

# UC Santa Barbara

## UC Santa Barbara Electronic Theses and Dissertations

### Title

Theoretical Generalizations of Topological Phases and Topological Entanglement Entropy

### Permalink

<https://escholarship.org/uc/item/77314761>

### Author

Patel, Kaushal

### Publication Date

2017

Peer reviewed|Thesis/dissertation

University of California  
Santa Barbara

# Theoretical Generalizations of Topological Phases and Topological Entanglement Entropy

A dissertation submitted in partial satisfaction  
of the requirements for the degree

Doctor of Philosophy  
in  
Physics

by

Kaushal Hasmukh Patel

Committee in charge:

Dr. Parsa Bonderson, Co-Chair  
Professor Chetan Nayak, Co-Chair  
Professor David Weld

September 2017

The Dissertation of Kaushal Hasmukh Patel is approved.

---

Professor David Weld

---

Professor Chetan Nayak, Committee Co-Chair

---

Dr. Parsa Bonderson, Committee Co-Chair

August 2017

Theoretical Generalizations of Topological Phases and Topological Entanglement  
Entropy

Copyright © 2017

by

Kaushal Hasmukh Patel

To my grandfather...

## Acknowledgements

It takes a village to raise a graduate student, and I have many people to thank for their support and for shaping me into the person I am today.

First and foremost, I thank my advisor Parsa Bonderson for being a brilliant mentor. His diligence and standard for perfection have been both humbling and inspiring, and I hope their effect on me never wear off. At the end of the day, I can only hope that I have reciprocated even some tiny fraction of the joy and knowledge he has given me.

I also thank the many outstanding Microsoft researchers and professors at UCSB, especially Chetan Nayak and David Weld, who have served on my thesis defense committee. I am grateful for my collaborators and colleagues, with whom I have had many insightful conversations about physics, graduate school, and life in general.

No words could describe the sacrifice my parents have made for me, and I am hopelessly indebted to them. My brother and my other close friends and family have also had played a huge role in my success in graduate school. I could always count on their love, even on the darkest of days.

Finally, in my final year, I have had the pleasure of meeting and marrying a wonderful woman, whose youthful spirit and heartening encouragement has carried me across the finish line. Thank you, Shweta.

# Curriculum Vitæ

## Kaushal Hasmukh Patel

### Education

- 2017 Ph.D. in Physics, University of California, Santa Barbara.  
2014 M.A. in Physics, University of California, Santa Barbara.  
2011 B.S. in Math and Physics, McGill University.

### Publications

1. Parsa Bonderson, Christina Knapp, and Kaushal Patel, “Anyonic Entanglement and Topological Entanglement Entropy.” arXiv:1706.09420.
2. Parsa Bonderson, Meng Cheng, Kaushal Patel, and Eugeniu Plamedeala, “Topological Enrichment of Luttinger’s Theorem.” arXiv:1601.07902.
3. Parsa Bonderson, Kaushal Patel, Kirill Shtengell, and Steve Simon, ”Topological Flux Phases.” In Preparation.

## Abstract

Theoretical Generalizations of Topological Phases and Topological Entanglement

Entropy

by

Kaushal Hasmukh Patel

In this thesis, we explore topological phases, study their properties, and present some novel extensions of them. Our study of topological phases begins on simplified theoretical models and provides a tractable setting to discuss the otherwise abstract mathematics involved, while maintaining the power to capture many experimentally salient features of these phases. We generalize these theoretical models and discover new phases of matter, topological flux phases, which are topological phases with a uniform anyonic flux. Other extensions of topological phases we study are fractionalized Fermi liquids, which are gapless topological phases with non-trivial interactions between gapless and topological sectors. Finally, we also focus on one peculiar property of topological phases, topological entanglement entropy, which captures the fact that some information is distributed globally in topological phase and can only be accessed with a topologically non-trivial measurement.

# Contents

|  |            |
|--|------------|
| <b>Curriculum Vitae</b>  | <b>vi</b>  |
| <b>Abstract</b>  | <b>vii</b> |
| <b>1 Introduction</b>  | <b>1</b>   |
| <b>2 Topological Flux Phases</b>                                   | <b>4</b>   |
| 2.1 Introduction . . . . .   | 4          |
| 2.2 String-Net Models . . . . .                                    | 5          |
| 2.3 Flux Phases . . . . .  | 23         |
| 2.4 Abelian Flux Phases . . . . .                                  | 27         |
| 2.5 Non-Abelian Flux Phases . . . . .                              | 34         |
| <b>3 Topological Enrichment of Luttinger’s Theorem</b>             | <b>49</b>  |
| 3.1 Introduction . . . . .   | 49         |
| 3.2 Oshikawa’s Argument . . . . .                                  | 51         |
| 3.3 Symmetry Fractionalization . . . . .                           | 54         |
| 3.4 Fractionalized Fermi Liquid . . . . .                          | 62         |
| 3.5 Discussion . . . . .   | 68         |
| <b>4 Anyonic Entanglement and Topological Entanglement Entropy</b> | <b>70</b>  |
| 4.1 Introduction . . . . .   | 70         |
| 4.2 Entropy . . . . .  | 72         |
| 4.3 Anyonic Entropy and Entanglement . . . . .                     | 77         |
| 4.4 Anyon Models for Higher Genus Surfaces . . . . .               | 100        |
| 4.5 Topological Entanglement Entropy in Anyon Models II . . . . .  | 115        |
| 4.6 Discussion . . . . .   | 164        |
| <b>A</b>   | <b>172</b> |
| A.1 $\mathbb{Z}_2^{(1/2)}$ (Doubled Semion) . . . . .              | 172        |
| A.2 String Operators . . . . .                                     | 174        |
| A.3 Corrections to $\mathcal{S}$ and $\mathcal{T}$ . . . . .       | 176        |

|                     |  |            |
|---------------------|--|------------|
| A.4                 | Ising String Operators . . . . .   | 178        |
| A.5                 | GSD from Verlinde Equation . . . . .                                       | 180        |
| A.6                 | GSD for Doubled Chern-Simons Theories . . . . .                            | 181        |
| A.7                 | $\mathbb{Z}_2^{(1/2)}$ Flux Phase . . . . .                                | 186        |
| A.8                 | $\mathbb{Z}_N$ Flux Phases . . . . .                                       | 188        |
| A.9                 | Abelian vs. Non-Abelian Fluxes . . . . .                                   | 192        |
| A.10                | Ising Change of Basis . . . . .  | 193        |
| A.11                | Properties of Spectacle Operators . . . . .                                | 197        |
| A.12                | Proof of Topological Protection . . . . .                                  | 200        |
| <b>B</b>            |  | <b>206</b> |
| B.1                 | Luttinger’s Theorem for Kondo Model . . . . .                              | 206        |
| B.2                 | Gauge Equivalence Between Flux Threading and Creating Anyon Loop . . . . . | 208        |
| <b>C</b>            |  | <b>212</b> |
| C.1                 | Anyon Models on a Sphere . . . . .   | 212        |
| C.2                 | Examples of Braided Tensor Categories . . . . .                            | 222        |
| C.3                 | Proofs . . . . .   | 225        |
| <b>Bibliography</b> |  | <b>233</b> |

# Chapter 1

## Introduction

According to Landau's theory of phase transitions, different phases of matter correspond to different manifestations of symmetries, and transitions between these phases occur when the corresponding symmetries are broken or restored [1]. Specifically, we can identify a local order parameter whose symmetry, or lack thereof, distinguishes between phases. For example, solid and liquid phases of matter can be distinguished by the symmetry of their density: the density of a liquid has continuous rotational and translational symmetry, which is broken down to discrete rotational and translational symmetry in the solid phase. Similarly, the magnetized and unmagnetized phases of the quantum Ising model can be distinguished by the symmetry of their magnetization: the magnetization of the unmagnetized phase has  $\mathbb{Z}_2$  Ising symmetry, which is broken in the magnetized phase.

Landau theory provides a unified description of many different phases and phase transitions, but there are some remarkable cases where it does not apply, such as the BKT transition [2, 3], integer quantum Hall effect [4, 5], and fractional quantum Hall effect [6]. These examples of phases that can not be understood with Landau theory often share one key ingredient: a non-trivial role played by topology. The exemplars of such

phases are called topological phases of matter, and exhibit some fascinating properties, e.g. robust ground state degeneracy, topological entanglement entropy, and excitations with exotic exchange statistics [7, 8, 9, 10, 11, 12, 13]. These properties open the door for exciting and novel applications, for example in quantum computing [14, 15, 16].

Symmetry can fail to distinguish different topological phases: two distinct topological phases can have identical symmetries. However, where group theory fails, category theory prevails. While originally discovered in an attempt to formalize and unify abstract concepts of various mathematical structures [17], category theory also provides a natural description of the universal properties of topological phases [18, 19]. Similar to how different phases in Landau theory correspond to different symmetry groups, different topological phases correspond to different categories of a special type. In this thesis, we use the language of category theories to explore topological phases, study their properties, and present some novel extensions of them. This thesis is organized as follows.

In Chapter 2, we introduce topological phases from a purely theoretical perspective, starting with lattice models called string-net models. We use these models to explore certain properties of topological phases, such as robust ground state degeneracy and the exotic excitations. We also modify string-net models to realize topological flux phases, which helps us explore concepts such as symmetry enriched topological phases, anyon condensation, and topological-protected non-Abelian braiding. This chapter is based on work in progress by Parsa Bonderson, Kaushal Patel, Kirill Shtengel, and Steven Simon, (content reproduced with permission of authors.)

In Chapter 3, we study gapless topological phases called fractionalized Fermi liquids, which are Fermi liquids coexisting with symmetry enriched topological order. We generalize Luttinger's theorem for Fermi liquids to fractionalized Fermi liquids. We find that, in the linear relation between the Fermi volume and the density of fermions, the contribution of the density is changed by the filling fraction associated with the topologically

---

ordered sector, which is determined by how the symmetries fractionalize. Conversely, this places constraints on the allowed symmetry enriched topological orders that can manifest in a fractionalized Fermi liquid with a given Fermi volume and density of fermions. This chapter is based on “Topological Enrichment of Luttinger’s Theorem” by Parsa Bonderson, Meng Cheng, Kaushal Patel, and Eugeniu Plamadela, arXiv:1601.07902, (content reproduced with permission of authors.)

In Chapter 4, we provide an intuitive understanding for topological entanglement entropy and present a method of deriving it for general system configurations of a topological phase, including surfaces of arbitrary genus, punctures, and quasiparticle content, for both bosonic and fermionic topological phases. In the process, we also develop different notions of anyonic entropy and formalize diagrammatic notation for topological phases on higher genus surfaces. Our results recover and extend prior results for anyonic entanglement and the topological entanglement entropy. This chapter is based on “Anyonic Entanglement and Topological Entanglement Entropy” by Parsa Bonderson, Christina Knapp, and Kaushal Patel, arXiv:1706.09420, (content reproduced with permission of authors.)

# Chapter 2

## Topological Flux Phases

### 2.1 Introduction

The study of topological phases of matter has exploded in recent years, in part due to their fundamental beauty, and in part due to the dream of applying these systems to quantum information processing [14, 15, 16]. Experimental realizations of topological phases include fractional quantum Hall effect [6, 20] (FQHE) and, potentially, quantum spin liquid materials [21, 22, 23].

String-net models provide extremely useful exactly solvable lattice models for a large class of (2+1)D topological phases; namely, lattice gauge theories and doubled Chern-Simons theories [24]. The Hamiltonians of string-net models are defined so that their ground states did not contain any flux passing through the plaquettes of the lattice. In this paper, we modify the Hamiltonians so that they favor a nontrivial flux through every plaquette, to form what we call flux phases. These flux phases can differ from the original trivial flux phases in several important ways.

Abelian flux phases of string-net models turn out to be symmetry enriched topological versions of their trivial flux counterpart. Specifically, the discrete translation symmetry of

the lattice is fractionalized in these flux phases. That is, when an anyon is translated along a trivial path, e.g. around a single plaquette, its wavefunction may acquire a nontrivial phase, precisely due its braiding around the nontrivial flux in that plaquette. We show that all Abelian flux phases can be understood with this symmetry fractionalization framework.

Non-Abelian flux phases of string-net models are more exotic and cannot be classified by symmetry fractionalization. While they may not be exactly solvable in general, the  $\sigma$  flux phase of the Ising string-net model we study in this paper does turn out to be exactly solvable. We find that it has an extensive ground state degeneracy, originating from the non-Abelian nature of the  $\sigma$  flux, and offers some notion of topological protected non-Abelian braiding. We also find that its extensive degeneracy is gapped out by local perturbations, and the resulting perturbed phase is none other than the toric code phase. We view this perturbation into the toric code phase as anyon condensation.

The outline of this paper is as follows. We begin with a brief review of string-net models in Sec. 2.2, and review the  $\mathbb{Z}_2$  string-net model and Ising string-net model. We then introduce flux phases of string-net models in Sec. 2.3, and show how to tune the Hamiltonian in order to realize them. We study Abelian flux phases in Sec. 2.4, and show that they can be understood as simple examples of symmetry fractionalization. Finally, we study the non-Abelian flux phases in Sec. 2.5, focusing mainly on the  $\sigma$  flux phase of the Ising string-net model.

## 2.2 String-Net Models

String-net lattice models were proposed by Levin and Wen [24] as a mechanism of obtaining a class of topological phases, whose emergent, low-energy degrees of freedom are described by topological quantum field theories (TQFTs). These models constitute

a Hamiltonian realization of the Turaev-Viro state sum models [25], which construct the partition functions of the corresponding TQFTs. String-net models have proven to be a useful tool for analyzing topological phases and have led to a range of new insights.

A 2D string-net model is constructed on a trivalent lattice (defined on a 2D surface) using a fusion tensor category (FTC)  $\mathcal{C}$ , which can be defined by a set of parameters  $\{\{|i\rangle, \delta_{ijk}, d_i, F_{klm}^{ijm}\}$ , which are required to satisfy certain consistency conditions. The lattice degrees of freedom live on the links of the lattice and the orthonormal basis states of each link are given by  $|i\rangle$ . The elements  $\{|i\rangle$  are interpreted as “string types” in the context of the string-net models.  $\delta_{ijk}$  encode the branching rules that determine whether three string types  $i$ ,  $j$ , and  $k$  are allowed to meet at a vertex in the ground state.  $d_i$  is the quantum dimension of the string type  $i$ , which is the associated weight ascribed to the creation of a loop of type  $i$ .  $F_{klm}^{ijm}$  are the  $F$ -symbols, which encode reconnection rules or fusion associativity of string types, similar to  $6j$ -symbols in traditional angular momentum addition. We will give more details of these parameters below.

When a string-net model is constructed from a FTC  $\mathcal{C}$  and has the “trivial flux” condition imposed by the plaquette terms, the resulting low energy effective theory of the system is a TQFT. The emergent quasiparticles of such systems are anyons whose universal properties, such as their fusion and braiding, are described by a modular tensor category (MTC) denoted  $D(\mathcal{C})$ , which is the Drinfeld center or quantum double of  $\mathcal{C}$ .

In this section, we review the construction of string-net models and two key examples of string-net models: (1) the  $\mathbb{Z}_2$  model, which realizes the  $D(\mathbb{Z}_2)$  or “toric code” phase, and the Ising model, which realizes the  $D(\text{Ising}) = \text{Ising} \times \overline{\text{Ising}}$  phase. These two models will serve as important examples throughout the remainder of this paper. We also review the  $\mathbb{Z}_2^{(1/2)}$  model, which realizes the  $D(\mathbb{Z}_2^{(1/2)})$  (doubled semion) phase in Appendix A.1. This section may be skipped or skimmed by those familiar with string-net models.

### 2.2.1 Model

String-net models may be constructed on any directed trivalent lattice or graph. For a model with  $n$  string types, a *lattice state* is given by assigning a label  $i \in \{0, 1, \dots, n-1\}$  to each of the directed links of the lattice. These different labels are thought of as the different string types. The Hilbert space is spanned by the set of all possible lattice states, with the inner product between two lattice states defined as 1 if they are identical, and 0 otherwise.

Any trivalent graph can be used, in principle, but it is convenient to choose the honeycomb lattice (hexagonal lattice with basis), because of its symmetry. Most manifolds, e.g. the sphere, cannot be tiled by a honeycomb lattice, so we will implicitly assume an appropriate trivalent graph when discussing such manifolds. The model, described below, is adapted to arbitrary trivalent graphs by a straightforward generalization of the plaquette term.

The Hamiltonian of the string-net model with trivial flux is

$$\mathbf{H}^{(0)} = - \sum_{\mathbf{v}} \mathbf{Q}_{\mathbf{v}} - \sum_{\mathbf{p}} \mathbf{B}_{\mathbf{p}}^{(0)}, \quad (2.1)$$

where  $\mathbf{v}$  stands for the vertices of the lattice, and  $\mathbf{p}$  the plaquettes. The operators  $\mathbf{Q}_{\mathbf{v}}$  and  $\mathbf{B}_{\mathbf{p}}^{(0)}$  are commuting projectors, and therefore  $\mathbf{H}^{(0)}$  is exactly solvable.

The operator  $\mathbf{Q}_{\mathbf{v}}$  acts on the vertex  $\mathbf{v}$  as

$$\mathbf{Q}_{\mathbf{v}} \left| \begin{array}{c} \nearrow j \\ \leftarrow i \\ \searrow k \end{array} \right\rangle = \delta_{ijk} \left| \begin{array}{c} \nearrow j \\ \leftarrow i \\ \searrow k \end{array} \right\rangle, \quad (2.2)$$

where  $\delta_{ijk}$  are the *branching rules*. The branching rules specify which triples of string

types are allowed to meet at the vertices of the ground state:

$$\delta_{ijk} = \begin{cases} 1 & \text{if } i, j, k \text{ allowed to meet,} \\ 0 & \text{otherwise.} \end{cases} \quad (2.3)$$

(The branching rules are independent of the order that the string types meet at a vertex.)

Lattice states which obey the branching rules at every vertex are called *string-nets*.

The branching rules  $\delta_{ijk}$  represent the fusion rules

$$i \times j = \sum_k N_{ij}^k k \quad (2.4)$$

of a FTC  $\mathcal{C}$ , through the relation  $N_{ij}^k = \delta_{ij\bar{k}}$ , where  $\bar{k}$  is the charge conjugate or dual of  $k$ .<sup>1</sup> As such, they must obey the following conditions:

1. There exists a unique “vacuum” string, which we label 0. In the string-net model, the 0 string is interpreted as an unoccupied link and it branches trivially with other strings.
2. For every string type  $i$ , there is a dual string type  $\bar{i}$ , which is the unique string type that obeys  $\delta_{0j\bar{k}} = \delta_{jk}$  for all  $j$ . (The two-index  $\delta$  symbol is the usual Kronecker delta, not to be confused with the three-index branching rules  $\delta_{ijk}$ .) The dual string represents a string oriented in the opposite direction:

$$|\bar{i}\leftarrow\rangle = |\rightarrow i\rangle. \quad (2.5)$$

If  $i = \bar{i}$ , then  $i$  is self-dual and it can be drawn without an arrow. The vacuum string is always required to be self-dual  $0 = \bar{0}$ .

---

<sup>1</sup>We note that, more generally, one can take  $N_{ij}^k$  to be positive integers.

3. The branching rules satisfy

$$\sum_m \delta_{ijm} \delta_{\bar{m}kl} = \sum_n \delta_{iln} \delta_{jk\bar{n}}. \quad (2.6)$$

This relation represents the recoupling of the branching rules (associativity of fusion).

4. The branching rules satisfy  $\delta_{ijk} = \delta_{jki} = \delta_{jik} = \delta_{\bar{i}\bar{j}\bar{k}}$ , for all  $i, j$ , and  $k$ . These relations represent invariance under rotation, reflection, and string type conjugation of the branching rules, respectively.

The operator  $\mathbf{B}_p^{(0)}$  is defined to be

$$\mathbf{B}_p^{(0)} = \sum_s \frac{d_s}{\mathcal{D}_C^2} \mathbf{B}_p^s, \quad (2.7)$$

where  $\mathbf{B}_p^s$  acts on the plaquette  $p$  as

$$\mathbf{B}_p^s \left| \begin{array}{c} \psi \\ \begin{array}{c} \text{g} \quad \text{h} \quad \text{g}' \\ \text{a} \quad \text{b} \quad \text{c} \\ \text{l} \quad \text{k} \quad \text{i} \\ \text{f} \quad \text{j} \quad \text{d} \\ \text{e} \end{array} \end{array} \right\rangle = \sum_{g'h'i'j'k'l'} F_{\bar{s}g'l'}^{a\bar{l}g} F_{\bar{s}h'g'}^{b\bar{g}h} F_{\bar{s}i'h'}^{c\bar{h}i} F_{\bar{s}j'i'}^{d\bar{i}j} F_{\bar{s}k'j'}^{e\bar{j}k} F_{\bar{s}l'k'}^{f\bar{k}l} \left| \begin{array}{c} \psi \\ \begin{array}{c} \text{g}' \quad \text{h}' \quad \text{g} \\ \text{a}' \quad \text{b}' \quad \text{c}' \\ \text{l}' \quad \text{k}' \quad \text{i}' \\ \text{f}' \quad \text{j}' \quad \text{d}' \\ \text{e}' \end{array} \end{array} \right\rangle. \quad (2.8)$$

In these expressions,  $d_i$  are the *quantum dimensions* of the FTC  $\mathcal{C}$ , which take nonzero values. In the string-net model,  $d_i$  is the weight ascribed to annihilating a loop of charge  $i$ .  $\mathcal{D}_C = \sqrt{\sum_i d_i^2}$  is the *total quantum dimension* of  $\mathcal{C}$ .  $F_{klm}^{ijm}$  are the *F-symbols* of  $\mathcal{C}$ , which encode associativity of fusion in the state space. Since these quantities are taken from a FTC, they must obey the conditions:

1.  $d_i d_j = \sum_k \delta_{i\bar{j}\bar{k}} d_k$ . Note that this implies  $d_0 = 1$  and  $d_i = d_{\bar{i}}$ .

2.  $F_{kln}^{ijm}$  is inadmissible if any of  $\delta_{ijm}$ ,  $\delta_{\bar{m}kl}$ ,  $\delta_{iln}$ , or  $\delta_{\bar{n}jk}$  are equal to 0, in which case, we set  $F_{kln}^{ijm} = 0$ . Otherwise,  $F_{kln}^{ijm}$  is admissible (i.e. when  $\delta_{ijm}\delta_{\bar{m}kl} = \delta_{iln}\delta_{\bar{n}jk} = 1$ ).
3. Pentagon equation:

$$\sum_n F_{k\bar{p}n}^{mlq} F_{mn\bar{s}}^{jip} F_{lk\bar{r}}^{j\bar{s}n} = F_{\bar{q}k\bar{r}}^{jip} F_{ml\bar{s}}^{riq}. \quad (2.9)$$

This consistency relation requires that different paths of  $F$ -move applications that begin in the same configuration and end in the same configuration yield the same amplitude.

We also wish to impose the following additional constraints:

1. Tetrahedral symmetries:

$$F_{kln}^{ijm} = F_{jin}^{lk\bar{m}} = F_{lk\bar{n}}^{jim} = F_{\bar{k}nl}^{imj} \frac{v_m v_n}{v_j v_l} \quad (2.10)$$

These relations are obtained from a tetrahedron whose edges correspond to the six string types involved, by reflecting along different planes. This can be viewed as encoding reflection invariance of the  $F$ -moves.

2.  $F_{\bar{j}i0}^{ijk} = \frac{v_k}{v_i v_j} \delta_{ijk}$ , where  $v_i = v_{\bar{i}} = \sqrt{d_i}$  and  $v_0 = 1$ . This condition, together with Eq. (2.10) implies rotational invariance of the  $F$ -moves (i.e. there is no preferred direction), since they provide the conditions for strict isotopy invariance [26]. (More specifically, it implies that the Frobenius-Schur indicators  $\varkappa_i \equiv d_i F_{i\bar{i}0}^{i\bar{i}0} = 1$  for all  $i$  and  $F_{\bar{j}i0}^{ijk} = F_{i\bar{i}k}^{j\bar{j}0} = \frac{v_k}{v_i v_j} \delta_{ijk}$ .)
3.  $F_{\bar{k}l\bar{n}}^{i\bar{j}\bar{m}} = (F_{kln}^{ijm})^*$ . This condition, together with the relation  $F_{kln}^{ijm} = F_{\bar{l}\bar{i}\bar{m}}^{j\bar{k}n}$  derived from Eq. (2.10), and the relation  $\sum_n F_{kln}^{ijm} F_{li\bar{p}}^{j\bar{k}\bar{n}} = \delta_{mp}$  derived from rotational invariance, implies that the  $F$ -moves are unitary. It is also straightforward to see that this condition implies that  $\mathbf{B}_p^{(0)}$  is Hermitian.

In other words, imposing these extra conditions means we are restricting to a FTC  $\mathcal{C}$  that is unitary (in the sense that the  $F$ -symbols are unitary, but the quantum dimensions are not required to be positive) and completely invariant under rotation and reflection (isotopy and spatial parity).

We note that more general string-net models may be defined. In particular, one may consider models based on FTCs that have fusion multiplicities or which are non-unitary. One may also use FTCs that are not completely invariant under rotation and reflection, with appropriate modification of the model construction. However, we will not consider such generalizations in our paper.

Given a set of string types and their corresponding branching rules, Ocneanu rigidity [27] guarantees that there are only a finite number of distinct sets of  $d_i$  and  $F$ -symbols, up to gauge transformations, that can satisfy the above conditions. Each of these gauge-equivalent set of quantities describes a distinct FTC and leads to a different string-net model representing distinct topological phases. (Using  $d_i$  and  $F$ -symbols related by gauge transformations yield Hamiltonians and corresponding ground states that are related by the application of product of local unitary operators. As such, they represent the same phase of matter.)

Due to the special choice of the coefficients  $d_s/\mathcal{D}_{\mathcal{C}}^2$  in Eq. (2.7), the plaquette terms  $\mathbf{B}_p^{(0)}$  energetically favor there being no flux passing through the plaquettes of the ground states. These zero-flux states corresponds to the ground state subspace of a topological phase in which the ground states have a smooth continuum limit. In Sec. 2.3, we will tune these coefficients to create modified plaquette terms  $\mathbf{B}_p^{(i)}$  that energetically favor a nontrivial flux  $i$  passing through the plaquettes of the ground state, resulting in what we call “topological flux phases.”

## Ground States

Since the Hamiltonian is a sum of commuting projectors, it can be solved exactly. A ground state  $|0\rangle$  of the string-net Hamiltonian is a superposition of lattice states

$$|0\rangle = \frac{1}{N} \sum_X \Phi(|X\rangle)|X\rangle, \quad (2.11)$$

where  $N$  is a normalization constant and  $\Phi(|X\rangle)$  is the amplitude of the lattice state  $|X\rangle$ .

The ground states of the Hamiltonian maximizes every  $\mathbf{Q}_v$  and every  $\mathbf{B}_p^{(0)}$ . In order to maximize every  $\mathbf{Q}_v$ , a ground state  $|0\rangle$  must be a linear combination of string-nets, i.e.  $\Phi(|X\rangle) = 0$  if  $|X\rangle$  is not a string-net. In order to maximize every  $\mathbf{B}_p^{(0)}$ , the amplitudes  $\Phi(|X\rangle)$  must obey the following *local relations*:

1.  $\Phi(|\rightarrow i \rightarrow\rangle) = \Phi(|\rightarrow i \curvearrowright\rangle)$  indicating that strings can be continuously deformed (isotopy).
2.  $\Phi(|\circ_i\rangle) = d_i \Phi(|\ )\rangle$  indicating that the relative amplitude for a loop of string type  $i$  is its quantum dimension.
3.  $\Phi\left(|\begin{array}{c} i \quad k \quad j \\ \circlearrowleft \end{array}\rangle\right) = \delta_{ij} \Phi\left(|\begin{array}{c} i \quad k \quad j \\ \circlearrowright \end{array}\rangle\right)$  indicating the conservation of string type, i.e. that the branching rules hold at all scales.
4.  $\Phi\left(|\begin{array}{c} i \quad m \quad l \\ \leftarrow j \quad \rightarrow k \end{array}\rangle\right) = \sum_n F_{kln}^{ijm} \Phi\left(|\begin{array}{c} i \quad l \\ \leftarrow j \quad \rightarrow k \\ \leftarrow n \end{array}\rangle\right)$  indicating that the amplitudes for recoupling string-nets is determined by the  $F$ -symbols.

where the diagrams in these relations represent some local region of a string-net state  $|X\rangle$ . These relations are schematic in the sense that, while string-net states are defined on the lattice, we allow the strings to be smoothly deformed off the lattice structure (onto the corresponding 2D manifold it tiles) when applying these relations in a local region, as

long as we return to the lattice structure for the sake of comparing with another string-net state. These relations hold because  $\mathbf{H}^{(0)}$  is in the zero-flux phase. For nontrivial topological flux phases, these local relations will generally no longer hold. States for which these relations hold are referred to as *string-net condensates*.

On a closed surface of genus zero, i.e. the sphere or the infinite plane, the local relations can always relate the amplitude of two different string-nets. Thus, there is a unique ground state on such manifolds. On more general surfaces, the local relations cannot always relate the amplitude of two different string-nets. As a result, there may be degenerate ground states. Two string-net configurations that cannot be related by any number of applications of the local relations belong to different ground states. This ground state degeneracy, which is topologically protected against local perturbations, is determined by Eq. (A.30). These ground states can only be related by application of operators that act nontrivially on regions of macroscopic extent, for example a string operator that winds around a nontrivial cycle of the manifold. This is discussed in more detail below.

## Excitations

Since the ground states simultaneously maximizes every  $\mathbf{Q}_v$  and  $\mathbf{B}_p^{(0)}$ , excited states must violate at least one  $\mathbf{Q}_v$  or  $\mathbf{B}_p^{(0)}$ . Thus, the excited states are separated from the ground states by a constant energy gap. Because the energy of an excited state can be attributed to the violation of specific vertex and plaquette terms, we can view such states as possessing quasiparticles localized at the positions of the violated vertices and plaquettes. These states possessing quasiparticles can be obtained from the ground state by applying open string operators (Wilson line operators), which we now review.

A *string operator*  $\mathbf{W}_a$  of anyon type  $\mathbf{a}$  is represented pictorially by a directed path along the lattice labeled  $\mathbf{a}$ , as shown in Fig. 2.1. The string operators carry a (specific)

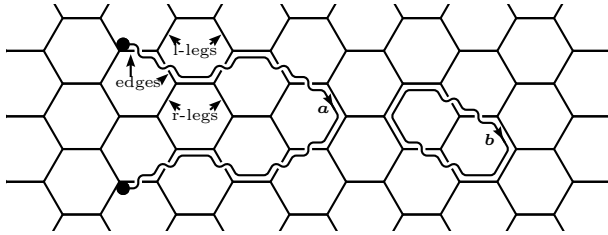


Figure 2.1: Open string operator  $W_a$  and closed string operator  $W_b$ .

superposition of lattice string type labels  $j \in \mathcal{C}$ . When the string operator path runs along the lattice without crossing any links, its action on string-net states is given by fusing the string into the lattice using the local relations of  $\mathcal{C}$ . Additionally, the string operators are defined to have a (one-sided) braiding over links of the lattice and to be isotopy invariant (with fixed endpoints, when the string is open) when applied to ground states of the (zero-flux) string-net condensed phase. Consistency with the reversal of link orientations requires the string operators to satisfy

$$\begin{array}{c} \rightarrow \\ \rightarrow \end{array} \text{---} = \begin{array}{c} \rightarrow \\ \rightarrow \end{array} \text{---} . \tag{2.12}$$

Isotopy invariance of the string operators over the string-net condensate ground states is obtained by requiring that the string operators can be deformed freely over the vertices

$$\begin{array}{c} \rightarrow \\ \rightarrow \end{array} \text{---} = \begin{array}{c} \rightarrow \\ \rightarrow \end{array} \text{---} , \tag{2.13}$$

when the lattice state satisfies the branching rules at the vertex (see Appendix A.2 for details), and over the plaquettes

$$\left| \begin{array}{c} \rightarrow \\ \rightarrow \end{array} \text{---} \right\rangle = \left| \begin{array}{c} \rightarrow \\ \rightarrow \end{array} \text{---} \right\rangle , \tag{2.14}$$

where the lattice state satisfies the branching rules and zero-flux condition at the pla-

quette. Imposing these requirements on the string operators is equivalent to imposing the conditions on the braiding amplitudes.

Since the string operators satisfy these conditions, we can think of them as *fluctuating* with respect to the (zero-flux) string-net condensed ground states. This means that, when applied to the ground states of the string-net condense phase, the location of the string operator is not observable. (If the string operator is open, the location of its endpoints are observable.) For nontrivial flux phases, the fluctuating property of string operators will no longer hold in general, and it may be possible to observe the location of the string when applied to the ground states.

Due to Ocneanu rigidity, there can only be a finite number of string operators that satisfy these conditions for any particular string-net model. We emphasize that there will generally be more distinct types of string operators than there are lattice string types (i.e. degrees of freedom per link). In particular, while the lattice string types correspond to the simple objects in the underlying FTC  $\mathcal{C}$ , the string operator types correspond to the anyon types (topological charges) in the emergent topological phase, which is described by the MTC  $D(\mathcal{C})$ . We will label the emergent anyon types (and their corresponding string operator types) as  $\mathbf{a} \in D(\mathcal{C})$  in bold to distinguish them from the underlying string types  $i \in \mathcal{C}$  of the string-net model.

A *closed* string operator commutes with the (zero-flux) Hamiltonian. As such, applying a closed string operator to a ground state results in a ground state. On a manifold with nontrivial topology, where there are degenerate ground states, a closed string operator can cause a transition between ground states if it is non-contractible, e.g. if it wraps around a nontrivial cycle of a torus. A closed string operator that is contractible takes a ground state to itself, up to a factor of the loop weight (expectation of a contractible

closed string operator in a ground state)

$$\ell_{\mathbf{a}} = \langle 0 | \circ \mathbf{a} | 0 \rangle = \sum_j n_{\mathbf{a},j} d_j. \quad (2.15)$$

An *open* string operator  $\mathbf{W}_{\mathbf{a}}$  commutes with the Hamiltonian everywhere except at its endpoints. Consequently, a state obtained by applying an open string operator to a ground state results in an excited state that violates  $\mathbf{Q}_v$  and/or  $\mathbf{B}_p^{(0)}$  for the vertices and/or plaquettes at the string endpoints. This can be interpreted as the creation of localized quasiparticle excitations  $\mathbf{a}$  and  $\bar{\mathbf{a}}$  at the endpoints of the open string operator. (A directed open string of type  $\mathbf{a}$  starts at a quasiparticle of type  $\bar{\mathbf{a}}$  and ends at a quasiparticle of type  $\mathbf{a}$ .) As such, the fusion and braiding properties of  $D(\mathcal{C})$  can be obtained from these string operators. Rather than obtain all the basic data, we focus on certain important gauge invariant quantities that are believed to fully specify a MTC (up to gauge freedom), namely the modular  $\mathcal{S}$ -matrix and  $\mathcal{T}$ -matrix.

We begin by noting that in order for a MTC to (diagrammatically) describe anyonic states of quasiparticles, it must be unitary and have a positive definite inner product, which means its quantum dimensions must be positive. In terms of its  $F$ -symbols (one should be careful to distinguish between the  $F$ -symbols of  $D(\mathcal{C})$  considered here, and those of  $\mathcal{C}$  used to define the lattice model), the quantum dimension of an anyon type may be defined to be

$$d_{\mathbf{a}} = d_{\bar{\mathbf{a}}} = |[F_{\mathbf{a}}^{\mathbf{a}\bar{\mathbf{a}}\mathbf{a}}]_{00}]^{-1} \quad (2.16)$$

and the Frobenius-Schur indicators are phases given by

$$\chi_{\mathbf{a}} = \chi_{\bar{\mathbf{a}}}^* = d_{\mathbf{a}} [F_{\mathbf{a}}^{\mathbf{a}\bar{\mathbf{a}}\mathbf{a}}]_{00}. \quad (2.17)$$

With these definitions,  $d_{\mathbf{a}} \geq 1$  and the dimension of the anyonic state space associated

with  $n$  anyons of topological charge  $\mathbf{a}$  scales as  $d_{\mathbf{a}}^n$  as  $n \rightarrow \infty$ . An anyon is *Abelian* if  $d_{\mathbf{a}} = 1$ , while it is *non-Abelian* if  $d_{\mathbf{a}} > 1$ . Also, when  $\mathbf{a} = \bar{\mathbf{a}}$ ,  $\varkappa_{\mathbf{a}} = \pm 1$  is a gauge invariant quantity. When  $\mathbf{a} \neq \bar{\mathbf{a}}$ ,  $\varkappa_{\mathbf{a}}$  is gauge dependent, and can be set to 1 if so desired. (The term ‘‘Frobenius-Schur indicator’’ is often reserved for the case when  $\mathbf{a} = \bar{\mathbf{a}}$ , but we use it more generally.)

In terms of the string operators’s loop weight, defined in Eq. (2.15), these quantities associated with the quasiparticle types are given by

$$d_{\mathbf{a}} = |\ell_{\mathbf{a}}|, \quad (2.18)$$

$$\varkappa_{\mathbf{a}} = \ell_{\mathbf{a}}/|\ell_{\mathbf{a}}|. \quad (2.19)$$

This emphasizes a distinction between the closed string operator loops applying to the 2D lattice states and the ‘‘loops’’ formed by taking inner products of anyonic states using the diagrammatic formalism. For the FTC  $\mathcal{C}$  of the lattice model, the Frobenius-Schur indicators of the string types (link variables) were required to be  $\varkappa_j = 1$  for all  $j$ , but the quantum dimensions  $d_j$  were not required to be positive numbers. Similarly, the string operator lines are required to be isotopy invariant when acting on the string-net condensate ground states, and their loop values  $\ell_{\mathbf{a}}$  need not be positive. On the other hand, for the emergent MTC  $\mathcal{D}(\mathcal{C})$  describing the anyonic quasiparticle excitations, the quantum dimensions are required to be  $d_{\mathbf{a}} \geq 1$  for all  $\mathbf{a}$ , since this corresponds to a positive definite inner product, but the Frobenius-Schur indicators  $\varkappa_{\mathbf{a}}$  are not required to equal 1.

The total quantum dimension of the emergent theory  $\mathcal{D}(\mathcal{C})$  is related to that of the underlying FTC  $\mathcal{C}$  by

$$\mathcal{D}_{\mathcal{D}(\mathcal{C})} = \sqrt{\sum_{\mathbf{a}} d_{\mathbf{a}}^2} = \sum_j d_j^2 = \mathcal{D}_{\mathcal{C}}^2. \quad (2.20)$$

The exchange statistics of the anyons are captured by the topological  $\mathcal{S}$  and  $\mathcal{T}$  matrices

$$\mathcal{S}_{ab} = \frac{\varkappa_a \varkappa_b}{\mathcal{D}_{D(\mathcal{C})}} \langle 0 | a \text{ } \overbrace{\text{ } }^{\text{ } } b | 0 \rangle \quad (2.21)$$

$$\mathcal{T}_{ab} = \frac{1}{d_a} \langle 0 | \text{ } \overbrace{\text{ } }^{\text{ } } a | 0 \rangle \delta_{ab}, \quad (2.22)$$

where the diagrams schematically represent string operators applied to the lattice states. These definitions include Frobenius-Schur factors that account for the distinction between the string operators applying to 2D lattice states and the diagrammatic representation of the corresponding quantities in the emergent topological state space, as explained in Appendix A.3.

When the FTC  $\mathcal{C}$  describes the fusion and recoupling structure of a MTC  $\mathcal{M}$ , i.e. there exists a consistent way of introducing a braiding structure for  $\mathcal{C}$  with a unitary  $S$ -matrix, then the quantum double of  $\mathcal{C}$  will be described by  $D(\mathcal{C}) = \mathcal{M} \times \bar{\mathcal{M}}$ . In this case, one can envision the emergent theory by doubling the manifold into two surfaces on either side of the lattice, with  $\mathcal{M}$  living on one surface and  $\bar{\mathcal{M}}$  living on the other. In this way, a quasiparticle of topological charge  $\mathbf{a} = (a_L, a_R)$  can be thought of as localizing topological charge  $a_L \in \mathcal{M}$  on the surface above the lattice and  $a_R \in \bar{\mathcal{M}}$  on the surface below the lattice. The quantum dimension of  $(a_L, a_R)$  is  $d_{(a_L, a_R)} = d_{a_L} d_{a_R}$ .

Another large class of theories are obtained when the FTC  $\mathcal{C} = \text{Rep}(G)$ , for which the set of topological charges are the irreducible representations of a finite group  $G$ , the fusion rules are given by tensor products of representations, the  $F$ -symbols are given by the corresponding  $6j$ -symbols, and the dimension of an irreducible representation is its corresponding quantum dimension. In this case, the quantum double of  $\mathcal{C}$  is the discrete gauge theory  $D(G)$  for gauge group  $G$ . [28] The resulting anyon types may take the form of: a pure flux  $(\alpha, I)$ , where  $\alpha$  is a conjugacy class of  $G$ ; a pure charge

$(\{e\}, R^{(G)})$ , where  $R^{(G)}$  is an irreducible representation of  $G$ ; or a dyon (flux-charge composite)  $(\alpha, R^{(C(\alpha))})$ , where  $\alpha$  is a conjugacy class of  $G$  and  $R^{(C(\alpha))}$  is an irreducible representation of the centralizer  $C(\alpha)$  of (an element in)  $\alpha$ . The quantum dimension of  $(\alpha, R^{(C(\alpha))})$  is  $d_{(\alpha, R^{(C(\alpha))})} = |\alpha| \dim R^{(C(\alpha))}$ .<sup>2</sup>

We now describe two examples in more detail.

### 2.2.2 $\mathbb{Z}_2$ (Toric Code)

The  $\mathbb{Z}_2$  model uses the FTC  $\mathcal{C} = \text{Rep}(\mathbb{Z}_2)$  given by:

- String types 0 and 1,
- Allowed branchings  $\{0, 0, 0\}$ ,  $\{0, 1, 1\}$ ,
- Quantum dimensions  $d_0 = d_1 = 1$ , and
- All admissible  $F_{klm}^{ijn} = 1$ .

The Hamiltonian is

$$\mathbf{H}_{\mathbb{Z}_2}^{(0)} = - \sum_{\mathbf{v}} \mathbf{Q}_{\mathbf{v}} - \sum_{\mathbf{p}} \frac{1}{2} (\mathbf{B}_{\mathbf{p}}^0 + \mathbf{B}_{\mathbf{p}}^1). \quad (2.23)$$

The ground state in the plane is the sum of all possible lattice configurations of closed loops of lattice strings with equal amplitude (string-nets are simply configurations of closed loops in this example):

$$|0\rangle = \sum_{|X\rangle \in \substack{\text{closed loop} \\ \text{string-nets}}} |X\rangle. \quad (2.24)$$

---

<sup>2</sup>One may also obtain the discrete gauge theory  $D(G)$  from the FTC  $\mathcal{C} = \text{Vec}(G)$ , where the topological charges are the group elements, the fusion rules are given by group multiplication, the  $F$ -symbols are trivial (equal 1 when admissible), and quantum dimensions all equal 1. However, in this case, the fusion rules are not necessarily commutative, unless  $G$  is Abelian, so one must use one of the more general string-net model constructions.

If we represent the strings as spin- $\frac{1}{2}$  degrees of freedom, where the 0 string is  $|+z\rangle$  and the 1 string is  $|-z\rangle$ , then  $\mathbf{Q}_v$  and  $\mathbf{B}_p^{(0)}$  can be written in terms of Pauli matrices:

$$\mathbf{Q}_v = \frac{1}{2} \left( 1 + \prod_{i \in v \text{ legs}} \sigma_i^z \right) \quad (2.25)$$

$$\mathbf{B}_p^{(0)} = \frac{1}{2} \left( 1 + \prod_{i \in p \text{ edges}} \sigma_i^x \right) \cdot \prod_{v \in p \text{ vertices}} \mathbf{Q}_v \quad (2.26)$$

Omitting the  $\prod_v \mathbf{Q}_v$  term in  $\mathbf{B}_p^{(0)}$ , which acts trivially on the ground state, this Hamiltonian is equivalent to Kitaev's toric code Hamiltonian [15]

$$\mathbf{H} = - \sum_v \prod_{i \in v \text{ legs}} \sigma_i^z - \sum_p \prod_{i \in p \text{ edges}} \sigma_i^x, \quad (2.27)$$

up to a factor of 2 and an overall energy shift.

There are four string operators, which correspond to the topological charges of the  $D(\mathbb{Z}_2)$  MTC. When acting along a path P, they can be written in terms of Pauli matrices:

$$\mathbf{W}_I = I, \quad (2.28)$$

$$\mathbf{W}_e = \prod_{p \in P \text{ edges}} \sigma_p^x, \quad (2.29)$$

$$\mathbf{W}_m = \prod_{r \in P \text{ r-legs}} \sigma_r^z, \quad (2.30)$$

$$\mathbf{W}_f = \prod_{p \in P \text{ edges}} \sigma_p^x \cdot \prod_{r \in P \text{ r-legs}} \sigma_r^z. \quad (2.31)$$

Here, P edges are the links along the path of the string operator, and P r-legs are the links exiting to the right when traversing the path in some fixed direction, as shown in Fig. 2.1. And open string operator  $\mathbf{W}_e$  creates a  $\mathbf{Q}_v$  violating electric charge  $e$  at each of its endpoints,  $\mathbf{W}_m$  creates a  $\mathbf{B}_p^{(0)}$  violating magnetic flux  $m$ , and  $\mathbf{W}_f$  creates a bound

state  $\mathbf{f}$  of  $\mathbf{e}$  and  $\mathbf{m}$ . (If we do not omit the  $\prod_v \mathbf{Q}_v$  term in the definition of  $\mathbf{B}_p^{(0)}$ , then  $\mathbf{W}_e$  also creates three  $\mathbf{B}_p^{(0)}$  violations at each endpoint.)

The  $\mathcal{S}$  and  $\mathcal{T}$  matrices are

$$\mathcal{S} = \frac{1}{2} \begin{bmatrix} 1 & 1 & 1 & 1 \\ 1 & 1 & -1 & -1 \\ 1 & -1 & 1 & -1 \\ 1 & -1 & -1 & 1 \end{bmatrix}, \quad (2.32)$$

$$\mathcal{T} = \text{diag}[1, 1, 1, -1]. \quad (2.33)$$

The rows and columns of  $\mathcal{S}$  and  $\mathcal{T}$  are labeled by  $\mathbf{I}$ ,  $\mathbf{e}$ ,  $\mathbf{m}$ , and  $\mathbf{f}$ , in order. Using Eq. (A.30), the ground state degeneracy on a genus  $g$  surface is  $4^g$ .

### 2.2.3 Ising (Ising $\times$ $\overline{\text{Ising}}$ )

The Ising model uses the Ising FTC  $\mathcal{C} = \text{IFC}$ :

- String types 0 ( $\vdots$ ), 1 ( $\mid$ ), and 2 ( $\parallel$ ), (which we call  $I$ ,  $\sigma$ , and  $\psi$ , respectively),
- Allowed branchings  $\{I, I, I\}$ ,  $\{I, \sigma, \sigma\}$ ,  $\{I, \psi, \psi\}$ ,  $\{\sigma, \sigma, \psi\}$ ,
- Quantum dimensions  $d_I = d_\psi = 1$ ,  $d_\sigma = \sqrt{2}$ , and
- Nontrivial  $F$ -symbols:

$$F_{\sigma\sigma I}^{\sigma\sigma I} = F_{\sigma\sigma\psi}^{\sigma\sigma I} = F_{\sigma\sigma I}^{\sigma\sigma\psi} = -F_{\sigma\sigma\psi}^{\sigma\sigma\psi} = 1/\sqrt{2}, \quad (2.34)$$

$$F_{\sigma\psi\sigma}^{\sigma\psi\sigma} = F_{\psi\sigma\sigma}^{\psi\sigma\sigma} = -1. \quad (2.35)$$

All other admissible  $F_{klm}^{ijn} = 1$ .

The Hamiltonian is

$$\mathbf{H}_{\text{Ising}}^{(I)} = - \sum_{\mathbf{v}} \mathbf{Q}_{\mathbf{v}} - \sum_{\mathbf{p}} \frac{1}{4} \left( \mathbf{B}_{\mathbf{p}}^I + \sqrt{2} \mathbf{B}_{\mathbf{p}}^{\sigma} + \mathbf{B}_{\mathbf{p}}^{\psi} \right). \quad (2.36)$$

Unlike with the  $\mathbb{Z}_2$  model, we have no explicit closed-form expression for the ground states, though it can be constructed using the local relations of Sec. 2.2.1.

The Ising FTC describes the fusion structure of the Ising MTC. Thus, there are nine distinct types of string operators, which correspond to the topological charges of the  $D(\text{Ising}) = \text{Ising} \times \overline{\text{Ising}}$  MTC. We label them  $\mathbf{a} = (a_L, a_R)$ , where  $a_L, a_R \in \{I, \sigma, \psi\}$ . (See Appendix A.4 for details.)

The  $\mathcal{S}$  and  $\mathcal{T}$  matrices of  $D(\text{Ising})$  are:

$$\mathcal{S} = \mathcal{S}_{\text{Ising}} \otimes \mathcal{S}_{\text{Ising}}^*, \quad (2.37)$$

$$\mathcal{T} = \mathcal{T}_{\text{Ising}} \otimes \mathcal{T}_{\text{Ising}}^*, \quad (2.38)$$

where the modular matrices of the Ising MTC are given by

$$\mathcal{S}_{\text{Ising}} = \frac{1}{2} \begin{bmatrix} 1 & \sqrt{2} & 1 \\ \sqrt{2} & 0 & -\sqrt{2} \\ 1 & -\sqrt{2} & 1 \end{bmatrix}, \quad (2.39)$$

$$\mathcal{T}_{\text{Ising}} = \text{diag}[1, e^{i\pi/8}, -1], \quad (2.40)$$

where the rows and columns are labeled by  $I$ ,  $\sigma$ , and  $\psi$ , in order. Using Eq. A.30, the ground state degeneracy of  $D(\text{Ising})$  on a genus  $g$  surface is  $4^{g-1}(2^g + 1)^2$ .

The anyons carrying the  $\sigma$  topological charge have non-Abelian statistics. For exam-

ple, the  $(\sigma, I)$  anyon has  $d_{(\sigma, I)} = \sqrt{2}$ , because two  $(\sigma, I) \times (\sigma, I) = (I, I) + (\psi, I)$ . A full braid of two  $(\sigma, I)$  anyons around each other has the same effect as transferring a  $(\psi, I)$  topological charge between them, up to a phase, i.e.

$$\begin{array}{c} \text{↻} \\ \text{---} \\ (\sigma, I) \quad (\sigma, I) \end{array} = e^{-i\pi/4} \begin{array}{c} \text{---} \\ \text{---} \\ (\sigma, I) \quad (\sigma, I) \end{array} \begin{array}{c} \uparrow \\ \text{---} \\ \uparrow \\ (\psi, I) \end{array}. \quad (2.41)$$

## 2.3 Flux Phases

In this section, we introduce flux phases of string-net models. The phases described in Sec. 2.2 are in the zero-flux phase of the string-net models, where the ground state(s) can be found using the local string-net relations (described by a FTC  $\mathcal{C}$ ). The quasiparticle string operators were thought of as fluctuating with respect to the ground states as a result of the zero-flux condition allowing them to be freely deformed over plaquettes. However, for a string-net model with  $n$  strings, one can obtain  $n$  different phases (including the zero-flux phase) by modifying the plaquette term of the Hamiltonian to energetically favor one of the  $n$  different “flux” values through the plaquettes. Consequently, the ground states of these nontrivial flux phases will have the corresponding flux through plaquettes, so the local relations may not all apply for the ground states and the string operators may not fluctuate freely.

Defining fusion matrices  $N_i$  in terms of the fusion rules (branching rules) as  $[N_i]_{jk} = N_{ij}^k = \delta_{ij\bar{k}}$  (see Sec. 2.2.1), we find the following properties. Commutativity and associativity of the fusion rules implies that the fusion matrices are all normal matrices that mutually commute with each other, so they can be simultaneously diagonalized. That is,  $N_i = P\Lambda^{(i)}P^\dagger$ , where  $\Lambda^{(i)}$  is the diagonal matrix of the eigenvalues of  $N_i$  and  $P$  is a unitary matrix whose columns are the orthonormal eigenvectors of the fusion matrices. The existence of a unique 0 string and unique dual strings implies that  $[P]_{ij} = [\Lambda^{(i)}]_{jj}[P]_{0j}$

and  $[\Lambda^{(i)}]_{jj} = [\Lambda^{(i)}]_{jj}^*$ . Since  $P$  is unitary,  $[P]_{0j} \neq 0$  and we have  $[\Lambda^{(i)}]_{jj} = \frac{[P]_{ij}}{[P]_{0j}}$ . This yields the generalized Verlinde equation

$$[N_i]_{jk} = \sum_l \frac{[P]_{il}[P]_{jl}[P]_{kl}^*}{[P]_{0l}}. \quad (2.42)$$

By multiplying the columns of  $P$  with appropriate phases, we can choose  $[P]_{0i}$  to be real. With this convention, we have  $[P]_{ij} = [P]_{ij}^*$ . Lastly, since  $\sum_k [N_i]_{jk} d_k = d_i d_j$ , the vector of quantum dimensions is an eigenvector for all  $N_i$ , which we choose to be the 0th column, so that  $[P]_{i0} = d_i / \mathcal{D}_C$ .

We now use the  $P$  matrix to define an operator for plaquette  $p$  that energetically favors a flux of type  $i \in \{0, 1, \dots, n-1\}$  through the plaquette, which is given by

$$\mathbf{B}_p^{(i)} = \sum_s a_s^{(i)} \mathbf{B}_p^s, \quad (2.43)$$

$$a_s^{(i)} = [P]_{0i} [P]_{si}^*. \quad (2.44)$$

We notice that these are orthogonal projectors, as

$$\begin{aligned} \mathbf{B}_p^{(i)} \mathbf{B}_p^{(j)} &= \sum_{s,t} a_s^{(i)} a_t^{(j)} \mathbf{B}_p^s \mathbf{B}_p^t \\ &= \sum_{s,t,u} a_s^{(i)} a_t^{(j)} [N_s]_{tu} \mathbf{B}_p^u \\ &= \sum_{s,t,u,v} [P]_{0i} [P]_{si}^* [P]_{0j} [P]_{tj}^* \frac{[P]_{sv} [P]_{tv} [P]_{uv}^*}{[P]_{0v}} \mathbf{B}_p^u \\ &= \sum_u \delta_{ij} [P]_{0i} [P]_{ui}^* \mathbf{B}_p^u \\ &= \delta_{ij} \mathbf{B}_p^{(i)}. \end{aligned} \quad (2.45)$$

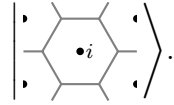
The eigenstates of  $\mathbf{B}_p^{(i)}$  are the states of definite flux passing through the plaquette  $p$ .

Specifically, the state with  $i$  flux in  $p$  has eigenvalue 1, whereas states with other fluxes have eigenvalue 0.

With these plaquette operators, the  $i$ -flux phase of the string-net model has the corresponding fixed point Hamiltonian

$$\mathbf{H}^{(i)} = - \sum_{\mathbf{v}} \mathbf{Q}_{\mathbf{v}} - \sum_{\mathbf{p}} \mathbf{B}_{\mathbf{p}}^{(i)}. \quad (2.46)$$

The ground states of the  $i$ -flux phase will have an  $i$ -flux through every plaquette, which we depict as a gray honeycomb lattice with a dot labeled  $i$  in the center of each plaquette:



If the emergent anyons form a doubled Chern-Simons theory, then the  $i$ -flux phase corresponds to having an  $(i, i)$  anyon in every plaquette, or equivalently, having an  $i$  string passing through every plaquette. This is because in this case, we can let  $P = \mathcal{S}_{\mathcal{C}}$  and  $a_s^{(i)} = [\mathcal{S}_{\mathcal{C}}]_{0i} [\mathcal{S}_{\mathcal{C}}]_{si}^*$ , where  $\mathcal{S}_{\mathcal{C}}$  is the  $\mathcal{S}$  matrix obtained when making the underlying UFC into an MTC. Using

$$\begin{array}{c} \uparrow j \\ \circlearrowleft \\ \downarrow i \end{array} = \frac{[\mathcal{S}_{\mathcal{C}}]_{ij}}{[\mathcal{S}_{\mathcal{C}}]_{0j}} \begin{array}{c} j \\ | \end{array}, \quad (2.47)$$

we see that applying  $\mathbf{B}_{\mathbf{p}}^{(i)}$  on a plaquette that has a flux  $j$  passing through it gives:

$$\begin{aligned} \mathbf{B}_{\mathbf{p}}^{(i)} \left| \begin{array}{c} \cdot \\ \cdot \\ \cdot \\ \cdot \\ \cdot \\ \cdot \end{array} \right\rangle &= \sum_s [\mathcal{S}_{\mathcal{C}}]_{0i} [\mathcal{S}_{\mathcal{C}}]_{si}^* \left| \begin{array}{c} \cdot \\ \cdot \\ \cdot \\ \cdot \\ \cdot \\ \cdot \end{array} \right\rangle \\ &= \sum_s \frac{[\mathcal{S}_{\mathcal{C}}]_{0i} [\mathcal{S}_{\mathcal{C}}]_{si}^* [\mathcal{S}_{\mathcal{C}}]_{sj}}{[\mathcal{S}_{\mathcal{C}}]_{0j}} \left| \begin{array}{c} \cdot \\ \cdot \\ \cdot \\ \cdot \\ \cdot \\ \cdot \end{array} \right\rangle \\ &= \delta_{ij} \left| \begin{array}{c} \cdot \\ \cdot \\ \cdot \\ \cdot \\ \cdot \\ \cdot \end{array} \right\rangle. \end{aligned} \quad (2.48)$$

If the emergent anyons describe a discrete gauge theory, then a flux phase should correspond to having some  $(\alpha, I)$  flux in every plaquette.

For both doubled Chern-Simons theories and discrete gauge theories, a flux phase is defined to be Abelian if the corresponding anyon occupying the plaquettes is Abelian, and non-Abelian otherwise. (In general, it is unclear whether a flux phase must correspond to having a particular anyon in every plaquette. So, we provide a more general definition of Abelian and non-Abelian flux phases in App. A.9.)

Let the order of a flux be the minimum number of corresponding anyons required to obtain a  $(I, I)$  anyon from their fusion. Flux phases where the order of the flux is incommensurate with the number of plaquettes in the lattice, e.g. the flux phases of the  $\mathbb{Z}_2$  model and the Ising model on a lattice with an odd number of plaquettes, are actually frustrated: it is impossible to have a certain flux through every plaquette. This leads to an extensive ground state degeneracy, essentially due to the location of the frustrated plaquette(s).

The string operators derived in the smooth phase can still be used in flux phases to produce excitations. However, string operators cannot necessarily be passed over plaquettes centers freely. For example,  $\mathbf{W}_{(\sigma, I)}$  is no longer fluctuating in the  $\sigma$  flux phase of the Ising model:

$$\left| \begin{array}{c} \text{---} \\ \text{---} \end{array} \right\rangle = e^{-\pi i/4} \left| \begin{array}{c} \text{---} \\ \text{---} \end{array} \right\rangle \neq \left| \begin{array}{c} \text{---} \\ \text{---} \end{array} \right\rangle, \quad (2.49)$$

where we have used Eq. (2.41). (String operators can still be passed over vertices.)

Even though the flux phases are defined by the specific  $\mathbf{B}_p^{(i)}$ , they characterize all possible  $\mathbf{B}_p$ . This is because any magnetic operator can be written as  $\mathbf{B}_p = \sum_s a_s \mathbf{B}_p^s$ , where  $a_s^* = a_s$  for Hermiticity, or equivalently,  $\mathbf{B}_p = \sum_i b_i \mathbf{B}_p^{(i)}$ , where  $b_i = b_i^* = \sum_s [P]_{0i}^{-1} [P]_{si} a_s$ . The ground state(s) of this  $\mathbf{B}_p$  has a  $j$  flux passing through every

plaquette, where  $j$  corresponds to the largest  $b_j$  in  $\sum_i b_i \mathbf{B}_p^{(i)}$ . So, the system is in the  $j$  flux phase. Thus, any  $\mathbf{B}_p$  belongs to some flux phase. The boundary between the  $j$  flux phase and  $k$  flux phase is realized when both  $b_j = b_k$  are both the largest coefficients, and in this case the system exhibits a level crossing between the ground state(s) of the  $j$  flux phase and the ground state(s) of the  $k$  flux phase.

## 2.4 Abelian Flux Phases

In this section, we study two examples of Abelian flux phases: the flux phase of the  $\mathbb{Z}_2$  model, and the  $\psi$  flux phase of the Ising model. (We also study the flux phase of the  $\mathbb{Z}_2^{(1/2)}$  model in App. A.7 and the flux phases of the  $\mathbb{Z}_n$  and  $\mathbb{Z}_n^{(1/2)}$  models in App. A.8.) We show that in general, Abelian flux phases can be understood as simple examples of translation symmetry fractionalization.

### 2.4.1 $\mathbb{Z}_2$ Flux Phase

The Hamiltonian is

$$\mathbf{H}_{\mathbb{Z}_2}^{(1)} = - \sum_{\mathbf{v}} \mathbf{Q}_{\mathbf{v}} - \sum_{\mathbf{p}} \frac{1}{2} (\mathbf{B}_{\mathbf{p}}^0 - \mathbf{B}_{\mathbf{p}}^1) \quad (2.50)$$

$$= - \sum_{\mathbf{v}} \frac{1}{2} \left( 1 + \prod_{i \in \mathbf{v} \text{ legs}} \sigma_i^z \right) - \sum_{\mathbf{p}} \frac{1}{2} \left( 1 - \prod_{i \in \mathbf{p} \text{ edges}} \sigma_i^x \right), \quad (2.51)$$

where we have again omitted the  $\prod_{\mathbf{v}} \mathbf{Q}_{\mathbf{v}}$  in the definition of  $\mathbf{B}_{\mathbf{p}}^{(1)}$ .

The ground state corresponds to having an  $\mathbf{m}$  anyon (i.e.  $\pi$  flux) in every plaquette.

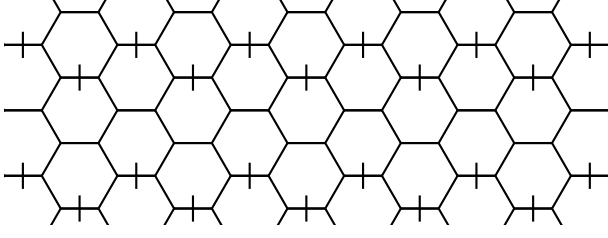


Figure 2.2: Change of Basis

It is given by

$$|0\rangle = \sum_{|X\rangle \in \substack{\text{closed loop} \\ \text{string-nets}}} (-1)^{n_{\text{P}}(|X\rangle)} |X\rangle, \quad (2.52)$$

where  $n_{\text{P}}(|X\rangle)$  is the number of plaquettes contained by closed loops in  $|X\rangle$ . Using Eq. A.30, the ground state degeneracy for a lattice with an even number of plaquettes  $N$  on a manifold of genus  $g$  is  $\mathcal{N}_{g, \{\mathbf{m}, \dots, \mathbf{m}\}} = 4^g$ , where  $\{\mathbf{m}, \dots, \mathbf{m}\}$  represents  $N$  number of  $\mathbf{m}$ . For a lattice with an odd number of plaquettes, the system is actually frustrated and the ground state degeneracy is  $4^g N$ .

The four string operators of the smooth phase can still be applied in the flux phase to create excitations, but the  $\mathbf{W}_e$  and  $\mathbf{W}_f$  string operators now acquire a factor of  $-1$  every time they are passed over a plaquette.

### Even Plaquette Solution

We can use a change of basis to solve  $\mathbf{H}_{\mathbb{Z}_2}^{(1)}$  for a lattice with an even number of plaquettes. To specify the change of basis we choose a dimer covering on the dual lattice. In other words, we mark links on the lattice in such a way that each hexagon has exactly one marked link, as shown in Fig. 2.2. We apply the change of basis

$$\Lambda = \Lambda^{-1} = \prod_{i \in \substack{\text{marked} \\ \text{links}}} \Lambda_i, \quad (2.53)$$

where

$$\Lambda_i = \sigma_i^z = \begin{bmatrix} 1 & 0 \\ 0 & -1 \end{bmatrix} \quad (2.54)$$

multiplies the amplitude of a lattice state by  $-1$  if the link  $i$  is occupied by a 1 string. Since every hexagon has exactly one marked link, and

$$\sigma_i^z \sigma_j^x \sigma_i^z = \begin{cases} \sigma_j^x, & i \neq j \\ -\sigma_j^x, & i = j \end{cases}, \quad (2.55)$$

the change of basis transforms the flux Hamiltonian into the smooth Hamiltonian:

$$\Lambda^{-1} H_{\mathbb{Z}_2}^{(1)} \Lambda = H_{\mathbb{Z}_2}^{(0)}. \quad (2.56)$$

Thus, we can understand the flux phase by applying the change of basis to the smooth phase results.

The ground state in the flux phase is:

$$|0\rangle = \sum_{|X\rangle \in \substack{\text{closed loop} \\ \text{string-nets}}} (-1)^{n_M(|X\rangle)} |X\rangle, \quad (2.57)$$

where  $n_M(|X\rangle) = n_P(|X\rangle)$  is the number of marked links occupied by 1 strings in  $|X\rangle$ . This agrees with Eq. (2.52).

The four modified string operators of the flux phase, which pass through plaquettes freely, are  $\mathbf{W}_I$ ,  $(-1)^{n_M(P)} \mathbf{W}_e$ ,  $\mathbf{W}_m$ ,  $(-1)^{n_M(P)} \mathbf{W}_f$ , where  $n_M(P)$  is the number of marked links along the path  $P$ .

### 2.4.2 Ising $\psi$ Flux Phase

The Hamiltonian is:

$$\mathbf{H}_{\text{Ising}}^{(\psi)} = - \sum_{\mathbf{v}} \mathbf{Q}_{\mathbf{v}} - \sum_{\mathbf{p}} \frac{1}{4} \left( \mathbf{B}_{\mathbf{p}}^I - \sqrt{2} \mathbf{B}_{\mathbf{p}}^{\sigma} + \mathbf{B}_{\mathbf{p}}^{\psi} \right). \quad (2.58)$$

Since the Ising UFTC can be made into a MTC, the ground state corresponds to having a  $(\psi, \psi)$  anyon in every plaquette, or equivalently, having a  $\psi$  string passing through every plaquette. Unlike with the flux phase of the  $\mathbb{Z}_2$  model, there is no explicit formula for the ground state, though it can be constructed using the local relations of Sec. 2.2.1 as long we respect the presence of the  $\psi$  flux: the relations can be applied in a region without any flux, and passing a  $\sigma$  string through a  $\psi$  flux introduces a factor of  $-1$ . Using Eq. A.30, the ground state degeneracy for a lattice with  $N$  plaquettes on a manifold of genus  $g$  is  $\mathcal{N}_{g, \{(\psi, \psi), \dots, (\psi, \psi)\}} = 4^{g-1} (1 + (-1)^N 2^{g+1} + 4^g)$ , where  $\{(\psi, \psi), \dots, (\psi, \psi)\}$  represents  $N$  number of  $(\psi, \psi)$ .

The nine string operators of the smooth phase can still be applied in the flux phase to create excitations. However,  $\mathbf{W}_{(I, \sigma)}$ ,  $\mathbf{W}_{(\sigma, I)}$ ,  $\mathbf{W}_{(\sigma, \psi)}$ , and  $\mathbf{W}_{(\psi, \sigma)}$  acquire a factor of  $-1$  every time they are passed over a plaquette center.

#### Even Plaquette Solution

As with the flux phase of the  $\mathbb{Z}_2$  model, we can use a change of basis to solve  $\mathbf{H}_{\text{Ising}}^{(\psi)}$  for a lattice with an even number of plaquettes. We mark links on the lattice in such a way that each hexagon has exactly one marked link, as shown in Fig. 2.2, and apply the change of basis  $\mathbf{\Lambda}$ :

$$\mathbf{\Lambda} = \mathbf{\Lambda}^{-1} = \prod_{i \in \text{marked links}} \mathbf{\Lambda}_i, \quad (2.59)$$

where

$$\Lambda_i = \text{diag}(1, -1, 1) \quad (2.60)$$

multiplies the amplitude of a lattice state by  $-1$  if its link  $i$  is occupied by a  $\sigma$  string. We show in App. A.10 that this change of basis transforms the flux Hamiltonian into the smooth Hamiltonian:

$$\Lambda^{-1} \mathbf{H}_{\text{Ising}}^{(\psi)} \Lambda = \mathbf{H}_{\text{Ising}}^{(I)}. \quad (2.61)$$

Thus, we can understand the flux phase by applying the change of basis to the smooth phase results.

For example, suppose the ground state of the smooth phase is

$$|0\rangle = \sum_{|X\rangle} \Phi(|X\rangle) |X\rangle, \quad (2.62)$$

Then, the ground state in the  $\psi$  flux phase is

$$|0\rangle = \sum_{|X\rangle} (-1)^{n_M(|X\rangle)} \Phi(|X\rangle) |X\rangle. \quad (2.63)$$

where  $n_M(|X\rangle)$  is the number of marked links occupied by  $\sigma$  strings in  $|X\rangle$ . Similarly, the modified string operators of the  $\psi$  flux phase, which pass through plaquettes freely, are  $(-1)^{n_M(P)} \mathbf{W}_{(I,\sigma)}$ ,  $(-1)^{n_M(P)} \mathbf{W}_{(\sigma,I)}$ ,  $(-1)^{n_M(P)} \mathbf{W}_{(\sigma,\psi)}$ , and  $(-1)^{n_M(P)} \mathbf{W}_{(\psi,\sigma)}$ , where  $n_M(P)$  is the number of marked links along the path  $P$ . (The other string operators do not need to be modified.)

### 2.4.3 Symmetry Fractionalization

Topological phases with symmetry lead to symmetry-enriched topological phases, which cannot be adiabatically connected by a path of gapped Hamiltonians without

breaking the symmetry.[29, 30] In these phases, the symmetry is fractionalized: the anyons carry fractional quantum numbers corresponding to the symmetry. For example, in the fractional quantum Hall effect, the U(1) symmetry is fractionalized and the anyons carry fractional charge.[20]

For string-net model, abelian flux phases are SET phases whose translational symmetry has been fractionalized, as we will show below. This is in accordance with other work that has understood translational symmetry fractionalization as having a background anyonic flux.[29, 30, 31] In general, only a subset of SET phases with translational symmetry fractionalization can be obtained as flux phases (via modified plaquette operators). We expect that the remaining fractionalization classes can be obtained by additionally modifying the vertex terms.

Consider a system in a topological phase with a symmetry described by the group  $G$ , whose element  $\mathbf{g}$  acts on the Hilbert space as the unitary on-site operators  $\mathbf{R}_{\mathbf{g}}$ . Let  $|\Psi_{\{\mathbf{a}_1, \dots, \mathbf{a}_n\}}\rangle$  be a state with anyons  $\mathbf{a}_1, \dots, \mathbf{a}_n$ . Assuming the action of the symmetry does not permute the anyons, it can be decomposed into unitary operators acting locally on the anyons:

$$\mathbf{R}_{\mathbf{g}}|\Psi_{\{\mathbf{a}_1, \dots, \mathbf{a}_n\}}\rangle = \prod_{i=1}^n \mathbf{U}_{\mathbf{g}}^{(i)}|\Psi_{\{\mathbf{a}_1, \dots, \mathbf{a}_n\}}\rangle. \quad (2.64)$$

The local operators form a projective representation of  $G$ ,

$$\mathbf{U}_{\mathbf{g}}^{(i)}\mathbf{U}_{\mathbf{h}}^{(i)}|\Psi_{\{\mathbf{a}_1, \dots, \mathbf{a}_n\}}\rangle = \eta_{\mathbf{a}_i}(\mathbf{g}, \mathbf{h})\mathbf{U}_{\mathbf{gh}}^{(i)}|\Psi_{\{\mathbf{a}_1, \dots, \mathbf{a}_n\}}\rangle, \quad (2.65)$$

where  $\eta_{\mathbf{a}}(\mathbf{g}, \mathbf{h}) \in \text{U}(1)$ .

The phases  $\eta_{\mathbf{a}}(\mathbf{g}, \mathbf{h})$  must satisfy certain constraints, due to the associativity of  $\mathbf{U}_{\mathbf{g}}^{(i)}$  and the fact that  $\mathbf{R}_{\mathbf{g}}\mathbf{R}_{\mathbf{h}} = \mathbf{R}_{\mathbf{gh}}$ . Additionally,  $\eta_{\mathbf{a}}(\mathbf{g}, \mathbf{h})$  have some redundancy, because  $\mathbf{U}_{\mathbf{g}}^{(i)}$  can be “trivially” redefined by a phase. It turns out that the solutions for  $\eta_{\mathbf{a}}(\mathbf{g}, \mathbf{h})$ ,

modulo the aforementioned redundancy, are classified by the second cohomology group  $H^2(G, \mathcal{A})$ , where  $\mathcal{A}$  is the group of Abelian anyons under fusion. In our case, since the translation symmetry group of a lattice is  $\mathbb{Z} \times \mathbb{Z}$  and  $H^2(\mathbb{Z} \times \mathbb{Z}, \mathcal{A}) = \mathcal{A}$ . Therefore, each translational symmetry fractionalization class is specified by an Abelian anyon, which can be thought of as a background anyonic flux.

The Abelian flux phases are simple examples of translation symmetry fractionalization. For example, the flux phase of the  $\mathbb{Z}_2$  model corresponds to the fractionalization class specified by the anyon  $\mathbf{m}$ , i.e. every plaquette has an  $\mathbf{m}$ , and the  $\psi$  flux phase of the Ising model is specified by  $(\psi, \psi)$ , i.e. every plaquette has a  $(\psi, \psi)$ ,

More generally, the  $\mathbb{Z}_n$  model has  $n^2$  Abelian anyons  $\mathbf{a} = (a_1, a_2)$ , where  $a_1, a_2 \in \{0, \dots, n-1\}$ , that obey  $\mathbb{Z}_n \times \mathbb{Z}_n$  fusion rules. The  $j$  flux phase corresponds to having a  $(0, j)$  boson in every plaquette. In this phase,

$$\mathbf{U}_x^{(\mathbf{a})} \mathbf{U}_y^{(\mathbf{a})} = e^{2\pi i a_1 j/n} \mathbf{U}_y^{(\mathbf{a})} \mathbf{U}_x^{(\mathbf{a})}. \quad (2.66)$$

In other words, when an anyon  $(a_1, a_2)$  is transported around a plaquette, the wavefunction acquires a phase  $e^{2\pi i a_1 j/n}$ , which is exactly the phase acquired upon braiding  $(a_1, a_2)$  around  $(0, j)$ .

Similarly, the  $\mathbb{Z}_n^{(1/2)}$  model has  $n^2$  Abelian anyons  $\mathbf{a} = (a_A, a_B)$ , where  $a_A, a_B \in \{0, \dots, n-1\}$ , that obey  $\mathbb{Z}_n \times \mathbb{Z}_n$  fusion rules. In this case, the  $j$  flux phase corresponds to having a  $(j, j)$  boson in every plaquette. In this phase,

$$\mathbf{U}_x^{(\mathbf{a})} \mathbf{U}_y^{(\mathbf{a})} = e^{2\pi i (a_A - a_B) j/n} \mathbf{U}_y^{(\mathbf{a})} \mathbf{U}_x^{(\mathbf{a})}. \quad (2.67)$$

In other words, when an anyon  $(a_A, a_B)$  is transported around a plaquette, the wavefunction acquires a phase  $e^{2\pi i (a_A - a_B) j/n}$ , which is exactly the phase acquired upon braiding

$(a_A, a_B)$  around  $(j, j)$ .

Flux phases in which the background anyonic flux corresponds to an Abelian topological charge can be interpreted as a translationally invariant topological phase in which the translational symmetry is fractionalized.[29, 30, 31] In particular, the background anyonic flux per unit cell corresponds to the Abelian topological charge, denoted  $\mathbf{b}(T_{\hat{e}_2}, T_{\hat{e}_1})$ , specifies the symmetry fractionalization class through the invariant relation

$$\mathbf{b}(T_{\hat{e}_2}, T_{\hat{e}_1}) = \mathbf{w}(T_{\hat{e}_2}, T_{\hat{e}_1}) \times \overline{\mathbf{w}(T_{\hat{e}_1}, T_{\hat{e}_2})}, \quad (2.68)$$

where  $T_{\hat{e}_j}$  is the translational symmetry group generator for translation in the  $\hat{e}_j$  direction. These are classified by  $H^2(\mathbb{Z}^2, \mathcal{A})$ , where  $\mathcal{A}$  is the group defined by the Abelian anyons (of the emergent topological order), with group multiplication specified by the fusion rules.

## 2.5 Non-Abelian Flux Phases

In this section, we study the non-Abelian  $\sigma$  flux phase of the Ising model. We find that the model has an extensive ground state degeneracy, and exhibits topologically protected non-Abelian braiding. Furthermore, we find that this extensive degeneracy is gapped out by generic local perturbations, and that the resulting perturbed phase is the toric code phase. Finally, we discuss some general properties of non-Abelian flux phases.

### 2.5.1 Ising $\sigma$ Flux Phase

The Hamiltonian is

$$H_{\text{Ising}}^{(\sigma)} = - \sum_{\mathbf{v}} Q_{\mathbf{v}} - \sum_{\mathbf{p}} \frac{1}{2} (B_{\mathbf{p}}^I - B_{\mathbf{p}}^\psi). \quad (2.69)$$

Since the Ising UFTC can be made into a MTC, the ground state corresponds to having a  $(\sigma, \sigma)$  anyon in every plaquette, or equivalently, having a  $\sigma$  string passing through every plaquette. Unlike with the flux phase of the  $\mathbb{Z}_2$  model and the  $\psi$  flux phase of the Ising model, we cannot use local relations at all to find the ground state. This is because passing a  $\sigma$  string through a  $\sigma$  flux leaves  $\psi$  string tails that cannot be removed. Using Eq. A.30, the ground state degeneracy for a lattice with an even number of plaquettes  $N$  on a manifold of genus  $g$  is  $\mathcal{N}_{g, \{(\sigma, \sigma), \dots, (\sigma, \sigma)\}} = 2^{N-2} 16^g$ , where  $\{(\sigma, \sigma), \dots, (\sigma, \sigma)\}$  represents  $N$  number of  $(\sigma, \sigma)$ . For a lattice with an odd number of plaquettes, the system is actually frustrated and the ground state degeneracy is  $2^{N-2} 16^g N$ .

Of the nine string operators of the smooth phase, only  $\mathbf{W}_{(I,I)}$  and  $\mathbf{W}_{(\psi,\psi)}$  are still fluctuating, (and actually do not create excitations.)  $\mathbf{W}_{(I,\psi)}$  and  $\mathbf{W}_{(\psi,I)}$  acquire a factor of  $-1$  every time they are passed over a plaquette, and  $\mathbf{W}_{(I,\sigma)}$ ,  $\mathbf{W}_{(\sigma,I)}$ ,  $\mathbf{W}_{(\sigma,\sigma)}$ ,  $\mathbf{W}_{(\sigma,\psi)}$ , and  $\mathbf{W}_{(\psi,\sigma)}$  cannot be passed over plaquettes at all.

### Even Plaquette Solution

For a lattice with an even number of plaquettes, we can use the results of the flux phase of  $\mathbb{Z}_2$  model to obtain a ground state. Consider momentarily limiting the Hilbert space basis to the set of string-nets with only  $I$  and  $\psi$  strings. If we represent the strings as spin- $\frac{1}{2}$  particles, where the  $I$  string is  $|+z\rangle$  and the  $\psi$  string is  $|-z\rangle$ , then the  $\mathbf{H}_{\text{Ising}}^{(\sigma)}$  acting on this subspace can be written in terms of Pauli matrices:

$$\begin{aligned} \mathbf{H}_{\text{Ising}\setminus\sigma}^{(\sigma)} = & - \sum_{\mathbf{v}} \frac{1}{2} \left( 1 + \prod_{\mathbf{i} \in \mathbf{v} \text{ legs}} \sigma_{\mathbf{i}}^z \right) \\ & - \sum_{\mathbf{p}} \frac{1}{2} \left( 1 - \prod_{\mathbf{i} \in \mathbf{p} \text{ edges}} \sigma_{\mathbf{i}}^x \right), \end{aligned} \quad (2.70)$$

which is identical to  $\mathbf{H}_{\mathbb{Z}_2}^{(1)}$  of Eq. (2.51). Therefore, its ground state is

$$|0\rangle = \sum_{|X\rangle \in \text{closed } \psi \text{ loop string-nets}} (-1)^{n_M(|X\rangle)} |X\rangle, \quad (2.71)$$

where  $n_M(|X\rangle)$  is the number of  $\psi$  strings that occupy marked links in the string-net  $|X\rangle$ .

This ground state does not contain any links occupied by  $\sigma$  strings. In order to introduce  $\sigma$  strings, we may attempt to act on this ground state with a closed  $\mathbf{W}_{(\sigma,I)}$  that encloses a single plaquette. Although this closed string operator cannot create excitations, it annihilates the ground state:

$$\left| \left\langle \left[ \text{hexagon with } \sigma \text{ string} \right] \right\rangle \right| = 0. \quad (2.72)$$

However, consider two closed  $\mathbf{W}_{(\sigma,I)}$  enclosing adjacent plaquettes  $p_1$  and  $p_2$  connected by  $\mathbf{W}_{(\psi,I)}$ , which we call a *minimal spectacle operator*  $\mathbf{S}_{p_1 p_2}$ :

$$\mathbf{S}_{p_1 p_2} \left[ \text{two adjacent hexagons } p_1, p_2 \text{ with } \psi \text{ string} \right] \equiv \frac{1}{2} \left[ \text{two adjacent hexagons } p_1, p_2 \text{ with } \sigma \text{ strings} \right] \quad (2.73)$$

Acting  $\mathbf{S}_{p_1 p_2}$  on this ground state does result in a new ground state, which is also a sum of closed  $\psi$  loop string-nets but with the links enclosing  $p_1$  and  $p_2$  occupied by  $\sigma$  strings. By applying minimal spectacle operators on top of or next to each other, we can create larger spectacle operators:

$$\left[ \text{three hexagons with } \psi \text{ string} \right] \propto \left[ \text{three hexagons with } \sigma \text{ strings} \right] \quad (2.74)$$

(2.75)

Therefore, we can create a wide variety of spectacle operators, which, when acted on the ground state given by Eq. (2.71), result in a new ground states. Spectacle operators are Hermitian, unitary, mutually commuting, and commute with the Hamiltonian. These properties are proven in App. A.11. Note that the path of  $\mathbf{W}_{(\psi,I)}$  in the spectacle operators is unimportant, since it can be passed over plaquettes with a factor of  $-1$ . Therefore, only  $p_1$  and  $p_2$  are needed to specify  $\mathbf{S}_{p_1 p_2}$ . We will often specify the plaquettes of  $\mathbf{S}_{p_1 p_2}$  using diagrams and leave the subscripts  $p_1$  and  $p_2$  implicit.

Thus, we have an extensive ground state degeneracy due to the spectacle operators. To count this degeneracy, we note that all spectacle operators can be constructed out of minimal spectacle operators. All that matters is which plaquettes contain the  $\mathbf{W}_{(\sigma,I)}$  loops; the  $\mathbf{W}_{(\psi,I)}$  string operators connecting them are fluctuating (up to an unimportant factor of  $-1$ ). Because each of the  $N$  plaquettes may or may not contain a  $\mathbf{W}_{(\sigma,I)}$  loop, but the total number of  $\mathbf{W}_{(\sigma,I)}$  loops must be even, there are  $2^{N-1}$  possible ways of acting spectacle operators. However, this double counts the number of unique spectacle operators. This is because when acting on a ground state, a configuration of minimal spectacle operators acting on plaquettes  $\{p_i\}$  is equivalent to the configuration of minimal spectacle operators acting on every plaquette but  $\{p_i\}$ . For example,

(2.76)

Thus, the correct extensive degeneracy is  $2^{N-2}$ . This extensive degeneracy essentially

originates from the degeneracy of the fusion tree formed by fusing the  $\sigma$  fluxes above and below the lattice, as explained in App. A.6.3 and App. A.10.

The rest of the degeneracy can be determined by considering closed string operators that wrap around the nontrivial cycles of the manifold. For example, consider a lattice with an even number of plaquettes on a torus. The ground state degeneracy is  $16 \times 2^{N-2}$ . We can count this degeneracy as 16 base ground states, each with a  $2^{N-2}$  degeneracy spanned by spectacle operators. We label these states as  $|I, I; \alpha\rangle$ ,  $|I, \sigma; \alpha\rangle$ ,  $|I, \sigma'; \alpha\rangle$ ,  $|I, \psi; \alpha\rangle$ ,  $|\sigma, I; \alpha\rangle$ ,  $|\sigma', I; \alpha\rangle$ ,  $|\sigma, \sigma; \alpha\rangle$ ,  $|\sigma, \sigma'; \alpha\rangle$ ,  $|\sigma', \sigma; \alpha\rangle$ ,  $|\sigma', \sigma'; \alpha\rangle$ ,  $|\sigma, \psi; \alpha\rangle$ ,  $|\sigma', \psi; \alpha\rangle$ ,  $|\psi, I; \alpha\rangle$ ,  $|\psi, \sigma; \alpha\rangle$ ,  $|\psi, \sigma'; \alpha\rangle$ , and  $|\psi, \psi; \alpha\rangle$ , where  $\alpha \in \{1, \dots, 2^{N-2}\}$ . Here,  $|I, I; 1\rangle$  is the ground state given by Eq. (2.71),  $|I, I; \alpha\rangle$  is  $|I, I; 1\rangle$  acted on by a configuration  $\alpha$  of spectacle operators, and  $|i, j; \alpha\rangle$  is  $|I, I; \alpha\rangle$  with a  $\mathbf{W}_{(i,I)}$  wrapping around one of the nontrivial cycles and a  $\mathbf{W}_{(j,I)}$  wrapping around the other.

$$|i, j; 1\rangle : \quad \begin{array}{c} \text{Diagram of a torus with two loops: a vertical loop labeled } (i, I) \text{ and a horizontal loop labeled } (j, I). \end{array} \quad (2.77)$$

The  $\sigma'$  string is a  $\mathbf{W}_{(\sigma, I)}$  string with half of a spectacle operator attached.

$$|\sigma', I; 1\rangle : \quad \begin{array}{c} \text{Diagram of a torus with a vertical loop labeled } (\sigma, I) \text{ and a horizontal loop labeled } (j, I). \end{array} \quad (2.78)$$

### Projective Non-Abelian Braiding

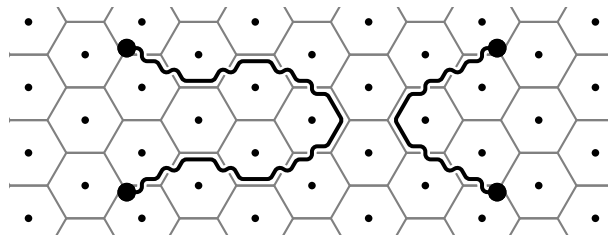
A topological phase is usually defined (in the thermodynamic limit) to have a robust ground state degeneracy that depends only on the topology of the manifold the system is supported by and a finite energy gap for excitations. These properties are ostensi-

bly crucial to the topological protection of the ground states and of the braiding of quasiparticle excitations. However, the requirement of a finite excitation gap can actually be relaxed: quasi-topological phases can be gapless and yet exhibit topological protection.[32] Indeed, almost all experimentally realized topological phases are actually gapless. The Hall bar in the fractional quantum hall effect, for example, contains gapless phonons and photons.

The Ising  $\sigma$  flux phase may be roughly thought of as gapless, because of its extensive ground state degeneracy. Strictly speaking, it is not a gapless phase, because as we show in the later sections, this extensive ground state degeneracy can be gapped out by local perturbations. Nevertheless, we can ask whether topological protection exists against perturbations that do not lift this extensive ground state degeneracy. We show that the non-Abelian braiding of  $\sigma$  anyons is in fact topologically protected.

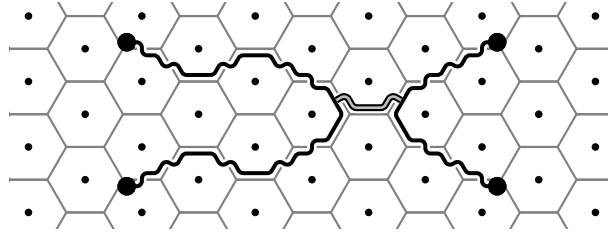
Consider the case when a lattice with an even number of plaquettes is supported by a sphere, and only perturbations that commute with spectacle operators are allowed. The ground state degeneracy is  $2^{N-2}$ , spanned by spectacle operators. We label these orthogonal states as  $|\alpha\rangle$ , where  $\alpha \in \{1, \dots, 2^{N-2}\}$  represents a configuration of spectacle operators.

Let  $\mathbf{O}^{(I)}$  be composed of two non-intersecting open  $\mathbf{W}_{(\sigma,I)}$ , as shown below.



When acting on the ground state subspace this operator creates the subspace  $\mathcal{H}^{(I)}$  spanned by  $|\alpha^{(0)}\rangle = \mathbf{O}^{(I)}|\alpha\rangle$ . Let  $\mathbf{O}^{(\psi)}$  be  $\mathbf{O}^{(I)}$  with a  $\mathbf{W}_{(\psi,I)}$  connecting the two  $\mathbf{W}_{(\sigma,I)}$ ,

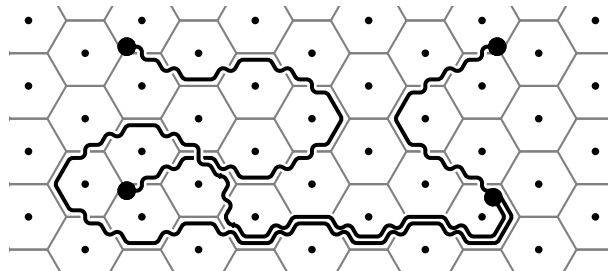
as shown below.



When acting on the ground state Hilbert space this operator creates the Hilbert space  $\mathcal{H}^{(\psi)}$ , spanned by  $|\alpha^{(\psi)}\rangle = \mathbf{O}^{(\psi)}|\alpha\rangle$ . (Note that the exact form of the strings composing the  $\mathbf{O}^{(I)}$  and  $\mathbf{O}^{(\psi)}$  is unimportant as long as the four endpoints of  $\mathbf{W}_{(\sigma,I)}$  are sufficiently separated. The placement of  $\mathbf{W}_{(\psi,I)}$  is unimportant as it can be moved around, acquiring a factor of  $-1$  as it passes over a plaquette center.)

States in both Hilbert spaces  $\mathcal{H}^{(I)}$  and  $\mathcal{H}^{(\psi)}$  have the same energy and, furthermore, we prove in App. A.12 that the spaces are topologically protected against any local operator if the simply connected cover of the support of that operator does not contain endpoints from both the  $\mathbf{W}_{(\sigma,I)}$ .

Let us restrict ourselves to  $\mathcal{H}^{(I)} \oplus \mathcal{H}^{(\psi)}$ , spanned by  $2 \times 2^{N-2}$  degenerate energy eigenstates  $|\Sigma\rangle$ , where  $|\Sigma\rangle$  is  $|\alpha^{(I)}\rangle$  or  $|\alpha^{(\psi)}\rangle$  for some  $\alpha$ . We wish to adiabatically evolve the  $\mathbf{H}_{IS}^{(\sigma)}(t)$  from  $t = 0$  to  $t = T$  so that we end up braiding an endpoint of one of the  $\mathbf{W}_{(\sigma,I)}$  around an endpoint of the other  $\mathbf{W}_{(\sigma,I)}$ .



We require that the path of the braid encloses an even number of plaquettes and is sufficiently distant from the two nonparticipating  $(\sigma, I)$  endpoints

Let us assume we have energy eigenstates  $|\Sigma(t)\rangle$  at time  $t$ , i.e.  $\mathbf{H}_{\text{Ising}}^{(\sigma)}(t)|\Sigma(t)\rangle = E(t)|\Sigma(t)\rangle$ . Since the evolution is cyclic, i.e.  $\mathbf{H}_{\text{Ising}}^{(\sigma)}(0) = \mathbf{H}_{\text{Ising}}^{(\sigma)}(T)$ , we have

$$|\Sigma(T)\rangle = \sum_{\Theta} [\mathbf{B}]_{\Sigma\Theta} |\Theta(0)\rangle, \quad (2.79)$$

where  $[\mathbf{B}]_{\Sigma\Theta} = \langle \Theta(0) | \Sigma(T) \rangle$  is the holonomy matrix. If we start with an eigenstate  $|\psi_{\Sigma}(0)\rangle = |\Sigma(0)\rangle$ , then the final state is given by:

$$|\psi_{\Sigma}(T)\rangle = e^{-\frac{i}{\hbar} \int_0^T E(t) dt} \mathbf{U} \mathbf{B} |\Sigma(0)\rangle, \quad (2.80)$$

where

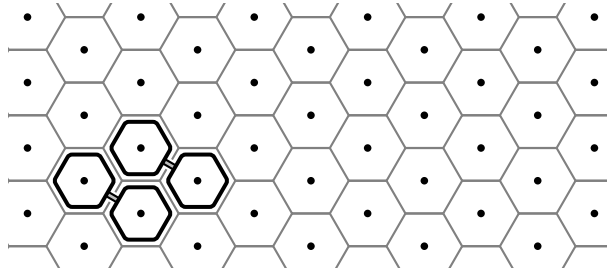
$$\mathbf{U} = \mathcal{P} \exp \left( i \int_0^T \mathbf{A}(t) dt \right) \quad (2.81)$$

is the Berry matrix, and

$$[\mathbf{A}(t)]_{\Sigma\Theta} = i \langle \Sigma(t) | \frac{d}{dt} | \Theta(t) \rangle \quad (2.82)$$

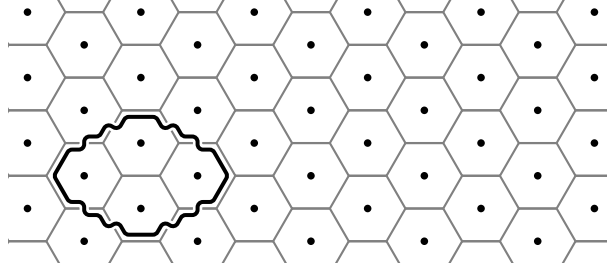
is the Berry connection.

To understand  $\mathbf{B}$ , consider the starting with a ground state  $|\alpha^{(I)}\rangle$ . For every such  $\alpha$ , there is a unique  $\beta$  such that  $|\beta^{(I)}\rangle = \mathbf{S}|\alpha^{(I)}\rangle$ , where the operator  $\mathbf{S}$  is the product of minimal spectacle operators enclosing the braided region, as shown below.

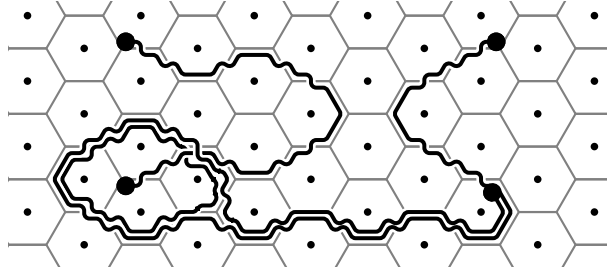


Such a spectacle operator must exist because the braiding encloses an even number of

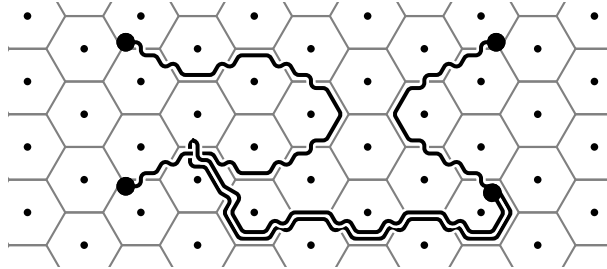
plaquettes. This operator is equivalent to a single  $\mathbf{W}_{(\sigma,I)}$  loop enclosing the braided region.



Therefore, replacing  $|\alpha^{(I)}\rangle$  with  $\mathcal{S}|\beta^{(I)}\rangle$  yields the following diagram.

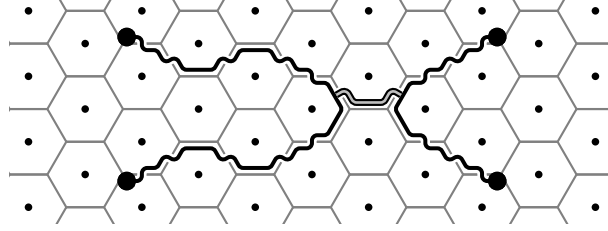


Fusing the  $\mathbf{W}_{(\sigma,I)}$  simplifies the diagram.



Here, we have removed the  $\mathbf{W}_{(\psi,I)}$  that results from the fusion by freely creating a  $\mathbf{W}_{(\psi,I)}$  enclosing the braided region from the ground state  $|\beta\rangle$  and fusing the two  $\mathbf{W}_{(\psi,I)}$ . Using Eq. (2.41) and the fact that  $\mathbf{W}_{(\psi,I)}$  can be passed over plaquette centers with a factor of

–1, this can be reduced to a state proportional to  $|\beta^{(2)}\rangle$ .



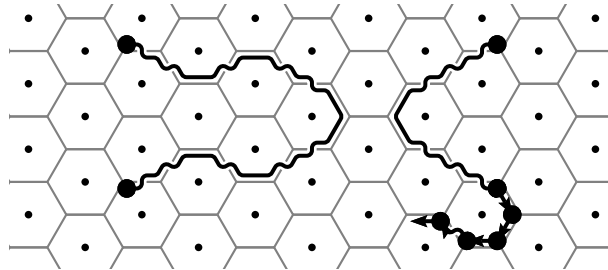
Thus,  $\mathbf{B}$  takes states in  $\mathcal{H}^{(I)}$  to states in  $\mathcal{H}^{(\psi)}$  and vice versa:

$$\mathbf{B} = \begin{bmatrix} \mathbf{0} & \mathbf{b}^{(\psi) \rightarrow (I)} \\ \mathbf{b}^{(I) \rightarrow (\psi)} & \mathbf{0} \end{bmatrix}. \quad (2.83)$$

Furthermore,  $\mathbf{b}^{(\psi) \rightarrow (I)} = \mathbf{b}^{(I) \rightarrow (\psi)}$  because the  $\mathbf{W}_{(\psi, I)}$  of  $\mathbf{O}^{(\psi)}$  can be moved arbitrarily far away so that the braiding process cannot be affected by it. This can always be done provided the path of the braid is sufficiently distant from the two nonparticipating  $\mathbf{W}_{(\sigma, I)}$  endpoints. Thus, we conclude that  $\mathbf{B}$  is block off-diagonal, and both the blocks are identical:

$$\mathbf{B} = \begin{bmatrix} \mathbf{0} & \mathbf{b} \\ \mathbf{b} & \mathbf{0} \end{bmatrix}. \quad (2.84)$$

To understand  $\mathbf{U}$ , we can view the adiabatic evolution as a series of small local hoppings of the endpoint being braided.



Each of these hoppings is facilitated by local operators and therefore forbidden from taking a state in  $\mathcal{H}^{(I)}$  to a state in  $\mathcal{H}^{(\psi)}$  due to topological protection proved in App. A.12. Therefore,  $\mathbf{A}$  takes states in  $\mathcal{H}^{(I)}$  to states in  $\mathcal{H}^{(I)}$  and states in  $\mathcal{H}^{(\psi)}$  to states in  $\mathcal{H}^{(\psi)}$ :

$$\mathbf{A} = \begin{bmatrix} \mathbf{a}^{(I) \rightarrow (I)} & \mathbf{0} \\ \mathbf{0} & \mathbf{a}^{(\psi) \rightarrow (\psi)} \end{bmatrix}. \quad (2.85)$$

Furthermore,  $\mathbf{a}^{(I) \rightarrow (I)} = \mathbf{a}^{(\psi) \rightarrow (\psi)}$ , because the  $\mathbf{W}_{(\psi, I)}$  of  $\mathbf{O}^{(\psi)}$  can be moved arbitrarily far away so that the braiding process cannot be affected by it. Thus, we conclude that  $\mathbf{U}$  is block diagonal, and both the blocks are identical.

$$\mathbf{U} = \begin{bmatrix} \mathbf{u} & \mathbf{0} \\ \mathbf{0} & \mathbf{u} \end{bmatrix}. \quad (2.86)$$

Since  $\mathbf{B}$  is block off-diagonal and  $\mathbf{U}$  is block diagonal, the adiabatic braiding process maps states in  $\mathcal{H}^{(I)}$  to states in  $\mathcal{H}^{(\psi)}$  and vice versa. This is similar to the non-Abelian braiding of  $(\sigma, I)$  anyons that would occur in the smooth topological phase, as shown in Eq. (2.41).

Thus, the Ising  $\sigma$  flux phase exhibits topologically protected non-Abelian braiding even in the presence of an extensive ground state degeneracy. In the next sections, we show that this extensive degeneracy can be gapped out by local perturbations, and the resulting system is actually in the toric code phase. In this phase, the above braiding of  $\sigma$  anyons can be viewed as braiding of confined defects. [30]

### Condensation into Toric Code

Recall from Sec. 2.5.1 that the ground state degeneracy of the Ising  $\sigma$  flux phase on a lattice with an even number of plaquettes supported by a torus is  $16 \times 2^{N-2}$ ,

spanned by  $2^{N-2}$  spectacle operators and 16 different configurations of string operators acting around nontrivial cycles of the torus. If we perturb the system with the local operator  $\sum_i \mathbf{V}_i$ , where  $\mathbf{V}_i$  penalizes a  $\sigma$  string occupying link  $i$ , then the states acted on by spectacle operators become gapped and  $\mathbf{W}_{(I,\sigma)}$ ,  $\mathbf{W}_{(\sigma,I)}$ ,  $\mathbf{W}_{(\sigma,\psi)}$ , and  $\mathbf{W}_{(\psi,\sigma)}$  become confined. As a result, only four of  $16 \times 2^{N-2}$  original ground states remain ground states after the perturbation:  $|I, I; 1\rangle$ ,  $|I, \psi; 1\rangle$ ,  $|\psi, I; 1\rangle$ , and  $|\psi, \psi; 1\rangle$ . These four states are equal superpositions of closed  $\psi$  string loops on a torus, i.e. the toric code ground states.

The appearance of the toric code phase here is to be expected: as previously remarked in Sec. 2.5.1, the Hamiltonian  $\mathbf{H}_{\text{Ising}\setminus\sigma}^{(\sigma)}$  of the Ising  $\sigma$  flux phase in the absence of  $\sigma$  strings is equivalent to the toric code Hamiltonian  $\mathbf{H}_{\mathbb{Z}_2}^{(0)}$ . Interestingly, however, the transition into the toric code phase can also be understood as the condensation of the  $(\psi, \psi)$  boson.[33] The  $(\psi, \psi)$  boson is allowed to condense because an open  $\mathbf{W}_{(\psi,\psi)}$  does not create excitations at its endpoints in the  $\sigma$  flux phase. The reason it condenses is because the local operator  $\mathbf{V}_i$  can be essentially thought of as creating (or annihilating)  $(\psi, \psi)$  bosons in the two adjacent plaquettes that share the  $i$  link as an edge. Thus, the perturbation  $\sum_i \mathbf{V}_i$  allows for spontaneous pair creation and annihilation of  $(\psi, \psi)$  bosons, encouraging the formation of its bose condensate.

In the condensed phase, the new anyon spectrum is given by:

$$\tilde{\mathbf{I}} = (I, I) + (\psi, \psi) \quad (2.87)$$

$$\tilde{\mathbf{e}} = (\sigma, \sigma)_1 \quad (2.88)$$

$$\tilde{\mathbf{m}} = (\sigma, \sigma)_2 \quad (2.89)$$

$$\tilde{\mathbf{f}} = (I, \psi) + (\psi, I) \quad (2.90)$$

$$\tilde{\boldsymbol{\sigma}}_+ = (\sigma, I) + (\sigma, \psi) \quad (2.91)$$

$$\tilde{\boldsymbol{\sigma}}_- = (I, \sigma) + (\psi, I) \quad (2.92)$$

This new spectrum exhibits all three features of anyon condensation: identification, confinement, and splitting of anyons. We explain them in detail below, using the diagrammatic action of string operators described in App. A.2 and the details of the Ising string operators given by Table A.1 of App. A.4.

The following anyons are identified:  $(I, I) \sim (\psi, \psi)$ ,  $(I, \psi) \sim (\psi, I)$ ,  $(\sigma, I) \sim (\sigma, \psi)$ , and  $(I, \sigma) \sim (\psi, \sigma)$ . Their identification occurs because their string operators only differ by how they act on  $\sigma$  strings, which are absent in the low energy subspace. For example, both  $\mathbf{W}_{(I,I)}$  and  $\mathbf{W}_{(\psi,\psi)}$  act trivially on  $I$  and  $\psi$  strings:

$$\begin{array}{c} \diagup \\ \diagdown \end{array} = \begin{array}{c} \times \\ \times \end{array} \quad (2.93)$$

$$\begin{array}{c} \diagup \\ \diagdown \end{array} = \begin{array}{c} \diagup \\ \diagdown \end{array} \quad (2.94)$$

Thus, they are indistinguishable and must be identified.

The  $\tilde{\sigma}_+$  and  $\tilde{\sigma}_-$  anyons are confined. Their confinement occurs because they are composed of anyons with different topological spin, and thus braid nontrivially with the vacuum. It can also be explained by the fact that they create  $\sigma$  strings when acting on  $I$  or  $\psi$  strings. For example, consider  $\mathbf{W}_{(\sigma,I)}$  and  $\mathbf{W}_{(\sigma,\psi)}$ :

$$\begin{array}{c} \diagup \\ \diagdown \end{array} = \begin{array}{c} \diagup \\ \diagdown \end{array} \quad (2.95)$$

$$\begin{array}{c} \diagup \\ \diagdown \end{array} = i \begin{array}{c} \diagup \\ \diagdown \end{array} \quad (2.96)$$

Therefore, they cost energy proportional to their length and are confined.

The  $(\sigma, \sigma)$  anyon is split into two anyons:  $\tilde{\epsilon}$  and  $\tilde{m}$ . To understand this splitting, recall that a string operator is acted on the lattice by drawing the operator over the fattened lattice, resolving every overcrossing using the  $\Omega$  symbols, joining the string tails between adjacent overcrossings, discarding the diagrams where these joined strings do

not match, and finally using the  $F$  symbols to express the diagram in terms of strings on the lattice. For  $\mathbf{W}_{(\sigma,\sigma)}$ , the rules for resolving overcrossings over  $I$  and  $\psi$  strings are given by:

$$\begin{array}{c} \diagup \\ \diagdown \end{array} = \begin{array}{c} \cdot \\ \cdot \\ \diagdown \\ \diagup \end{array} + \begin{array}{c} \diagup \\ \diagdown \end{array} \quad (2.97)$$

$$\begin{array}{c} \diagdown \\ \diagup \end{array} = - \begin{array}{c} \diagup \\ \diagdown \end{array} + \begin{array}{c} \diagdown \\ \diagup \end{array} \quad (2.98)$$

Consider acting this operator on a string-net. Starting at one endpoint and resolving the first overcrossing gives a superposition of two diagrams, one with two  $I$  string tails (first rules on right-hand sides of the above equations) and another with two  $\psi$  string tails (second rules on the right-hand sides). Let us focus on the  $I$  strings case. Resolving the next overcrossing will again give a superposition of two diagrams, but we can immediately discard the diagram with  $\psi$  string tails at the second overcrossing because it would not match with the  $I$  strings we chose at the first overcrossing. So, choosing the  $I$  string tails case at the first overcrossing fixes the rest of the overcrossings. Thus, there are actually only two diagrams superimposed: one where we only use the first rules on the right-hand side of the above equations, and the other where we only use the second rules. These rules correspond to the  $\tilde{m}$  and  $\tilde{e}$  particle of the toric code, respectively.

Note that the transition to the toric code depends crucially on the density of the  $\sigma$  flux present in the ground state. When the  $\sigma$  flux is dense, e.g. one flux in every plaquette as in the  $\sigma$  flux phase, then local interactions between the fluxes can lift the extensive ground state degeneracy and drive the transition. However, if the  $\sigma$  fluxes are sparse and well-separated, then we would expect the degeneracy to be protected against local perturbations.

## 2.5.2 General Properties

The Ising  $\sigma$  flux phase was exactly solvable due to the deep connection between Ising  $\times \overline{\text{Ising}}$  and the toric code. In general, we do not expect non-Abelian flux phases to be exactly solvable, and therefore expect them to be playgrounds of many rich properties.

Non-Abelian flux phases will generally have an extensive ground state degeneracy. More specifically, a flux phase with a non-Abelian anyon  $\mathbf{a}$  in every plaquette will have ground state degeneracy of  $d_{\mathbf{a}}^N$  for large  $N$ , where  $N$  is the number of plaquettes. For doubled Chern-Simons theories, this extensive degeneracy originates from the degeneracy of the fusion tree formed by fusing the non-Abelian fluxes, as demonstrated in App. A.6 and App. A.10.

We expect that this degeneracy will be lifted by generic local perturbations. However, it is unclear in general whether it will be lifted into a gapless spectrum of states or simply gapped out (as with the Ising  $\sigma$  flux phase). The former case would be interesting because if the phase also exhibits topological protected braiding, then it would be a lattice model of a true quasi-topological phase. The latter case would also be interesting because the resulting phase may be a different topological phase, and this topological phase transition may be an example of anyon condensation. For example, we expect certain non-Abelian flux phases of  $SU(2)_k$  to undergo condensation.[33]

# Chapter 3

## Topological Enrichment of Luttinger's Theorem

### 3.1 Introduction

Free electrons in a translationally invariant system form a Fermi sea. Interacting electrons may be described by Landau's Fermi liquid theory, which, when applicable, asserts that interactions between electrons do not qualitatively modify the free electron picture, at most dressing the electrons as quasiparticles, which are fermions with renormalized quantities, such as mass. In particular, the Fermi volume  $V_F$  of these emergent quasiparticles is precisely determined by the filling fraction  $\nu$  of the underlying electrons per unit cell:

$$\nu = \frac{V_F}{(2\pi)^D} \pmod{1}, \quad (3.1)$$

where the relation holds modulo an integer, which physically represents the number of filled bands. This relation, fixing the Fermi volume for a specified electron density, is the content of Luttinger's theorem [34], which is a rare example of an exact result for an

interacting system.

While Luttinger’s theorem was originally proved perturbatively, it was later recast as a “quantization” condition for Fermi liquids by Oshikawa [35], who proved it non-perturbatively by drawing inspiration from Laughlin’s flux threading argument [5, 36, 37] and Lieb, Schultz, and Mattis’s variational argument [38]. Later, it was found that Luttinger’s theorem may require modification for a fractionalized Fermi liquid, i.e. a Fermi liquid that is accompanied by symmetry enriched topological (SET) order, and that this modification, at least for some simple cases, may be understood by generalizing Oshikawa’s arguments [39, 40, 41].

In this paper, we apply Oshikawa’s arguments to 2D systems with general SET order [30]. By studying the interplay between symmetries, topological order, and the Fermi sea, we derive a topologically enriched generalization of Luttinger’s theorem for fractionalized Fermi liquids:

$$\nu - \nu_{\text{topo}} = \frac{V_F}{(2\pi)^2} \pmod{1}, \quad (3.2)$$

where, assuming that the underlying degrees of freedom effectively decouple into an SET sector and a Fermi liquid sector,  $\nu_{\text{topo}}$  is the filling fraction of the SET sector. For 2D systems, there is a precise general definition of  $\nu_{\text{topo}}$ ; it is the U(1) charge of the background anyonic flux per unit cell that is specified by the SET order [31], as we will describe. In higher dimensions, we expect a similar definition (and verify it for specific 3D examples), but a general formalism of higher dimensional topological and SET order is currently lacking. Our result reaffirms the intuition that the underlying degrees of freedom that topologically order should not contribute to the Fermi volume.

A consequence of the topologically enriched Luttinger’s theorem is that experimental observation of a Fermi volume that deviates from that of an ordinary Fermi liquid may point to the existence of a fractionalized Fermi liquid phase. Moreover, the SET order

that is allowed for a given deviation is constrained by the corresponding value of  $\nu_{\text{topo}}$ .

Our paper is organized as follows. In Sec. 3.2, we review Oshikawa's proof of Luttinger's theorem. In Sec. 3.3, we review 2D symmetry fractionalization, focusing on U(1) and translational symmetries, and show that flux threading argument places a constraint on which SET phases are allowed at some given filling. In Sec. 3.4, we derive the topologically enriched version of Luttinger's theorem for a general 2D fractionalized Fermi liquid, apply it to the  $\mathbb{Z}_2$  fractionalized Fermi liquid (FL\*), and examine some examples of 3D  $\mathbb{Z}_2$  fractionalized Fermi liquids. Finally, in Sec. 4.6, we discuss further possible applications and generalizations of our work.

## 3.2 Oshikawa's Argument

In essence, Oshikawa's argument involves starting with a periodic system in its ground state, adiabatically inserting a flux along one of the directions, applying a large gauge transformation to remove the flux, and finally comparing the resulting state with the original state in order to derive constraints for the system. This yields the commensurability condition if the system is gapped [42], and Luttinger's theorem if the system is gapless with a Fermi surface of charged quasiparticles [35]. We review these arguments in more detail.

We consider a  $D$  dimensional periodic system of size  $L_1 \times \cdots \times L_D$  with a global U(1) symmetry and a corresponding filling fraction, specifying the density per unit cell  $\nu = p/q$  for some coprime integers  $p$  and  $q$ . We assume the system is described by a translationally invariant Hamiltonian  $\mathbf{H}(0)$  and is in a ground state  $|\Psi(0)\rangle$ . Let the state  $|\Psi(0)\rangle$  be an eigenstate of the translation operator  $\mathbf{R}_{T_1}$  with eigenvalue  $e^{iP_1(0)}$ , i.e. it has momentum  $P_1(0)$ . (We set  $\hbar = e = 1$ .)

Next, we consider adiabatically inserting a U(1) flux so that a uniform electric field

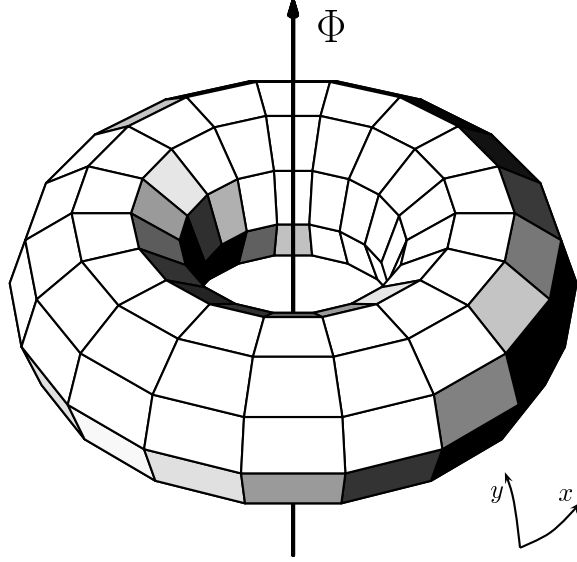


Figure 3.1: A 2D periodic lattice depicted as a torus. A flux inserted to induce a uniform electric field in the  $x$ -direction can be thought of as threading the handle of the torus.

is induced along the  $\hat{x}_1$ -direction, for which the Hamiltonian is  $\mathbf{H}(\Phi)$  and adiabatic path of ground states is given by  $|\Psi(\Phi)\rangle$ . In the 2D case, where the periodic system is effectively a torus, the flux can be thought of as threading the handle of the torus, as illustrated in Fig. 3.1. Since inserting a  $2\pi$  flux returns the system to the same point in configuration space, the spectra of  $\mathbf{H}(2\pi)$  and  $\mathbf{H}(0)$  are identical, and there exists a large gauge transformation  $\mathcal{G}$  that removes the flux:  $\mathcal{G}\mathbf{H}(2\pi)\mathcal{G}^{-1} = \mathbf{H}(0)$ . Therefore,  $\mathcal{G}|\Psi(2\pi)\rangle$  must be an eigenstate of  $\mathbf{H}(0)$ . Also, since  $[\mathbf{R}_{T_1}, \mathbf{H}(\Phi)] = 0$  throughout the flux threading process,  $|\Psi(2\pi)\rangle$  has momentum  $P_1(0)$ , and since  $\mathcal{G}\mathbf{R}_{T_1}\mathcal{G}^{-1} = e^{i2\pi\nu L_2 \cdots L_D} \mathbf{R}_{T_1}$ , the state  $\mathcal{G}|\Psi(2\pi)\rangle$  has momentum  $P_1(0) + 2\pi\nu L_2 \cdots L_D \pmod{2\pi}$ .

If the system is gapped and remains gapped throughout the flux threading process, then the adiabatic theorem guarantees that  $\mathcal{G}|\Psi(2\pi)\rangle$  is a ground state of  $\mathbf{H}(0)$ <sup>1</sup>. By choosing arbitrary integers  $L_2, \dots, L_D$  that are coprime with  $q$ , we find  $q$  degenerate ground states with different momenta. In the absence of topological order, these degen-

<sup>1</sup>For subtleties regarding adiabatic flux insertion and quasi-adiabatic evolution of gapped, degenerate Hamiltonians, see Ref. [43].

erate ground states must be the result of spontaneous translational symmetry breaking. Their period in the  $\hat{x}_1$ -direction must be an integer multiple of  $q$ , and therefore the new unit cell, which is the original unit cell enlarged by a factor of  $q$ , has an integer filling fraction. This is Oshikawa's commensurability condition [42], which was later rigorously proven for 2D systems by Hastings [44]. In the presence of topological order, translational symmetry need not be spontaneously broken, since topological phases can have translationally-invariant, degenerate ground states on a torus. In 2D, however, only certain topological orders can coexist with U(1) and translational symmetry for a given  $\nu$ , as we will explain in Sec. 3.3.4. In the rest of this paper, we assume there is no spontaneous symmetry breaking in the system.

If the system is gapless, then  $\mathcal{G}|\Psi(2\pi)\rangle$  is no longer necessarily a ground state. However, it is still true that its momentum is shifted by  $2\pi\nu L_2 \cdots L_D$ , and this shift can be compared with the momentum shift of the emergent degrees of freedom. For example, if the system is a Fermi liquid of charge 1 quasiparticles, then threading the flux applies a Galilean boost to the Fermi sea, shifting the momentum of each of the  $N_F$  quasiparticles by  $2\pi/L_1$ . Equating the two momentum shifts yields the constraint

$$\nu = \frac{V_F}{(2\pi)^D} + \frac{n}{L_2 \cdots L_D}, \quad (3.3)$$

for some integer  $n$ , where  $V_F \equiv (2\pi)^D N_F / L_1 \cdots L_D$  is the Fermi volume. Similarly, inserting flux along the other directions yields more constraints on  $\nu$ , which are compatible for coprime integers  $L_1, \dots, L_D$  iff

$$\nu = \frac{V_F}{(2\pi)^D} \pmod{1}. \quad (3.4)$$

This is Oshikawa's derivation of Luttinger's theorem [35]. In Appendix B.1, we provide

a derivation of Luttinger's theorem for the 2D Kondo model, under the assumption that it is in a Fermi liquid phase.

### 3.3 Symmetry Fractionalization

A symmetric system with topological order can manifest distinct SET phases, which cannot be adiabatically connected to each other while respecting the symmetry [30]. A distinguishing signature of these phases is symmetry fractionalization [29, 30], a phenomenon that allows quasiparticles to carry fractionalized quantum numbers of the symmetry. For example, U(1) fractionalization leads to quasiparticles with fractional charge [6, 20], while translational symmetry fractionalization leads to a nontrivial background anyonic flux in the system [45, 31]. (Both of these examples will be described in more detail.)

In general, symmetry fractionalization in a 2D topologically ordered phase is classified by the cohomology group  $H_\rho^2(G, \mathcal{A})$ , where  $G$  is the symmetry group,  $\mathcal{A}$  is the group of Abelian anyons under fusion, and  $\rho$  is the symmetry action, which may permute anyon types. We first review the derivation of this classification and, in doing so, introduce relevant notation and concepts. (See Ref. [30] for more details.) We will assume that the topological order is bosonic and that symmetries are unitary. We also focus on the case where the symmetry action  $\rho$  does not permute anyon types, which must be the case for symmetries described by a continuous and connected group, such as U(1).

#### 3.3.1 Review of On-Site Symmetry Fractionalization

Consider a symmetric 2D system in a topological phase with symmetry group  $G$ , whose elements  $\mathbf{g}$  act linearly on the Hilbert space by the unitary on-site operators  $\mathbf{R}_\mathbf{g} = \prod_{k \in I} \mathbf{R}_\mathbf{g}^{(k)}$ . Let  $|\Psi_{\{a_1, \dots, a_n\}}\rangle$  be a state with  $n$  quasiparticles carrying topological

charges  $a_1, \dots, a_n$ , respectively, which collectively fuse to the trivial (vacuum) topological charge. Assuming the action of the symmetry does not permute anyon types, it takes the form

$$\mathbf{R}_{\mathbf{g}}|\Psi_{\{a_1, \dots, a_n\}}\rangle = \prod_{j=1}^n \mathbf{U}_{\mathbf{g}}^{(j)}|\Psi_{\{a_1, \dots, a_n\}}\rangle, \quad (3.5)$$

where  $\mathbf{U}_{\mathbf{g}}^{(j)}$  are unitary operators whose nontrivial action is localized in a neighborhood of the  $j$ th quasiparticle. The local operators form projective representation of  $G$ , with multiplication given by

$$\mathbf{U}_{\mathbf{g}}^{(j)}\mathbf{U}_{\mathbf{h}}^{(j)}|\Psi_{\{a_1, \dots, a_n\}}\rangle = \eta_{a_j}(\mathbf{g}, \mathbf{h})\mathbf{U}_{\mathbf{gh}}^{(j)}|\Psi_{\{a_1, \dots, a_n\}}\rangle, \quad (3.6)$$

where  $\eta_a(\mathbf{g}, \mathbf{h}) \in \text{U}(1)$ .

The phases  $\eta_a(\mathbf{g}, \mathbf{h})$  must satisfy certain constraints, which provide a classification of the possible way symmetry can be fractionalized. Since  $\mathbf{R}_{\mathbf{g}}\mathbf{R}_{\mathbf{h}} = \mathbf{R}_{\mathbf{gh}}$ , the fact that Eq. (3.5) holds for any configuration of topological charges allowed by fusion requires that

$$\eta_a(\mathbf{g}, \mathbf{h})\eta_b(\mathbf{g}, \mathbf{h}) = \eta_c(\mathbf{g}, \mathbf{h}), \quad (3.7)$$

whenever  $c$  is an allowed fusion outcome of  $a$  and  $b$ , i.e.  $N_{ab}^c \neq 0$ . This property allows us to write the projective phases as [30]

$$\eta_a(\mathbf{g}, \mathbf{h}) = M_{a, \mathbf{w}(\mathbf{g}, \mathbf{h})}, \quad (3.8)$$

where  $\mathbf{w}(\mathbf{g}, \mathbf{h}) \in C^2(G, \mathcal{A})$  is an  $\mathcal{A}$ -valued 2-cochain, i.e. a  $\mathcal{A}$ -valued function on  $G^2$ , and  $M_{a,b}$  is the mutual braiding statistics between anyons  $a$  and  $b$ .

Associativity of the local operators requires that

$$\eta_a(\mathbf{h}, \mathbf{k})\eta_a(\mathbf{g}, \mathbf{hk}) = \eta_a(\mathbf{gh}, \mathbf{k})\eta_a(\mathbf{g}, \mathbf{h}). \quad (3.9)$$

This implies  $\mathbf{w}(\mathbf{g}, \mathbf{h}) \in Z^2(G, \mathcal{A})$  is a 2-cocycle, i.e. that

$$\mathbf{w}(\mathbf{h}, \mathbf{k}) \times \mathbf{w}(\mathbf{g}, \mathbf{hk}) = \mathbf{w}(\mathbf{gh}, \mathbf{k}) \times \mathbf{w}(\mathbf{g}, \mathbf{h}). \quad (3.10)$$

However,  $\eta_a(\mathbf{g}, \mathbf{h})$  have some redundancy. The local operators  $U_{\mathbf{g}}^{(j)}$  can be “trivially” redefined to  $\tilde{U}_{\mathbf{g}}^{(j)}$ , such that

$$\tilde{U}_{\mathbf{g}}^{(j)}|\Psi_{\{a_1, \dots, a_n\}}\rangle = \zeta_{a_j}(\mathbf{g})U_{\mathbf{g}}^{(j)}|\Psi_{\{a_1, \dots, a_n\}}\rangle, \quad (3.11)$$

where  $\zeta_a(\mathbf{g}) \in U(1)$ , as long as  $\zeta_a(\mathbf{g})\zeta_b(\mathbf{g}) = \zeta_c(\mathbf{g})$  whenever  $c$  is an allowed fusion outcome of  $a$  and  $b$ . Under this redefinition,

$$\tilde{\eta}_a(\mathbf{g}, \mathbf{h}) = \frac{\zeta_a(\mathbf{gh})}{\zeta_a(\mathbf{h})\zeta_a(\mathbf{g})}\eta_a(\mathbf{g}, \mathbf{h}), \quad (3.12)$$

and therefore projective phases  $\eta_a(\mathbf{g}, \mathbf{h})$  related by such transformations are physically equivalent. Since they respect fusion, the redefinition phases can similarly be written as  $\zeta_a(\mathbf{g}) = M_{a, \mathfrak{z}(\mathbf{g})}$ , where  $\mathfrak{z}(\mathbf{g}) \in C^1(G, \mathcal{A})$  is a 1-cochain. In this way, the redundancy of the local operators corresponds to a redundancy of the 2-cocycles  $\mathbf{w}(\mathbf{g}, \mathbf{h})$  given by redefinition by 2-coboundaries  $d\mathfrak{z}(\mathbf{g}, \mathbf{h}) = \mathfrak{z}(\mathbf{h}) \times \overline{\mathfrak{z}(\mathbf{gh})} \times \mathfrak{z}(\mathbf{g}) \in B^2(G, \mathcal{A})$ . Thus, the possible manner in which symmetry can fractionalize, as encoded in the allowed projective phases  $\eta_a(\mathbf{g}, \mathbf{h})$  modulo the redundancy, is classified by the elements of the second cohomology group

$$[\mathbf{w}(\mathbf{g}, \mathbf{h})] \in H^2(G, \mathcal{A}) = \frac{Z^2(G, \mathcal{A})}{B^2(G, \mathcal{A})}. \quad (3.13)$$

### 3.3.2 U(1) Symmetry Fractionalization

Consider a system with an on-site U(1) symmetry, which may be a subgroup of the full symmetry group. For example, it can be the U(1) associated with particle number conservation or U(1) < SO(3) associated with spin rotational symmetry. Let us label the elements of U(1) as  $\theta \in [0, 2\pi)$ , and their local action on the anyons as  $\mathbf{U}_\theta^{(j)}$ . We can choose the 2-cocycles

$$\mathbf{w}(\theta_1, \theta_2) = v^{(\theta_1 + \theta_2 - [\theta_1 + \theta_2]_{2\pi})/2\pi}, \quad (3.14)$$

where  $v \in \mathcal{A}$ , to represent the distinct cohomology classes  $[\mathbf{w}] \in H^2(\text{U}(1), \mathcal{A}) = \mathcal{A}$ . While  $\mathbf{w}(\theta_1, \theta_2)$  is not gauge invariant, since it can be redefined by 2-coboundaries,  $v = \mathbf{w}(\theta, 2\pi - \theta)$  is gauge invariant. Therefore, we label U(1) fractionalization classes by  $v$ . Physically, the anyon  $v$  is associated with the “vison,” which is the quasiparticle created by threading a  $2\pi$  U(1) flux [31].

Let  $Q_a$  be the U(1) charge of anyon  $a$ . Rotating a state by an arbitrary  $\theta$  results in

$$\mathbf{R}_\theta |\Psi_{\{a_1, \dots, a_n\}}\rangle = e^{i\theta Q} |\Psi_{\{a_1, \dots, a_n\}}\rangle, \quad (3.15)$$

where the total charge  $Q = \sum_j Q_{a_j}$  must be an integer, since  $\mathbf{R}_0 = \mathbf{R}_{2\pi}$ . Meanwhile, the local operators act as

$$\mathbf{U}_\theta^{(j)} |\Psi_{\{a_1, \dots, a_n\}}\rangle = e^{i\theta Q_{a_j}} |\Psi_{\{a_1, \dots, a_n\}}\rangle, \quad (3.16)$$

where  $Q_a$  need not be integers. This action of  $\mathbf{U}_\theta^{(j)}$  is not gauge invariant, but a gauge invariant statement can be obtained by applying a complete  $2\pi$  rotation [with the use of Eq. (3.8)]:

$$\mathbf{U}_\theta^{(j)} \mathbf{U}_{2\pi - \theta}^{(j)} |\Psi_{\{a_1, \dots, a_n\}}\rangle = M_{a_j, v} |\Psi_{\{a_1, \dots, a_n\}}\rangle. \quad (3.17)$$

Thus, the anyon  $a$  has a possibly fractional charge  $Q_a$ , which is given by the relation

$$e^{i2\pi Q_a} = M_{a,v}. \quad (3.18)$$

### 3.3.3 Translational Symmetry Fractionalization

Consider a 2D system in a topological phase with  $\mathbb{Z}^2$  translational symmetry. The fractionalization of this symmetry requires a straightforward modification of the on-site formalism. In particular, the state vector  $|\Psi_{\{a_1, \dots, a_n\}}\rangle$  on the right hand side of Eq. (3.5) must have the positions of its quasiparticles translated (according to the applied translation operator) with respect to  $|\Psi_{\{a_1, \dots, a_n\}}\rangle$  on the left hand side, and the local unitary operators  $\mathbf{U}_{\mathbf{g}}^{(j)}$  should be understood to act nontrivially in a neighborhood of the translated quasiparticle positions [30]. Let us label the generators of translation as  $T_x$  and  $T_y$  and their corresponding local unitary operators as  $\mathbf{U}_x^{(j)}$  and  $\mathbf{U}_y^{(j)}$ .

We can choose the 2-cocycles

$$\mathbf{w}(T_x^{m_x} T_y^{m_y}, T_x^{n_x} T_y^{n_y}) = b^{m_y n_x}, \quad (3.19)$$

where  $b \in \mathcal{A}$ , to represent the distinct cohomology classes  $[\mathbf{w}] \in H^2(\mathbb{Z}^2, \mathcal{A}) = \mathcal{A}$ . While  $\mathbf{w}(T_x^{m_x} T_y^{m_y}, T_x^{n_x} T_y^{n_y})$  is not gauge invariant, since it can be redefined by 2-coboundaries, the quantity  $\mathbf{w}(T_y, T_x) \times \overline{\mathbf{w}(T_x, T_y)} = b$  is gauge invariant and, moreover, completely specifies cohomology class. Therefore, we can label translational symmetry fractionalization classes by  $b \in \mathcal{A}$ .

Physically, the anyon  $b$  can be thought of as the background anyonic flux per unit

cell. This is because

$$\begin{aligned}
& (U_{T_y}^{(j)})^{-1} (U_{T_x}^{(j)})^{-1} U_{T_y}^{(j)} U_{T_x}^{(j)} |\Psi_{\{a_1, \dots, a_n\}}\rangle \\
&= \frac{\eta_{a_j}(T_y, T_x)}{\eta_{a_j}(T_x, T_y)} |\Psi_{\{a_1, \dots, a_n\}}\rangle \\
&= M_{a_j, \mathbf{w}(T_y, T_x)} M_{a_j, \overline{\mathbf{w}(T_x, T_y)}} |\Psi_{\{a_1, \dots, a_n\}}\rangle \\
&= M_{a_j, b} |\Psi_{\{a_1, \dots, a_n\}}\rangle.
\end{aligned} \tag{3.20}$$

That is, when an anyon  $a$  is transported around a unit cell, the wavefunction acquires a phase corresponding to braiding  $a$  around  $b$ .

### 3.3.4 Flux Threading Argument

Consider a system with both on-site  $U(1)$  symmetry and  $\mathbb{Z}^2$  translational symmetry. Using Künneth formula for group cohomology, one has [31]

$$H^2(U(1) \times \mathbb{Z}^2, \mathcal{A}) = H^2(U(1), \mathcal{A}) \times H^2(\mathbb{Z}^2, \mathcal{A}), \tag{3.21}$$

which means that the fractionalization for the combined symmetries are determined by that of the  $U(1)$  and translational symmetries, which can be independently specified. Suppose the system belongs to  $U(1)$  fractionalization class  $v$  and translational symmetry fractionalization class  $b$ .

If we consider a state that has  $2\pi$   $U(1)$  flux through a handle of the torus and transport an anyon  $a$  around the handle, so that it winds around the flux once, the wavefunction will acquire the Aharonov-Bohm phase  $e^{i2\pi Q_a}$ . By Eq. (3.18), this is identical to the phase  $M_{a,v}$  that is acquired by braiding  $a$  around  $v$ . Therefore, the effect of threading the flux through a handle of the torus should be gauge equivalent to creating a vison

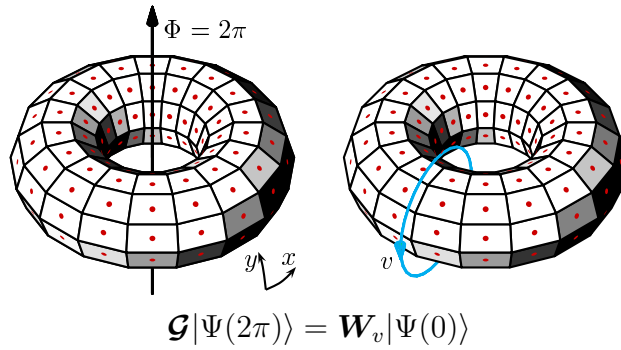


Figure 3.2: Threading a  $2\pi$  flux through the handle of the torus creates a  $v$  anyon loop (blue). The dots represent the anyonic flux per unit cell  $b$  (red).

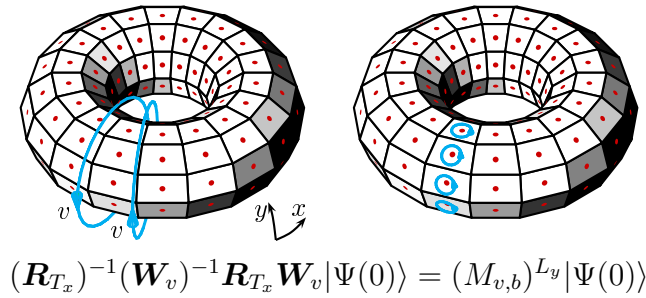


Figure 3.3: The  $\mathbf{R}_{T_x}$  eigenvalue of  $\mathbf{W}_v|\Psi(0)\rangle$  is determined by the mutual braiding statistics between  $v$  and  $b$ . To go from the l.h.s. to the r.h.s., we partially fused the adjacent  $v$  anyon loops, being careful not to pass them through the anyonic flux  $b$  lines emanating from the center of every cell of the torus.

loop that wraps around the handle, as illustrated in Fig. 3.2. That is

$$\mathcal{G}|\Psi(2\pi)\rangle = \mathbf{W}_v|\Psi(0)\rangle, \quad (3.22)$$

where  $\mathbf{W}_v$  is an operator that creates a  $v$  anyon loop wrapping around the handle of the torus.<sup>2</sup> (See Appendix B.2 for a more direct argument.)

The state  $\mathbf{W}_v|\Psi(0)\rangle$  has momentum  $P_x(0) + 2\pi Q_b L_y \pmod{2\pi}$ , since

$$(\mathbf{R}_{T_x})^{-1}(\mathbf{W}_v)^{-1}\mathbf{R}_{T_x}\mathbf{W}_v|\Psi(0)\rangle = (M_{v,b})^{L_y}|\Psi(0)\rangle, \quad (3.23)$$

which can be understood from the relation in Fig. 3.3. On the other hand, we know the state  $\mathcal{G}|\Psi(2\pi)\rangle$  has momentum  $P_x(0) + 2\pi\nu L_y \pmod{2\pi}$ . Equating the momenta of  $\mathcal{G}|\Psi(2\pi)\rangle$  and  $\mathbf{W}_v|\Psi(0)\rangle$ , and repeating the argument in the other direction yields

$$\nu = Q_b \equiv \nu_{\text{topo}} \pmod{1}. \quad (3.24)$$

In other words, the filling fraction of a 2D SET phase is equal to the U(1) charge of the background anyonic flux per unit cell.

Eq. (3.24), which relates microscopic and emergent properties of the system, can be viewed as a constraint on the allowed SET order that may exist at a given filling. For example, consider the Ising anyon model, which contains Abelian anyons  $I$  and  $\psi$ , and non-Abelian anyon  $\sigma$ . The fact that  $M_{I,I} = M_{I,\psi} = M_{\psi,\psi} = 1$  implies that  $Q_b = 0$  for any fractionalization pattern, and so it is impossible to have the pure Ising topological order at a non-integer fractional filling.

---

<sup>2</sup>The application of  $\mathbf{W}_v$  to a ground state is equivalent to creating a  $v - \bar{v}$  pair of anyons, adiabatically transporting  $v$  around the cycle of the torus, and then annihilating the pair to vacuum.

### 3.4 Fractionalized Fermi Liquid

A fractionalized Fermi liquid is a gapless system with U(1) and translational SET order, whose gapless modes are well-described by Fermi liquid theory, and whose symmetries are fractionalized. We assume that topological excitations and gapless excitations coexist, but are effectively decoupled from one another, i.e. the system decouples into an SET sector and a Fermi liquid sector, and is consequently in a strong quasi-topological phase [32]. We consider a 2D system for which the SET order belongs to U(1) fractionalization class  $v$  and translational symmetry fractionalization class  $b$ .

Similar to the situation described in Sec. 3.3.4, starting from a ground state  $|\Psi(0)\rangle$  of a fractionalized Fermi liquid and threading a  $2\pi$  flux through the handle of a torus is gauge equivalent to applying a vison loop that wraps around the handle to the state  $|\Psi'(0)\rangle$ ,

$$\mathcal{G}|\Psi(2\pi)\rangle = \mathbf{W}_v|\Psi'(0)\rangle, \quad (3.25)$$

where  $|\Psi'(0)\rangle$  is  $|\Psi(0)\rangle$  with a Galilean boosted Fermi sea, so that it is in the same topological sector as  $|\Psi(0)\rangle$ , but has a shifted momentum. Note that the assumption of the decoupling between the SET sector and the Fermi liquid sector is crucial here, since it allows us to separate the effect of flux threading on the SET sector, i.e. wrapping a vison loop around the handle, from its effect on the Fermi liquid sector, i.e. boosting the Fermi sea. If the topological excitations were to interact with the Fermi liquid quasiparticles in a manner that nontrivially coupled the SET sector and the Fermi liquid sector, then the effect of flux threading may not be so cleanly separable.

The state  $|\Psi'(0)\rangle$  has momentum  $P_x(0) + 2\pi N_F/L_x \pmod{2\pi}$ , due to the Fermi liquid quasiparticles. As explained in Sec. 3.3.4, the state  $\mathbf{W}_v|\Psi'(0)\rangle$  has momentum  $2\pi Q_b L_y$  relative to the state  $|\Psi'(0)\rangle$ . On the other hand, we know the state  $\mathcal{G}|\Psi(2\pi)\rangle$  has momentum  $P_x(0) + 2\pi\nu L_y \pmod{2\pi}$ . Equating the momenta of  $\mathcal{G}|\Psi(2\pi)\rangle$  and  $\mathbf{W}_v|\Psi'(0)\rangle$

and repeating the argument in the other direction yields Luttinger's theorem for a 2D fractionalized Fermi liquid:

$$\nu = Q_b + \frac{V_F}{(2\pi)^2} \pmod{1}. \quad (3.26)$$

This is essentially a combination of Eq. (3.4) and Eq. (3.24). We see that the background anyonic flux can appropriate some of the charge available to the emergent degrees of freedom, thus changing the Fermi volume. Or, put differently, the Fermi volume is determined by the filling fraction of the Fermi liquid sector:

$$\nu - \nu_{\text{topo}} = \frac{V_F}{(2\pi)^2} \pmod{1}. \quad (3.27)$$

### 3.4.1 $\mathbb{Z}_2$ Fractionalized Fermi Liquid: FL\*

Consider a 2D periodic lattice with  $\nu_c = \nu_{c\uparrow} + \nu_{c\downarrow}$  conduction electrons and  $\nu_s$  spin- $\frac{1}{2}$  localized spins per unit cell, governed by the Kondo model Hamiltonian

$$\begin{aligned} \mathbf{H} = & -t \sum_{\langle jk \rangle, \alpha} (\mathbf{c}_{j\alpha}^\dagger \mathbf{c}_{k\alpha} + \text{h.c.}) + U \sum_j \mathbf{n}_{j\uparrow} \mathbf{n}_{j\downarrow} \\ & + K \sum_j \vec{\mathbf{s}}_j \cdot \vec{\mathbf{S}}_j + J \sum_{\langle jk \rangle} \vec{\mathbf{S}}_j \cdot \vec{\mathbf{S}}_k, \end{aligned} \quad (3.28)$$

where  $\vec{\mathbf{s}}_j = \sum_{\alpha\beta} \mathbf{c}_{j\alpha}^\dagger \vec{\sigma}_{\alpha\beta} \mathbf{c}_{j\beta} / 2$ . As explained in App. B.1, the above Hamiltonian has two global U(1) symmetries, denoted U(1) $_{\uparrow}$  and U(1) $_{\downarrow}$ , which correspond to the independently conserved quantities  $\nu_{c\uparrow} + m_s \nu_s$  and  $\nu_{c\downarrow} - m_s \nu_s$ , respectively, where  $m_s$  is the magnetization per localized spin.

In the ordinary Fermi liquid phase of the Kondo model, these two symmetries lead

to the Luttinger's theorems

$$\nu_{c\uparrow} + \left(\frac{1}{2} + m_s\right)\nu_s = \frac{V_{F\uparrow}}{(2\pi)^2} \pmod{1}, \quad (3.29)$$

$$\nu_{c\downarrow} + \left(\frac{1}{2} - m_s\right)\nu_s = \frac{V_{F\downarrow}}{(2\pi)^2} \pmod{1}, \quad (3.30)$$

which can be combined to give the spin-summed Luttinger's theorem

$$\nu_c + \nu_s = \frac{V_F}{(2\pi)^2} \pmod{2}. \quad (3.31)$$

See App. B.1 for details.

If the Kondo model is placed on a geometrically frustrated lattice, e.g. triangular lattice, then at low temperatures and small enough values of  $K$ , the localized spins are believed to topologically order. In this case, the system may enter the so-called FL\* phase of the Kondo model [39, 46, 47], which is a fractionalized Fermi liquid. Let us assume that  $K = 0$ , so that the electrons are decoupled from the spins, and that the spins form a  $\mathbb{Z}_2$  spin liquid with toric code topological order.

In this case, the localized spins carry  $U(1)_\uparrow$  and  $U(1)_\downarrow$  charge values of  $1/2$ . Consequently, the Luttinger's theorems are modified by  $\nu_{\text{topo}} = \nu_s/2$  to give

$$\nu_{c\uparrow} + m_s\nu_s = \frac{V_{F\uparrow}}{(2\pi)^2} \pmod{1}, \quad (3.32)$$

$$\nu_{c\downarrow} - m_s\nu_s = \frac{V_{F\downarrow}}{(2\pi)^2} \pmod{1}, \quad (3.33)$$

which can be combined to give the spin-summed Luttinger's theorem for the FL\* phase

$$\nu_c = \frac{V_F}{(2\pi)^2} \pmod{2}. \quad (3.34)$$

We emphasize that this result for the FL\* phase differs from the result in Eq. (3.31) for the ordinary Fermi liquid phase when the number of localized spins per unit cell  $\nu_s$  is odd. This difference can be understood by studying symmetry fractionalization of the  $\mathbb{Z}_2$  spin liquid, as we now explain in more detail.

Recall that the toric code [15] has four types of anyons: trivial excitations  $I$ , bosons  $e$  and  $m$ , and fermionic composites  $f = e \times m$ . They are all Abelian and obey  $\mathbb{Z}_2 \times \mathbb{Z}_2$  fusion rules. The nontrivial braiding statistics are  $M_{e,m} = M_{e,f} = M_{m,f} = -1$ . Let the  $U(1)_\uparrow$  and  $U(1)_\downarrow$  symmetry fractionalization class be specified by  $v = m$ . In this case,  $Q_I = Q_m = 0$  and  $Q_e = Q_f = 1/2$ , i.e.  $e$  is a spin- $\frac{1}{2}$  spinon,  $m$  is a spinless vison, and  $f$  is a spin- $\frac{1}{2}$  fermion.<sup>3</sup> If  $\nu_s$  is even, then, by Eq. (3.24), the translational symmetry fractionalization class is either  $b = I$  or  $b = m$ , and Eq. (3.31) agrees with Eq. (3.34). However, if  $\nu_s$  is odd, then the translational symmetry fractionalization class is either  $b = e$  or  $b = f$ . In this case, Eq. (3.31) and Eq. (3.34) clearly disagree, and the topological enrichment of Luttinger's theorem for the FL\* phase is manifest.

### 3.4.2 3D $\mathbb{Z}_2$ Fractionalized Fermi Liquid

Consider a spinless Fermi liquid that is accompanied by 3D bosonic toric code ( $\mathbb{Z}_2$  gauge theory) topological order. The 3D bosonic toric code has four types of topological

---

<sup>3</sup>Observe that the spin symmetry of the localized spins has been fractionalized. To see this, first note that while the localized spins have  $SU(2)$  spin symmetry, the relevant symmetry group is actually  $SU(2)$  modded by its center  $\mathbb{Z}_2$ :  $SU(2)/\mathbb{Z}_2 = SO(3)$ . In other words, the Hilbert space factorizes into two disjoint subspaces, and the  $SU(2)$  operators act as a direct product of  $SO(3)$  operators on each subspace. The representations of  $SO(3)$  are classified by  $\mathbb{Z}$ , i.e. integer spins. Indeed, local operators such as  $\mathbf{S}_j^+$  and  $\mathbf{S}_j^-$  change the spin by an integer. Thus, an excitation must normally have integer spin. However, in the  $\mathbb{Z}_2$  spin liquid, the  $e$  and  $f$  are spin- $\frac{1}{2}$  excitations.

Alternatively, we may view the localized spins as electrons, in which case the relevant symmetry group is the product of the  $SU(2)$  spin symmetry group and the  $U(1)$  charge symmetry group, modded by its center  $\mathbb{Z}_2$ :  $SU(2) \times U(1)/\mathbb{Z}_2 = U(2)$ . The representations of  $U(2)$  are classified by  $(s, q)$ , where  $2s$  and  $q$  are integers whose sum is even. Therefore, a particle with spin  $s$  and charge  $q$  must obey  $2s + q \bmod 2 = 0$ . The electron, for instance, transforms as the  $(\frac{1}{2}, 1)$  representation. However, in the  $\mathbb{Z}_2$  spin liquid, the  $e$  and  $f$  are spin- $\frac{1}{2}$  chargeless excitations.

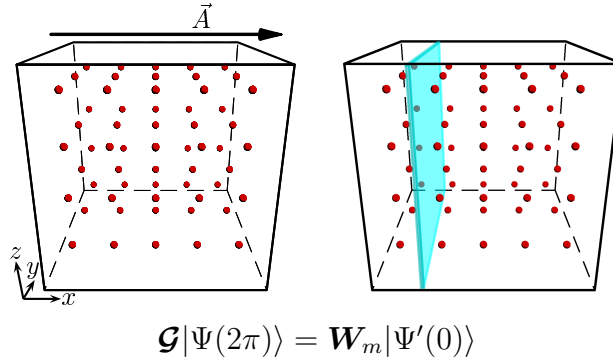


Figure 3.4: Inserting a  $2\pi$  flux along the  $x$  direction is equivalent to having an  $m$  membrane (blue) in the  $yz$  plane. The dots represent an  $e$  occupying every cell (red). (The underlying 3D periodic lattice is not shown.)

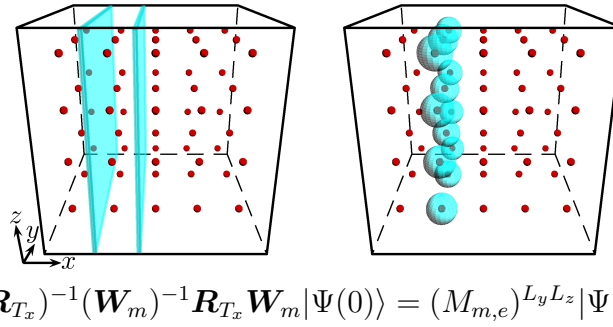


Figure 3.5: The  $\mathbf{R}_{T_x}$  eigenvalue of  $\mathbf{W}_m|\Psi(0)\rangle$  is determined by the mutual braiding statistics between  $m$  and  $e$ . To go from the l.h.s. to the r.h.s., we have partially fused the adjacent  $m$  membranes, being careful not to pass them through the  $e$  at the center of every cell.

excitations: trivial excitations  $I$ , point excitations  $e$ , loop excitations  $m$ , and composite loop excitations  $f = e \times m$  [48, 49]. Topological loop excitations are created along the boundary of a fluctuating surface operator, similar to how topological point excitations are created at the endpoints of fluctuating string operators. While the fusion rules and exchange statistics of excitations in a 3D topological order are more intricate than in 2D, our discussion will simply rely on the fact that  $M_{e,m} = -1$ , which now expresses the phase obtained by taking an  $e$  quasiparticle around a circuit that links a  $m$  loop once. As in 2D, the topological enrichment of Luttinger's theorem can be understood in terms of the symmetry fractionalization. Although 3D symmetry fractionalization currently lacks a general formalism, it has been recently studied for the 3D toric code [50].

Suppose that  $U(1)$  charge symmetry is fractionalized such that  $e$  is charge- $\frac{1}{2}$ , and translational symmetry is fractionalized such that an  $e$  occupies every unit cell, and hence we have  $\nu_{\text{topo}} = 1/2$ . Then, at least for our purposes, inserting a flux such that a uniform electric field is induced along the  $x$ -direction is gauge equivalent to introducing an  $m$  membrane in the  $yz$ -plane, as shown in Fig. 3.4, since transporting an  $e$  anyon along the  $x$ -direction around a nontrivial cycle of the torus results in the wavefunction acquiring a phase of  $-1$  in both cases. (Since the  $m$  membrane is created by a non-contractible surface operator  $\mathbf{W}_m$  that has no boundary, it does not create an  $m$  loop excitation, but still acts nontrivially on the ground states.) Mathematically, this is expressed as  $\mathcal{G}|\Psi(2\pi)\rangle = \mathbf{W}_m|\Psi'(0)\rangle$ , where  $|\Psi'(0)\rangle$  is in the same topological sector as  $|\Psi(0)\rangle$ .

The state  $|\Psi'(0)\rangle$  has momentum  $P_x(0) + 2\pi N_F/L_x \pmod{2\pi}$ , due to the Fermi liquid quasiparticles. The state  $\mathbf{W}_m|\Psi'(0)\rangle$  has momentum  $\pi L_y L_z$  relative to  $|\Psi'(0)\rangle$ , since

$$(\mathbf{R}_{T_x})^{-1}(\mathbf{W}_m)^{-1}\mathbf{R}_{T_x}\mathbf{W}_m|\Psi(0)\rangle = (M_{m,e})^{L_y L_z}|\Psi(0)\rangle, \quad (3.35)$$

which can be understood from the relation in Fig. 3.5. On the other hand, we know that

the state  $\mathcal{G}|\Psi(2\pi)\rangle$  has momentum  $P_x(0) + 2\pi\nu L_y L_z \pmod{2\pi}$ . Equating the momenta of  $\mathcal{G}|\Psi(2\pi)\rangle$  and  $\mathbf{W}_v|\Psi(0)\rangle$  and repeating the argument in the other directions yields the topologically enriched Luttinger's theorem

$$\nu - \frac{1}{2} = \frac{V_F}{(2\pi)^3} \pmod{1}. \quad (3.36)$$

In the context of the 3D Kondo model, a fractionalized Fermi liquid phase is realized when the localized spins acquire the 3D bosonic toric code topological order. If the  $U(1)_\uparrow$  and  $U(1)_\downarrow$  symmetries are fractionalized such that  $e$  quasiparticles carry spin- $\frac{1}{2}$ , and the translational symmetry is fractionalized such that an  $e$  (or  $f$ ) occupies each unit cell, then the topologically enriched Luttinger's theorem is

$$\nu_c + \nu_s - 1 = \frac{V_F}{(2\pi)^3} \pmod{2}. \quad (3.37)$$

### 3.5 Discussion

We have extended Oshikawa's arguments to systems that possess SET order. For fractionalized Fermi liquids, this led to a topologically enriched version of Luttinger's theorem. The modified Luttinger's theorem of Eq. (3.2) determines how the presence of topological order can change the Fermi volume. From the opposite perspective, this relation places strict constraints on the possible SET order allowed to manifest in a fractionalized Fermi liquid with an experimentally observed Fermi volume that deviates from the naïve value expected for an ordinary Fermi liquid.

While we have focused on systems whose SET sector and Fermi liquid sector are effectively decoupled, it would be interesting to apply our arguments to other gapless topological systems, e.g.  $\mathbb{Z}_2$  and  $U(1)$  gapless spin liquids. For gapless spin liquids, the

challenge is understanding their symmetry fractionalization and their behavior under flux threading, particularly when there are nontrivial interactions between the gapless topological excitations and the gapless Fermi liquid quasiparticles. In general, it would be interesting to relax our assumption that the SET sector and Fermi liquid sector of a fractionalized Fermi liquid are decoupled. Introducing some interaction that mixes these sectors would drive the system into a weak quasi-topological phase, and may nontrivially modify our results.

Finally, a natural extension of our arguments would be to fully understand their generalization to higher dimensional systems. As mentioned, we expect Eq. (3.2) to hold for a general  $D$ -dimensional fractionalized Fermi liquid, but our ability to establish this relation is limited by the fact that the theory of higher dimensional topological order and symmetry enrichment is not yet fully developed.

# Chapter 4

## Anyonic Entanglement and Topological Entanglement Entropy

### 4.1 Introduction

Entanglement, “the characteristic trait of quantum mechanics” [51], underlies some of the most exotic phenomena in condensed matter physics, including quantum critical points [52, 53], quantum spin liquids [54], and topologically ordered phases of matter [14, 16]. Topological order occurs in gapped, many-body systems whose microscopic degrees of freedom possess daedal entanglement in their ground states. In particular, topological phases exhibit emergent universal phenomena that depend only on the global (topological) properties of the system, making them robust to local perturbations and incapable of being identified by any local probe of the system. Among the most intriguing of such emergent phenomena is the ability to support anyons – quasiparticle excitations with a topological (nonlocal) state space and exotic exchange statistics characterized by braiding [9, 10, 11, 12, 13].

Beyond their fundamental interest as exemplars of the ways nature can give rise to

emergent properties that are not intrinsic to the microscopic degrees of freedom, anyons provide a technologically promising platform for quantum information processing. Topological quantum computing [15, 55, 16], the nonlocal storage and manipulation of quantum information in an anyonic system, is robust against errors due to local perturbations and noise from the environment.

The topological entanglement entropy (TEE) [7, 8] is a signature of topological order that has been the focus of numerous theoretical [48, 56, 57, 58, 59, 60, 61, 62, 63, 64] and numerical studies [65, 66, 67, 68, 69, 70, 71, 72, 73, 74, 75, 76, 77, 78]. Despite these efforts, an intuitive understanding of the origin and form of the TEE has remained elusive and only an inchoate connection between the TEE and the anyonic excitations of the system has been established.

In this work, we examine entanglement and entropy of anyonic systems. In doing so, we demonstrate that TEE is a natural consequence of the conservation of topological charge. We obtain our results using anyon models, which are the algebraic description of the long-ranged, low-energy effective theories of quasiparticles. Mathematically, anyon models are known as unitary modular tensor categories (UMTCs) and apply beyond the context of anyons [12, 79, 13, 18, 19, 80, 81]. We use the formalism for anyonic density matrices developed in Refs. [82, 83]. Our analysis applies to bosonic topological phases of matter on compact, orientable surfaces in two spatial dimensions.

This paper is organized as follows. In Section 4.2, we briefly review classical and quantum entropy. In Section 4.3, we discuss anyonic entanglement, introducing the anyonic entanglement entropy (AEE) and entropy of anyonic charge entanglement, as well as presenting a new derivation of the TEE for a disk in the plane. In Section 4.4, we discuss the state space of anyon models on higher genus surfaces. In Section 4.5, we apply this formalism to derive the TEE on higher genus surfaces. In Section 3.5, we conclude and place our results in the broader context of lattice models, topological defects,

fermionic topological phases, non-orientable surfaces, and three-dimensional topological phases.

## 4.2 Entropy

### 4.2.1 Classical and Quantum Entropies

Entropy is the measure of uncertainty in a state of a physical system. Classically, if an unknown variable  $X$  has value  $x$  with probability  $p_x$ , the Shannon entropy is

$$H(\{p_x\}) \equiv - \sum_x p_x \log p_x. \quad (4.1)$$

The Shannon entropy quantifies our uncertainty in the value of  $X$ , or equivalently, how much information we gain by learning the value of  $X$ .

The classical Rényi entropy of order  $\alpha$  is defined by

$$H_\alpha(\{p_x\}) \equiv \frac{1}{1-\alpha} \log \left( \sum_x p_x^\alpha \right) \quad (4.2)$$

for  $\alpha > 0$ . Note that  $\lim_{\alpha \rightarrow 1} H_\alpha(\{p_x\}) = H(\{p_x\})$ , thus the Rényi entropies may be understood as a generalization of the Shannon entropies. The Rényi entropies are normalized to vanish for a pure state ( $\{p_x\} = \{\delta_{xy}\}$  for some  $y$ ) and to be maximized for a uniform distribution ( $\{p_x\} = \{1/N\}$ ).

Classical entropies can be easily extended to describe quantum states by replacing probability distributions with density matrices and sums with traces over the degrees of freedom in the system. The quantum analogue of the Shannon entropy for a quantum

state  $\rho$  is the von Neumann entropy,

$$S(\rho) \equiv -\text{Tr}(\rho \log \rho), \quad (4.3)$$

which can be re-expressed as the Shannon entropy of the eigenvalues  $\lambda_x$  of  $\rho$ ,

$$S(\rho) = H(\{\lambda_x\}) = -\sum_x \lambda_x \log \lambda_x. \quad (4.4)$$

The quantum Rényi entropy of order  $\alpha$  is similarly generalized as

$$S^{(\alpha)}(\rho) \equiv \frac{1}{1-\alpha} \log[\text{Tr}(\rho^\alpha)]. \quad (4.5)$$

There exist many other entropy-related quantities. The relative entropy measures the closeness of two quantum states  $\rho$  and  $\sigma$ :

$$S(\rho||\sigma) \equiv \text{Tr}(\rho \log \rho) - \text{Tr}(\rho \log \sigma). \quad (4.6)$$

The mutual information measures how much information is shared between two subsystems. That is, if a system with state  $\rho$  has two subsystems  $A$  and  $B$ , then the mutual information is

$$I(A : B) \equiv S(\rho_A) + S(\rho_B) - S(\rho), \quad (4.7)$$

where  $\rho_A = \text{Tr}_B \rho$  and  $\rho_B = \text{Tr}_A \rho$ . Both the relative entropy and the mutual information can be defined for classical probability distributions in the natural way.

### 4.2.2 Entanglement Entropy

Consider partitioning a system into a region  $A$  and its complement  $\bar{A}$ . If we are interested only in  $A$ , then we would like to describe the state with degrees of freedom local to  $A$ , rather than the state of the full system,  $\rho$ . When the Hilbert space of the system admits a factorization

$$\mathcal{H} = \mathcal{H}_A \otimes \mathcal{H}_{\bar{A}}, \quad (4.8)$$

where  $\mathcal{H}_A$  has support in  $A$ , then we can define the reduced density matrix  $\rho_A$  by

$$\rho_A = \text{Tr}_{\bar{A}} \rho. \quad (4.9)$$

The partial trace  $\text{Tr}_{\bar{A}}$  means we sum over all degrees of freedom local to  $\bar{A}$ , essentially retaining only the information associated with  $A$ . For any operator  $O = O_A \otimes O_{\bar{A}}$ , where  $O_A$  has support in  $A$ , the partial trace is the unique operator satisfying  $\text{Tr}(\rho O) = \text{Tr}_A(\rho_A O_A)$  [84].

Note that  $\rho_A$  is a pure state only when  $\rho = \rho_A \otimes \rho_B$  is separable and  $\rho_A = |\psi_A\rangle\langle\psi_A|$ . In general, if there is some entanglement between  $A$  and  $\bar{A}$ ,  $\rho_A$  will be a mixed state. The von Neumann entropy of the reduced density matrix,

$$S(\rho_A) \equiv -\text{Tr}_A[\rho_A \log \rho_A], \quad (4.10)$$

is a measure of this entanglement; it can only decrease when acted upon by operators local to  $A$ . We call  $S(\rho_A)$  the entanglement entropy. If  $\rho$  for the full system is a pure state, then  $S(\rho_A)$  is the unique entanglement measure that is (1) invariant under operators acting only on  $A$ , (2) continuous, and (3) additive when there are several copies of the system.

### 4.2.3 Topological Entanglement Entropy

In a gapped two dimensional system partitioned into regions  $A$  and  $\bar{A}$  with smooth boundaries, the ground state of the  $A \cup \bar{A}$  is expected to have entanglement entropy that scales linearly with the boundary separating  $A$  and  $\bar{A}$ . If the state is topologically ordered, the entanglement entropy will have a universal constant correction to this “boundary law” that is completely determined by topological invariants [48, 7, 8]. The ground state wavefunction of a topological phase on the plane, partitioned into a disk  $A$  and its complement  $\bar{A}$ , has entanglement entropy

$$S_A = \alpha L + S_{\text{topo}} + \mathcal{O}(L^{-1}) \quad (4.11)$$

where  $L$  is the linear size of  $A$ ,  $\alpha$  is a non-universal constant dependent upon the short distance physics of the system, and

$$S_{\text{topo}} \equiv -\log \mathcal{D} \quad (4.12)$$

is the topological entanglement entropy (TEE) [7]. The quantity  $\mathcal{D}$  is the total quantum dimension of the system. For a topological phase whose corresponding TQFT is described by the UMTC  $\mathcal{C}$ , the total quantum dimension is defined by

$$\mathcal{D} = \sqrt{\sum_{a \in \mathcal{C}} d_a^2}, \quad (4.13)$$

where  $d_a$  is the quantum dimension of the anyon with topological charge  $a$  (see C.1 for a review). Eq. (4.11) also holds in the context of string-nets [8, 25, 85], see Section 4.6.1 for further discussion.

At first consideration,  $S_{\text{topo}}$  might seem like a rather crude quantity to use for charac-

| $\mathcal{D}^2$ | UMTCs  |
|-----------------|--|
| 1               | $\mathbb{Z}_1$ (Trivial)   |
| 2               | $\mathbb{Z}_2^{(p)}$ , $p = \frac{1}{2}, \frac{3}{2}$  |
| 3               | $\mathbb{Z}_3^{(p)}$ , $p = 1, 2$  |
| $\phi + 2$      | $\text{Fib}^{\pm 1}$   |
| 4               | $\mathbb{Z}_2^{(1/2)} \times \mathbb{Z}_2^{(3/2)}$ ; $\mathcal{K}_\nu$ , $\nu = 0, 1, \dots, 15$ |
| 5               | $\mathbb{Z}_5^{(p)}$ , $p = 1, 2$  |
| 6               | $\mathbb{Z}_6^{(p)}$ , $p = \frac{1}{2}, \frac{5}{2}, \frac{7}{2}, \frac{11}{2}$                 |
| 7               | $\mathbb{Z}_7^{(p)}$ , $p = 1, 3$  |
| $2(\phi + 2)$   | $\text{Fib}^{\pm 1} \times \mathbb{Z}_2^{(p)}$ , $p = \frac{1}{2}, \frac{3}{2}$                  |

Table 4.1: A TQFT in  $(2 + 1)\text{D}$  is described by a UMTC, which can be classified according to its value of the total quantum dimension  $\mathcal{D}$ . This table lists all distinct UMTCs with  $\mathcal{D}^2 < 8$ , as determined from Refs. [82, 88, 89]. ( $\phi = \frac{1+\sqrt{5}}{2} \approx 1.6$  is the Golden ratio.) For most values of  $\mathcal{D}$ , there are very few possible UMTCs. Moreover, the UMTCs with a given value of  $\mathcal{D}$  are usually very closely related. Additional details may be found in C.2.

terizing a topological phase, as it is a single number. Indeed, other entanglement-based probes of the system, such as the “entanglement spectrum” [86], will generally provide more information about the system. However, topological order is highly constrained, so the information contained in the single number  $S_{\text{topo}}$  can be used, with a bit of algebraic effort, to significantly narrow the field of possibilities when trying to identify a topological phase. Indeed, for many cases, knowing  $S_{\text{topo}}$  is sufficient to completely determine the topological order (up to chirality). To be more specific, in the context of anyon models, if  $N$  refers to the number of anyon types in a theory, one can easily show (from the fusion rules) that  $N \leq \mathcal{D}^2$ . It was shown in Ref. [87] that, for a given rank  $N$ , there are only a finite number of possible UMTCs. It follows that there are only a finite number of possible UMTCs for a particular value of  $\mathcal{D}$ . Moreover, the UMTCs with a given value of  $\mathcal{D}$  are usually very closely related. In Table 4.1, we list all UMTCs for  $\mathcal{D}^2 < 8$ .

Since the seminal works of Refs. [7, 8], TEE has received a significant amount of attention. Theoretical studies have investigated the connections between TEE and ground

state degeneracy [61], derived the TEE for Chern-Simons theories on higher genus surfaces [56, 63], derived TEE for certain systems with topological defects [60], and explored the TEE in the context of  $(3+1)$ -dimensional topological phases [57, 59, 62, 64]. In numerical studies, TEE has become a useful quantity for identifying topological phases [65, 66, 67, 68, 69, 70, 72, 73, 74, 75, 76, 77, 78] (though it has been demonstrated that the accuracy of numerical extractions of TEE requires some caution [68, 71]). Nonetheless, the meaning and origin of  $S_{\text{topo}}$  has remained somewhat nebulous. In this paper, we attempt to demystify these concepts by analyzing entanglement entropy and TEE in the context of anyon models.

Our calculations of the entanglement entropy and the TEE only take into account the long-range physics encoded in the TQFT describing the topological phase. If the system is away from the purely topological, zero correlation length limit, microscopic details of the system will modify the length-dependent terms in Eq. (4.11). However, the universal contribution to the entanglement entropy,  $S_{\text{topo}}$ , will be the same.

For an arbitrary compact, orientable surface (possibly including genus, punctures, and quasiparticles) partitioned into regions  $A$  and  $\bar{A}$ , the entanglement entropy between  $A$  and  $\bar{A}$  takes the form

$$S_A = \sum_{k=1}^N \left( \alpha L_k - \log \mathcal{D} + \sum_c p_c^{(k)} \log d_c \right) + \tilde{S}(\tilde{\rho}_A) + \mathcal{O}(L_k^{-1}), \quad (4.14)$$

where  $k = 1, \dots, N$  labels the connected components of the partition boundary between  $A$  and  $\bar{A}$ ;  $L_k$  is the length of the  $k$ th connected component of the partition boundary;  $\tilde{\rho}_A$  is the anyonic reduced density matrix for region  $A$  (including boundaries);  $p_c^{(k)}$  the probability of the state  $\tilde{\rho}_A$  being in a configuration wherein the  $k$ th joint boundary component carries topological charge  $c$ ;  $d_c$  is the quantum dimension of topological charge  $c$ ; and  $\tilde{S}(\tilde{\rho})$  is the anyonic entropy of the anyonic state  $\tilde{\rho}$ . These quantities will be defined

and explained in detail in this paper.

### 4.3 Anyonic Entropy and Entanglement

We proceed by applying the standard notions of entropy, discussed in Section 4.2, to anyon models, reviewed in C.1. In doing so, we elucidate the unique ways in which entanglement arises in a topologically ordered system. For clarity, we denote an anyonic state (density matrix) and its associated entropy with a tilde;  $\tilde{\rho}$  and  $\tilde{S}(\tilde{\rho})$  respectively.

The anyonic von Neumann entropy is

$$\tilde{S}(\tilde{\rho}) = -\widetilde{\text{Tr}}(\tilde{\rho} \log \tilde{\rho}), \quad (4.15)$$

where  $\widetilde{\text{Tr}}$  denotes the quantum trace, see C.1. In C.3, we prove that the anyonic von Neumann entropy has many of the important properties that the conventional von Neumann entropy has. Moreover, when the state has Abelian total charge, the quantum trace is equivalent to the conventional trace, in which case the anyonic density matrix  $\tilde{\rho}$  is a properly normalized conventional density matrix and  $\tilde{S}(\tilde{\rho}) = S(\tilde{\rho})$ .

The anyonic Rényi entropy is

$$\tilde{S}^{(\alpha)}(\tilde{\rho}) = \frac{1}{1-\alpha} \log \widetilde{\text{Tr}}(\tilde{\rho}^\alpha). \quad (4.16)$$

The relation between the conventional von Neumann and Rényi entropies holds for the anyonic counterparts:

$$\lim_{\alpha \rightarrow 1} \tilde{S}^{(\alpha)}(\tilde{\rho}) = \tilde{S}(\tilde{\rho}). \quad (4.17)$$

### 4.3.1 Pure States and Mixed States

An anyonic state on the sphere (or plane with no topological charge on the boundary) must have trivial total fusion channel. This constraint derives from the conservation of topological charge; a single anyon with nontrivial charge cannot be created from the vacuum. This simple statement has important consequences for anyonic entanglement, which we now explore.

Similar to the conventional quantum states, we define an *anyonic pure state* to be the ones whose anyonic density matrix  $\tilde{\rho}$  has vanishing anyonic von Neumann entropy, or equivalently,  $\widetilde{\text{Tr}}(\tilde{\rho}^2) = 1$ . When  $\widetilde{\text{Tr}}(\tilde{\rho}^2) < 1$ , the anyonic state is mixed.

Our intuition from conventional quantum mechanics can be misleading when applied to anyonic states. As an illustrative example, consider the density matrix of a single anyon with definite charge  $a$ :

$$\tilde{\rho}_a = \frac{1}{d_a} |a\rangle \langle a| = \frac{1}{d_a} I_a = \frac{1}{d_a} \left| \begin{array}{c} \uparrow \\ a \end{array} \right. . \quad (4.18)$$

One can write  $|a\rangle \langle a|$  as  $|a, 0; a\rangle \langle a, 0; a|$  to maintain the proper association of bras and kets with trivalent vertices. At first glance, Eq. (4.18) may appear to be a pure state, as there is no degeneracy in the local state space associated with a single anyon. However, it must be kept in mind that, due to conservation of topological charge, a single anyon cannot truly exist by itself. Such a nontrivial state must be obtained from the state of multiple anyons by tracing out all but one, e.g.,

$$\tilde{\rho}_a = \widetilde{\text{Tr}}_{\bar{a}} \left( \frac{1}{d_a} \begin{array}{c} \begin{array}{c} \nearrow a \\ \searrow \bar{a} \end{array} \\ \begin{array}{c} \nwarrow a \\ \nearrow \bar{a} \end{array} \end{array} \right) = \frac{1}{d_a} \begin{array}{c} \begin{array}{c} \nearrow a \\ \searrow \bar{a} \end{array} \\ \begin{array}{c} \nwarrow a \\ \nearrow \bar{a} \end{array} \end{array} = \frac{1}{d_a} \left| \begin{array}{c} \uparrow \\ a \end{array} \right. . \quad (4.19)$$

If the charge  $a$  of the remaining anyon is non-Abelian, and hence  $d_a > 1$ , this state is not

pure, as can be seen from

$$\widetilde{\text{Tr}} [\tilde{\rho}_a^2] = 1/d_a < 1. \quad (4.20)$$

The remaining single anyon is in an anyonic mixed state as a consequence of the anyonic entanglement it had with the other anyons from the traced out subsystem. This simple example highlights the type entanglement we wish to quantify.

One can check that  $\tilde{S}(\tilde{\rho}_a)$  is nonzero. The anyonic Rényi entropy of  $\tilde{\rho}$  is

$$\begin{aligned} \tilde{S}^{(\alpha)}(\tilde{\rho}_a) &= \frac{1}{1-\alpha} \log \widetilde{\text{Tr}}(\tilde{\rho}_a^\alpha) = \frac{1}{1-\alpha} \log \widetilde{\text{Tr}} \left( \frac{1}{d_a^\alpha} \begin{array}{c} | \\ \hline a \\ \hline | \end{array} \right) = \frac{1}{1-\alpha} \log \left( \frac{1}{d_a^\alpha} \begin{array}{c} \text{hexagon} \\ \hline a \\ \hline \text{hexagon} \end{array} \right) \\ &= \frac{1}{1-\alpha} \log d_a^{1-\alpha} = \log d_a. \end{aligned} \quad (4.21)$$

Taking the (trivial in this example) limit  $\alpha \rightarrow 1$ , we see

$$\tilde{S}(\tilde{\rho}_a) = \log d_a \equiv \tilde{S}_a, \quad (4.22)$$

which is nonzero when  $a$  is non-Abelian. Eq. (4.22) is the anyonic entropy associated with the topological charge  $a$ , due solely to the topological nature of the system. Recall from regular quantum mechanics that a quantum system with a  $d$ -dimensional Hilbert space has  $\log d$  as its maximal von Neumann entropy. From this perspective, one may think of this anyonic entropy as arising from some locally inaccessible internal degrees of freedom of anyons. This is precisely what gives rise to the nonlocal topological state space associated with non-Abelian anyons.

Let  $|\psi_c\rangle$  denote a state with overall topological charge  $c$ . From the above example, we see that an anyonic pure state has anyonic density matrix  $\tilde{\rho}$  that can be written as  $\tilde{\rho} = |\psi_c\rangle\langle\psi_c|$ , such that  $c$  is Abelian. The term “anyonic pure state” is sometimes defined to only include states with trivial overall topological charge 0, but here we expand

the definition to include states with overall Abelian charge, because from the entropic perspective they have all the same properties.

A general state of a system of two anyons can be diagonalized into sectors of distinct charge. Let  $\tilde{\rho}_{AB}$  be the state of a system of two anyons  $A$  and  $B$ , where the capital letters denote that there can be sums over external fusion trees. We can write

$$\tilde{\rho}_{AB} = \sum_{c, \mu_c} \frac{p_{\mu_c}^{AB}}{d_c} |\mu_c\rangle \langle \mu_c| = \sum_{c, \mu_c} \frac{p_{\mu_c}^{AB}}{d_c} \sum_{\substack{a, b, \alpha, \\ a', b', \alpha'}} \frac{\psi_{a, b, c, \alpha}^{(\mu)} \left( \psi_{a', b', c, \alpha'}^{(\mu)} \right)^* \sqrt{d_c}}{(d_a d_b d_{a'} d_{b'})^{1/4}} \begin{array}{c} a \quad b \\ \diagdown \quad \diagup \\ \alpha \\ \diagup \quad \diagdown \\ c \\ \diagdown \quad \diagup \\ a' \quad b' \end{array}, \quad (4.23)$$

where the state vectors

$$|\mu_c\rangle = \sum_{a, b, \alpha} \psi_{a, b, c, \alpha}^{(\mu)} \left( \frac{d_c}{d_a d_b} \right)^{1/4} \begin{array}{c} a \quad b \\ \diagdown \quad \diagup \\ \alpha \\ \diagup \quad \diagdown \\ c \end{array}, \quad (4.24)$$

have coefficients  $\psi_{a, b, c, \alpha}^{(\mu)}$  chosen such that

$$\langle \nu_c | \mu_c \rangle = \sum_{a, b, \alpha} \psi_{a, b, c, \alpha}^{(\mu)} \left( \psi_{a, b, c, \alpha}^{(\nu)} \right)^* \left| \begin{array}{c} a \quad b \\ \diagdown \quad \diagup \\ \alpha \\ \diagup \quad \diagdown \\ c \end{array} \right. = \delta_{\mu, \nu} I_c. \quad (4.25)$$

The decomposition can always be done in terms of vectors  $|\mu_c\rangle$  with definite overall charge  $c$  because superpositions of different values of overall topological charge are always incoherent, i.e. the density matrix is always block diagonal in sectors of distinct overall topological charge  $c$ .

The anyonic von Neumann entropy of  $\tilde{\rho}_{AB}$  is

$$\begin{aligned} \tilde{S}(\tilde{\rho}_{AB}) &= -\partial_\alpha \left( \widetilde{\text{Tr}}(\tilde{\rho}_{AB})^\alpha \right)_{\alpha=1} = -\partial_\alpha \left( \sum_{\mu_c, c} d_c \left( \frac{p_{\mu_c}^{AB}}{d_c} \right)^\alpha \right)_{\alpha=1} \\ &= -\sum_{c, \mu_c} p_{\mu_c}^{AB} \log \left( \frac{p_{\mu_c}^{AB}}{d_c} \right) = \sum_c H(\{p_{\mu_c}^{AB}\}) + \sum_c p_c^{AB} \tilde{S}_c, \end{aligned} \quad (4.26)$$

where

$$p_c^{AB} = \sum_{\mu_c} p_{\mu_c}^{AB} \quad (4.27)$$

is the probability of the state having overall topological charge  $c$ . In particular, the only way for Abelian anyonic states to have nonzero entropy is through incoherent superpositions of the charges of localized anyons, which is just the Shannon entropy of classical origin. This represents the fact that there are no fusion degeneracies to evoke a multidimensional state space for Abelian anyons.

One might be tempted to think of the term

$$\sum_{c, \mu_c} p_{\mu_c}^{AB} \tilde{S}_c \quad (4.28)$$

as the “topological” contribution to the entropy of this system, since it results from the overall charge of the system, and it appears to be the difference between the anyonic entropy and the entropy of a non-anyonic system with orthonormal decomposition coefficients  $p_{\mu_c}^{AB}$ . However, this is a misleading superficiality and one cannot partition the provenance of entropy in this manner. The fusion category structure of anyon models is not a simple tensor product and the topological effects and qualities of the system are subtly encoded throughout the fusion channel description of an anyonic state.

### 4.3.2 Anyonic Entanglement

Having gained some insight from the examples of the previous section, we turn now to characterizations of anyonic entanglement. In ordinary quantum mechanics, entanglement arises from correlations between local degrees of freedom. For example, in the Bell state

$$|\Phi^+\rangle = \frac{1}{\sqrt{2}} (|0\rangle_A \otimes |0\rangle_B + |1\rangle_A \otimes |1\rangle_B) \quad (4.29)$$

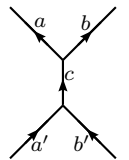
all degrees of freedom of the system are local to either qubit  $A$  or qubit  $B$ , and the state of qubit  $A$  is correlated with that of qubit  $B$ . In a topological phase, the anyonic Hilbert space generally does not admit a tensor product structure. Thus, there exist nonlocal emergent degrees of freedom which cannot be assigned to a particular region, e.g. the total topological charge of a collection of anyons. These nonlocal degrees of freedom arise from topological correlations in the system and imprint signatures in the entanglement of the state.

One probe of the system's topological correlations is the *entropy of anyonic charge entanglement*

$$\tilde{S}_{\text{ace}}(A : B) = \tilde{S}(D_{A:B}[\tilde{\rho}]) - \tilde{S}(\tilde{\rho}), \quad (4.30)$$

where  $D_{A:B}$  is the charge line decoherence superoperator that severs charge lines in the density matrix that connect the subsystems  $A$  and  $B$ .  $D_{A:B}$  may be enacted by a vertical  $\omega_0$ -loop applied to the diagrammatic density matrix that encloses topological charge lines connecting the two regions. This definition of  $\tilde{S}_{\text{ace}}(A : B)$  is intended to extract only the entropy associated directly with the anyonic charge lines that connect the two subsystems  $A$  and  $B$  (as will be made more clear).

More explicitly, if subsystems  $A$  and  $B$  are connected by the diagram (suppressing vertex labels and the fusion trees of anyons within subsystems  $A$  and  $B$ )



$$, \quad (4.31)$$

then  $D_{A:B}$  acts on the system by applying the  $\omega_0$ -loop as shown below [90]:

$$\begin{array}{c} \diagup a \\ \diagdown b \\ \omega_0 \\ \diagup e \\ \diagdown \\ \diagdown a' \\ \diagup b' \end{array} = \sum_e [F_{a'b'}^{ab}]_{ce} \begin{array}{c} a \\ \omega_0 \\ b \\ \diagdown e \\ \diagup \\ a' \\ b' \end{array} = \sqrt{\frac{d_c}{d_a d_b}} \delta_{a,a'} \delta_{b,b'} \begin{array}{c} | \\ a \\ | \\ | \\ b \\ | \end{array}. \quad (4.32)$$

The state  $\tilde{\rho}_{AB}$  has no *anyonic charge entanglement* between subsystems  $A$  and  $B$  if

$$\tilde{\rho}_{AB} \in V_{A'_1, \dots, A'_m}^{A_1, \dots, A_m} \otimes V_{B'_1, \dots, B'_n}^{B_1, \dots, B_n}, \quad (4.33)$$

which implies that  $\tilde{\rho}_{AB} = D_{A:B}[\tilde{\rho}_{AB}]$ . Again, the capital letters imply that there can be sums over external fusion trees. Diagrammatically,  $\tilde{\rho}_{AB}$  can be written such that no nontrivial charge lines connect the anyons of subsystem  $A$  with those of subsystem  $B$  [83].

Alternatively, we can investigate the entanglement using the anyonic analogue to Eq. (4.10). For a state  $\tilde{\rho}_{AB}$  in region  $A \cup B$ , the *anyonic entanglement entropy* (AEE) of  $A$  with  $B$  is

$$\tilde{S}(\tilde{\rho}_A) \equiv -\widetilde{\text{Tr}}(\tilde{\rho}_A \log \tilde{\rho}_A), \quad (4.34)$$

where  $\tilde{\rho}_A = \widetilde{\text{Tr}}_B(\tilde{\rho}_{AB})$  is the reduced density matrix of subregion  $A$ .

The AEE captures all correlations between the two subsystems, while the entropy of anyonic charge entanglement extracts the correlations due to nontrivial dimension of the charge line connecting the two subsystems. This distinction becomes more apparent

when comparing the following three states:

$$\tilde{\rho}_1 \equiv \sum_a p_a \tilde{\rho}_a \otimes \tilde{\rho}_{\bar{a}} = \sum_a \frac{p_a}{d_a^2} \left| a \right\rangle \left| \bar{a} \right\rangle \quad (4.35)$$

$$\tilde{\rho}_2 \equiv \sum_a \frac{p_a}{d_a} \begin{array}{c} \swarrow \bar{a} \\ \searrow a \\ \swarrow a \\ \searrow \bar{a} \end{array} \quad (4.36)$$

$$\tilde{\rho}_3 \equiv \sum_{a,a'} \sqrt{\frac{p_a p_{a'}}{d_a d_{a'}}} \begin{array}{c} \swarrow \bar{a} \\ \searrow a \\ \swarrow a' \\ \searrow \bar{a}' \end{array}. \quad (4.37)$$

By comparing  $\tilde{\rho}_j$  with  $\tilde{\rho}_j^2$ , one can easily check that  $\tilde{\rho}_1$  is a mixed state,  $\tilde{\rho}_2$  is a mixed state unless  $p_a = \delta_{a,b}$  for a particular charge  $b$ , and  $\tilde{\rho}_3$  is a pure state. (We note that when  $p_a = \delta_{a,b}$  for a particular charge  $b$ , the states  $\tilde{\rho}_1$  and  $\tilde{\rho}_2$  can be obtained from each other through the use of an interferometric “forced measurement” procedure [91]. With these operational resources, either of these states may be used as entanglement resources for an anyonic analogue of quantum state teleportation [92, 91].)

The states  $\tilde{\rho}_1$ ,  $\tilde{\rho}_2$ , and  $\tilde{\rho}_3$  have exactly the same reduced density matrix

$$\tilde{\rho}_A = \widetilde{\text{Tr}}_A (\tilde{\rho}_1) = \widetilde{\text{Tr}}_A (\tilde{\rho}_2) = \widetilde{\text{Tr}}_A (\tilde{\rho}_3) = \sum_a \frac{p_a}{d_a} \left| a \right\rangle, \quad (4.38)$$

and, therefore, the same AEE

$$\tilde{S}(\tilde{\rho}_A) = H(\{p_a\}) + \sum_a p_a \tilde{S}_a. \quad (4.39)$$

However, the states have distinct entropy of anyonic charge entanglement:

$$\tilde{S}_{\text{ace}}(\tilde{\rho}_1) = 0 \quad (4.40)$$

$$\tilde{S}_{\text{ace}}(\tilde{\rho}_2) = 2 \sum_a p_a \tilde{S}_a \quad (4.41)$$

$$\tilde{S}_{\text{ace}}(\tilde{\rho}_3) = H(\{p_a\}) + 2 \sum_a p_a \tilde{S}_a. \quad (4.42)$$

Eq. (4.40) is easily seen from the fact that no charge lines connect  $A$  with  $\bar{A}$  in  $\tilde{\rho}_1$ . Eq. (4.41) differs from Eq. (4.42) because, even though  $D_{A:\bar{A}}[\tilde{\rho}_2] = D_{A:\bar{A}}[\tilde{\rho}_3] = \tilde{\rho}_1$ ,  $\tilde{S}(\tilde{\rho}_2) \neq \tilde{S}(\tilde{\rho}_3)$ .

For a slightly more in-depth example of how to calculate  $\tilde{S}(\tilde{\rho})$  and  $\tilde{S}_{\text{ace}}(\tilde{\rho})$ , consider the pure state

$$|\psi\rangle = \sum_{\substack{\vec{a}, \vec{e}, \vec{\mu}, \\ \vec{b}, \vec{f}, \vec{\nu}, c}} \frac{\psi_{\vec{a}, \vec{e}, \vec{\mu}, \vec{b}, \vec{f}, \vec{\nu}, c}}}{(d_{\vec{a}} d_{\vec{b}})^{1/4}} \quad (4.43)$$

For brevity, we write the product of quantum dimension factors as  $d_{\vec{a}} = d_{a_1} d_{a_2} \dots d_{a_n}$  and the index  $\vec{a}$  to mean  $a_1, a_2, \dots, a_n$ ; and use similar abbreviations  $\vec{b}$ ,  $\vec{e}$ ,  $\vec{f}$ ,  $\vec{\mu}$ , and  $\vec{\nu}$ . We calculate the entropy of anyonic charge entanglement between the left charges  $a_i$  and the right charges  $b_i$ .

The decohered state  $D_{A:B} \left[ |\psi\rangle \langle\psi| \right]$  is

$$\begin{aligned}
 D_{A:B} \left[ |\psi\rangle \langle\psi| \right] &= \sum_{\substack{\vec{a}, \vec{e}, \vec{\mu}, \\ \vec{b}, \vec{f}, \vec{\nu}, c \\ \vec{a}', \vec{e}', \vec{\mu}', \\ \vec{b}', \vec{f}', \vec{\nu}', c'}}} \frac{\psi_{\vec{a}, \vec{e}, \vec{\mu}, \vec{b}, \vec{f}, \vec{\nu}, c} \psi_{\vec{a}', \vec{e}', \vec{\mu}', \vec{b}', \vec{f}', \vec{\nu}', c'}^*}{(d_{\vec{a}} d_{\vec{b}} d_{\vec{a}'} d_{\vec{b}'})^{1/4}} \quad \begin{array}{c} \begin{array}{c} a_1 \ a_2 \ \dots \ a_n \ b_n \ b_2 \ b_1 \\ \mu_2 \ e_2 \ \dots \ \mu_n \ \nu_n \\ \swarrow \ \searrow \ \downarrow \ \swarrow \ \searrow \\ \mu_n \ \nu_n \\ \downarrow \ \downarrow \\ c \ \bar{c} \\ \downarrow \ \downarrow \\ \omega_0 \\ \downarrow \ \downarrow \\ \mu_n' \ \nu_n' \\ \swarrow \ \searrow \ \downarrow \ \swarrow \ \searrow \\ \mu_2' \ e_2' \ \dots \ \mu_n' \ \nu_2' \\ \downarrow \ \downarrow \\ c' \ \bar{c}' \end{array} \end{array} \quad (4.44) \\
 &= \sum_{\substack{\vec{a}, \vec{e}, \vec{\mu}, \\ \vec{b}, \vec{f}, \vec{\nu}, c \\ \vec{a}', \vec{e}', \vec{\mu}', \\ \vec{b}', \vec{f}', \vec{\nu}'}} \frac{\psi_{\vec{a}, \vec{e}, \vec{\mu}, \vec{b}, \vec{f}, \vec{\nu}, c} \psi_{\vec{a}', \vec{e}', \vec{\mu}', \vec{b}', \vec{f}', \vec{\nu}', c'}^*}{(d_{\vec{a}} d_{\vec{b}} d_{\vec{a}'} d_{\vec{b}'})^{1/4}} \frac{1}{d_c} \quad \begin{array}{c} \begin{array}{c} a_1 \ a_2 \ \dots \ a_n \ b_n \ b_2 \ b_1 \\ \mu_2 \ e_2 \ \dots \ \mu_n \ \nu_n \\ \swarrow \ \searrow \ \downarrow \ \swarrow \ \searrow \\ \mu_n \ \nu_n \\ \downarrow \ \downarrow \\ c \ \bar{c} \\ \downarrow \ \downarrow \\ \mu_n' \ \nu_n' \\ \swarrow \ \searrow \ \downarrow \ \swarrow \ \searrow \\ \mu_2' \ e_2' \ \dots \ \mu_n' \ \nu_2' \\ \downarrow \ \downarrow \\ c' \ \bar{c}' \end{array} \end{array}
 \end{aligned}$$

The second equality follows from

$$\begin{array}{c} \begin{array}{c} c \ \bar{c} \\ \swarrow \ \searrow \\ \omega_0 \\ \swarrow \ \searrow \\ c' \ \bar{c}' \end{array} = \sum_e \left[ (F_{c'c\bar{c}'}^{-1}) \right]_{0e} \begin{array}{c} c \ \bar{c} \\ \swarrow \ \searrow \\ \omega_0 \\ \swarrow \ \searrow \\ e \\ \downarrow \ \downarrow \\ c' \ \bar{c}' \end{array} = \left[ (F_{c\bar{c}\bar{c}}^{-1}) \right]_{00} \delta_{c,c'} \begin{array}{c} | \\ | \\ c \\ | \\ | \\ \bar{c} \\ | \\ | \\ c \\ | \\ | \\ \bar{c} \end{array} = \frac{\delta_{c,c'}}{d_c} \begin{array}{c} | \\ | \\ c \\ | \\ | \\ \bar{c} \\ | \\ | \\ c \\ | \\ | \\ \bar{c} \end{array}. \quad (4.45)
 \end{array}$$

The entropy of anyonic charge entanglement is

$$\begin{aligned}
 \tilde{S}_{\text{acc}}(|\psi\rangle \langle\psi|) &= \tilde{S} \left( \left[ D_{A:B} |\psi\rangle \langle\psi| \right] \right) - \tilde{S}(|\psi\rangle \langle\psi|) = - \sum_c p_c \log \left( \frac{p_c}{d_c^2} \right) - 0 \\
 &= H(\{p_c\}) + 2 \sum_c p_c \tilde{S}_c, \quad (4.46)
 \end{aligned}$$

where we have defined the probability of the anyons in subsystem  $A$  fusing to  $c$  (or the

anyons in subsystem  $B$  fusing to  $\bar{c}$ ) to be

$$p_c = \sum_{\substack{\vec{a}, \vec{e}, \vec{\mu}, \\ \vec{b}, \vec{f}, \vec{\nu}}} \psi_{\vec{a}, \vec{e}, \vec{\mu}, \vec{b}, \vec{f}, \vec{\nu}, c} \psi_{\vec{a}, \vec{e}, \vec{\mu}, \vec{b}, \vec{f}, \vec{\nu}, c}^* \quad (4.47)$$

We emphasize that the  $\tilde{S}_{\text{ace}}$  has isolated entropic quantities that are solely associated with the anyonic charge lines connecting the subsystems  $A$  and  $B$ : the details of the state within the two subsystems are unimportant, as only the probability of the overall topological charge of each subsystem contributes to  $\tilde{S}_{\text{ace}}$ . Notice that Eqs. (4.46) and (4.42) are identical. The first term in Eq. (4.46) is the classical Shannon entropy of the probability distribution  $\{p_c\}$  associated with the charge  $c$  lines connecting the subsystems  $A$  and  $B$ . The second term, which is nonzero only if at least one of the charge lines connecting subsystems  $A$  and  $B$  is non-Abelian, is the anyonic entropy associated with the charge  $c$  lines themselves.

We can check (e.g. using the method of Lagrange multipliers) that Eq. (4.46) is maximized by  $p_a = d_a^2/\mathcal{D}^2$ , and the corresponding maximum value is

$$\max_{|\psi\rangle} \left[ \tilde{S}_{\text{ace}}(|\psi\rangle\langle\psi|) \right] = 2 \log \mathcal{D}. \quad (4.48)$$

In fact, this is the maximum value of  $\tilde{S}_{\text{ace}}$  for a general (possibly mixed) state whose overall topological charge is trivial. We return to this point in the next section when discussing anyon pair-production.

We now calculate the AEE for the pure state given in Eq. (4.43). Tracing over the  $b$

charges gives the reduced density matrix for the  $a$  charges

$$\tilde{\rho}_A = \sum_{\substack{\vec{a}, \vec{e}, \vec{\mu}, \\ \vec{a}', \vec{e}', \vec{\mu}', \\ \vec{b}, \vec{f}, \vec{v}, c}} \frac{\psi_{\vec{a}, \vec{e}, \vec{\mu}, \vec{b}, \vec{f}, \vec{v}, c} \psi_{\vec{a}', \vec{e}', \vec{\mu}', \vec{b}, \vec{f}, \vec{v}, c}^*}{(d_{\vec{a}} d_{\vec{a}'})^{1/4} \sqrt{d_c}} \quad \cdot \quad \begin{array}{c} a_1 \quad a_2 \quad a_n \\ \swarrow \quad \searrow \quad \nearrow \\ \mu_2 \quad e_2 \\ \downarrow \\ \mu_n \\ | \\ c \\ | \\ \mu'_n \\ \swarrow \quad \searrow \quad \nearrow \\ \mu'_2 \quad e'_2 \\ \downarrow \\ a'_1 \quad a'_2 \quad a'_n \end{array} \quad (4.49)$$

We can define a matrix  $M_c$  whose components are given by

$$[M_c]_{(\vec{a}, \vec{e}, \vec{\mu}), (\vec{a}', \vec{e}', \vec{\mu}')} = \sum_{\vec{b}, \vec{f}, \vec{v}} \psi_{\vec{a}, \vec{e}, \vec{\mu}, \vec{b}, \vec{f}, \vec{v}, c} \psi_{\vec{a}', \vec{e}', \vec{\mu}', \vec{b}, \vec{f}, \vec{v}, c}^* \quad (4.50)$$

Then, one can easily check that

$$\tilde{\rho}_A^\alpha = \sum_{\substack{\vec{a}, \vec{e}, \vec{\mu}, \\ \vec{a}', \vec{e}', \vec{\mu}', \\ c}} \frac{[M_c^\alpha]_{(\vec{a}, \vec{e}, \vec{\mu}), (\vec{a}', \vec{e}', \vec{\mu}')}}{d_c^{\alpha-1} (d_{\vec{a}} d_{\vec{a}'})^{1/4} \sqrt{d_c}} \quad , \quad \begin{array}{c} a_1 \quad a_2 \quad a_n \\ \swarrow \quad \searrow \quad \nearrow \\ \mu_2 \quad e_2 \\ \downarrow \\ \mu_n \\ | \\ c \\ | \\ \mu'_n \\ \swarrow \quad \searrow \quad \nearrow \\ \mu'_2 \quad e'_2 \\ \downarrow \\ a'_1 \quad a'_2 \quad a'_n \end{array} \quad (4.51)$$

from which it follows that

$$\widetilde{\text{Tr}}[\tilde{\rho}_A^\alpha] = \sum_c \frac{\text{Tr}[M_c^\alpha]}{d_c^\alpha} d_c = \sum_{c,j} \left( \frac{\lambda_c^{(j)}}{d_c} \right)^\alpha d_c \quad (4.52)$$

In the last equality, we have defined  $\lambda_c^{(j)}$  to be the  $j$ th eigenvalue of  $M_c$ . Therefore, the AEE is

$$\tilde{S}[\tilde{\rho}_A] = - \sum_{c,j} \lambda_c^{(j)} \log \left( \frac{\lambda_c^{(j)}}{d_c} \right) = \sum_c H(\{\lambda_c^{(j)}\}) + \sum_c p_c \tilde{S}_c \quad (4.53)$$

where in the last equality we have noted that  $\sum_j \lambda_c^{(j)} = p_c$  from Eq. (4.47). The above

result could have equivalently been achieved by first performing a Schmidt decomposition on the state  $|\psi\rangle$ .

Several previous works have investigated anyonic entanglement through the entanglement entropy. Ref. [93] used a skein theory approach to evaluate the bipartite entanglement entropy of a pure state in the context of  $SU(2)_k$  Chern-Simons theory. Ref. [94] defined an operational entanglement measure, based on Eq. (4.10), for bipartite anyonic pure states with vacuum total charge. More generally, Ref. [95] used anyon models to evaluate the AEE on surfaces of arbitrary genus, constructing the reduced density matrix from a given partitioning of a surface. We give an alternative construction in Section 4.4.2. All three of the above-mentioned works identify the second term of Eq. (4.53) as the TEE for an anyonic system. In this paper, we reserve the term TEE for  $S_{\text{topo}} = -\log \mathcal{D}$  of Refs. [7, 8], which cannot be derived using the methods of Refs. [93, 94, 95]. In the next section, we explain how  $S_{\text{topo}}$  may be wheedled out of the anyonic state description.

### 4.3.3 Topological Entanglement Entropy in Anyon Models I

The extraction of the TEE in the context of anyonic states is subtle. Consider a sphere partitioned into two disks: region  $A$  and its complement, region  $\bar{A}$ . In order to obtain the (microscopic) density matrix for the subsystem  $A$ , we trace out the subsystem  $\bar{A}$ . Topologically, we view this as first cutting the system along the partition boundary  $\partial A = \partial \bar{A}$  to yield two disjoint compact systems (disks)  $A$  and  $\bar{A}$ , for which  $\partial A \neq \partial \bar{A}$ , and then tracing out  $\bar{A}$ . When the system is cut into disjoint compact subsystems, each resulting connected genus zero surface must individually have trivial total topological charge. Thus, if the interior of a resulting disk contains topological charge  $c$ , e.g. from a collection of quasiparticles in that region, then its boundary must carry a total topological charge of  $\bar{c}$ .

In the case of the ground state on the sphere, there are no topological excitations in the system, so  $\text{int}(A)$  and  $\text{int}(\bar{A})$  have trivial topological charge ( $c = \bar{c} = 0$ ). Before cutting the surface, the anyonic state representing this configuration is the trivial (vacuum) state, i.e. the empty diagram. If we use the trivial anyonic state  $|0\rangle$ , the corresponding AEE obviously vanishes, so one might naïvely expect the TEE between regions  $A$  and  $\bar{A}$  to also vanish. This deduction is clearly invalid [7, 8].

The resolution to this apparent discrepancy is that a spatial cut of the system is an operation that is both topological and microscopic. That is, a cut has effects on length scales that are large compared to the topological correlation length  $\xi$  and length scales that are small compared to the regularization length  $\ell$ , i.e. the lattice spacing or magnetic length (roughly the correlation length). In particular, degrees of freedom along either side of the spatial partition boundary effectively change from being adjacent to being infinitely separated as a result of a spatial cut (i.e. from strongly-interacting to non-interacting). This process evinces anyonic correlations across the partition boundary that could not be resolved within the uncut system, because they exist below the regularization length, which is why they were not captured by the anyonic state describing the system before cutting. That is, one can think of cutting as locally creating many anyons along the newly created boundaries, but since the total topological charge of each boundary is trivial, there is a projection of the total charge of these anyons along each boundary. In this section, we provide a heuristic description of these subtle anyonic correlations that exist across a spatial partition and explain how the topological charge projection imposed on the partition boundaries by the cutting operation generates the decrease in entropy (increase in order) characterized by the TEE. We will return to a more rigorous derivation of these in Section 4.5.

Since we are interested in the correlations across the partition boundary, let us begin by focusing on the local correlations across the boundary between degrees of freedom in

a small disk-like region  $\mathcal{B}_1$  straddling the partition boundary between  $A$  and  $\bar{A}$ , whose linear size is on the order of the regularization length  $\ell$ . (As a notational note, we will denote regions that do not strictly belong to  $A$ , or which result from a discretization of  $A$ , with calligraphic letters.) We choose  $\mathcal{B}_1$  in this way to represent a short segment of the partition boundary. However, if we cut the system along the partition boundary, then we must similarly partition the region  $\mathcal{B}_1$  along the same partition boundary. For this, we define  $\partial\mathcal{A}_1 = A \cap \mathcal{B}_1$  and  $\partial\bar{\mathcal{A}}_1 = \bar{A} \cap \mathcal{B}_1$ , and wish to consider the correlations between degrees of freedom in regions  $\partial\mathcal{A}_1$  and  $\partial\bar{\mathcal{A}}_1$ . In general, there will be non-universal contributions to the entanglement entropy from the microscopic details of the local correlations. We are, however, interested in extracting the universal contributions to the entanglement entropy, so we focus on the anyonic correlations captured by the anyonic state formalism.

Since we are now considering a region  $\mathcal{B}_1$  whose size is smaller than the resolution length scale, we can heuristically think of the region as being microscopically populated with pair-created anyons; the separation of these anyons is too small to resolve their individual existence, and since they are pair-created from vacuum, the total topological charge within region  $\mathcal{B}_1$  is trivial, as it should be. In this picture, the region  $\partial\mathcal{A}_1$  will contain topological charge  $a_1$  and  $\partial\bar{\mathcal{A}}_1$  will necessarily contain the (pair-created partner) topological charge  $\bar{a}_1$ , with some probability  $p_{a_1}$ . When the entire uncut system is in the ground state, we expect that pair-produced anyons of region  $\mathcal{B}_1$  will be unentangled with regions that are disjoint from  $\mathcal{B}_1$ , so the anyonic correlations between regions  $\partial\mathcal{A}_1$  and  $\partial\bar{\mathcal{A}}_1$  can be represented by a two-anyon pure state. Moreover, we expect the anyonic state representing the local anyonic correlations at the regularization scale to have maximal anyonic charge line entanglement between the two subsystems. Therefore, the density matrix describing quasiparticle pair production is the pure state of Eq. (4.37) with  $p_{a_1} =$

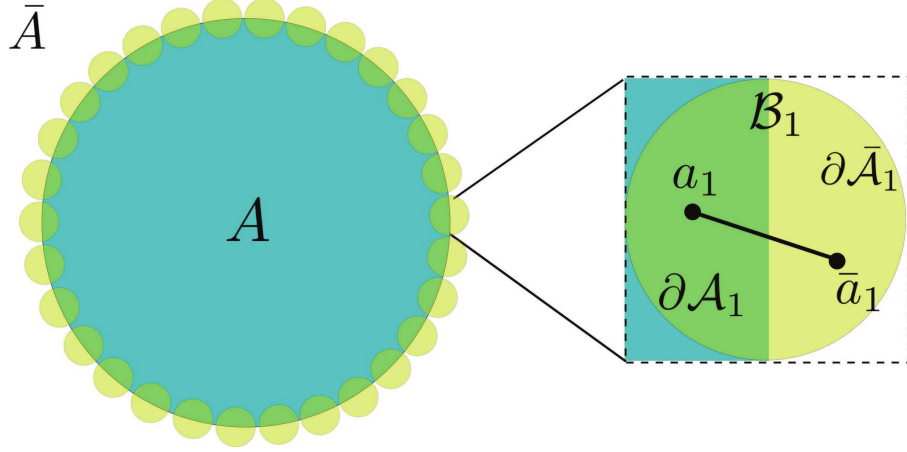


Figure 4.1: The boundary between subsystems  $A$  (blue) and  $\bar{A}$  (white) is covered by a disjoint set of small disk-like regions  $\mathcal{B}_j$  (yellow), each of which is partitioned into subregions  $\partial\mathcal{A}_j$  and  $\partial\bar{\mathcal{A}}_j$ , which are contained in regions  $A$  and  $\bar{A}$ , respectively. Cutting along the partition evinces local anyonic correlations between regions  $\partial\mathcal{A}_j$  and  $\partial\bar{\mathcal{A}}_j$  that can heuristically be thought of in terms of pair-created anyons in a maximally anyonic charge entangled state, which could not be resolved as separate anyons for the uncut system in the ground state. Cutting the system into disconnected, compact regions  $A$  and  $\bar{A}$  imposes a topological constraint that the total topological charge of regions  $A$  is trivial (after the cut). This yields a topological correlation of the boundary anyons of region  $A$ , which is the origin of the TEE  $S_{\text{topo}} \equiv -\log \mathcal{D}$ .

$d_{a_1}^2/\mathcal{D}^2$  [see discussion around Eq. (4.48)]:

$$\tilde{\rho}_{\mathcal{B}_1} = \sum_{a_1, a'_1} \frac{d_{a_1} d'_{a_1}}{\mathcal{D}^2} \frac{1}{\sqrt{d_{a_1} d'_{a_1}}} \begin{array}{c} a_1 \quad \bar{a}_1 \\ \diagdown \quad \diagup \\ \diagup \quad \diagdown \\ a'_1 \quad \bar{a}'_1 \end{array}. \quad (4.54)$$

If we trace out the anyon in region  $\partial\bar{\mathcal{A}}_1$ , the density matrix for region  $\partial\mathcal{A}_1$  is given by

$$\tilde{\rho}_{\partial\mathcal{A}_1} = \widetilde{\text{Tr}}_{\partial\bar{\mathcal{A}}_1}[\tilde{\rho}_{\mathcal{B}_1}] = \sum_{a_1} \frac{d_{a_1}}{\mathcal{D}^2} \left| \begin{array}{c} a_1 \\ \vdots \end{array} \right\rangle. \quad (4.55)$$

We now envision covering the partition boundary  $\partial A$  with similar small disk-like regions  $\mathcal{B}_1, \dots, \mathcal{B}_n$  that are all disjoint from each other, as shown in Figure 4.1. These divide the boundary  $\partial A$  into  $n$  segments  $\partial\mathcal{A}_j = \partial A \cap \mathcal{B}_j$  associated with the local

boundary regions. In this way, the boundary length is roughly  $L \sim n\ell$ . The same description of  $\mathcal{B}_1$  above applies to each region  $\mathcal{B}_j$ . Thus, if we start with the ground state of the uncut system and trace out  $\bar{A}$ , we expect the state of subsystem  $A$  after cutting to have an anyon corresponding to each segment of the discretized boundary, which is similarly described by the reduced density matrix

$$\tilde{\rho}_{\partial\mathcal{A}_j} = \sum_{a_j} \frac{d_{a_j}}{\mathcal{D}^2} \left| \begin{array}{c} a_j \\ \hline \end{array} \right. . \quad (4.56)$$

However, the anyonic reduced density matrix for subsystem  $A$  is not simply given by the tensor product

$$\tilde{\rho}_{\partial\mathcal{A}} \equiv \tilde{\rho}_{\partial\mathcal{A}_1} \otimes \cdots \otimes \tilde{\rho}_{\partial\mathcal{A}_n} \quad (4.57)$$

of those of the local boundary regions  $\partial\mathcal{A}_j$ . The compact region  $A$  must have trivial total topological charge, so it is necessary to apply a projection of the overall topological charge onto the trivial charge. Denoting the anyonic reduced density matrix that takes into account the localized boundary charges as  $\tilde{\rho}_A$ , we have

$$\begin{aligned} \tilde{\rho}_A &\equiv \frac{\Pi_0 \tilde{\rho}_{\partial\mathcal{A}} \Pi_0}{\widetilde{\text{Tr}}[\Pi_0 \tilde{\rho}_{\partial\mathcal{A}} \Pi_0]} = \frac{\Pi_0 (\tilde{\rho}_{\partial\mathcal{A}_1} \otimes \cdots \otimes \tilde{\rho}_{\partial\mathcal{A}_n}) \Pi_0}{\widetilde{\text{Tr}}[\Pi_0 (\tilde{\rho}_{\partial\mathcal{A}_1} \otimes \cdots \otimes \tilde{\rho}_{\partial\mathcal{A}_n}) \Pi_0]} \\ &= \sum_{\bar{a}} \frac{d_{\bar{a}}}{\mathcal{D}^{2n}} \omega_0 \left[ \begin{array}{c} a_1 \ a_2 \ \cdots \ a_n \\ \uparrow \ \uparrow \ \uparrow \ \uparrow \\ \hline \uparrow \ \uparrow \ \uparrow \ \uparrow \\ \hline \end{array} \right] = \sum_{\bar{a}, \bar{e}, \bar{\mu}} \frac{\sqrt{d_{\bar{a}}}}{\mathcal{D}^{2n-2}} \left[ \begin{array}{c} a_1 \ a_2 \ a_3 \ \cdots \ a_{n-1} \ a_n \\ \swarrow \ \searrow \ \swarrow \ \searrow \ \swarrow \ \searrow \\ \mu_2 \ \mu_3 \ \cdots \ \mu_{n-1} \ \bar{a}_n \\ \swarrow \ \searrow \ \swarrow \ \searrow \\ \mu_{n-1} \ \bar{a}_n \\ \swarrow \ \searrow \\ \mu_3 \ \mu_2 \ \cdots \ \mu_3 \ \mu_2 \\ \swarrow \ \searrow \ \swarrow \ \searrow \\ a_1 \ a_2 \ a_3 \ \cdots \ a_{n-1} \ a_n \end{array} \right] . \quad (4.58) \end{aligned}$$

The last equality of Eq. (4.58) is obtained by performing a series of  $F$ -moves to write the

state in a tree-like form, so that the  $\omega_0$ -loop is applied to a single charge line.

It follows that, when taking into account the anyonic correlations along the partition boundary, the anyonic entanglement entropy for the ground state is given by

$$\tilde{S}(\tilde{\rho}_{\mathcal{A}}) = n\tilde{S}(\tilde{\rho}_{\partial\mathcal{A}_j}) - 2\log\mathcal{D}, \quad (4.59)$$

where we have written the anyonic entropy of a single “boundary anyon” as

$$\tilde{S}(\tilde{\rho}_{\partial\mathcal{A}_j}) = -\sum_{a_j} \frac{d_{a_j}^2}{\mathcal{D}^2} \log\left(\frac{d_{a_j}}{\mathcal{D}^2}\right). \quad (4.60)$$

The explicit derivation of  $\tilde{S}(\tilde{\rho}_{\mathcal{A}})$  from  $\tilde{\rho}_{\mathcal{A}}$  will be given in Section 4.5.

A few comments are in order:

1. There is a subtle over-counting in this heuristic description of the anyonic correlations across the boundary that produces twice the actual amount of entanglement entropy between  $A$  and  $\bar{A}$ . After correcting this inadvertent doubling found in Eq. (4.59), the contribution to the entanglement entropy between regions  $A$  and  $\bar{A}$  is given by

$$\tilde{S}_A = \frac{1}{2}\tilde{S}(\tilde{\rho}_{\mathcal{A}}) = \frac{n}{2}\tilde{S}(\tilde{\rho}_{\partial\mathcal{A}_j}) - \log\mathcal{D}. \quad (4.61)$$

We address this point at the end of this section.

2. The first term of Eq. (4.61) describes a linear dependence of the anyonic entanglement entropy on the length  $L$  of the boundary, since  $n \sim L/\ell$ . The boundary length-dependent term  $\alpha L$  of the entanglement entropy Eq. (4.11), in general, will have non-universal contributions from the microscopic details of the physical system. The term  $\frac{n}{2}\tilde{S}(\tilde{\rho}_{\partial\mathcal{A}_j})$  reflects a contribution to this from the topological sector of the theory, for which the non-universal aspect is determined by the short-distance

regularization of the theory, i.e. giving  $\alpha_{\text{topo}} = \frac{1}{2} \tilde{S}(\tilde{\rho}_{\partial\mathcal{A}_j}) \ell^{-1}$ .

3. The second term is the universal  $O(1)$  topological contributions to the entanglement entropy  $S_{\text{topo}} \equiv -\log \mathcal{D}$ , i.e. the term that is independent of the size or shape of the boundary. The origin of this term is the topological constraint that boundary anyons collectively have total topological charge 0. This can be understood from considering the difference between the entropy of the boundary anyons before and after application of the topological charge projection, that is

$$\tilde{S}(\tilde{\rho}_{\partial\mathcal{A}}) - \tilde{S}(\tilde{\rho}_{\mathcal{A}}) = -2S_{\text{topo}} = 2 \log \mathcal{D}. \quad (4.62)$$

Thus, we view  $S_{\text{topo}}$  the reduction in the entanglement entropy due to the topological constraint that the total topological charge of the compact subsystem  $A$  must be trivial (after cutting the original system), which imposes a correlation of the boundary anyons charges. Notice that Eq. (4.62) is the multipartite mutual information between the boundary anyons of regions  $\partial\mathcal{A}_1, \dots, \partial\mathcal{A}_n$ , which is a measure of the correlation between them, or the amount of information that is shared by them. This information is only accessible by considering the boundary regions collectively. From this perspective,  $\mathcal{D}$  can be thought of as the ‘‘dimension’’ of the state space associated with a group of random anyons whose collective topological charge is 0.

When the system is not in the ground state, but has quasiparticle excitations, we can use this argument by including the anyonic state of the quasiparticles. We denote the reduced density matrix describing the quasiparticles in the interior of region  $A$  as  $\tilde{\rho}_{\text{int}(A)}$ . In the case where there is a single quasiparticle of topological charge  $c$  in region  $A$ , we have  $\tilde{\rho}_{\text{int}(A)} = \tilde{\rho}_c$ . Following the same arguments for this case, the anyonic reduced

density matrix (including the localized boundary anyons) for the compact region  $A$  after the cut is

$$\begin{aligned}
\tilde{\rho}_A &\equiv \frac{\Pi_0 (\tilde{\rho}_c \otimes \tilde{\rho}_{\partial A}) \Pi_0}{\widetilde{\text{Tr}} \left[ \Pi_0 (\tilde{\rho}_c \otimes \tilde{\rho}_{\partial A}) \Pi_0 \right]} = \sum_{\bar{a}} \frac{d_{\bar{a}}}{\mathcal{D}^{2n}} \frac{1}{d_c} \omega_0 \begin{array}{c} a_1 \ a_2 \ \dots \ a_n \ c \\ \uparrow \ \uparrow \ \dots \ \uparrow \ \uparrow \\ \hline \uparrow \ \uparrow \ \dots \ \uparrow \ \uparrow \\ \omega_0 \end{array} \\
&= \sum_{\bar{a}, \bar{e}, \bar{\mu}} \frac{\sqrt{d_{\bar{a}}}}{\mathcal{D}^{2n-2} d_c^{3/2}} \begin{array}{c} a_1 \ a_2 \ a_3 \ \dots \ a_n \ c \\ \swarrow \ \searrow \ \swarrow \ \dots \ \swarrow \ \searrow \\ \mu_2 \ e_2 \ \mu_3 \ e_3 \ \dots \ e_{n-2} \ \mu_{n-1} \ \bar{c} \\ \swarrow \ \searrow \ \swarrow \ \dots \ \swarrow \ \searrow \\ \mu_{n-1} \ \bar{c} \ \mu_{n-1} \ \bar{c} \\ \swarrow \ \searrow \ \swarrow \ \dots \ \swarrow \ \searrow \\ \mu_3 \ e_3 \ \mu_2 \ e_2 \ \mu_3 \ e_3 \ \dots \ \mu_2 \ e_2 \ \mu_3 \ e_3 \\ \swarrow \ \searrow \ \swarrow \ \dots \ \swarrow \ \searrow \\ a_1 \ a_2 \ a_3 \ \dots \ a_n \ c \end{array} . \tag{4.63}
\end{aligned}$$

The corresponding anyonic entanglement entropy is given by

$$\tilde{S}(\tilde{\rho}_A) = n\tilde{S}(\tilde{\rho}_{\partial A_j}) + 2S_{\text{topo}} + \tilde{S}_c, \tag{4.64}$$

where  $\tilde{S}_c = \log d_c$  is the anyonic entropy associated with the topological charge  $c$ , as in Eq. (4.22). For anyonic states,  $\tilde{S}_c$  was associated with the system having overall topological charge  $c$ . Here,  $\tilde{S}_c$  is associated with the the topological charge  $\bar{c}$  on the boundary formed by the partition, which is the same thing as the interior of  $A$  having overall topological charge  $c$ .

In the case of a more general configuration of quasiparticles, it is straightforward to see that the reduced density matrix

$$\tilde{\rho}_A \equiv \frac{\Pi_0 (\tilde{\rho}_{\text{int}(A)} \otimes \tilde{\rho}_{\partial A}) \Pi_0}{\widetilde{\text{Tr}} \left[ \Pi_0 (\tilde{\rho}_{\text{int}(A)} \otimes \tilde{\rho}_{\partial A}) \Pi_0 \right]} = \frac{\Pi_0 (\tilde{\rho}_{\text{int}(A)} \otimes \tilde{\rho}_{\partial A_1} \otimes \dots \otimes \tilde{\rho}_{\partial A_n}) \Pi_0}{\widetilde{\text{Tr}} \left[ \Pi_0 (\tilde{\rho}_{\text{int}(A)} \otimes \tilde{\rho}_{\partial A_1} \otimes \dots \otimes \tilde{\rho}_{\partial A_n}) \Pi_0 \right]} \tag{4.65}$$

yields

$$\tilde{S}(\tilde{\rho}_A) = n\tilde{S}(\tilde{\rho}_{\partial A_j}) + 2S_{\text{topo}} + \tilde{S}(\tilde{\rho}_{\text{int}(A)}), \quad (4.66)$$

where  $\tilde{S}(\tilde{\rho}_{\text{int}(A)})$  is the anyonic entanglement entropy of the quasiparticles contained within region  $A$  (before the cut), as defined in Eq. (4.53). For the purposes of separating the contributions of the quasiparticles and the partition boundary to the entanglement entropy, it is useful to write this last term as

$$\tilde{S}(\tilde{\rho}_{\text{int}(A)}) = \sum_c p_c \tilde{S}_c + \tilde{S}(\tilde{\rho}_A), \quad (4.67)$$

where  $p_c$  is the probability of the anyonic state  $\tilde{\rho}_A$  being in a configuration with topological charge  $c$  on the partition boundary.

This leads us to one additional comment:

4. The contribution to the entanglement entropy coming from the quasiparticle content and total topological charge on the partition boundary for region  $A$  is not inadvertently doubled in this heuristic argument, so the total contribution of the anyonic correlations to the entanglement entropy between regions  $A$  and  $\bar{A}$  is given by

$$\tilde{S}_A = \frac{n}{2}\tilde{S}(\tilde{\rho}_{\partial A_j}) + S_{\text{topo}} + \sum_c p_c \tilde{S}_c + \tilde{S}(\tilde{\rho}_A). \quad (4.68)$$

The fallacious doubling of the boundary contribution to the entanglement entropy discussed above resulted from the improper assumption that the local anyonic correlations across the boundary could be represented by localized anyons at fixed locations along the partition boundary in the manner described above. For example, a system in a chiral topological phase on a surface with boundary (e.g. a disk) will have a chiral, gapless CFT on the edge. Unlike in the (gapped) bulk, anyonic excitations on such an edge cannot be localized at a fixed point in space. While the heuristic picture described in this section

is, strictly speaking, incorrect, the concept contains some truth and can be salvaged to represent a doubling of the degrees of freedom. This may be understood from a number of related perspectives.

One of these perspectives, which we will detail and utilize in Section 4.5, stems from the method used in Ref. [7] to derive the TEE. In particular, the Kitaev-Preskill derivation involves (conceptually) introducing a time-reversal conjugate copy of the system and connecting the two systems at various locations by wormholes threaded by trivial topological flux. By locating such wormholes along the partition boundary (which is mirrored on the conjugate copy of the surface), the partition boundary will pass through the wormholes. In the doubled system with wormholes, the partition cut will cut the tubes connecting the (now doubled) regions  $\mathbb{A}$  and  $\bar{\mathbb{A}}$  (respectively corresponding to the un-doubled regions  $A$  and  $\bar{A}$  of the original surface), giving rise to boundaries (the circles along which the tubes are cut) which carry topological charge values. The anyonic state  $\tilde{\rho}_{\mathbb{A}}$  turns out to be equivalent to the anyonic state  $\tilde{\rho}_A$  described above (see Section 4.5 for details). The doubling of the boundary contribution to the entanglement entropy arises in this picture because the system itself was doubled.

This doubling can also be understood in the context of state-sum and string-net models. From this perspective, the Kitaev-Preskill surface doubling is interpreted as representing the two chiral sectors of the emergent TQFT. More specifically, for a (spherical) fusion tensor category  $\mathcal{F}$  that describes the fusion structure of a MTC  $\mathcal{C}$ , the emergent TQFT associated with a state-sum or string-net model based on  $\mathcal{F}$  is the Drinfeld quantum double  $D(\mathcal{F}) = \mathcal{C} \times \bar{\mathcal{C}}$ . One can think of  $\mathcal{C}$  as living on one surface and its time-reversal conjugate  $\bar{\mathcal{C}}$  on another, and the wormholes connecting these surfaces represent the plaquette centers of the string-net lattice model (which is the lattice dual of the state-sum triangulation). In this way, the lattice degrees of freedom on the links, which are described by  $\mathcal{F}$ , are what is captured by the anyonic state  $\tilde{\rho}_A$  at the partition

boundary. As such, the lattice model with degrees of freedom in  $\mathcal{F}$  provides a microscopic regularization and correct accounting of the entropy for the TQFT  $\mathcal{D}(\mathcal{F})$ , which is double that of  $\mathcal{C}$ ; for example,  $\mathcal{D}_{\mathcal{F}} = \mathcal{D}_{\mathcal{C}} = \sqrt{\mathcal{D}_{\mathcal{D}(\mathcal{F})}}$ . (See Section 4.6.1 for more details.)

Another perspective on the boundary entropy doubling comes from considering the boundary degrees of freedom as an edge CFT, e.g. for a chiral topological phase. As mentioned, such an edge cannot localize topological charge at specific locations along the edge. Moreover, one cannot simply break such an edge into segments, as the chiral CFT cannot terminate at the segment endpoints. In order to break the edge into segments in a manner that is well-defined for the CFT, one can use a boundary CFT [96] (“boundary” here refers to the endpoints of a 1D spatial segment on which the  $(1+1)$ D CFT lives, not the 1D boundary of the 2D bulk region). Such boundary CFTs always have both holomorphic and anti-holomorphic modes that are coupled to each other by the boundary conditions, so the edge CFT degrees of freedom are necessarily doubled. This can also be understood as another perspective on the Kitaev-Preskill derivation, wherein doubling the surface and introducing wormholes creates boundary segments on the conjugate surface carrying CFT modes that propagate in the opposite direction as that of the original boundary. In other words, the boundary edge is split up into boundary circles of the tubes connecting regions  $\mathbb{A}$  and  $\bar{\mathbb{A}}$  and the edge segment on the original surface can be viewed as carrying the holomorphic modes while the edge segment on the conjugate surface carries the anti-holomorphic modes.

In Section 4.5, we provide the more rigorous derivation of Eqs. (4.58) and (4.61) using a generalization of the Kitaev-Preskill arguments. This approach requires TQFT methods in which we evaluate anyon diagrams associated with the topological state space of higher genus surfaces. To aid our discussion, we develop the formalism of anyon models for higher genus surfaces in the next section.

## 4.4 Anyon Models for Higher Genus Surfaces

We now generalize the anyon model formalism, reviewed in C.1 for a surface of genus zero, to higher genus, orientable, compact surfaces (possibly with boundary). The genus  $g$  of a surface is the number of handles on it. The topology of an orientable, compact surface is classified by its genus  $g$  and the number  $n$  of punctures, i.e., connected boundary components.

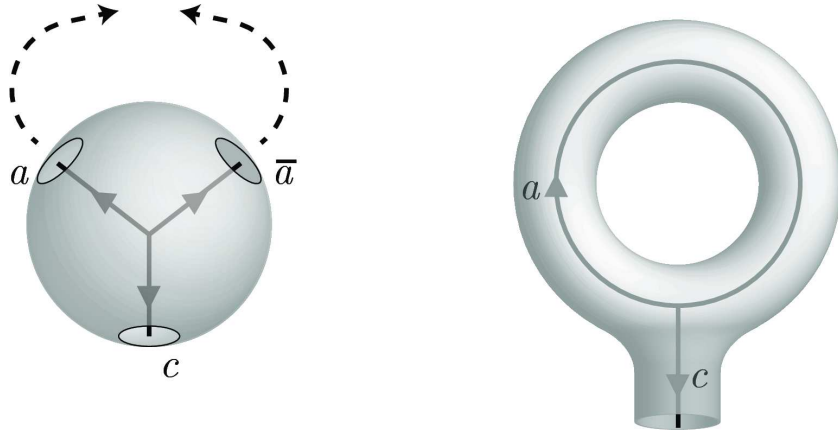
The state space of anyon models on higher genus surfaces has previously been discussed by Ref. [97] and applied to anyonic entanglement in Ref. [95]. Our presentation differs from that of Ref. [97] in notation and normalization conventions, but the fundamental understanding is the same. Our discussion of anyonic entanglement, particularly our derivation of the reduced density matrix, differs from that of Ref. [95].

Ref. [95] focuses on the entanglement of anyonic states associated with the quasiparticles in a subregion of the higher genus surface, rather than the entanglement between different regions of the surfaces. Thus, when partitioning the surface into regions  $A$  and  $\bar{A}$ , Ref. [95] traces over the topological charge lines threading the boundary between  $A$  and  $\bar{A}$ . In our treatment, we wish to examine both the entanglement associated with the anyonic states as well as the entanglement between  $A$  and  $\bar{A}$ . We therefore include the charge lines threading the boundary between  $A$  and  $\bar{A}$  in our reduced density matrix  $\tilde{\rho}_A$ , which is what allows us to calculate  $S_{\text{topo}}$  in Section 4.5.

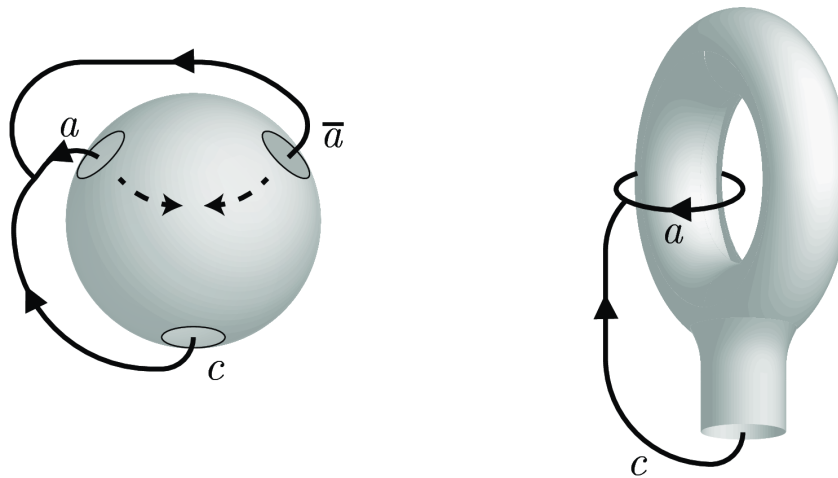
### 4.4.1 Topological State Space of a Higher Genus Surface

The topological Hilbert space of a compact surface with genus  $g$  and  $n$  punctures can be constructed from that of the  $(2g + n)$ -punctured sphere with puncture labels  $a_1, \bar{a}_1, \dots, a_g, \bar{a}_g$  and  $c_1, \dots, c_n$ . The Hilbert space can be spanned by two canonical bases: the “inside” basis and the “outside” basis.

The inside basis is formed by expressing the fusion tree for the punctures inside the sphere and gluing the punctures labeled  $a_1, \dots, a_g$  to their respective punctures labeled  $\bar{a}_1, \dots, \bar{a}_g$  outside the sphere. This leaves all the anyonic charge lines enclosed in the interior of the resulting surface or ending at a remaining puncture.

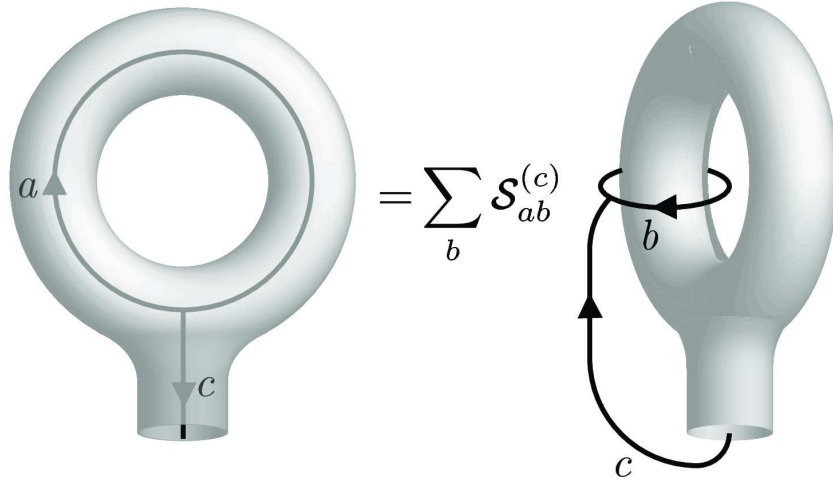


The outside basis is formed by expressing the fusion tree for the punctures outside the sphere and gluing the punctures labeled  $a_1, \dots, a_g$  to their respective punctures labeled  $\bar{a}_1, \dots, \bar{a}_g$  inside (through) the sphere. This leaves all the anyonic charge lines in the region exterior to the resulting surface or ending at a remaining puncture.



The modular  $\mathcal{S}$ -transformations interchange the two complementary cycles associated with a given handle and, thus, provides a basis change between the inside and outside

bases.



In the following, we primarily work with the inside basis.

### Basis

The topological Hilbert space on a sphere is constructed from the fusion and splitting spaces  $V_{ab}^e$  and  $V_e^{ab}$ , see C.1 for a review. These vector spaces are supplemented on a higher genus surface by spaces involving topological charge lines circling non-contractible cycles, which we denote as  $V_e^{(a)}$  and  $V_{(a)}^e$ . The space  $V_e^{(a)}$  is spanned by the vectors

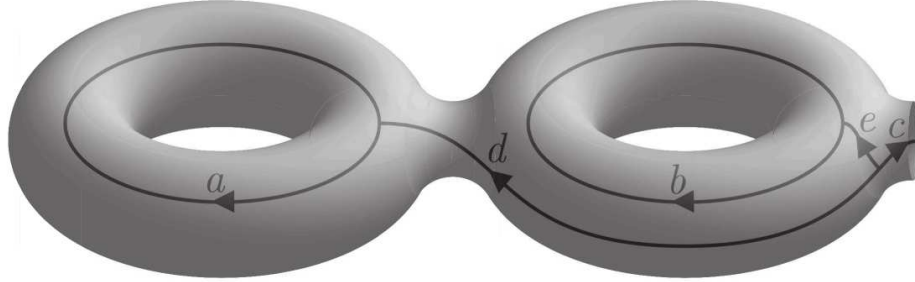
$$|(a); e, \mu\rangle = d_e^{1/4} \begin{array}{c} \diamond \\ \otimes \\ a \\ \mu \\ e \end{array}, \quad (4.69)$$

where  $e$  can be any anyon such that  $N_{a\bar{a}}^e \neq 0$ . The symbol  $\otimes$  represents a non-contractible cycle associated with a handle of the surface, for either the inside or outside basis. The topological charge line  $a$  circling the non-contractible cycle is written in bra/ket notation as  $(a)$  in order to distinguish it from the charges labeling boundaries or quasiparticles.

The dual space  $V_{(a)}^e$  is spanned by the covectors

$$\langle (a); e, \mu | = d_e^{1/4} \begin{array}{c} \uparrow e \\ \mu \\ \diamond \\ \otimes \\ a \end{array}, \quad (4.70)$$

Larger spaces are constructed by taking tensor products. For example, consider the anyonic Hilbert space  $V_0^{(a)(b)c}$  of a genus  $g = 2$  surface with topological charge lines  $a$  and  $b$  wrapping around its two handles and an anyon  $c$  on its surface.



This Hilbert space can be constructed as

$$V_0^{(a)(b)c} \cong \bigoplus_{d,e} V_d^{(a)} \otimes V_e^{(b)} \otimes V_{\bar{c}}^{de} \otimes V_0^{\bar{c}c}, \quad (4.71)$$

which is spanned by the vectors

$$|(a); d, \mu \rangle |(b); e, \nu \rangle |d, e; \bar{c}, \alpha \rangle |\bar{c}, c; 0 \rangle = \frac{1}{d_c^{1/4}} \begin{array}{c} \diamond \quad \diamond \\ \otimes \quad \otimes \\ a \quad b \\ \mu \quad \nu \\ \downarrow \quad \downarrow \\ d \quad e \\ \alpha \quad \bar{c} \\ \downarrow \quad \downarrow \\ c \end{array}, \quad (4.72)$$

where  $\mu = 1, \dots, N_{a\bar{a}}^d$ ,  $\nu = 1, \dots, N_{b\bar{b}}^e$ , and  $d$  and  $e$  are any anyons such that  $N_{a\bar{a}}^d \geq 1$ ,  $N_{b\bar{b}}^e \geq 1$ , and  $N_{d\bar{e}}^{\bar{c}} \geq 1$ .

In general, the space  $V_e^{(z_1)\dots(z_g)a_1\dots a_n}$  for a subsystem containing anyons  $a_1, \dots, a_n$  and

genus  $g$  is spanned by

$$\begin{aligned}
 & |\vec{z}; \vec{x}, \vec{\omega}\rangle |\vec{x}, \vec{y}, \vec{\chi}; d\rangle |\vec{a}, \vec{b}, \vec{\alpha}; c\rangle |d, c; e, \mu\rangle \\
 &= \left(\frac{d_e}{d_{\vec{a}}}\right)^{1/4} \text{Diagram}, \tag{4.73}
 \end{aligned}$$

We only use the bra/ket notation when the system is in the canonical basis written above. When applying  $F$ -moves that take the state out of the canonical basis, the diagrammatic representation of the topological Hilbert space is much easier to use, see e.g., the entropy calculations of Section 4.5.

Finally, we note that, when considering states on compact surfaces, the overall topological charge of each connected component of the surface (including their boundaries) is always the trivial charge 0. We return to this point in Section 4.4.1 when discussing subtleties of performing the partial quantum trace.

## Dimension

The dimension of  $V_0^{(z_1)\dots(z_g)a_1\dots a_n}$  is given by

$$\dim(V_0^{(z_1)\dots(z_g)a_1\dots a_n}) = N_{z_1 \bar{z}_1 \dots z_g \bar{z}_g a_1 \dots a_n}^0, \tag{4.74}$$

The dimension of the space of anyons  $a_1, \dots, a_n$  on a surface with genus  $g$  is

$$\mathcal{N}_{g;a_1\dots a_n} \equiv \sum_{\vec{z}} \dim(V_0^{(z_1)\dots(z_g)a_1\dots a_n}) = \sum_{\vec{z}} N_{z_1 \bar{z}_1 \dots z_g \bar{z}_g a_1 \dots a_n}^0, \tag{4.75}$$

which can also be expressed in terms of the  $\mathcal{S}$ -matrix (see Section C.1.2) as

$$\mathcal{N}_{g;a_1\dots a_n} = \sum_x \left(\frac{d_x}{\mathcal{D}}\right)^{2-n-2g} \mathcal{S}_{a_1x} \dots \mathcal{S}_{a_nx}. \quad (4.76)$$

In particular, if there are no anyons present, then

$$\mathcal{N}_{g;0} = \sum_x \left(\frac{d_x}{\mathcal{D}}\right)^{2-2g} \sim |\mathcal{C}_{\text{Abelian}}| \mathcal{D}^{2g-2} \quad (4.77)$$

for large  $g$ , where  $|\mathcal{C}_{\text{Abelian}}|$  is the number of distinct Abelian topological charges in  $\mathcal{C}$ .

### Inner Product

Inner products of states on surfaces with non-contractible cycles can be evaluated in the diagrammatic representation by cutting open the anyon lines encircling the non-contractible cycle, introducing a factor of  $1/\sqrt{d_a}$  for each anyon line  $a$  that is cut, and then stacking the diagrams. For example, consider a ground state on the torus

$$|(a)\rangle = \begin{array}{c} \diamond \\ \otimes \\ \swarrow \quad \searrow \\ a \end{array} \quad (4.78)$$

In order to compute the inner product of such states in the diagrammatic formalism, we first cut open the diagram, as though we are cutting open the corresponding handle of the surface (the torus), and multiply by a normalization factor for each of the new leaves of the diagram, giving

$$|(a)_{\text{cut}}\rangle = |a, \bar{a}; 0\rangle = \frac{1}{\sqrt{d_a}} \begin{array}{c} a \quad \bar{a} \\ \swarrow \quad \searrow \\ \end{array}. \quad (4.79)$$

Then, the inner product  $\langle(b)| (a)\rangle$  can be expressed as

$$\langle(b)| (a)\rangle = \langle(b)_{\text{cut}}| (a)_{\text{cut}}\rangle = \frac{1}{\sqrt{d_a d_b}} \begin{array}{c} b \quad \bar{b} \\ \swarrow \quad \searrow \\ \text{---} \\ \swarrow \quad \searrow \\ a \quad \bar{a} \end{array} = \delta_{a,b} \frac{1}{d_a} \begin{array}{c} \diamond \\ \swarrow \quad \searrow \\ a \end{array} = \delta_{a,b}. \quad (4.80)$$

In the above, we have included a dashed line to indicate where the topological charge lines were cut and glued together.

Similarly, for the states of a punctured torus,

$$\langle (a); c, \mu | = d_c^{1/4} \begin{array}{c} \uparrow c \\ \mu \\ \diamond \otimes \\ \leftarrow a \end{array}, \quad (4.81)$$

the corresponding states when the handle is cut open are given by

$$|(a)_{\text{cut}}; c, \mu\rangle = |a, \bar{a}; c, \mu\rangle = \left(\frac{d_e}{d_a^2}\right)^{1/4} \begin{array}{c} a \quad \bar{a} \\ \swarrow \quad \searrow \\ \mu \\ \uparrow c \end{array}. \quad (4.82)$$

The inner product of two basis states of the punctured torus is

$$\begin{aligned} \langle (b); e, \nu | (a); c, \mu\rangle &= \langle (b)_{\text{cut}}; e, \nu | (a)_{\text{cut}}; c, \mu\rangle = \left(\frac{d_c d_e}{d_a^2 d_b^2}\right)^{1/4} \begin{array}{c} \uparrow e \\ \nu \\ \diamond \\ \leftarrow b \quad \bar{b} \\ \swarrow \quad \searrow \\ a \quad \bar{a} \\ \mu \\ \uparrow c \end{array} \\ &= \delta_{a,b} \delta_{c,e} \delta_{\mu,\nu} \uparrow^c = \delta_{a,b} \delta_{c,e} \delta_{\mu,\nu} |c\rangle \langle c|. \end{aligned} \quad (4.83)$$

More complicated diagrams can be similarly evaluated. In the general case, each additional endpoint in the diagram (boundary of the surface) of charge  $a$  that results from cutting open a handle requires a normalization factor of  $d_a^{-1/4}$  in the diagrammatic representation of the “cut” state.

## Operators

The space  $V_{(Z'_1)\dots(Z'_g)A'_1\dots A'_n}^{(Z_1)\dots(Z_g)A_1\dots A_n}$  of operators acting on  $n$  anyons on a surface of genus  $g$  can be constructed as

$$V_{(Z'_1)\dots(Z'_g)A'_1\dots A'_n}^{(Z_1)\dots(Z_g)A_1\dots A_n} = \sum_{\vec{z}, \vec{z}', \vec{a}, \vec{a}'} \bigoplus_c V_{(z'_1)\dots(z'_g)a'_1\dots a'_n}^c \otimes V_c^{(z_1)\dots(z_g)a_1\dots a_n}. \quad (4.84)$$

For example, the identity operator acting on the state space of a punctured torus is

$$I = \sum_a I_{(a)} = \sum_{a,c,\mu} |(a); c, \mu\rangle \langle (a); c, \mu| = \sum_{a,c,\mu} \sqrt{d_c} \begin{array}{c} \text{⊗} \\ \text{⋈} \\ \text{⊗} \end{array}. \quad (4.85)$$

## Trace

The trace of an operator involving non-contractible cycles is defined, as usual, to be the sum of its diagonal elements, e.g.

$$\text{Tr}(|(a); c, \mu\rangle \langle (a'); c, \mu'|) = \delta_{a,a'} \delta_{\mu,\mu'}. \quad (4.86)$$

To evaluate the quantum trace  $\widetilde{\text{Tr}}$  for a system with charge lines circling non-contractible cycles, cut open the anyon lines circling the non-contractible cycle, introduce a factor  $1/\sqrt{d_a}$  for every cut charge line  $a$ , and join the outgoing charge lines of the operator's diagram back onto the incoming charge lines. In doing so, we remove the non-contractible cycles, which can be understood as mapping the system to the sphere with certain charge

lines identified [97]. As an example,

$$\begin{aligned}
\widetilde{\text{Tr}}(|(a); c, \mu\rangle \langle (a'); c, \mu'|) &= \widetilde{\text{Tr}}\left(\sqrt{d_c} \begin{array}{c} \text{\textcircled{a}} \\ \text{\textcircled{c}^\mu} \\ \text{\textcircled{a}'} \end{array}\right) = \sqrt{\frac{d_c}{d_a d_{a'}}} \delta_{a,a'} \delta_{\mu,\mu'} \begin{array}{c} \text{\textcircled{a}} \\ \text{\textcircled{c}^\mu} \\ \text{\textcircled{a}'} \end{array} \\
&= d_c \delta_{a,a'} \delta_{\mu,\mu'}.
\end{aligned} \tag{4.87}$$

The above agrees with Eq. (4.86) up to a factor of  $d_c$ . This corresponds to the general relation between the anyonic trace of an operator  $X \in V_{(z'_1)\dots(z'_g)a'_1\dots a'_n}^{(z_1)\dots(z_g)a_1\dots a_n}$  and the ordinary trace, given by

$$\widetilde{\text{Tr}}(X) = \sum_c d_c \text{Tr}([X]_c), \tag{4.88}$$

$$\text{Tr}(X) = \sum_c \frac{1}{d_c} \widetilde{\text{Tr}}([X]_c), \tag{4.89}$$

where

$$[X]_c = \Pi_c X \Pi_c \in V_c^{(z_1)\dots(z_g)a_1\dots a_n} \otimes V_{(z'_1)\dots(z'_g)a'_1\dots a'_n}^c \tag{4.90}$$

is the projection of  $X$  onto definite total charge  $c$ , with  $X = \sum_c [X]_c$ .

One can also compute the partial quantum trace of a surface of genus  $g$  by joining the charge lines and cycles of only the subset of anyons being traced out. First, one must specify which regions of the surface are being traced out, thereby identifying which anyons and cycles are being traced over. In doing so, one is implicitly specifying the path through which one performs the trace over anyonic charge lines<sup>1</sup>. In general, the partial

<sup>1</sup>When considering anyons in a planar surface, one sometimes traces out anyons by “taking the anyons to infinity.” This amounts to moving the anyons to the edge of the diagram by braiding them past other anyons, a process that is not necessarily unique when the partition is not specified. One must be more careful to specify the partition and to keep track of the boundary charges in a connected surface of higher genus, as will be further discussed in the next section.

quantum trace of  $X \in V_{(z'_1)\dots(z'_g)(v'_1)\dots(v'_h)a'_1\dots a'_n b'_1\dots b'_m}$  over the anyons  $b_1, \dots, b_m$  and handles  $v_1, \dots, v_h$  is related to the ordinary partial trace by

$$\widetilde{\text{Tr}}_{(v_1)\dots(v_h)b_1\dots b_m}(X) = \sum_{c,a} \frac{d_c}{d_a} [\text{Tr}_{(v_1)\dots(v_h)b_1\dots b_m}([X_c])]_a, \quad (4.91)$$

$$\text{Tr}_{(v_1)\dots(v_h)b_1\dots b_m}(X) = \sum_{c,a} \frac{d_a}{d_c} [\widetilde{\text{Tr}}_{(v_1)\dots(v_h)b_1\dots b_m}([X]_c)]_a. \quad (4.92)$$

### 4.4.2 Anyonic Density Matrices

An anyonic density matrix is a Hermitian, positive semi-definite anyonic operator normalized by the quantum trace,  $\widetilde{\text{Tr}}\tilde{\rho} = 1$ , that describes the topological state of the system. For any connected component of a compact surface, the overall topological charge, including boundary charges and quasiparticles, is 0. Thus, if one includes the boundaries (and their corresponding topological charges) that arise when tracing out portions of the system, the corresponding anyonic density matrix calculated from the quantum trace is equivalent to the ordinary density matrix calculated from the regular trace.

The anyonic density matrix determines the expectation value of anyonic operators acting on the system,  $\langle X \rangle = \widetilde{\text{Tr}}(\tilde{\rho}X)$ . On a higher genus surface,  $\tilde{\rho}$  can involve anyons living in the bulk or on the boundary of the surface, as well as anyonic charge lines circling non-contractible cycles of the surface.

The reduced anyonic density matrix  $\tilde{\rho}_A$  for a subsystem  $A$  is calculated by taking the partial quantum trace over the degrees of freedom belonging to the complement  $\bar{A}$ . For any operator  $X_A$  acting solely on degrees of freedom in  $A$ ,

$$\langle X_A \rangle = \widetilde{\text{Tr}}(\tilde{\rho}X_A) = \widetilde{\text{Tr}}_A(\tilde{\rho}_A X_A). \quad (4.93)$$

That is, the expectation value of  $X_A$  can be equivalently computed with the density matrix for the full system or with the reduced density matrix for  $A$ .

One must be careful to include boundary charges when computing reduced density matrices for surfaces with genus and multiple boundaries. In Section 4.3, we only considered states on genus zero surfaces with one partition boundary. To compute the reduced density matrix for a region  $A$ , we specified which topological charge lines belonged to  $A$  and which belonged to  $\bar{A}$ , then moved the charge lines in  $\bar{A}$  to the outside of the diagram and joined the incoming and outgoing lines. In doing so, we did not keep track of the charge associated with the boundary of  $A$ , which meant that we sometimes found a density matrix with nontrivial overall charge. This can be reconciled with conservation of topological charge by recognizing that, in the sphere or planar case, one is implicitly specifying a disk-like region  $A$  and tracing out the complementary region  $\bar{A}$ . Since there is a single boundary component for the disk, quasiparticles inside region  $A$  cannot braid with the boundary charge and, as long as the quasiparticles are kept far away from the boundary, they cannot fuse with it either. Therefore, one can safely trace out the boundary charge (or the charge at infinity), since the quasiparticles do not interact with the boundary charge topologically. If one wishes to treat the states of more general systems involving genus and boundaries, one must be careful to only trace out the parts of the states corresponding to regions of the surface that will be considered “inaccessible.”

The following method allows computation of the anyonic reduced density matrix for a region  $A$  on a general compact surface, assuming that the full system is in a pure state  $|\psi\rangle$ :

1. Write the density matrix  $|\psi\rangle\langle\psi|$  for the full system  $A \cup \bar{A}$  in a basis such that the charge lines for each connected component of region  $A$  are grouped together and there is a single charge line threading each boundary component connecting  $A$  with

- $\bar{A}$ .
2. Cut the system along the boundary  $\partial A \cap \partial \bar{A}$  between  $A$  and  $\bar{A}$  to form disjoint compact surfaces  $A$  and  $\bar{A}$ . For each charge line  $a_j$  that is cut, introduce a factor of  $d_{a_j}^{-1/2}$  to normalize the state in the basis  $|\psi_{\text{cut}}\rangle \langle \psi_{\text{cut}}|$ . Each charge line that is cut corresponds to a new pair of boundaries (carrying the corresponding charge) produced by cutting the surface, one of which belongs to  $A$  and the other to  $\bar{A}$ .
  3. Perform a partial quantum trace over the portion of the anyonic state corresponding  $\bar{A}$ . The resulting state  $\tilde{\rho}_A = \widetilde{\text{Tr}}_{\bar{A}} |\psi_{\text{cut}}\rangle \langle \psi_{\text{cut}}|$  is the reduced anyonic density matrix for  $A$ .

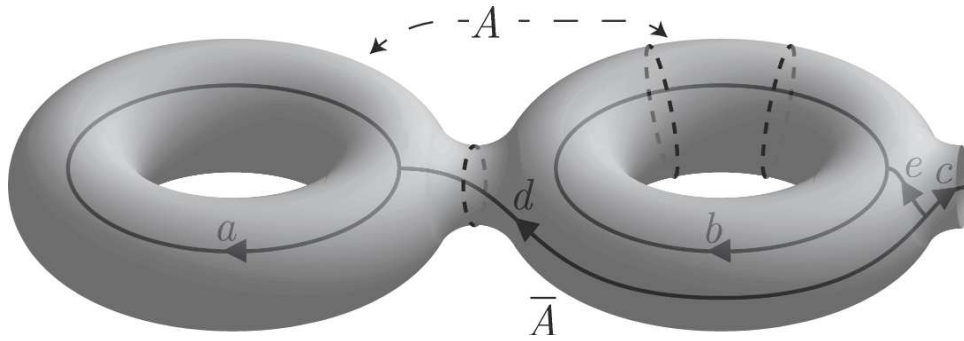
In step 1, the requirement that only one charge line threads each boundary component of  $\partial A$  comes from the TQFT statement that the charge associated with a puncture is equivalent to the charge line threading it. As it is not well-defined to think of multiple charges associated with the same puncture, before we introduce new punctures by cutting the surface, we must apply  $F$ -moves so that there is a single charge line threading each boundary component. In step 2, we again emphasize that each connected component of the surface, both before and after cutting, has total charge 0, when including the boundary charges. As a result, the partial quantum trace in step 3 will be equivalent to the regular partial trace. Our construction of the reduced density matrix differs from that of Ref. [95] in that we do not trace over the (new) boundary charges of  $A$  (see the discussion at the beginning of Section 4.4).

As a demonstrative example, we compute the anyonic reduced density matrices ob-

tained from the state (suppressing vertex labels)

$$|\psi\rangle = \sum_{a,b,c,d,e} \frac{\psi_{a,b,c,d,e}}{d_c^{1/4}} \quad \begin{array}{c} \text{---} \otimes \text{---} \\ \text{---} \otimes \text{---} \\ \text{---} \end{array} \quad (4.94)$$

of a surface with genus  $g = 2$  and  $n = 1$  puncture, when it is partitioned into the regions  $A$  and  $\bar{A}$  indicated by the dashed lines drawn on the surface:



Following the steps outlined above:

1. We write the full density matrix

$$\tilde{\rho} = |\psi\rangle \langle\psi| = \sum_{\substack{a,b,c,d,e \\ a',b',c',d',e'}} \frac{\psi_{a,b,c,d,e} \psi_{a',b',c',d',e'}^*}{(d_c d_{c'})^{1/4}} \quad \begin{array}{c} \text{---} \otimes \text{---} \\ \text{---} \otimes \text{---} \\ \text{---} \\ \text{---} \otimes \text{---} \\ \text{---} \otimes \text{---} \\ \text{---} \end{array} \quad (4.95)$$

2. We cut the surface:

$$|\psi_{\text{cut}}\rangle \langle\psi_{\text{cut}}| = \sum_{\substack{a,b,c,d,e \\ a',b',c',d',e'}} \frac{\psi_{a,b,c,d,e} \psi_{a',b',c',d',e'}^*}{(d_c d_{c'})^{1/4} d_b d_{b'} \sqrt{d_d d_{d'}}}$$
(4.96)

3. We trace over region  $\bar{A}$ :

$$\widetilde{\text{Tr}}_{\bar{A}} \left( \begin{array}{c} \text{Diagram (A)} \\ \text{Diagram (A-bar)} \end{array} \right) = \delta_{b,b'} \delta_{c,c'} \delta_{d,d'}$$
(4.97)

$$= d_b \sqrt{d_c d_d} \delta_{b,b'} \delta_{c,c'} \delta_{d,d'} \delta_{e,e'}$$

to find the reduced density matrix for  $A$ :

$$\tilde{\rho}_A = \widetilde{\text{Tr}}_{\bar{A}} |\psi_{\text{cut}}\rangle \langle\psi_{\text{cut}}| = \sum_{\substack{a,b,c, \\ d,e,a'}} \frac{\psi_{a,b,c,d,e} \psi_{a',b,c,d,e}^*}{d_b \sqrt{d_d}}$$
(4.98)

Alternatively, we can trace over the region  $A$ :

$$\begin{aligned}
 \widetilde{\text{Tr}}_A \left( \begin{array}{c} \text{Diagram 1} \\ \text{Diagram 2} \end{array} \right) &= \frac{\delta_{a,a'} \delta_{d,d'} \delta_{b,b'}}{d_a} \left( \begin{array}{c} \text{Diagram 3} \\ \text{Diagram 4} \end{array} \right) \\
 &= d_b \sqrt{d_d} \delta_{a,a'} \delta_{d,d'} \delta_{b,b'}
 \end{aligned} \tag{4.99}$$

to find the reduced density matrix for  $\bar{A}$ :

$$\tilde{\rho}_{\bar{A}} = \widetilde{\text{Tr}}_A |\psi_{\text{cut}}\rangle \langle \psi_{\text{cut}}| = \sum_{\substack{a,b,c,d,e, \\ c',e'}} \frac{\psi_{a,b,c,d,e} \psi_{a,b,c',d,e'}^*}{d_b \sqrt{d_c d_d}} \left( \begin{array}{c} \text{Diagram 5} \\ \text{Diagram 6} \end{array} \right). \tag{4.100}$$

### 4.4.3 Framing

Finally, when working with anyon models on a higher genus surface it is necessary to specify a framing of the charge lines. That is, charge lines should be thickened into ribbons, so that the diagram accurately keeps tracks of twists in a ribbon. These twists correspond to the phase a particle with fractional statistics picks up when undergoing a  $2\pi$  rotation. There is no canonical choice of framing for a general three manifold. There is, however, a definite law for how partition functions transform under a change of framing, i.e. under the modular  $\mathcal{T}$  transformations, known as Dehn twists. Thus, we must simply pick some framing and be consistent [98]. The framing can be defined as

the continuous map from the topological charge line inside the surface to a projection of the charge line on the surface, which defined a ribbon. One can think of the projection of the line onto the surface as being specified by the path along which quasiparticles were transported and fused in order to generate the corresponding state. Note that a Dehn twist of the surface will put a corresponding twist in the ribbon.

While the framing is technically necessary, we note that it will have no effect on the entanglement entropies we calculate in the following section. Similar to the conventional entanglement entropy of Section 4.2.2, the AEE is only a well-defined entanglement measure if the full system is in a pure state  $\tilde{\rho}_{A\bar{A}} = |\psi\rangle\langle\psi|$ . Writing the Schmidt decomposition of the state as  $|\psi\rangle = \sum_{\alpha} \lambda_{\alpha} |\psi_{\alpha}^A\rangle |\psi_{\alpha}^{\bar{A}}\rangle$ , we see the anyonic reduced density matrix for  $A$  will take the form  $\tilde{\rho}_A = \sum_{\alpha} |\lambda_{\alpha}|^2 |\psi_{\alpha}^A\rangle\langle\psi_{\alpha}^A|$ . The framing keeps track of twists in the diagram, which contribute a phase to the untwisted diagram. This phase of  $|\psi_{\alpha}^A\rangle$  will always be paired with its complex conjugate when considering the density matrix  $\tilde{\rho}_A$ , and thus will cancel out of the AEE calculations. We simplify our expressions in the next section by neglecting the framing, which should be interpreted as some implicit choice having been made.

## 4.5 Topological Entanglement Entropy in Anyon Models II

We are now in a position to compute the AEE for a bipartition of a topological state on a compact orientable surface with arbitrary genus and number of boundaries. Central to our method is the derivation of the reduced density matrix from the partitioning of the surface such that we account for correlations across the boundary. Our approach may be viewed as a generalization of the Kitaev-Preskill derivation of the TEE.

We first review the Kitaev-Preskill method for calculating the TEE, which used a geometric cancellation argument to isolate the TEE from the entanglement entropies of seven geometrically different partitions of the plane into a disk and its complement (we refer the reader to Ref. [7] for more details):

1. Pair the plane with its time-reversal conjugate surface.
2. Join the two surfaces by adiabatically inserting four wormholes that connect the surfaces and gluing the two planes together along a circle at infinity. “Adiabatic insertion” means that the system remains in its ground state during the entire process of inserting the wormholes. Thus, an anyon circling a wormhole should detect no difference from an anyon circling a region in the plane containing no topological excitations, i.e., each wormhole is threaded by a trivial topological charge line. The location of the wormholes corresponds to the “corners” of the different disk partitions of the plane.
3. For each choice of geometric partition, cut the surface along the partition boundary, which now runs along the regions between wormholes, i.e. around the tubes connecting the different partition regions. A partition cut divides the surface into disjoint compact, orientable surfaces with either three or four punctures, depending on the choice of partition.
4. Compute the state (reduced density matrix) and entanglement entropy of the resulting surfaces using standard TQFT methods. More specifically, this involves rewriting the state of the uncut doubled system in a basis that is more suitable to the ensuing cut by (a) applying modular  $\mathcal{S}$ -transformations to rewrite the trivial charge line through each wormhole as an  $\omega_0$ -loop circling the throat of the wormhole, and (b) applying  $F$ -moves to all the topological charge lines threading the

tubes that will be cut, so that there is a single topological charge line threading each boundary component generated by the partition cut (i.e. to obtain the basis states in which each resulting puncture has a definite value of topological charge).

5. Add and subtract the entanglement entropies of the seven geometric partitions such that their linear dependence cancels and the topological contribution survives.

We generalize the Kitaev-Preskill method to enable the computation of all topological contributions to the entanglement entropy, including the TEE and anyonic entanglement, for any compact region  $A$  of a 2D topological phase living on a compact, orientable surface  $M$  with any genus and number of punctures and/or quasiparticles using the following steps, which will be illustrated in detail for several examples:

1. Pair the surface  $M$  with its time-reversal conjugate  $M^*$ . (When embedded in 3D, we assume the original surface is enclosed by the conjugate surface.)
2. Adiabatically insert  $n$  wormholes along the original partition boundary  $\partial A$ . Each wormhole is threaded by a trivial topological charge line. The system will now look like two parallel surfaces connected by a series of tubes.<sup>2</sup> We denote this new surface by  $\mathbb{M}$  and the doubled regions corresponding to  $A$  and  $\bar{A}$  of the un-doubled system are denoted by  $\mathbb{A}$  and  $\bar{\mathbb{A}}$ , respectively. The partition boundary  $\partial\mathbb{A}$  has  $n$  connected components, each running along the regions between two wormholes, i.e. around the tubes connecting  $\mathbb{A}$  and  $\bar{\mathbb{A}}$ .
3. Cut  $\mathbb{M}$  along the partition boundary  $\partial\mathbb{A}$ . The partition cut divides the surface into disjoint compact, orientable surfaces  $\mathbb{A}$  and  $\bar{\mathbb{A}}$ , each of which obtains  $n$  new punctures from the cut, corresponding to the boundary components where regions  $\mathbb{A}$  and  $\bar{\mathbb{A}}$  were formerly connected.

---

<sup>2</sup>Not a big truck. [99]

4. Compute the state (reduced density matrix) and AEE entropy of the resulting surface  $\mathbb{A}$ . More specifically, this involves rewriting the state of the uncut doubled system in a basis that is more suitable to the ensuing cut by (a) applying modular  $\mathcal{S}$ -transformations to rewrite the trivial charge line through each wormhole as an  $\omega_0$ -loop circling the throat of the wormhole, and (b) applying  $F$ -moves to all the topological charge lines threading the tubes that will be cut, so that there is a single topological charge line threading each boundary component generated by the partition cut.
5. Taking  $n$  large,<sup>3</sup> the AEE of region  $\mathbb{A}$  will exhibit a term that is linear in  $n$ , which is identified as the contribution that is linear in the boundary length, and a constant term, which is identified as the topological contribution. The contributions from the boundary (i.e. the linear term and the TEE) are divided by two for the contribution to the entanglement entropy of  $A$ , the original (un-doubled) system.

Given the topological reduced density matrix for region  $\mathbb{A}$ , the AEE can be evaluated using the anyonic formalism discussed in Section 4.4. When there are punctures and/or quasiparticles in the system, one can choose whether or not to also double this content of the system, as long as one is careful to correctly attribute the corresponding contributions when accounting for the doubling. Similarly, if there is genus, one can choose different states (topological charge lines winding around the non-contractible cycles). We will utilize these options in our analysis when it simplifies the computations.

When writing the topological state of the doubled system with wormholes, one must be careful to identify the correct total number of non-contractible cycles of the surface  $\mathbb{M}$ . On the doubled infinite plane, there is a one-to-one correspondence between wormholes and non-contractible cycles. However, on the doubled sphere, the first wormhole inserted

---

<sup>3</sup>Taking  $n$  large corresponds to inserting as many wormholes along the boundary as possible. In other words, one inserts roughly one wormhole per regularization length, so  $n \sim L/\ell$ , as before.

does not create a non-contractible cycle, but simply yields the “connected sum” of the two spheres, which is a single sphere. Each subsequent wormhole inserted will then increase the genus of the resulting surface by one. A consequence of this is the the normalization on the doubled sphere will differ from the normalization on the doubled plane by a factor of  $\mathcal{D}$ , when written with  $\omega_0$ -loops encircling every wormhole. More generally, when we double a connected, compact surface of genus  $g$  and insert  $n$  wormholes attaching the doubled surfaces, the resulting surface will have genus  $2g + n - 1$ . This is, again, because the first wormhole inserted simply creates a connected sum of the two surfaces, and each subsequent wormhole increases the genus by one. We will restrict our attention to compact surfaces in order to make the analysis more rigorous, but similar methods can be used for non-compact surfaces.

One might be worried that inserting a large number of closely spaced wormholes would introduce non-contractible cycles whose lengths are too small to provide topological protection of the corresponding state degeneracies associated with them. In particular, if a cycle in  $\mathbb{M}$  is not long compared with the correlation length  $\xi$ , non-universal microscopic effects will generically lead to an energy splitting that favors different values of topological charge lines threading that cycle. This is, however, not a problem for our construction for the following reasons. The potentially small cycles introduced by inserting the wormholes are  $L_{\text{throat}}$ , the circumference of a given wormhole’s throat, and  $L_{\text{tube}}$ , the circumference of the tubes connecting regions  $\mathbb{A}$  and  $\bar{\mathbb{A}}$ . It is perfectly acceptable for  $L_{\text{throat}}$  to be small, because we are already requiring a specific value of topological charge line threading the throat of the wormhole, namely the trivial charge 0. As long as the Hamiltonian of the system is such that trivial charge line threading the wormhole is energetically favored by the adiabatic insertion of the wormhole, its throat circumference can be arbitrarily small (meaning down to the regularization length). In fact, this condition may be viewed as part of the definition of the process of adiabatically inserting a wormhole. On the

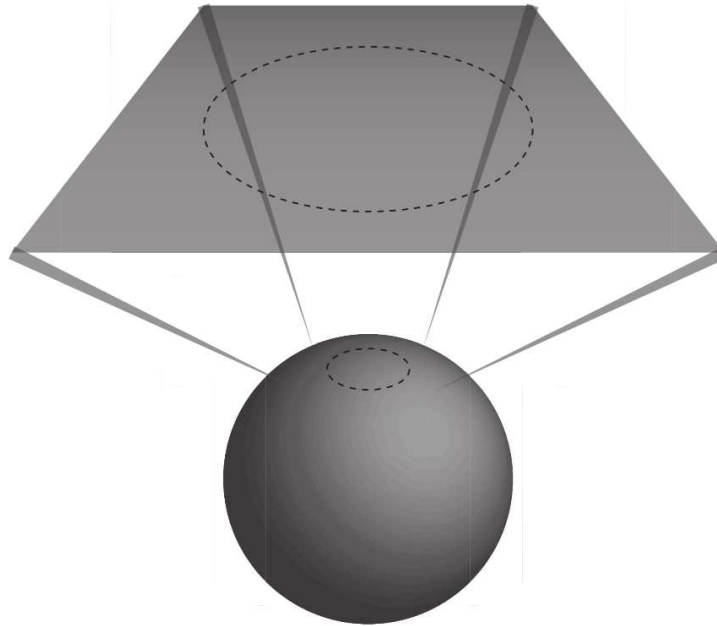
other hand, it is important that  $L_{\text{tube}}$  be much larger than  $\xi$ , because the ground state of  $\mathbb{M}$  will require superpositions of the values of topological charge line threading these cycles. At first glance, one might think that this should dissuade us from inserting wormholes separated by a distance  $d \approx \ell$ . However, the circumference of the tube is roughly  $L_{\text{tube}} \sim d + h$ , where  $h$  is the “height” of the wormholes, i.e. the spacing between conjugate surfaces. Since we are free to choose  $h$ , we can let it be arbitrarily large, which allows us to also have arbitrarily small  $d$  without sacrificing the necessary topological degeneracy.

There are several benefits of the method we present: (1) It applies beyond the ground state, to states containing anyonic excitations, i.e., boundaries and/or quasiparticles carrying topological charge. (2) It makes the origin of the TEE more explicit. (3) It captures the topological contribution to the boundary law term in the entanglement entropy. (4) It may be used to extract the TEE from the Rényi entropy for arbitrary topological phases.

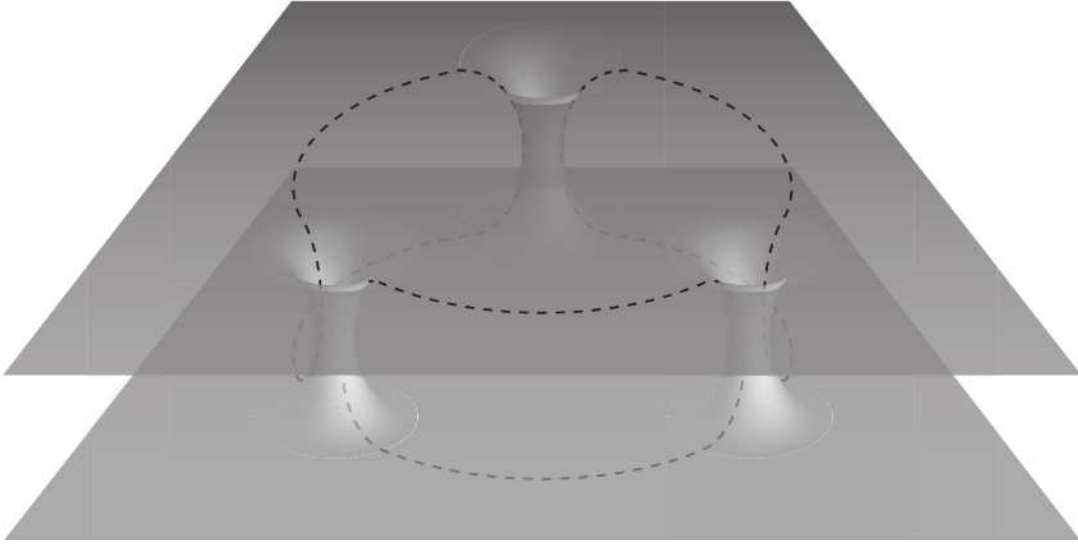
In this section, we use our method (described above) to calculate the topological contribution to the entanglement entropy. We first illustrate the approach in the simplest example of the ground state on a sphere partitioned into two disks, Section 4.5.1. We analyze this example in greater detail than subsequent examples, as it exhibits most of the crucial methodology that will be repeated. In Sections 4.5.2-4.5.5, we apply the same method to an excited state of a disk cut from the sphere, an annulus cut from the sphere, an annular segment cut from the torus, and a 3-punctured sphere cut from the sphere. In Section 4.5.6, we discuss the general form of the entanglement entropy for a subregion of a compact, orientable surface of arbitrary genus and number of punctures/quasiparticles.

### 4.5.1 Sphere Partitioned into Two Disks

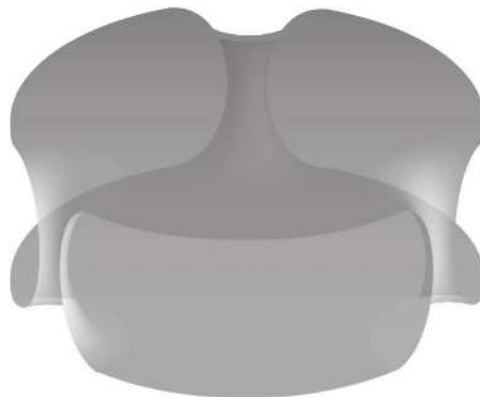
Before diving into the derivation of the reduced density matrix, we first comment on how to visualize the surfaces discussed in this section. Consider a sphere partitioned into two disks,  $A$  and  $\bar{A}$ . For ease of illustration, we zoom in so that locally the surface looks planar.

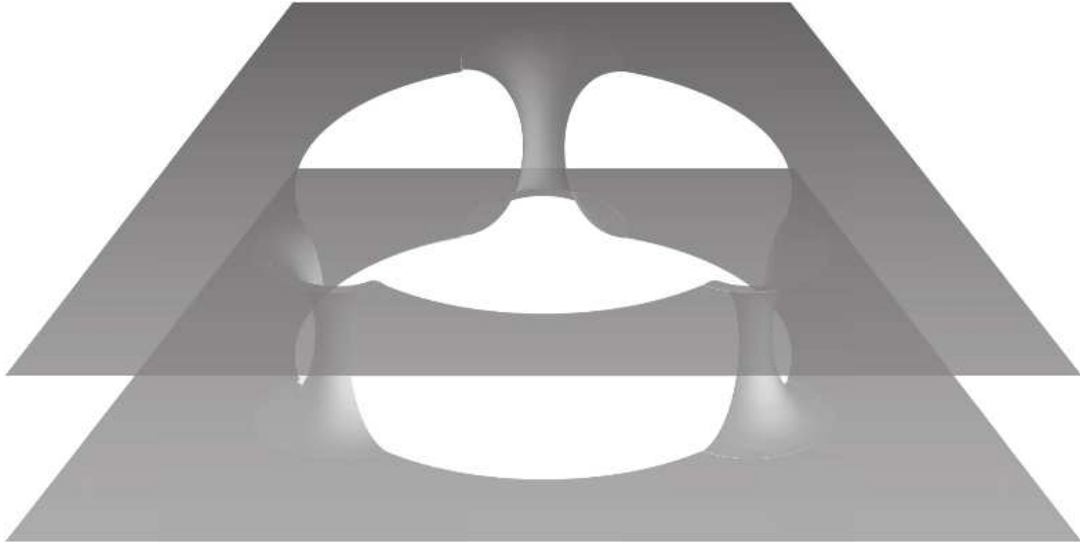


We pair the original surface  $M$  with its time-reversal conjugate  $M^*$ , and join the two surfaces by adiabatically inserting  $n$  wormholes along the partition boundary separating  $A$  from  $\bar{A}$ . The resulting surface  $\mathbb{M}$  has genus  $g = n - 1$ .



Here, we show the case with  $n = 3$  wormholes. The partition boundary is now broken into segments, each of which runs between two wormholes and pass through the wormholes between the upper layer region of  $\mathbb{M}$  and the lower layer region, as indicated in the above by dashed lines. In order to find the reduced density matrix for the doubled region  $\mathbb{A}$ , we cut the surface along the new partition boundary, resulting in the following surfaces for  $\mathbb{A}$  and  $\bar{\mathbb{A}}$ :



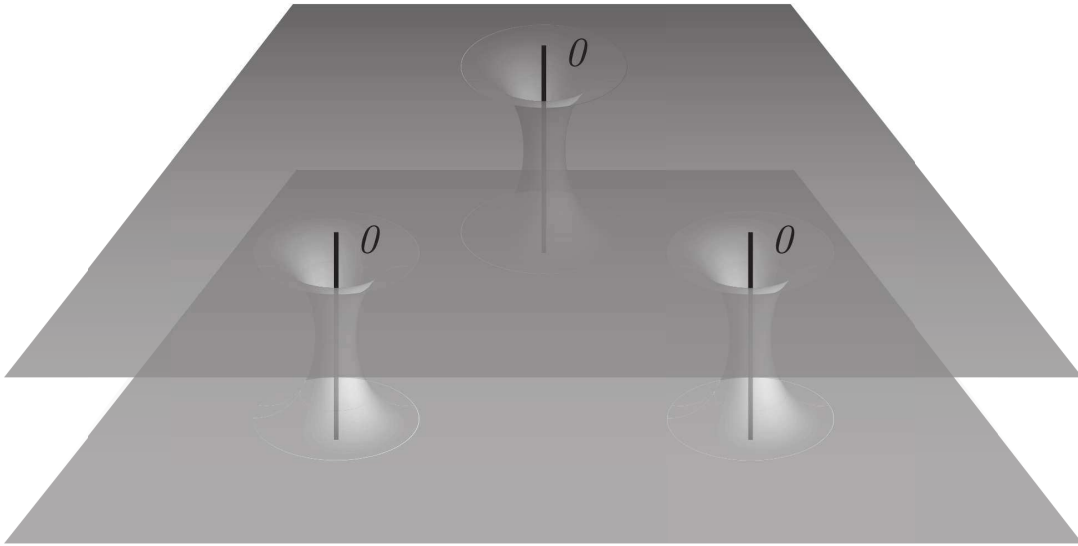


Each of these regions are topologically equivalent to a sphere with  $n$  punctures:

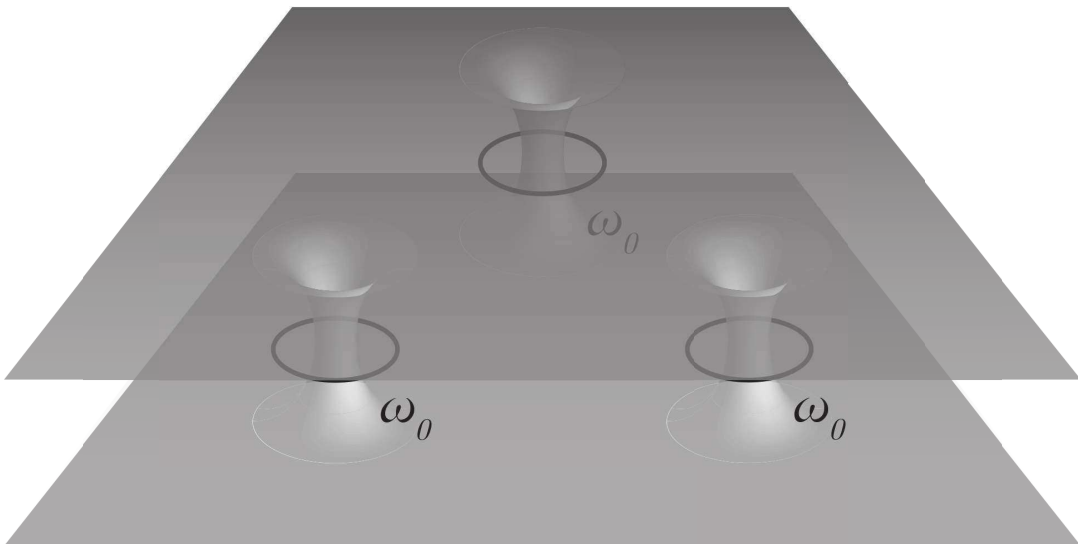


In the remainder of this section, we will omit the dashed lines indicating the partition boundary in the pictures of the surfaces, but we will include them in the corresponding anyon diagram representation of the state.

Having oriented ourselves to what the three-dimensional embedding of our surfaces look like, we are now ready to derive the corresponding anyonic reduced density matrix for  $\mathbb{A}$ . First, recall that adiabatic insertion implies that each wormhole is threaded by a trivial topological charge line.



We can use the modular  $\mathcal{S}$ -transformation to rewrite the topological charge line threading a given wormhole in terms of an  $\omega_0$ -loop circling the throat of that wormhole, up to an overall normalization factor of the state, essentially converting between the inside and outside bases (see Section 4.4.1).



This claim is justified by first isolating a given wormhole of the surface (when there is more than one wormhole), which locally takes the form of a punctured torus with charge line  $0$  through the handle. Next, one can apply the modular  $\mathcal{S}$ -transformation for a

punctured torus, described in Section 4.4.1. When the topological charge threading the handle is  $b = 0$  for a punctured torus, the charge on the puncture it is necessarily  $c = 0$ , i.e. the punctured torus state in the outside basis is  $| (0); 0 \rangle_{\text{outside}}$ . Applying the modular  $\mathcal{S}$ -transformation to the punctured torus state in the outside basis gives the state in terms of the inside basis

$$| (0); 0 \rangle_{\text{outside}} = \sum_a \mathcal{S}_{0a} | (a); 0 \rangle_{\text{inside}} = \sum_a \frac{d_a}{\mathcal{D}} | (a); 0 \rangle_{\text{inside}}, \quad (4.101)$$

which is the same as representing the state by having an  $\omega_0$ -loop circling the throat of that wormhole, up to an overall normalization factor. Thus, the state of the system can be re-expressed in the basis represented by topological charge lines that thread the region inside the surface  $\mathbb{M}$ .

Using the diagrammatic formalism, we can write the state as

$$|\psi\rangle = \mathcal{D}^{n-1} \begin{array}{c} \begin{array}{ccc} \omega_0 \circlearrowleft & \cdots & \omega_0 \circlearrowleft \\ \omega_0 \circlearrowleft & & \omega_0 \circlearrowleft \\ \omega_0 \circlearrowleft & \cdots & \omega_0 \circlearrowleft \end{array} \end{array}, \quad (4.102)$$

where the dashed line indicates the partition boundary, and we have introduced the notation  $\circlearrowleft$  to represent the throats of the wormholes around which the  $\omega_0$ -loops wind. This notation will be more convenient than expressing the state in terms of the non-contractible cycles associated with the genus, because the ensuing boundary partition cut is more naturally represented with respect to the wormholes. It is, however, straightforward to represent this state using the non-contractible cycles associated with the genus, and doing so makes clear the extra factor of  $\mathcal{D}^{-1}$  necessary for proper normalization. In particular, because the genus of the surface is  $g = n - 1$  (see the discussion at the begin-

ning of Section 4.5), one of the  $\omega_0$ -loops encircling a wormhole is redundant. This can be seen using the handle-slide property of the  $\omega_0$ -loop, which states that a topological charge line may be passed through a nontrivial cycle (or other charge lines) if the cycle is encircled by an  $\omega_0$ -loop:

$$(4.103)$$

One of the  $\omega_0$ -loops circling a wormhole can be deformed around the surface using handle-slide moves until it encircles nothing and can then simply be removed. If we treat that same wormhole as the one that is not contributing to the genus (i.e. the one responsible for first connecting the conjugate surfaces  $M$  and  $M^*$ ), then the state may be re-expressed in the notation of Section 4.4 for the state of a genus  $g = n - 1$  surface as

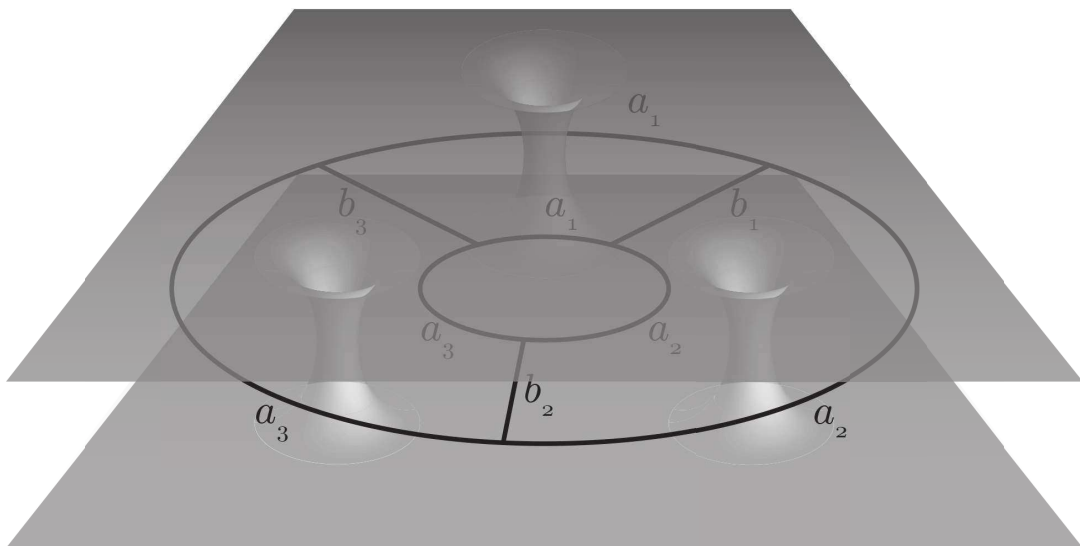
$$\begin{aligned}
 |\psi\rangle &= \mathcal{D}^{n-1} \omega_0 \begin{array}{c} \circlearrowleft \\ \otimes \end{array} \omega_0 \begin{array}{c} \circlearrowleft \\ \otimes \end{array} \cdots \omega_0 \begin{array}{c} \circlearrowleft \\ \otimes \end{array} \\
 &= \mathcal{D}^{n-1} \omega_0 \begin{array}{c} \circlearrowleft \\ \otimes \end{array} \cdots \omega_0 \begin{array}{c} \circlearrowleft \\ \otimes \end{array} \\
 &= \sum_{x_1, \dots, x_{n-1}} \frac{d_{x_1} \cdots d_{x_{n-1}}}{\mathcal{D}^{n-1}} x_1 \begin{array}{c} \circlearrowleft \\ \otimes \end{array} \cdots x_{n-1} \begin{array}{c} \circlearrowleft \\ \otimes \end{array} .
 \end{aligned} \tag{4.104}$$

Deforming the wormhole representation of the state of Eq. (4.102) and using Eq. (C.23), we can fuse together the charge lines threading the same boundary region, so that it is

expressed as (suppressing the fusion vertex labels)

$$\begin{aligned}
 |\psi\rangle &= \mathcal{D}^{n-1} \text{ (diagram with } \omega_0 \text{ labels)} \\
 &= \frac{1}{\mathcal{D}} \sum_{\vec{a}} \frac{d_{\vec{a}}}{\mathcal{D}^n} \text{ (diagram with } a_1, a_2, \dots, a_n \text{ labels)} \\
 &= \frac{1}{\mathcal{D}} \sum_{\vec{a}, \vec{b}} \frac{\sqrt{d_{\vec{b}}}}{\mathcal{D}^n} \text{ (diagram with } a_i, b_i \text{ labels)} .
 \end{aligned}
 \tag{4.105}$$

The corresponding anyon diagram embedded in three dimensions looks like



We can rewrite the state in a tree-like form using a series of  $F$ -moves <sup>4</sup>:

$$\begin{aligned}
|\psi\rangle &= \sum_{\vec{a}, \vec{b}, e_2, e'_2} \frac{\sqrt{d_{\vec{b}}}}{\mathcal{D}^{n+1}} [F_{a_3}^{a_1 b_1 b_2}]^\dagger_{e'_2 a_2} [F_{a_3}^{a_1 b_1 b_2}]_{a_2 e_2} \text{Diagram 1} \\
&= \sum_{\substack{a_1, a_3, \dots, a_n \\ \vec{b}, e_2, e'_2, e_3, e'_3}} \frac{\sqrt{d_{\vec{b}}}}{\mathcal{D}^{n+1}} \delta_{e_2, e'_2} [F_{a_4}^{a_1 e'_2 b_3}]^\dagger_{e'_3 a_3} [F_{a_4}^{a_1 e_2 b_3}]_{a_3 e_3} \text{Diagram 2} \\
&= \sum_{a_1, \vec{b}, \vec{e}} \frac{\sqrt{d_{\vec{b}}}}{\mathcal{D}^{n+1}} \text{Diagram 3} = \sum_{\vec{b}, e_2, \dots, e_{n-2}} \frac{\sqrt{d_{\vec{b}}}}{\mathcal{D}^{n-1}} \text{Diagram 4}
\end{aligned} \tag{4.106}$$

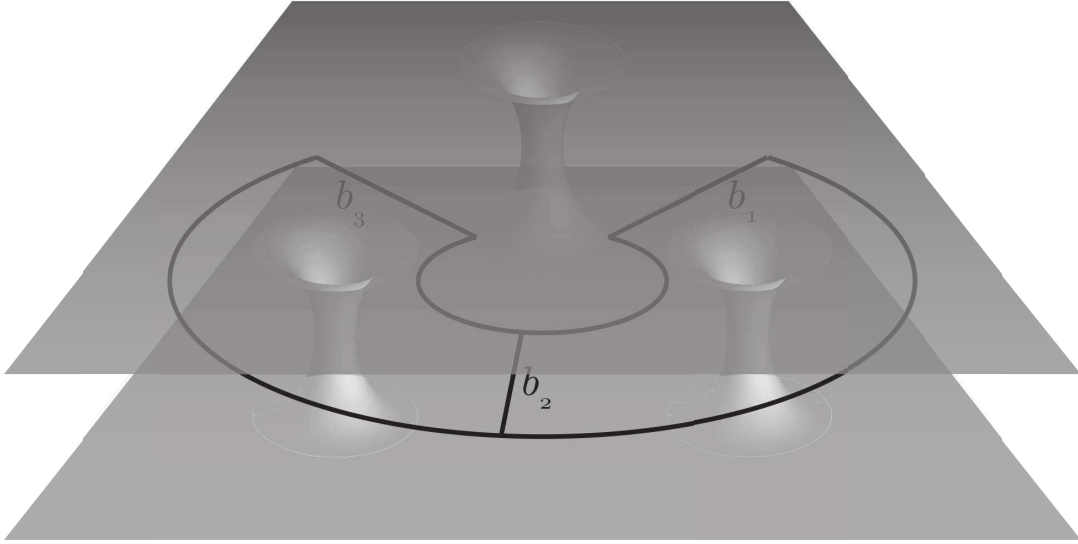
The unitarity of the  $F$ -symbols together with the summation over  $a_j$  results in  $\delta_{e_j, e'_j}$  factors (and similarly for the suppressed vertex labels). In the last line, we collapse a tadpole diagram in both  $\mathbb{A}$  and  $\bar{\mathbb{A}}$ , <sup>5</sup> which sets  $e_n = 0$  and  $e_{n-1} = \bar{b}_n$  and results in a factor of  $\mathcal{D}^2$  when  $a_1$  is summed over. In the following, we write  $\vec{e}$  to mean  $e_2, \dots, e_{n-2}$ . We note that the final expression could have alternatively been obtained from the state written as  $n$  wormholes with  $\omega_0$ -loops around only  $n - 1$  of the wormholes.

When embedded in three dimensional space, the anyon diagram corresponding to the

<sup>4</sup>This series of transformations also involves “bending” moves, i.e., vertex rotations [82]. The bending transformations also cancel out, so we leave them implicit to avoid excessive clutter.

<sup>5</sup>Note that the outer loop in the second to last expression of Eq. (4.106) can be deformed around the surface until it no longer encloses anything, i.e. it is truly a tadpole diagram.

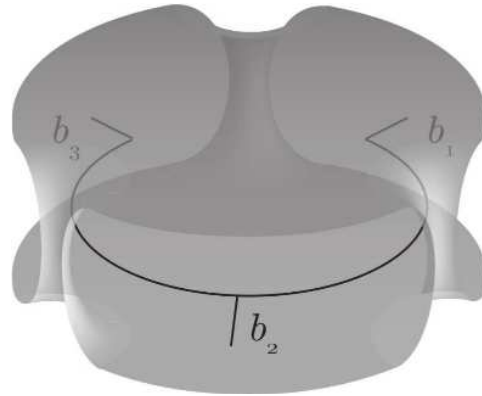
final representation of the state in Eq. (4.106) looks like



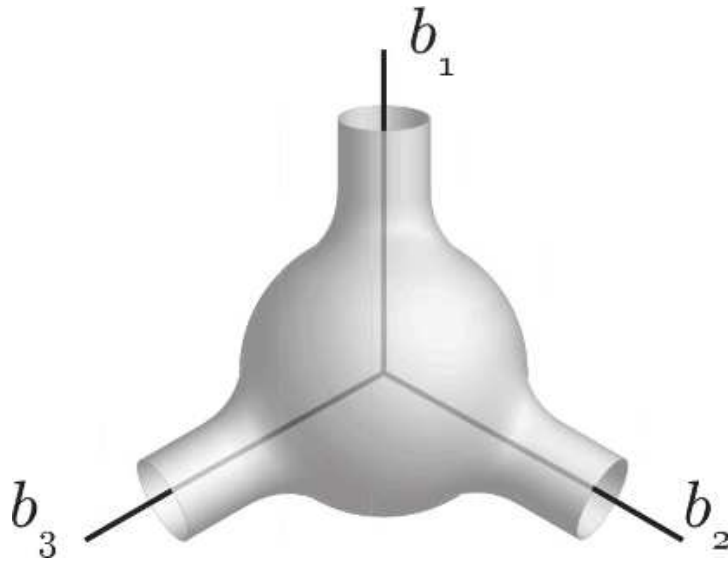
Now that each partition boundary component, i.e. each tube connecting  $\mathbb{A}$  to  $\bar{\mathbb{A}}$ , is threaded by a single topological charge line, when we cut the surface along the partition boundary between  $\mathbb{A}$  and  $\bar{\mathbb{A}}$ , indicated by the dashed lines in Eq. (4.106), each resulting boundary components of  $\mathbb{A}$  will correspondingly be ascribed the topological charge  $b_j$  of the charge line threading it, and similarly for the boundaries of  $\bar{\mathbb{A}}$ . The resulting state after cutting is

$$|\psi_{\text{cut}}\rangle = \sum_{\vec{b}, \vec{e}} \frac{1}{\mathcal{D}^{n-1}} \left( \begin{array}{c} b_1 \quad b_2 \quad b_3 \quad b_n \\ \swarrow \quad \swarrow \quad \swarrow \quad \swarrow \\ e_2 \quad e_3 \quad \dots \quad \bar{b}_n \\ \searrow \quad \searrow \quad \searrow \quad \searrow \\ \bar{b}_n \quad \dots \quad \bar{b}_n \end{array} \right) \left( \begin{array}{c} b_n \quad b_3 \quad b_2 \quad b_1 \\ \swarrow \quad \swarrow \quad \swarrow \quad \swarrow \\ e_2 \quad e_3 \quad \dots \quad \bar{b}_n \\ \searrow \quad \searrow \quad \searrow \quad \searrow \\ \bar{b}_n \quad \dots \quad \bar{b}_n \end{array} \right), \quad (4.107)$$

where the diagram for  $\mathbb{A}$  embedded in three dimensional space looks like



or, equivalently,



We can now find the reduced density matrix for  $\mathbb{A}$  by tracing over  $\bar{\mathbb{A}}$ ,

$$\begin{aligned} \tilde{\rho}_{\mathbb{A}} &= \widetilde{\text{Tr}}_{\bar{\mathbb{A}}} \left[ |\psi_{\text{cut}}\rangle \langle \psi_{\text{cut}}| \right] \\ &= \sum_{\vec{b}, \vec{e}, \vec{b}', \vec{e}'} \frac{1}{\mathcal{D}^{2n-2}} \end{aligned} \quad (4.108)$$

The quantum trace over  $\bar{\mathbb{A}}$  sets  $b_j = b'_j$  and  $e_j = e'_j$ , and evaluating the inner product yields a factor of  $\sqrt{d_{\vec{b}}}$ . Therefore, the anyonic reduced density matrix for  $A$  (restoring the vertex labels) is

$$\tilde{\rho}_{\mathbb{A}} = \sum_{\vec{b}, \vec{e}, \vec{\mu}} \frac{\sqrt{d_{\vec{b}}}}{\mathcal{D}^{2n-2}} \quad (4.109)$$

We note that this is precisely equal to the reduced density matrix  $\tilde{\rho}_A$  from Eq. (4.58).

From the reduced density matrix, we can calculate the anyonic Rényi entropy. First,

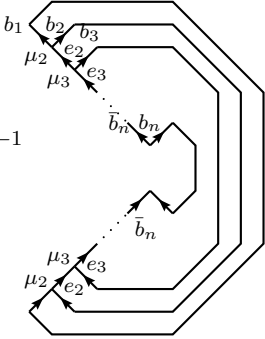
consider  $(\tilde{\rho}_{\mathbb{A}})^2$ :

$$(\tilde{\rho}_{\mathbb{A}})^2 = \sum_{\substack{\vec{b}, \vec{e}, \vec{\mu}, \\ \vec{e}', \vec{\mu}'}} \frac{d_{\vec{b}}}{\mathcal{D}^{4n-4}} \text{Diagram} = \sum_{\vec{b}, \vec{e}, \vec{\mu}} \frac{\sqrt{d_{\vec{b}}}}{\mathcal{D}^{2n-2}} \left( \frac{d_{\vec{b}}}{\mathcal{D}^{2n-2}} \right) \text{Diagram} \quad (4.110)$$

It is then easy to generalize to  $\tilde{\rho}_{\mathbb{A}}$  raised to an arbitrary power:

$$(\tilde{\rho}_{\mathbb{A}})^\alpha = \sum_{\vec{b}, \vec{e}, \vec{\mu}} \frac{\sqrt{d_{\vec{b}}}}{\mathcal{D}^{2n-2}} \left( \frac{d_{\vec{b}}}{\mathcal{D}^{2n-2}} \right)^{\alpha-1} \text{Diagram} \quad (4.111)$$

Performing the quantum trace over Eq. (4.111) yields

$$\begin{aligned} \widetilde{\text{Tr}}(\tilde{\rho}_{\mathbb{A}})^\alpha &= \sum_{\vec{b}, \vec{e}, \vec{\mu}} \frac{\sqrt{d_{\vec{b}}}}{\mathcal{D}^{2n-2}} \left( \frac{d_{\vec{b}}}{\mathcal{D}^{2n-2}} \right)^{\alpha-1} \\ &= \sum_{\vec{b}, \vec{e}, \vec{\mu}} \left( \frac{d_{\vec{b}}}{\mathcal{D}^{2n-2}} \right)^\alpha = \sum_{\vec{b}} N_{b_1 \dots b_n}^0 \left( \frac{d_{\vec{b}}}{\mathcal{D}^{2n-2}} \right)^\alpha, \end{aligned} \quad (4.112)$$


from which we see the anyonic Rényi entropy is

$$\tilde{S}^{(\alpha)}(\tilde{\rho}_{\mathbb{A}}) = \frac{1}{1-\alpha} \log \left[ \sum_{\vec{b}} N_{b_1 \dots b_n}^0 \left( \frac{d_{\vec{b}}}{\mathcal{D}^{2n-2}} \right)^\alpha \right]. \quad (4.113)$$

Taking the limit  $\alpha \rightarrow 1$  yields the (von Neumann) AEE:

$$\begin{aligned} \tilde{S}(\tilde{\rho}_{\mathbb{A}}) &= \lim_{\alpha \rightarrow 1} \tilde{S}^{(\alpha)}(\tilde{\rho}_{\mathbb{A}}) = - \sum_{\vec{b}} N_{b_1 \dots b_n}^0 \left( \frac{d_{\vec{b}}}{\mathcal{D}^{2n-2}} \right) \log \left( \frac{d_{\vec{b}}}{\mathcal{D}^{2n-2}} \right) \\ &= - \sum_{\vec{b}, \vec{e}} N_{b_1 b_2}^{e_2} N_{e_2 b_3}^{e_3} \dots N_{b_n, b_n}^0 \frac{d_{\vec{b}}}{\mathcal{D}^{2n-2}} \left[ \log \left( \frac{d_{b_1}}{\mathcal{D}^2} \right) + \dots + \log \left( \frac{d_{b_n}}{\mathcal{D}^2} \right) + 2 \log \mathcal{D} \right] \\ &= -n \sum_b \frac{d_b^2}{\mathcal{D}^2} \log \left( \frac{d_b}{\mathcal{D}^2} \right) - 2 \log \mathcal{D} \\ &= n \tilde{S}(\tilde{\rho}_{\partial \mathbb{A}_j}) + 2S_{\text{topo}}. \end{aligned} \quad (4.114)$$

In the second to last equality, we used Eq. (C.2) to sum over the multiplicities. In the last equality, we used  $S_{\text{topo}} \equiv -\log \mathcal{D}$  and the definition of the anyonic entropy of a “boundary anyon” given in Eq. (4.60), which now applies to the anyonic state of the topological charge on  $\partial \mathbb{A}_j$ , the  $j$ th connected component of  $\partial \mathbb{A}$ , i.e.  $\tilde{S}(\tilde{\rho}_{\partial \mathbb{A}_j}) = \tilde{S}(\tilde{\rho}_{\partial \mathcal{A}_j})$ .

At this point, the reason for the doubling of the topological contribution to the entanglement entropy coming from the partition boundary should be clear: we doubled the original region  $A$  and the original partition boundary in this method of computation. Thus, the topological contribution to the entanglement entropy for the original region  $A$  is given by

$$\tilde{S}_A = \frac{n}{2} \tilde{S}(\tilde{\rho}_{\partial A_j}) + S_{\text{topo}}. \quad (4.115)$$

As shown in Ref. [100] for string-net and quantum double models, using the Rényi entropy produces the same value of the TEE for any index  $\alpha$ . This can be seen for more general topological phases using our approach by rewriting Eq. (4.113) in powers of the boundary length. Consider the matrix

$$[K_\alpha]_{ee'} \equiv \sum_b N_{eb}^{e'} d_b^\alpha. \quad (4.116)$$

Since  $d_b = d_{\bar{b}}$  and  $N_{eb}^{e'} = N_{e'\bar{b}}^e$ , it follows that  $K_\alpha$  is normal and can, thus, be unitarily diagonalized, allowing us to write it as

$$[K_\alpha]_{ee'} = \sum_\mu \kappa_{\alpha,\mu} [v_{\alpha,\mu}]_e [v_{\alpha,\mu}]_{e'}^*. \quad (4.117)$$

where  $\kappa_{\alpha,\mu}$  is the  $\mu$ th eigenvalue with corresponding normalized eigenvector  $v_{\alpha,\mu}$ . We note that  $[K_\alpha]_{ee'} > 0$  for all  $e$  and  $e'$ , since there must be some value of  $b$  such that  $N_{eb}^{e'} \neq 0$ . Thus,  $K_\alpha$  obeys the Perron-Frobenius theorem, which implies that there is a unique eigenvector which has all positive real components (up to an overall scalar), and the corresponding eigenvalue of this eigenvector is positive and larger in magnitude than all other eigenvalues. We label this eigenvector by  $\mu = 0$ . It is straightforward to check that  $[v_\alpha]_e = d_e/\mathcal{D}$  is a normalized eigenvector, so it must be the  $\mu = 0$  eigenvector. Its

corresponding eigenvalue is

$$\kappa_{\alpha,0} = \sum_e d_e^{1+\alpha}. \quad (4.118)$$

Thus, we find that

$$\begin{aligned} \log \left( \sum_{\vec{b}} N_{b_1 \dots b_n}^0 d_{b_1}^\alpha \dots d_{b_n}^\alpha \right) &= \log \left( [(K_\alpha)^n]_{00} \right) = \log \left( \sum_{\mu} \kappa_{\alpha,\mu}^n [v_{\alpha,\mu}]_0 [v_{\alpha,\mu}]_0^* \right) \\ &= \log \left( \frac{\kappa_{\alpha,0}^n}{\mathcal{D}^{2n}} + \sum_{\mu \neq 0} \kappa_{\alpha,\mu}^n [v_{\alpha,\mu}]_0 [v_{\alpha,\mu}]_0^* \right) \\ &= n \log \kappa_{\alpha,0} - \log \mathcal{D}^{2n} + F(n, 0, K_\alpha). \end{aligned} \quad (4.119)$$

Here, we have defined

$$F(n, c, K_\alpha) \equiv \log \left( 1 + \frac{\mathcal{D}^{2n}}{d_c} \sum_{\mu \neq 0} \left( \frac{\kappa_{\alpha,\mu}}{\kappa_{\alpha,0}} \right)^n [v_{\alpha,\mu}]_0 [v_{\alpha,\mu}]_c^* \right), \quad (4.120)$$

which is exponentially suppressed in  $n$  for large  $n$ , since  $\kappa_{\alpha,\mu} < \kappa_{\alpha,0}$  for all  $\mu \neq 0$ . More specifically,  $|F(n, c, K_\alpha)| = \mathcal{O}(e^{-\lambda n})$ , where  $\lambda = -\log(\max_{\mu \neq 0} |\kappa_{\alpha,\mu}/\kappa_{\alpha,0}|)$  is a constant that only depends on the TQFT.

Plugging Eq. (4.119) back into Eq. (4.113), we have

$$\tilde{S}^{(\alpha)}(\tilde{\rho}_{\mathbb{A}}) = n \tilde{S}^{(\alpha)}(\tilde{\rho}_{\partial \mathbb{A}_j}) + 2S_{\text{topo}} + \frac{F(n, 0, K_\alpha)}{1 - \alpha}, \quad (4.121)$$

where we have denoted the anyonic Rényi entropy of a boundary anyon as

$$\tilde{S}^{(\alpha)}(\tilde{\rho}_{\partial \mathbb{A}_j}) = \tilde{S}^{(\alpha)}(\tilde{\rho}_{\partial \mathcal{A}_j}) = \frac{1}{1 - \alpha} \log \left( \frac{\kappa_{\alpha,0}}{\mathcal{D}^{2\alpha}} \right). \quad (4.122)$$

Eq. (4.121) has the same form as Eq. (4.11): a term that is linear in the length of the boundary ( $n \sim L/\ell$ ), a universal constant topological contribution, and sub-constant

corrections. Again, for the topological contribution to the entanglement Rényi entropy of the original (un-doubled) system, this should be divided by two

$$\tilde{S}_A^{(\alpha)} = \frac{n}{2} \tilde{S}^{(\alpha)}(\tilde{\rho}_{\partial\mathbb{A}_j}) + S_{\text{topo}} + \frac{F(n, 0, K_\alpha)}{2(1-\alpha)}. \quad (4.123)$$

Finally, we clarify why the original Kitaev-Preskill method of computing the TEE must be modified when using the Rényi entropy. Let  $\tilde{S}_n$  and  $\tilde{S}_n^{(\alpha)}$  denote the anyonic von Neumann and Rényi entanglement entropies, respectively, of the doubled region  $\mathbb{A}$  when  $n$  wormholes were inserted along the partition boundary in the doubling process, i.e.  $\mathbb{A}$  is an  $n$ -punctured sphere. The method of Ref. [7] utilized different geometric partitions of the systems into disks that resulted in 3-punctured and 4-punctured spheres after doubling and cutting, and showed that

$$S_{\text{topo}} = 2\tilde{S}_3 - \frac{3}{2}\tilde{S}_4. \quad (4.124)$$

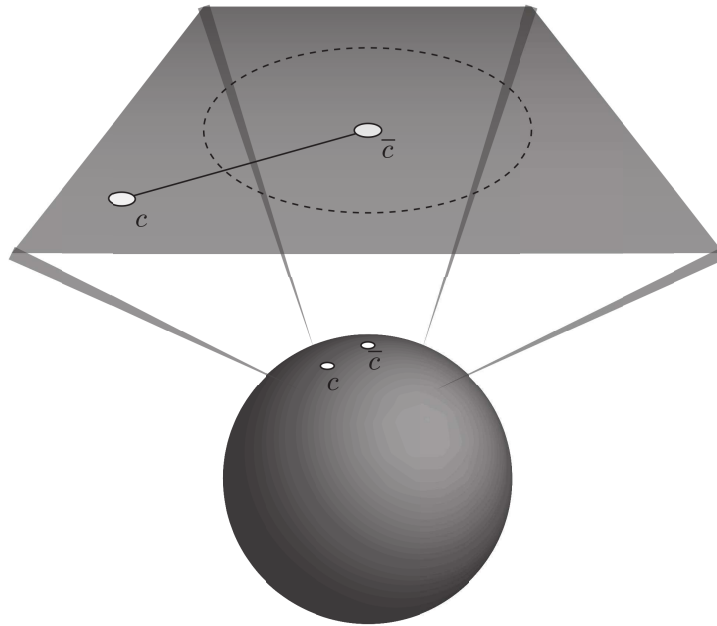
We see that this result holds given the form of Eq. (4.115). However, this result does not extend to the anyonic Rényi entropies, as can be seen from the form of Eq. (4.113):

$$2\tilde{S}_3^{(\alpha)} - \frac{3}{2}\tilde{S}_4^{(\alpha)} = S_{\text{topo}} + \frac{2F(3, 0, K_\alpha) - \frac{3}{2}F(4, 0, K_\alpha)}{1-\alpha}, \quad (4.125)$$

as the second term is some constant that depends on the TQFT, with no dependence on the boundary length. Our method recovers the boundary-law (linear length dependence) of the entanglement entropy and the TEE when utilizing Rényi entropies.

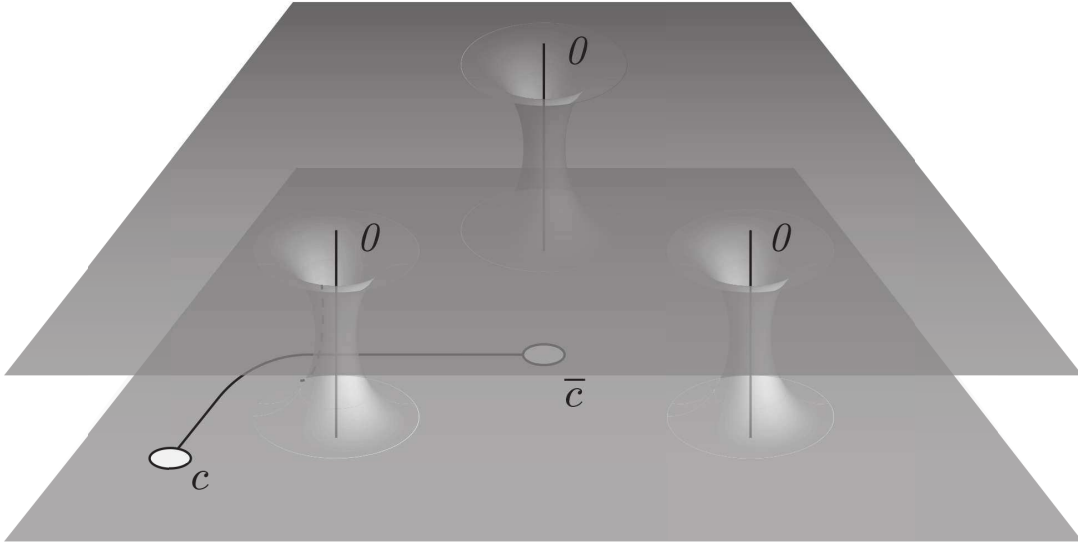
## 4.5.2 2-Punctured Sphere Partitioned into Two 1-Punctured Disks

We now extend the results of the previous section to the case when the disk  $A$  hosts an anyon  $c$ .



The line connecting  $c$  and  $\bar{c}$  along the surface can be thought of as the path through which the topological charges were created and moved to the shown positions.

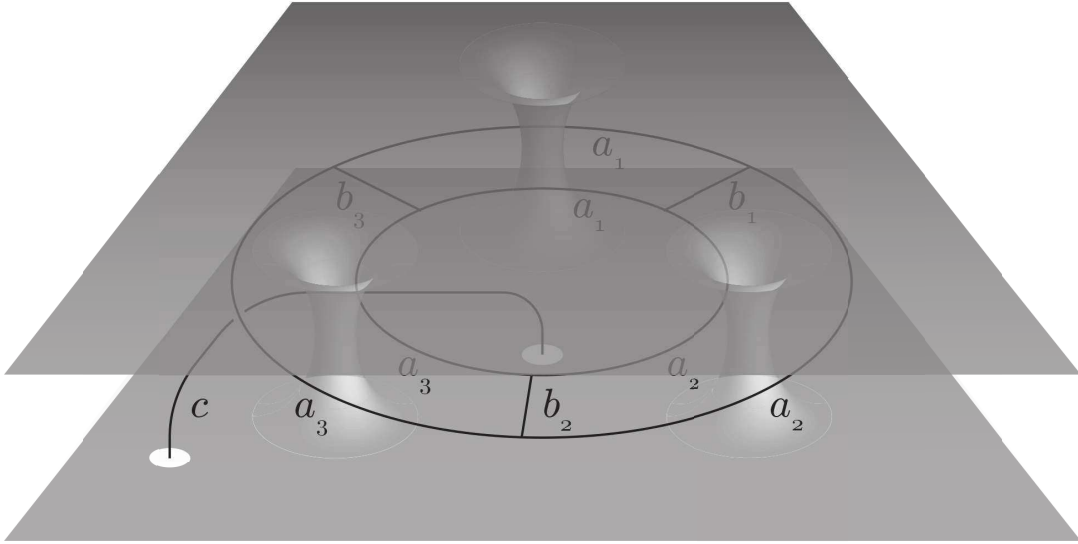
As before, we pair the system with its time-reversal conjugate, joining them by adiabatically inserting  $n$  wormholes along the boundary partition ( $n = 3$  in the following picture).



The derivation of the anyonic reduced density matrix for  $\mathbb{A}$  proceeds in much the same way as for the unpunctured disk in Section 4.5.1, with the only difference being that the topological charges  $c$  and  $\bar{c}$  are present. For instance, Eq. (4.105) is modified to

$$|\psi\rangle = \frac{1}{\mathcal{D}} \sum_{\vec{a}, \vec{b}} \frac{\sqrt{d_{\vec{b}}}}{\sqrt{d_{\vec{c}} \mathcal{D}^n}} \text{Diagram} \tag{4.126}$$

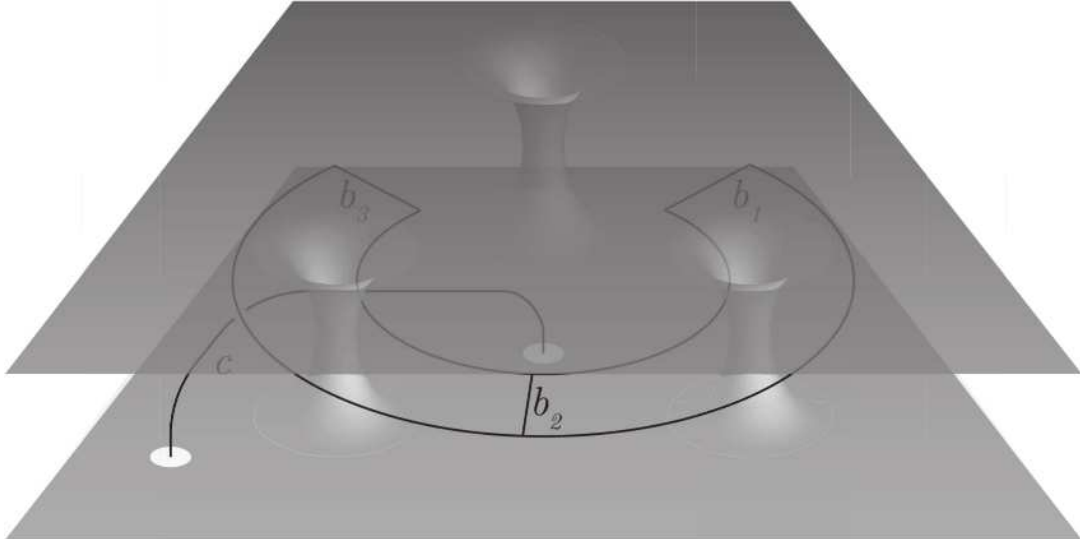
where the charge lines embedded in the doubled surface look like



As the charge line connecting  $c$  and  $\bar{c}$  lies below all other charge lines in the above picture, the steps illustrated in Eq. (4.106) (i.e.,  $F$ -moves to rewrite the state in tree-like form and collapsing the tadpoles in  $\mathbb{A}$  and  $\bar{\mathbb{A}}$ ) also apply to the excited state considered here. After applying these steps, we are left with the state in the form

$$|\psi\rangle = \sum_{\vec{b}, \vec{e}} \frac{\sqrt{d_{\vec{b}}}}{\sqrt{d_c} \mathcal{D}^{n-1}} \text{Diagram} \quad (4.127)$$

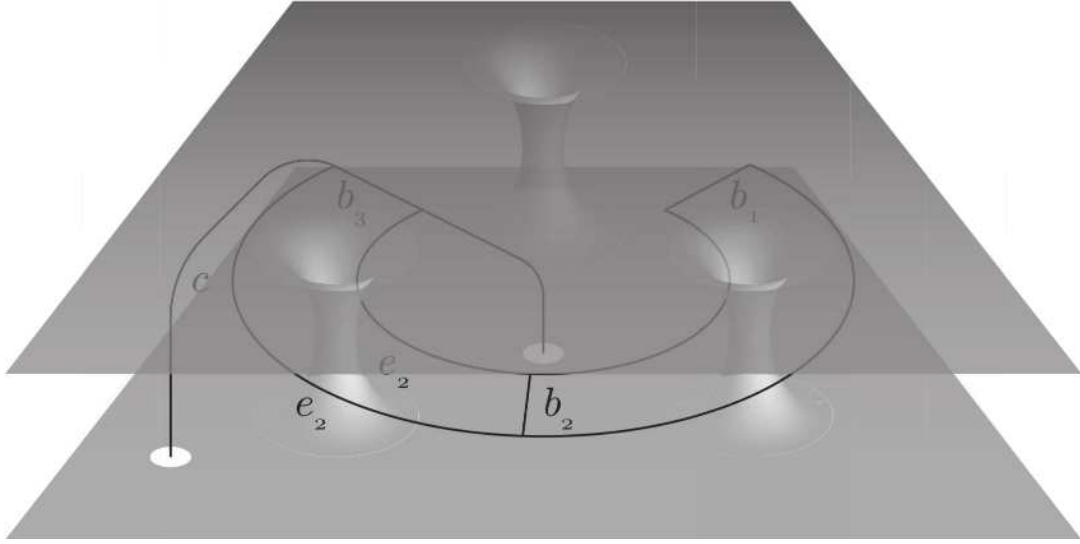
with corresponding three dimensional embedding



Now, before cutting the surface into  $\mathbb{A}$  and  $\bar{\mathbb{A}}$ , we must first fuse  $c$  with the topological charge line running through the same boundary region (taken in the picture to be  $b_3$  and in the diagram to be  $b_n$ ):

$$|\psi\rangle = \sum_{\vec{b}, \vec{e}} \frac{\sqrt{d_{\vec{b}}}}{d_c \mathcal{D}^{n-1}} \text{diagram} \tag{4.128}$$

In rewriting the state into this final form, we have used a braiding transformation that only contributes an overall phase to the state, which we therefore can drop. Additionally, we applied a partition of identity and have relabeled  $b_n$  as  $\bar{e}_{n-1}$  and instead used  $b_n$  to denote the fusion channel of  $\bar{e}_{n-1}$  and  $\bar{e}$  in the partition of identity. The shorthand notation  $\vec{e}$  now means  $e_2 \dots e_{n-1}$ . This diagrammatic state embedded in the doubled surface looks like



We can now cut the doubled surface, resulting in the state

$$|\psi_{\text{cut}}\rangle = \sum_{\vec{b}, \vec{e}} \frac{1}{d_c \mathcal{D}^{n-1}} \begin{array}{c} b_1 \quad b_2 \quad b_3 \qquad b_n \quad c \\ \swarrow \quad \swarrow \quad \swarrow \quad \swarrow \quad \swarrow \\ e_2 \quad e_3 \quad \dots \quad e_{n-2} \\ \searrow \quad \searrow \quad \searrow \quad \searrow \quad \searrow \\ \bar{c} \end{array} \begin{array}{c} \bar{c} \quad b_n \\ \swarrow \quad \swarrow \\ e_{n-2} \quad e_3 \quad e_2 \\ \searrow \quad \searrow \quad \searrow \\ c \quad b_3 \quad b_2 \quad b_1 \end{array} \quad (4.129)$$

Finally, we write the density matrix in the cut Hilbert space,  $\tilde{\rho} = |\psi_{\text{cut}}\rangle \langle \psi_{\text{cut}}|$ , and then trace over  $\bar{\mathbb{A}}$  to find the reduced anyonic density matrix (restoring the vertex labels):

$$\tilde{\rho}_{\mathbb{A}} = \sum_{\vec{b}, \vec{e}} \frac{\sqrt{d_{\bar{b}}}}{d_c^{3/2} \mathcal{D}^{2n-2}} \begin{array}{c} b_1 \quad b_2 \quad b_3 \qquad b_n \quad c \\ \swarrow \quad \swarrow \quad \swarrow \quad \swarrow \quad \swarrow \\ \mu_2 \quad e_2 \quad e_3 \quad \dots \quad e_{n-2} \\ \searrow \quad \searrow \quad \searrow \quad \searrow \quad \searrow \\ \mu_{n-1} \quad \bar{c} \end{array} \begin{array}{c} \mu_{n-1} \\ \swarrow \quad \swarrow \\ e_{n-2} \\ \searrow \quad \searrow \quad \searrow \\ \mu_3 \quad e_3 \quad e_2 \\ \swarrow \quad \swarrow \quad \swarrow \\ b_1 \quad b_2 \quad b_3 \qquad b_n \quad c \end{array} \quad (4.130)$$

Comparing Eq. (4.63) with Eq. (4.130), we see that the heuristic argument of Section 4.3.3 produced the same reduced anyonic density matrix  $\tilde{\rho}_{\mathcal{A}}$  for a disk containing a puncture or

quasiparticle of topological charge  $c$  as did our method (generalizing the Kitaev-Preskill method) using a doubled surface connected by wormholes.

Using the same steps outlined in Eqs. (4.116)-(4.120) for the unpunctured disk, we can calculate the anyonic Rényi entropy

$$\tilde{S}^{(\alpha)}(\tilde{\rho}_{\mathbb{A}}) = \frac{1}{1-\alpha} \log \left( \sum_{\vec{b}} N_{b_1 \dots b_n}^{\bar{c}} \left( \frac{d_{\vec{b}}}{d_c \mathcal{D}^{2n-2}} \right)^\alpha \right). \quad (4.131)$$

Taking the limit  $\alpha \rightarrow 1$  yields the (von Neumann) AEE

$$\tilde{S}(\tilde{\rho}_{\mathbb{A}}) = \lim_{\alpha \rightarrow 1} \tilde{S}^{(\alpha)}(\tilde{\rho}_{\mathbb{A}}) = n\tilde{S}(\tilde{\rho}_{\partial\mathbb{A}_j}) + 2S_{\text{topo}} + \tilde{S}_c, \quad (4.132)$$

which agrees with Eq. (4.64). Again, since we doubled the original surface in this method, both the area law term and the TEE appear with an extra factor of two. The  $\tilde{S}_c$  term is *not* doubled, because we did not double the punctures carrying charge  $c$  and  $\bar{c}$  of the original surface. Therefore, the topological contribution to the entanglement entropy of the original system in region  $A$  is

$$\tilde{S}_A = \frac{n}{2} \tilde{S}(\tilde{\rho}_{\partial\mathbb{A}_j}) + S_{\text{topo}} + \tilde{S}_c, \quad (4.133)$$

agreeing with Eq. (4.68).

As before, we can extract the topological contributions to the anyonic Rényi entropy by rewriting Eq. (4.131) in powers of the boundary length. We find

$$\tilde{S}^{(\alpha)}(\tilde{\rho}_{\mathbb{A}}) = n\tilde{S}^{(\alpha)}(\tilde{\rho}_{\partial\mathbb{A}_j}) + 2S_{\text{topo}} + \tilde{S}_c + \frac{F(n, \bar{c}, K_\alpha)}{1-\alpha}, \quad (4.134)$$

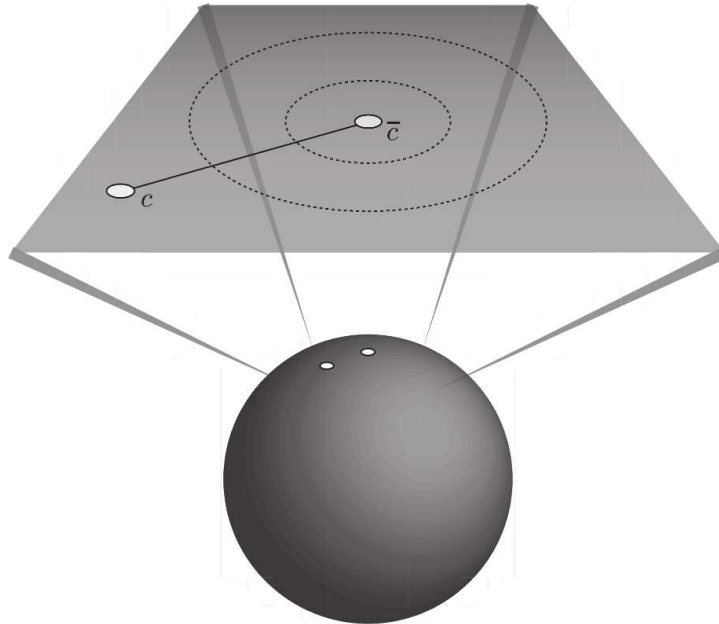
$$\tilde{S}_A^{(\alpha)} = \frac{n}{2} \tilde{S}^{(\alpha)}(\tilde{\rho}_{\partial\mathbb{A}_j}) + S_{\text{topo}} + \tilde{S}_c + \frac{F(n, \bar{c}, K_\alpha)}{2(1-\alpha)}, \quad (4.135)$$

where  $F(n, \bar{c}, K_\alpha)$  is exponentially suppressed in  $n$  for large  $n$ , which is essentially the regime in which the boundary length is large ( $n \sim L/\ell$ ).

We note that the geometric cancelation method used in Ref. [7] to isolate  $S_{\text{topo}}$  also cancels the  $\tilde{S}_c$  contribution due to a topological charge  $c$  in the region, so it does not isolate this term as well.

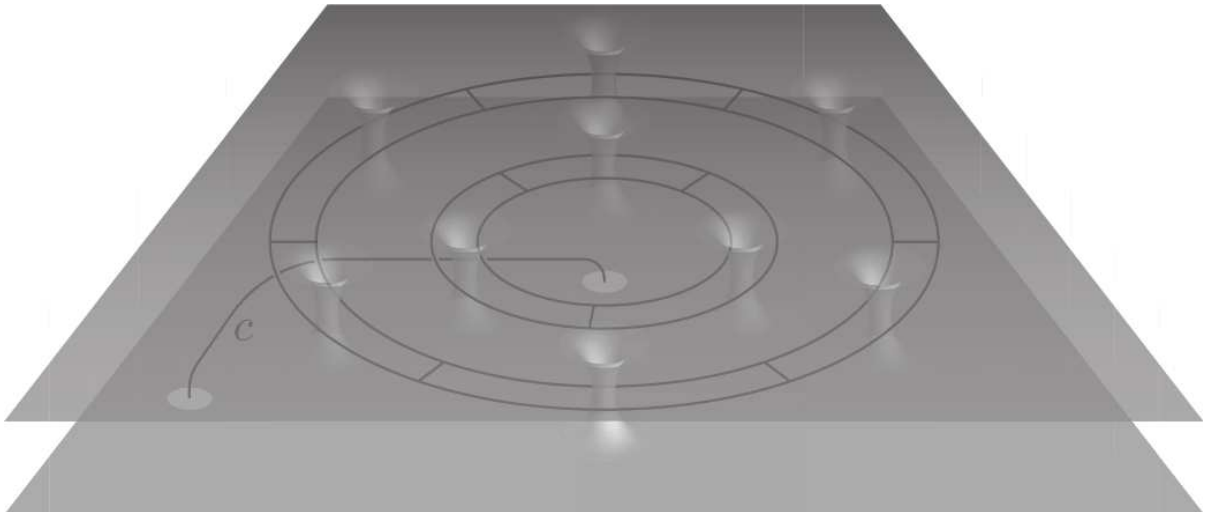
### 4.5.3 Punctured Sphere Partitioned into an Annulus and Two 1-Punctured Disks

We now consider a sphere with a pair of punctures (or quasiparticles) carrying topological charge  $c$  and  $\bar{c}$ . We apply our method for a partition of the system into an annular region  $A$ , chosen such that  $c$  and  $\bar{c}$  lie outside and on opposite sides of the annulus, i.e. each of the disks that form  $\bar{A}$  contains one of the punctures.



We follow the same approach as for the previous example of the disk. We create the manifold  $\mathbb{M}$  by pairing the system with its time-reversal conjugate and connecting the

surfaces through an array of wormholes adiabatically inserted along the partition boundary, which in this case is delineated by two concentric circles. We insert  $n$  wormholes along one boundary component and  $m$  wormholes along the other. Each wormhole is threaded by a trivial topological charge line. Then, analogous to Eq. (4.102) for the unpunctured disk, we apply a modular  $\mathcal{S}$ -transformation to express the state in the basis represented by topological charge lines in between the two surfaces, i.e. the inside basis. We then use  $F$ -moves to fuse the charge lines threading each new partition boundary component of the doubled surface with wormholes, similar to Eq. (4.105). The charge lines embedded in  $\mathbb{M}$  look like:



We now apply the same series of  $F$ -moves outlined in the first three equalities of Eq. (4.106).

The state can be written as (suppressing vertex labels)

$$|\psi\rangle = \sum_{\substack{\vec{a}, \vec{b}, \\ \vec{e}, \vec{f}, \\ g_1, h_1}} \frac{\sqrt{d_{\vec{a}} d_{\vec{b}}}}{\mathcal{D}^{n+m+1}} \frac{1}{\sqrt{d_c}} \quad (4.136)$$

where the dashed lines indicate the partition boundary between  $\mathbb{A}$  (corresponding to the annulus  $A$  of the un-doubled system) and  $\bar{\mathbb{A}}$  (corresponding to the two disks comprising  $\bar{A}$  of the un-doubled system). We can collapse the two tadpole diagrams in region  $\bar{\mathbb{A}}$  (the outermost  $g_1$  loop and the innermost  $h_1$  loop). In doing so,  $e_n$  and  $f_m$  are both required to equal the trivial charge 0. The remaining  $g_1$  and  $h_1$  loops in  $\mathbb{A}$  (which both encircle a

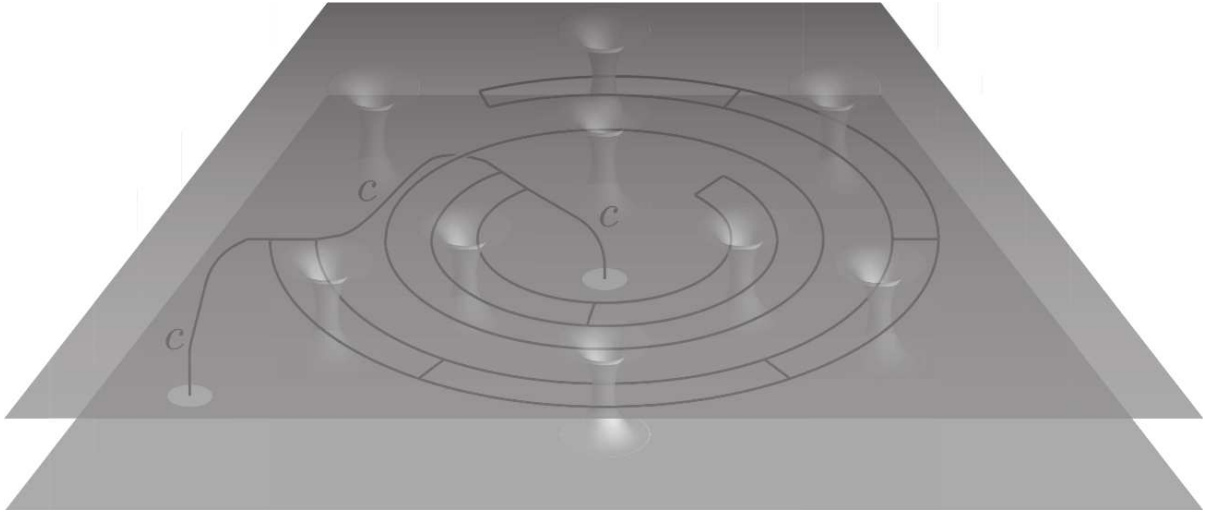
non-contractible cycle) can be fused together, resulting in the state:

$$|\psi\rangle = \sum_{\substack{\vec{a}, \vec{b}, k, \\ e_2, \dots, e_{n-2}, \\ f_2, \dots, f_{m-2}}} \frac{\sqrt{d_{\vec{a}} d_{\vec{b}}}}{\mathcal{D}^{n+m-2}} \frac{1}{\sqrt{d_c}} \frac{d_k}{\mathcal{D}} \quad (4.137)$$

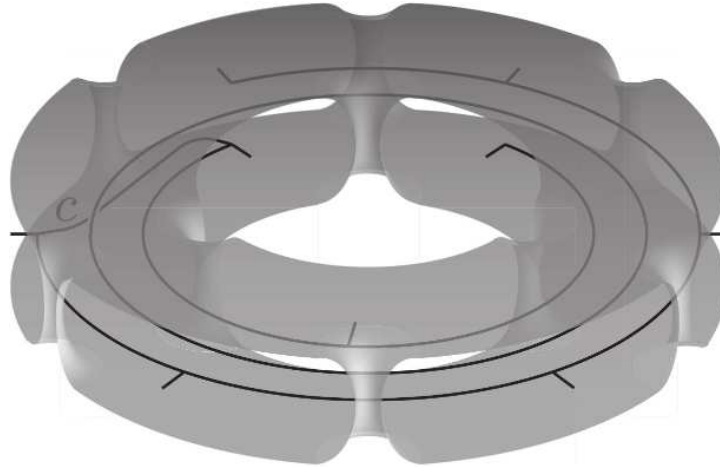
Here, we have used the property

$$\begin{aligned} \sum_{g,h} d_g d_h \begin{array}{c} \diamond \\ \text{\scriptsize } h \otimes \\ \text{\scriptsize } g \end{array} &= \sum_{g,h,k} d_g d_h N_{gh}^k \begin{array}{c} \diamond \\ \otimes \\ \text{\scriptsize } k \end{array} = \sum_{h,k} d_h^2 d_k \begin{array}{c} \diamond \\ \otimes \\ \text{\scriptsize } k \end{array} \\ &= \mathcal{D}^2 \sum_k d_k \begin{array}{c} \diamond \\ \otimes \\ \text{\scriptsize } k \end{array}. \end{aligned} \quad (4.138)$$

Note that the loop labeled by  $k$  in Eq. (4.137) is actually an  $\omega_0$ -loop circling one of the connected components of  $\bar{\mathbb{A}}$  (wrapping around a non-contractible cycle), because it is weighted by  $d_k$  in the sum over  $k$ . Similar to Eq. (4.128), we fuse the topological charge  $c$  line to the charge lines threading the same boundary regions, taken here to be  $b_m$  and  $a_n$ . The state embedded in the doubled surface looks like:



Finally, we cut along the partition boundary. After cutting, the region  $\mathbb{A}$  of the doubled system, which is an  $(n + m)$ -punctured torus (genus  $g = 1$ ), looks like



and the state  $|\psi_{\text{cut}}\rangle$  of the cut system (including  $\mathbb{A}$  and  $\bar{\mathbb{A}}$ ) can be represented diagrammatically as

$$|\psi_{\text{cut}}\rangle = \sum_{\vec{a}, \vec{b}, \vec{c}} \frac{1}{\mathcal{D}^{n+m-3}} \frac{1}{d_c^{3/2}} \begin{array}{c} \vec{c} \quad a_n \quad a_2 \quad a_1 \\ \swarrow \quad \downarrow \quad \searrow \\ \text{---} \quad \text{---} \quad \text{---} \\ \bar{\mathbb{A}} \end{array} \begin{array}{c} a_1 \quad a_2 \quad a_n \quad b_m \quad b_2 \quad b_1 \\ \swarrow \quad \downarrow \quad \searrow \quad \swarrow \quad \downarrow \quad \searrow \\ \omega_0 \quad \otimes \quad \vec{c} \quad \bar{\mathbb{A}} \\ \text{---} \quad \text{---} \quad \text{---} \\ \mathbb{A} \end{array} \begin{array}{c} b_1 \quad b_2 \quad b_m \quad c \\ \swarrow \quad \downarrow \quad \searrow \\ \text{---} \quad \text{---} \quad \text{---} \\ \bar{\mathbb{A}} \end{array} \quad (4.139)$$



diagrams. Note that

$$\widetilde{\text{Tr}} \left( \begin{array}{c} \text{Diagram 1} \\ \text{Diagram 2} \end{array} \right) = \sum_k \frac{d_k}{\mathcal{D}^4} \left( \begin{array}{c} \text{Diagram 3} \\ \text{Diagram 4} \end{array} \right) = \widetilde{\text{Tr}} \left( \begin{array}{c} \text{Diagram 5} \\ \text{Diagram 6} \end{array} \right) = \frac{d_c}{\mathcal{D}^2}. \quad (4.142)$$

Therefore,

$$(\tilde{\rho}_A)^2 = \sum_{\substack{\vec{a}, \vec{b}, \\ \vec{e}, \vec{f}, \\ \vec{\mu}, \vec{\nu}, \\ \vec{e}', \vec{f}', \\ \vec{\mu}', \vec{\nu}' \\ k}} \frac{1}{\mathcal{D}^{4(n+m-3)}} \frac{d_{\vec{a}} d_{\vec{b}}}{d_c^4} \frac{d_k^2}{\mathcal{D}^4} \frac{1}{d_k} \left( \begin{array}{c} \text{Diagram 7} \\ \text{Diagram 8} \\ \text{Diagram 9} \end{array} \right), \quad (4.143)$$

where the  $k$  loop with prefactor  $d_k/\mathcal{D}^4$  comes from taking the inner product of two

$\omega_0$ -loops. Evaluating the middle diagram, we find

$$(\tilde{\rho}_{\mathbb{A}})^2 = \sum_{\substack{\vec{a}, \vec{e}, \vec{\mu} \\ \vec{b}, \vec{f}, \vec{\nu}}} \frac{1}{\mathcal{D}^{2(n+m-3)}} \frac{\sqrt{d_{\vec{a}} d_{\vec{b}}}}{d_c^2} \left( \frac{d_{\vec{a}} d_{\vec{b}}}{\mathcal{D}^{2(n+m-2)} d_c^2} \right) \quad (4.144)$$

From the previous equation, it is straightforward to see that

$$(\tilde{\rho}_{\mathbb{A}})^\alpha = \sum_{\substack{\vec{a}, \vec{e}, \vec{\mu} \\ \vec{b}, \vec{f}, \vec{\nu}}} \frac{1}{\mathcal{D}^{2(n+m-3)}} \frac{\sqrt{d_{\vec{a}} d_{\vec{b}}}}{d_c^2} \left( \frac{d_{\vec{a}} d_{\vec{b}}}{\mathcal{D}^{2(n+m-2)} d_c^2} \right)^{\alpha-1} \quad (4.145)$$

Performing the quantum trace and summing over the vertex labels we find

$$\widetilde{\text{Tr}}(\tilde{\rho}_{\mathbb{A}})^\alpha = \sum_{\vec{a}, \vec{b}} \left( \frac{d_{\vec{a}} d_{\vec{b}}}{\mathcal{D}^{2(n+m-2)} d_c^2} \right)^\alpha N_{a_1 \dots a_n}^c N_{b_1 \dots b_m}^{\bar{c}} \quad (4.146)$$

The anyonic Rényi entropy is therefore

$$\tilde{S}^{(\alpha)}(\tilde{\rho}_{\mathbb{A}}) = \frac{1}{1-\alpha} \log \left( \sum_{\vec{a}, \vec{b}} N_{a_1 \dots a_n}^c N_{b_1 \dots b_m}^{\bar{c}} \left( \frac{d_{\vec{a}} d_{\vec{b}}}{\mathcal{D}^{2(n+m-2)} d_c^2} \right)^\alpha \right). \quad (4.147)$$

Taking the limit  $\alpha \rightarrow 1$  yields

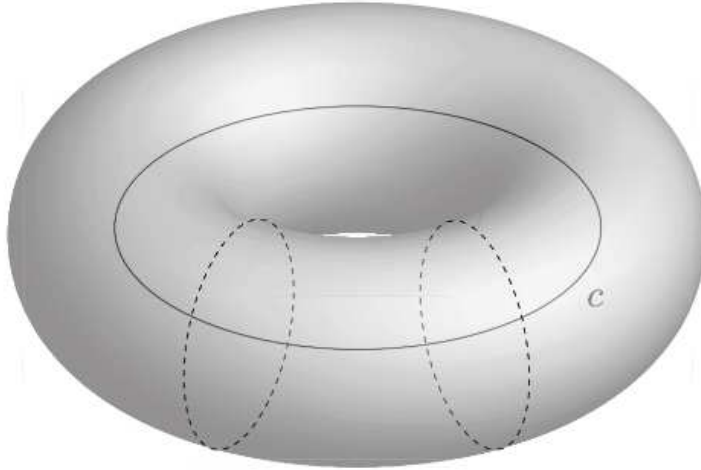
$$\tilde{S}(\tilde{\rho}_A) = -(n+m) \sum_a \frac{d_a^2}{\mathcal{D}^2} \log\left(\frac{d_a}{\mathcal{D}^2}\right) - 4 \log \mathcal{D} + 2 \log d_c. \quad (4.148)$$

Taking into account the doubling of the surface, the topological contribution to the entanglement entropy of the original (un-doubled) system is

$$\begin{aligned} \tilde{S}_A &= -\frac{n+m}{2} \sum_a \frac{d_a^2}{\mathcal{D}^2} \log\left(\frac{d_a}{\mathcal{D}^2}\right) - 2 \log \mathcal{D} + 2 \log d_c \\ &= -\frac{n+m}{2} \tilde{S}(\tilde{\rho}_{\partial A_j}) + 2S_{\text{topo}} + 2\tilde{S}_c. \end{aligned} \quad (4.149)$$

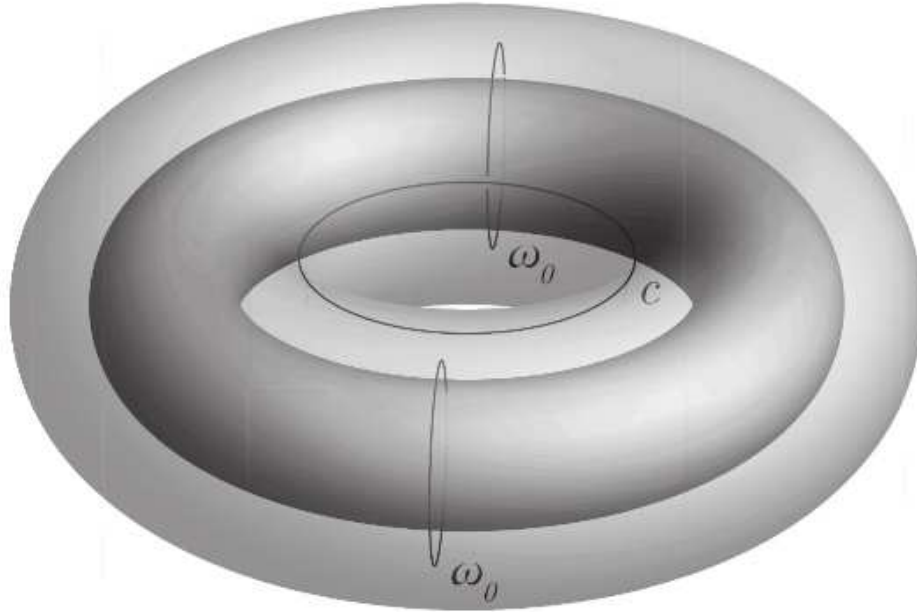
#### 4.5.4 Torus Partitioned into Two Cylinders (Two Annuli)

We now consider a torus in the ground state  $|(c); 0\rangle_{\text{inside}}$ , corresponding to a topological charge line  $c$  running in the longitudinal direction, i.e. in the inside basis, and apply our method for a partition the system into two cylindrical regions  $A$  and  $\bar{A}$ .

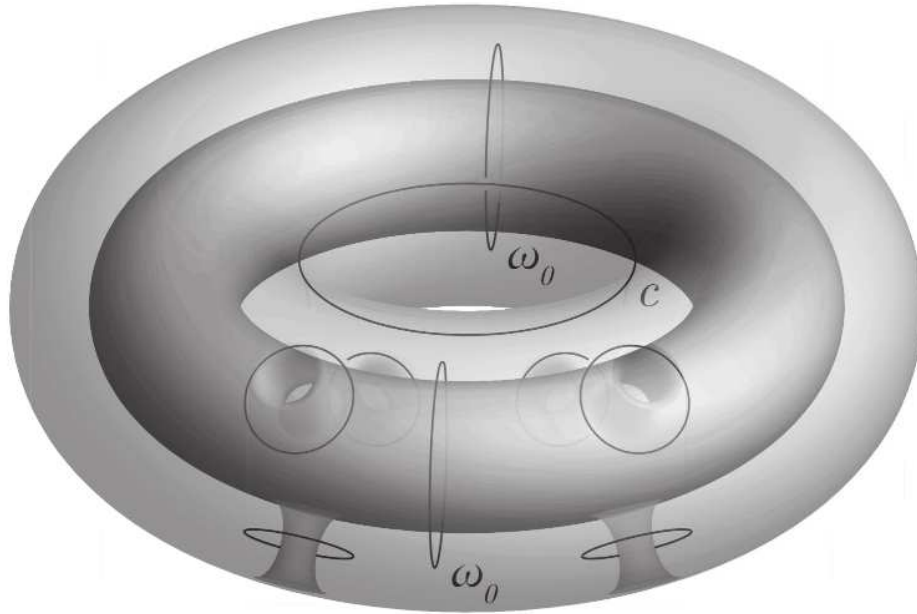


As with the previous examples, we pair the system with its time-reversal conjugate. Specifically, we introduce the conjugate inside the original torus, and choose it to be in

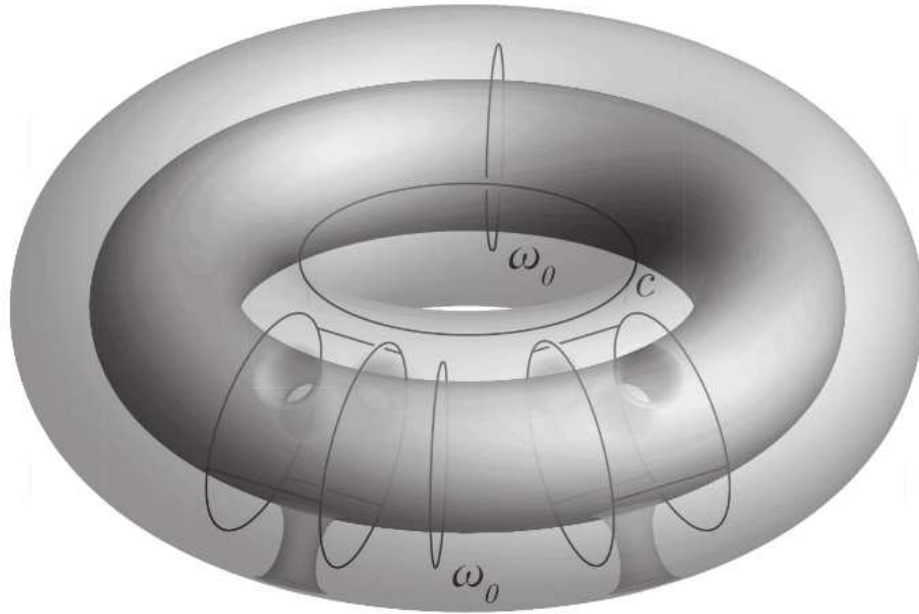
the its ground state  $|(0); 0\rangle_{\text{inside}}$ , as signified by the  $\omega_0$ -loops in the figure. (We draw two  $\omega_0$ -loops instead of just one, the utility of which will become clear later.)



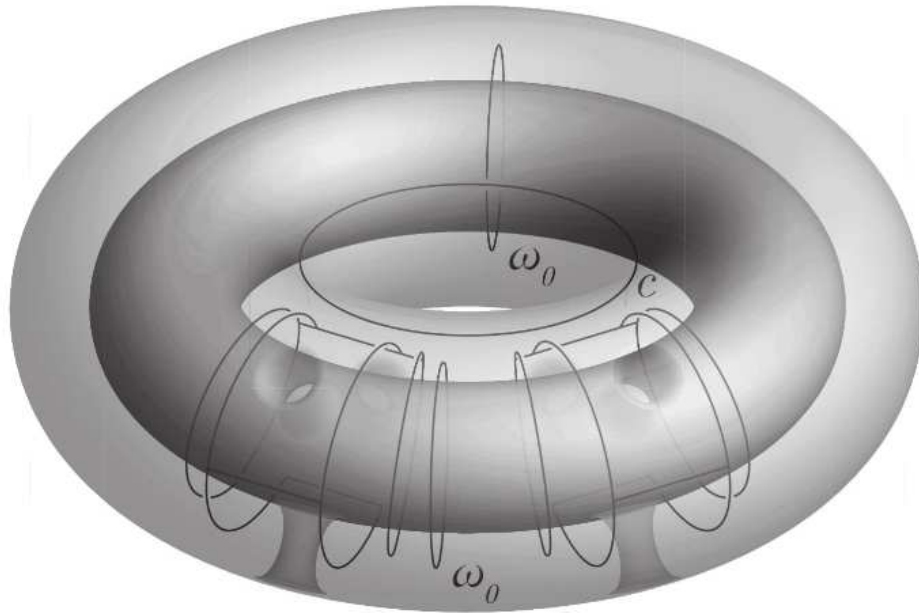
As before, to construct  $\mathbb{M}$  we adiabatically insert wormholes (threaded by trivial topological charge lines) along the partition boundary, with  $n$  wormholes along one of the boundary components and  $m$  wormholes along the other. Then we use the modular  $\mathcal{S}$ -transformation to re-express the state in the inside basis (where all the charge lines are between the two surfaces).



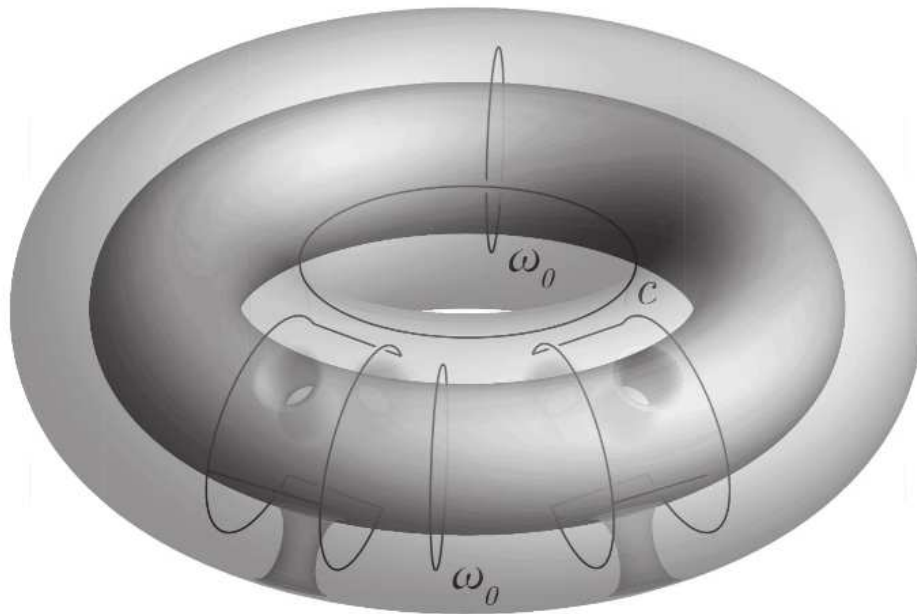
Analogous to Eq. (4.105) for the disk cut from the sphere, we apply a series of  $F$ -moves to fuse topological charge lines that thread the new boundary components between regions  $\mathbb{A}$  and  $\bar{\mathbb{A}}$ .



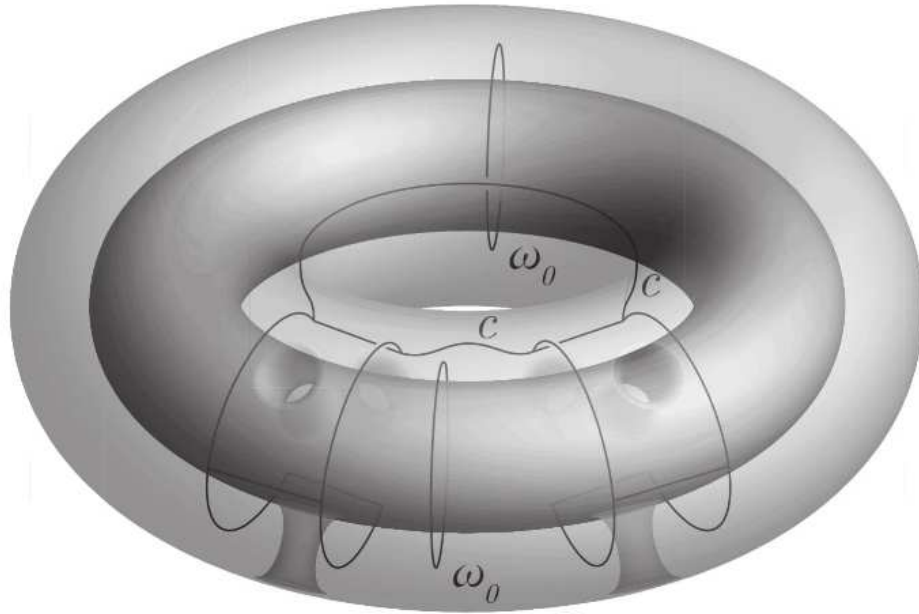
Similarly to the first three equalities in Eq. (4.106), we rewrite the state with further use of  $F$ -moves.



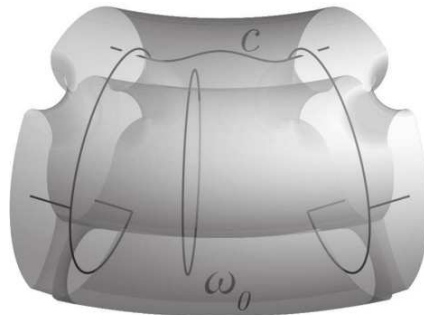
In the last equality of Eq. (4.106), we collapsed a tadpole diagram in both  $\mathbb{A}$  and  $\bar{\mathbb{A}}$ . In the present situation, the analogous “tadpole-like” diagrams now enclose a non-contractible cycle, i.e. the inner torus. Nonetheless, we can contract these loops using the handle-slide property of the  $\omega_0$ -loop, see Eq. (4.103). Thus, even though the tadpoles encircle a nontrivial cycle, they can be passed through it due to the presence of the  $\omega_0$ -loop. In this way, they become true tadpoles, and can be subsequently collapsed. (This step reveals the reason for beginning with two  $\omega_0$ -loops: there needs to be one on either side of the wormholes to help collapse the tadpoles.) The result is:



Fusing the topological charge  $c$  line into the other charge lines crossing the partition boundary, similar to Eq. (4.128), we have the state



Finally, we cut along the partition boundary to produce the cut state. Each of the resulting regions  $\mathbb{A}$  and  $\bar{\mathbb{A}}$  after cutting is a surface with genus  $g = 1$  and  $n + m$  punctures, and looks like:



Calculating the density matrix  $\tilde{\rho} = |\psi_{\text{cut}}\rangle \langle \psi_{\text{cut}}|$  and tracing out region  $\bar{\mathbb{A}}$  yields the reduced density matrix for region  $\mathbb{A}$ . Once again, there is a choice of basis for how to diagrammatically represent the region  $\mathbb{A}$ , which essentially amounts to either projecting the above picture to the plane as drawn, or turning the picture inside out so that the

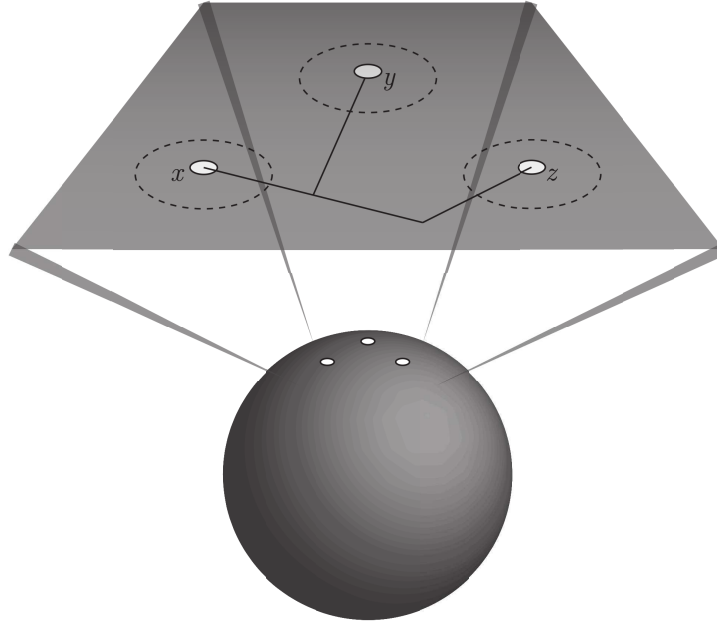
center tube becomes external to the region, resulting in the  $\omega_0$ -loop circling the  $c$  charge line. The former results in the reduced density matrix

$$\tilde{\rho}_{\mathbb{A}} = \sum_{\substack{\vec{a}, \vec{e}, \vec{\mu} \\ \vec{b}, \vec{f}, \vec{\nu}}} \frac{1}{\mathcal{D}^{2(n+m-3)}} \frac{\sqrt{d_{\vec{a}} d_{\vec{b}}}}{d_c^2} \quad , \quad (4.150)$$

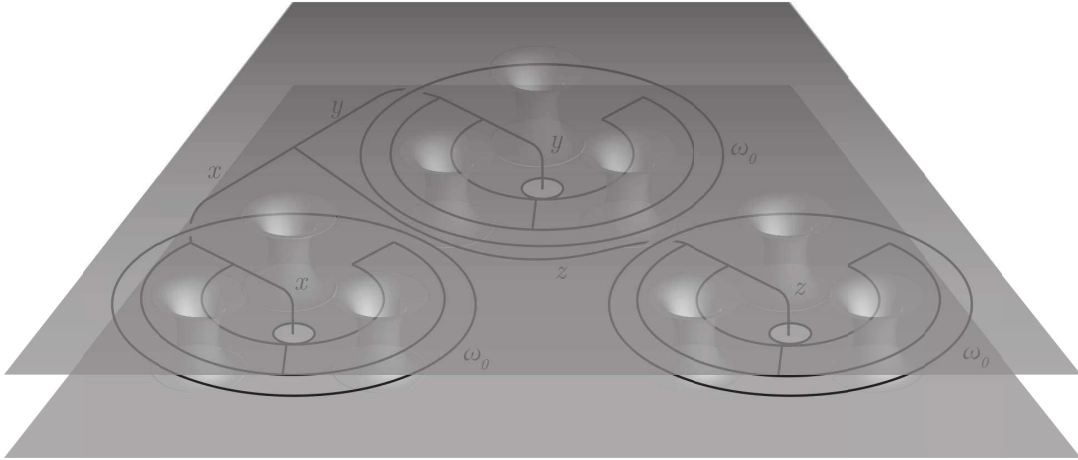
while the latter results in the reduced density matrix given in Eq. (4.141). Therefore, the reduced density matrix for the region  $\mathbb{A}$  of the doubled torus with wormholes is equivalent to that of the doubled region  $\mathbb{A}$  corresponding to when  $A$  was an annulus cut from a sphere, as we would expect from topological considerations. It follows that the anyonic Rényi entropy of region  $\mathbb{A}$  is given by Eq. (4.147) and the topological contribution to the entanglement entropy of  $A$ , the original (un-doubled) system, is given by Eq. (4.149).

### 4.5.5 3-Punctured Sphere Partitioned into a 3-Punctured Sphere and Three 1-Punctured Disks

As a final example, we consider a sphere containing three punctures (or quasiparticles) carrying topological charges  $x$ ,  $y$ , and  $z$ . We partition the region so that each puncture is contained in a separate disk, and apply our method for the three punctured sphere  $A$  that remains when the three disks are removed.



We follow the same steps as in the previous examples: (1) pair the system with its time-reversal conjugate, (2) insert wormholes threaded by trivial charge lines along the partition boundary, with  $l$ ,  $m$ , and  $n$  wormholes along the three different boundary components, respectively, (3) apply modular  $\mathcal{S}$ -transformations to express the state in the inside basis (all topological charge lines are between the two surfaces), (4) use  $F$ -moves to fuse topological charge lines that thread each new partition boundary component, (5) use further  $F$ -moves to write the state in a tree-like form, and (6) fuse the  $x$ ,  $y$ , and  $z$  charge lines to the topological charge line threading the same boundary component. Analogous to Eq. (4.136) for the annulus, after step (5) each disk in  $\bar{\mathbb{A}}$  will contain a tadpole that can be collapsed. Similar to Eq. (4.137), collapsing this tadpole results in an  $\omega_0$ -loop in  $\mathbb{A}$  encircling the corresponding region of  $\bar{\mathbb{A}}$ . Region  $\mathbb{A}$  is a surface with genus  $g = 2$  and  $l + m + n$  punctures. After performing steps (1)-(6), the state embedded in  $\mathbb{M}$  is



with the corresponding diagrammatic representation

$$|\psi\rangle = \sum_{\substack{\vec{a}, \vec{b}, \vec{c}, \\ \vec{e}, \vec{f}, \vec{g}}} \frac{\sqrt{d_{\vec{a}} d_{\vec{b}} d_{\vec{c}}}}{\mathcal{D}^{l+m+n-5} (d_x d_y d_z)^{3/4}} \quad . \quad (4.151)$$

The third  $\omega_0$ -loop can be brought around the other side of the sphere, so that it encloses the other two  $\omega_0$ -loops. Then, using the handle-slide property of Eq. (4.103), it can be slid over the other two  $\omega_0$ -loops, so that it does not enclose any non-contractible cycles. Finally, we can collapse this  $\omega_0$ -loop, using

$$\omega_0 = \sum_a \frac{d_a}{\mathcal{D}^2} \diamond_a = 1. \quad (4.152)$$

Thus, the state can be written as

$$|\psi\rangle = \sum_{\substack{\vec{a}, \vec{b}, \vec{c}, \\ \vec{e}, \vec{f}, \vec{g}}} \frac{\sqrt{d_{\vec{a}} d_{\vec{b}} d_{\vec{c}}}}{\mathcal{D}^{l+m+n-5} (d_x d_y d_z)^{3/4}} \cdot \text{Diagram} \quad (4.153)$$

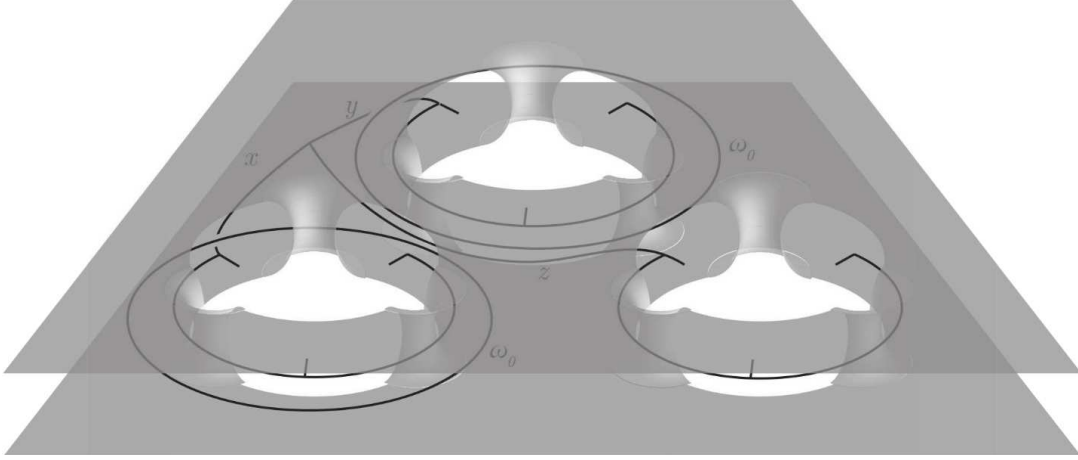
The diagram for equation 4.153 shows three circular regions arranged horizontally. Each region contains a network of anyons and lines. The left region has anyons labeled  $a_1, a_2$  and lines  $e_2$ . The middle region has anyons labeled  $b_1, b_2$  and lines  $f_2$ . The right region has anyons labeled  $c_1, c_2$  and lines  $g_2$ . External lines labeled  $x, y, z$  connect the regions. A dashed line represents a partition boundary.

Cutting along the partition boundary (dashed lines), we have

$$|\psi_{\text{cut}}\rangle = \sum_{\substack{\vec{a}, \vec{b}, \vec{c}, \\ \vec{e}, \vec{f}, \vec{g}}} \frac{1}{\mathcal{D}^{l+m+n-5} (d_x d_y d_z)^{3/4}} \cdot \text{Diagram} \quad (4.154)$$

The diagram for equation 4.154 shows the state after cutting along the partition boundary. It consists of two parts, (A) and (A-bar). Part (A) shows a network of anyons and lines with labels  $a_1, a_2, a_l, b_1, b_2, b_m, c_1, c_2, c_n$  and lines  $e_2, f_2, g_2$ . Two anyons labeled  $\omega_0$  are circled with an 'x' inside. Part (A-bar) shows the corresponding network with anyons  $a_1, a_2, a_l, b_1, b_2, b_m, c_1, c_2, c_n$  and lines  $e_2, f_2, g_2$ .

where we have chosen to represent the region  $\mathbb{A}$  in an analogous basis to that chosen in Eq. (4.139) for  $|\psi_{\text{cut}}\rangle$  of the annulus. The diagram for region  $\mathbb{A}$  embedded in three-dimensional space looks like



Finally, we can trace over region  $\bar{\mathbb{A}}$  to find the anyonic reduced density matrix for region  $\mathbb{A}$  (restoring the vertex labels):

$$\tilde{\rho}_{\mathbb{A}} = \sum_{\substack{\vec{a}, \vec{b}, \vec{c}, \\ \vec{e}, \vec{f}, \vec{g}, \\ \vec{\mu}, \vec{\nu}, \vec{\lambda}}} \frac{\sqrt{d_{\vec{a}} d_{\vec{b}} d_{\vec{c}}}}{\mathcal{D}^{2(l+m+n-5)} d_x d_y d_z} \quad (4.155)$$

Applying similar steps to those used in Eqs. (4.110)-(4.112) for the disk and in Eqs. (4.143)-(4.146) for the annulus, we find that the anyonic Rényi entropy is

$$\tilde{S}^{(\alpha)}(\tilde{\rho}_{\mathbb{A}}) = \frac{1}{1-\alpha} \log \left[ \sum_{\substack{\vec{a}, \vec{b}, \vec{c}, \vec{e}, \vec{f}, \vec{g}, \\ \vec{\mu}, \vec{\nu}, \vec{\lambda}}} \left( \frac{d_{\vec{a}} d_{\vec{b}} d_{\vec{c}}}{\mathcal{D}^{2(l+m+n-3)} d_x d_y d_z} \right)^\alpha \right]. \quad (4.156)$$

Taking the limit  $\alpha \rightarrow 1$  yields the AEE for region  $A$

$$\tilde{S}(\tilde{\rho}_A) = \lim_{\alpha \rightarrow 1} \tilde{S}^{(\alpha)}(\tilde{\rho}_A) = -(l+m+n) \sum_a \frac{d_a^2}{\mathcal{D}^2} \log \left( \frac{d_a}{\mathcal{D}} \right) - 6 \log \mathcal{D} + \log(d_x d_y d_z). \quad (4.157)$$

After taking into account the doubling of the surface, the topological contribution to the entanglement entropy for the original (un-doubled) region  $A$ , i.e. the 3-punctured sphere, is given by

$$\begin{aligned} \tilde{S}_A &= -\frac{l+m+n}{2} \sum_a \frac{d_a^2}{\mathcal{D}^2} \log \left( \frac{d_a}{\mathcal{D}} \right) - 3 \log \mathcal{D} + \log d_x + \log d_y + \log d_z \\ &= -\frac{l+m+n}{2} \tilde{S}(\tilde{\rho}_{\partial A_j}) - 3S_{\text{topo}} + \tilde{S}_x + \tilde{S}_y + \tilde{S}_z. \end{aligned} \quad (4.158)$$

We see the entanglement entropy of region  $A$  is equal to the sum of the entanglement entropies of three disks with matching boundary charge values [see Eq. (4.132)], as it should. Crucially, this implies that each separate boundary component of the region  $A$  contributes a universal  $\mathcal{O}(1)$  topological term  $\log(d_c/\mathcal{D})$  to the entanglement entropy, where  $c$  is the total topological charge on the corresponding boundary component.

### 4.5.6 General Result

Given the results of the prior examples, we can deduce the result for the general case of an arbitrary partitioning of a compact, orientable surface with genus  $g$  and arbitrary number of punctures or quasiparticles that carry topological charge. For a partitioning of the surface into regions  $A$  and  $\bar{A}$ , let us assume the joint boundary between  $A$  and  $\bar{A}$  (i.e.  $\partial A \cap \partial \bar{A}$ ) has  $N$  connected components,  $\partial A^{(1)}, \dots, \partial A^{(N)}$ . We denote the topological state of the system by  $\tilde{\rho}$ , which can be described using the anyonic formalism of fusion trees of topological charge lines of the punctures/quasiparticles and charge lines winding around non-contractible cycles. We denote the topological state of the (un-doubled)

region  $A$ , including the boundaries, by  $\tilde{\rho}_A$ . We denote by  $p_c^{(k)}$  the probability of the state  $\tilde{\rho}_A$  being in a configuration wherein  $\partial A^{(k)}$  carries topological charge  $c$ .

The topological contribution to the entanglement entropy associated with  $\partial A^{(k)}$  is

$$\tilde{S}_{\partial A^{(k)}} = -\frac{n_k}{2} \sum_a \frac{d_a^2}{\mathcal{D}^2} \log \left( \frac{d_a}{\mathcal{D}^2} \right) - \log \mathcal{D} + \sum_c p_c^{(k)} \log d_c \quad (4.159)$$

$$= \frac{n_k}{2} \tilde{S}(\tilde{\rho}_{\partial A_j}) + S_{\text{topo}} + \tilde{S}(\tilde{\rho}_{\partial A^{(k)}}). \quad (4.160)$$

Here,  $n_k \sim L_k/\ell$  is a non-universal quantity that is essentially the discretized length of the  $k$ th component of the partition boundary using some regularization.

The topological contribution to the entanglement entropy between regions  $A$  and  $\bar{A}$  is given by

$$\tilde{S}_A = \sum_{k=1}^N \tilde{S}_{\partial A^{(k)}} + \tilde{S}(\tilde{\rho}_A). \quad (4.161)$$

That is, it is the sum of the contributions from each of the partition boundary components and the anyonic entropy of the reduced density matrix of region  $A$  (including the boundary charges). Eq. (4.161) is consistent with previous studies on the entanglement entropy of orientable, higher genus surfaces supporting an  $SU(2)_k$  Chern-Simons theory [56, 63].

Generally, the superposition of charges on different partition boundary components cannot be described by independent probability distributions. As an example, the three-punctured sphere considered in Section 4.5.5 could be generalized to the case where the punctures have charges  $x$ ,  $y$ , and  $z$  with probability  $p_{xyz}$ . The constant terms in the AEE would then depend on the probability distribution  $\{p_{xyz}\}$  and it would not be possible to completely separate the terms associated with the disk containing charge  $x$  from the terms associated with the disk containing charge  $y$ . Therefore, we see that the entanglement entropy is highly state-dependent, even when we neglect the boundary-law

term. Nonetheless, the  $\mathcal{O}(1)$  partition boundary terms show up in a universal way by contributing a term  $\sum_c p_c^{(k)} \log\left(\frac{d_c}{\mathcal{D}}\right)$  for the corresponding  $k$ th component of the partition boundary.

Thus, we have determined that the entanglement entropy for a topological phase on an arbitrary compact, orientable surface (possibly including genus, punctures, and quasiparticles) partitioned into regions  $A$  and  $\bar{A}$  will take the form

$$S_A = \sum_{k=1}^N \left( \alpha L_k - \log \mathcal{D} + \sum_c p_c^{(k)} \log d_c \right) + \tilde{S}(\tilde{\rho}_A) + \mathcal{O}(L_k^{-1}), \quad (4.162)$$

where  $L_k$  is the length of the  $k$ th connected component of the partition boundary.

## 4.6 Discussion

In this paper, we have investigated the rich entanglement structure of two-dimensional topological phases with anyons by applying the standard notions of entropy to the diagrammatic representation of the TQFT. In Section 4.3, we probed the correlations between subsystems of anyons using the anyonic entanglement entropy (AEE) and the entropy of anyonic charge entanglement. We found that the fusion tensor category structure of the Hilbert space gives rise to entanglement associated with the topological charge line connecting two subsystems, a type of correlation not present in traditional quantum systems. We further found, in Sections 4.3.3 and 4.5, that the TEE is naturally explained from a decrease in the entropy (increase in order) evoked by a nonlocal (topological) constraint imposed on any region of the system by its topological order. The total fusion channel of topological charges encoding local correlations across the partition boundary is fixed when the system is cut, resulting in a very specific reduction of the AEE. We now place our results in a broader context. First, we discuss the relation of our results

to the string-net formalism of Ref. [85]. Then, we explain how our analysis also applies to topological defects and generalizes straightforwardly to fermionic topological phases. Finally, we discuss possible extensions of our methods to non-orientable surfaces and  $(3 + 1)$ -dimensional topologically ordered systems.

### 4.6.1 Relation to String-Net Models

String-nets are exactly solvable models of topological phases [85] in which “strings,” labeled by the elements of a unitary fusion tensor category (UFTC)  $\mathcal{F}$ , lie on the links of a lattice. A set of fusion rules constrains which strings may meet at a vertex. In general, the string-net model built from  $\mathcal{F}$  realizes a topological phase described by the Drinfeld center  $D(\mathcal{F})$  of  $\mathcal{F}$ . In the special case where  $\mathcal{F}$  describes the fusion structure of a MTC  $\mathcal{C}$ , the Drinfeld center takes the form  $D(\mathcal{F}) = \mathcal{C} \times \bar{\mathcal{C}}$ .

Ref. [8] found that the entanglement entropy of the (fixed point) string-net ground state of the plane partitioned into a disk region  $A$  whose boundary is crossed by  $n$  links of the lattice is

$$S_A = -n \sum_{i \in \mathcal{F}} \frac{d_i^2}{D} \log \left( \frac{d_i}{D} \right) - \log D, \quad (4.163)$$

where  $i$  and  $d_i$  are the labels and quantum dimensions, respectively, of the lattice strings.

The quantity

$$D = \mathcal{D}_{\mathcal{F}}^2 = \sum_{i \in \mathcal{F}} d_i^2 = \sqrt{\sum_{a \in D(\mathcal{F})} d_a^2} = \mathcal{D}_{D(\mathcal{F})} \quad (4.164)$$

is equal to the total quantum dimension  $\mathcal{D}_{D(\mathcal{F})}$  of the emergent TQFT  $D(\mathcal{F})$ .

In this paper, we found the entanglement entropy for a topological phase described by a UMTC  $\mathcal{C}$  by pairing the system with its time-reversal conjugate described by  $\bar{\mathcal{C}}$ , and inserting wormholes along the partition boundary to glue the two surfaces together. This process can be related to a string-net model based on the UFTC  $\mathcal{F}$  describing the fusion

structure of the UMTC  $\mathcal{C}$ . More specifically, the graph of anyon charge lines representing the state of the system in the basis where all anyon charge lines are between the two (doubled) layers of the surface (hosting  $\mathcal{C}$  and  $\bar{\mathcal{C}}$ ) is instead interpreted as the underlying lattice of the string-net model hosting  $\mathcal{F}$ . The lattice can be thought of as defining a surface (the original surface in the prior approach) and the wormholes are now thought of as passing through the (empty space at the) center of the plaquettes of the lattice. The plaquette operator  $B_p$  imposes trivial flux through the plaquettes, i.e. the  $\omega_0$ -loops circling the wormholes. Consequently, our result in Eq. (4.114), the AEE obtained from doubling a disk region of the original system, is identical to Eq. (4.163), the string-net result, when both  $a_j$  and  $i$  belong to  $\mathcal{C}$ , so that  $D = \mathcal{D}_{\mathcal{C}}^2$ .

Furthermore, when the UMTC  $\mathcal{C}$  describing the topological phase can itself be written as  $\mathcal{C} = \mathcal{E} \times \bar{\mathcal{E}}$  for some UMTC  $\mathcal{E}$ , then this phase can be realized by the string-net model built out of the UFTC  $\mathcal{E}$ .<sup>6</sup> In this case, Eq. (4.61), the topological contribution to the entanglement entropy for a topological phase described by  $\mathcal{C}$ , equals Eq. (4.163) for the corresponding string-net model built from  $\mathcal{E}$ , where  $a_j \in \mathcal{C}$  and  $i \in \mathcal{E}$ . While the TEE for a general UMTC  $\mathcal{C}$  always agrees with the string-net computation, since  $D = \mathcal{D}_{\mathcal{D}(\mathcal{F})}$ , it is interesting that the boundary length ( $n$ ) dependent terms match in this case where  $\mathcal{C} = \mathcal{E} \times \bar{\mathcal{E}}$ , that is

$$\frac{1}{2} \sum_{a \in \mathcal{C}} \frac{d_a^2}{\mathcal{D}_{\mathcal{C}}^2} \log \left( \frac{d_a}{\mathcal{D}_{\mathcal{C}}^2} \right) = \frac{1}{2} \sum_{\substack{a_L \in \mathcal{E} \\ a_R \in \bar{\mathcal{E}}}} \frac{d_{a_L}^2 d_{a_R}^2}{\mathcal{D}_{\mathcal{E}}^2 \mathcal{D}_{\bar{\mathcal{E}}}^2} \log \left( \frac{d_{a_L} d_{a_R}}{\mathcal{D}_{\mathcal{E}}^2 \mathcal{D}_{\bar{\mathcal{E}}}^2} \right) = \sum_{i \in \mathcal{E}} \frac{d_i^2}{D} \log \frac{d_i}{D}. \quad (4.165)$$

In the case where a UFTC  $\mathcal{F}$  does *not* describe the fusion structure of any UMTC, so that  $\mathcal{D}(\mathcal{F}) \neq \mathcal{E} \times \bar{\mathcal{E}}$  for any  $\mathcal{E}$ , it is not necessarily the case that there is equality between  $\frac{1}{2} \sum_{a \in \mathcal{D}(\mathcal{F})} \frac{d_a^2}{\mathcal{D}_{\mathcal{D}(\mathcal{F})}^2} \log \left( \frac{d_a}{\mathcal{D}_{\mathcal{D}(\mathcal{F})}^2} \right)$  and  $\sum_{i \in \mathcal{F}} \frac{d_i^2}{D} \log \frac{d_i}{D}$ , so the linear terms (proportional to  $n$ ) of Eq. (4.61) and Eq. (4.163) do not generally agree.

<sup>6</sup>In this case, the string-net lattice model provides a microscopic regularization of the theory.

Finally, we note that the string-net formalism gives an intuitive understanding for the form of  $S_{\text{topo}}$ . Consider a string-net model built out of an Abelian UFTC  $\mathcal{F}$ . Then  $d_i = 1$  for  $i \in \mathcal{F}$ , and  $D$  is simply the number of underlying string types  $D = |\mathcal{F}| = N$ . From Eq. (4.163), we see that the entanglement entropy is given by  $S_A = (n - 1) \log N$ . We can understand the form of  $S_A$  in this case as follows. The state space of each link in the lattice hosting the string-net has dimension  $N$ . Without conservation of topological charge, the entanglement entropy would be the sum of each link lying across the partition boundary, i.e.,  $n \log N$ . The constraint on the total charge of the lattice strings on the boundary essentially fixes the state of the last link, reducing the entanglement entropy by  $\log N = \log D = -S_{\text{topo}}$ . For a string-net built out of a UFTC  $\mathcal{F}$  describing a non-Abelian theory, the probability of a link carrying a given string is weighted by the quantum dimension of that string type, which also enters the entanglement entropy when a boundary component carries a corresponding topological charge.

### 4.6.2 Topological defects

The analysis in this paper also applies to  $(2 + 1)$ -dimensional topologically ordered systems that contain topological defects whose universal properties can be described by “ $G$ -crossed UMTCs.” This includes on-site symmetry defects [30] and translational symmetry defects [31]. In such cases, the topological defects in the system have fusion and associativity properties that are precisely the same as that of quasiparticles, and they have a generalization of braiding that incorporates the symmetry action. In particular, this means the defects have quantum dimensions in the same sense as do quasiparticles. There is also a generalization of modular transformations in the presence of defects and defect branch lines, which allows one to apply the methods of our paper in a straightforward manner. Specifically, a wormhole with trivial topological flux threading it can be re-

expressed in terms of the inside basis with topological charge lines circling the throat of the wormhole. In this case, if there is a  $\mathbf{g}$ -defect branch line around the location where the wormhole is inserted, the modular  $\mathcal{S}$ -transformation maps from the  $\mathbf{0}$ -sector for the outside basis, where topological charge lines threading the throat of the wormhole correspond to quasiparticles, to the  $\mathbf{g}$ -sector for the inside basis, where topological charge lines circling the throat of the wormhole correspond to  $\mathbf{g}$ -defects. Since the charge line through the wormhole is trivial, the amplitudes of the defect charge lines of the inside basis are proportional to their quantum dimensions, i.e.  $\mathcal{S}_{0a_{\mathbf{g}}}^{(\mathbf{0},\mathbf{g})} = \frac{d_{a_{\mathbf{g}}}}{\mathcal{D}_{\mathbf{0}}}$ , where the total quantum dimension  $\mathcal{D}_{\mathbf{0}}$  is that of the quasiparticle sector of the  $G$ -crossed theory, i.e. the total quantum dimension of the UMTC that describes the topological order without defects (see Ref. [30] for more details). It follows that the results in the presence of topological defects are exactly the same as in Eqs. (4.159)-(4.162), but the partition boundary components are now allowed to carry topological charges corresponding to quasiparticles or defects from the  $G$ -crossed MTC describing the system. This has been confirmed in the case of “twist defects” in the toric code model [60].

### 4.6.3 Fermionic Topological Phases

The analysis in this paper utilizes  $(2+1)$ -dimensional TQFTs, which describe bosonic topological phases of matter in two spatial dimensions. However, the results are straightforwardly generalized to fermionic topological phases by utilizing  $(2+1)$ -dimensional fermionic TQFTs, also known as topological spin theories [101]. A fermionic topological phase includes a physical fermion  $\psi$ , which has trivial braiding statistics with all quasiparticles in the theory, i.e. the physical fermion is transparent. The quasiparticles of the theory (including the physical fermion) are described by a super-modular tensor category (SMTC)  $\mathcal{C}_{\mathbf{0}}$ , which is a unitary braided tensor category in which the fermion  $\psi$  is trans-

| $\hat{\mathcal{D}}^2$ | SMTCs $\mathcal{C}_0$   |
|-----------------------|---|
| 1                     | $\mathbb{Z}_2^{(1)}$ (Trivial)  |
| 2                     | $\mathbb{Z}_2^{(1)} \times \mathbb{Z}_2^{(1/2)}$                                |
| 3                     | $\mathbb{Z}_2^{(1)} \times \mathbb{Z}_3^{(p)}$ , $p = 1, 2$                     |
| $\phi + 2$            | $\mathbb{Z}_2^{(1)} \times \text{Fib}^{\pm 1}$                                  |
| 4                     | $\mathbb{Z}_2^{(1)} \times \mathcal{K}_\nu$ , $\nu = 0, 1, \dots, 7$            |
| 5                     | $\mathbb{Z}_2^{(1)} \times \mathbb{Z}_5^{(p)}$ , $p = 1, 2$                     |
| 6                     | $\mathbb{Z}_2^{(1)} \times \mathbb{Z}_6^{(p)}$ , $p = \frac{1}{2}, \frac{5}{2}$ |
| $4 + 2\sqrt{2}$       | $\text{SO}(3)_6$  |
| 7                     | $\mathbb{Z}_2^{(1)} \times \mathbb{Z}_7^{(p)}$ , $p = 1, 3$                     |

Table 4.2: The quasiparticle sector of a fermionic TQFT in  $(2+1)\text{D}$  is described by a SMTC, which can be classified according to its value of the super total quantum dimension  $\hat{\mathcal{D}}$ . This table lists all distinct SMTCs with  $\hat{\mathcal{D}}^2 \leq 7$ , as determined from Refs. [82, 103, 89]. ( $\phi = \frac{1+\sqrt{5}}{2} \approx 1.6$  is the Golden ratio.) For most values of  $\hat{\mathcal{D}}$ , there are very few possible SMTCs. Moreover, the SMTCs with a given value of  $\hat{\mathcal{D}}$  are usually very closely related. Additional details may be found in C.2.

parent and the braiding is only two-fold degenerate, i.e. the degeneracy associated with the fermion. While charges in a bosonic topological phase are described by superselection sectors  $a$  of the corresponding UMTC, for the fermionic case we must think in terms of supersectors,  $\hat{a} = \{a, a \times \psi\}$ , with associated quantum dimension  $d_{\hat{a}} = d_a$ . Forming supersectors, we find that the topological  $S$ -matrix takes the form  $S = S_{\text{fermion}} \otimes \hat{S}$ , where  $S_{\text{fermion}}$  is the degenerate  $2 \times 2$   $S$ -matrix of a trivial fermion theory (i.e. the only topological charges are the vacuum and the fermion) and  $\hat{S}$  is the  $S$ -matrix of supersectors. The two-fold braiding degeneracy is equivalent to the condition that  $\hat{S}$  is unitary. For modular transformations of the fermionic topological phase, we must specify the spin structure for every nontrivial cycle of the surface (i.e., we must fix periodic or antiperiodic boundary conditions of the  $\psi$  Wilson loop for every nontrivial cycle), as this plays a crucial role in the structure of the fermionic modular transformations (see Ref. [102] for further details).

Given a fermionic TQFT, one can carry out the same steps and analogous calculations

for fermionic topological phases as in the method presented in this paper for bosonic topological phases. The main differences in the analysis will be that each wormhole will carry a trivial supersector flux  $\hat{0} = \{0, \psi\}$ , the choice of spin structures on the surfaces must be specified, and fermionic modular transformations, which act on spin structures, are used. It turns out, however, that the choice of spin structure does not affect the TEE result. We find that the TEE associated with each distinct partition boundary component for a fermionic topological phase is

$$\hat{S}_{\text{topo}} = -\log \hat{\mathcal{D}}, \quad (4.166)$$

where we have defined the super total quantum dimension by

$$\hat{\mathcal{D}} = \sqrt{\sum_{\hat{a} \in \hat{\mathcal{C}}_0} d_a^2} = \sqrt{\frac{1}{2} \sum_{a \in \mathcal{C}_0} d_a^2}. \quad (4.167)$$

This result has been confirmed for various fermionic fractional quantum Hall states [66, 67, 58, 68, 74, 75, 78].

Similar to the case of UMTCs, there are only a finite number of possible SMTCs for a particular value of  $\hat{\mathcal{D}}$ . In Table 4.2, we list all SMTCs for  $\hat{\mathcal{D}}^2 \leq 7$ .

#### 4.6.4 Non-orientable surfaces

An interesting future direction would be to generalize our analysis to study the entanglement entropy on non-orientable surfaces. We expect the construction of the reduced density matrix outlined in the beginning of Section 4.5 will differ for non-orientable surfaces in step 3. That is, the  $\mathcal{S}$ -transformation on a non-orientable surface will no longer necessarily result in an  $\omega_0$ -loop. Rather, the superposition of charges circling each wormhole will be a subset of all charges in the theory (see Ref. [104] for a discussion of state

sums on non-orientable surfaces). Nonetheless, we anticipate that the TEE will still originate from the conservation of topological charge.

### 4.6.5 Three dimensional topological phases

Finally, one could also extend our method of calculating the entanglement entropy to  $(3 + 1)$ -dimensional topological phases. Previous investigations of the TEE in  $(3 + 1)$ -dimensions have utilized a linear combination of spatial regions to isolate the boundary-independent contribution to the entanglement entropy, similarly to the  $(2+1)$ -dimensional Kitaev-Preskill method [57, 59, 62, 64]. Dividing the partition boundary into smaller regions, as in our method for  $(2 + 1)$ -dimensions, could elucidate how the conservation of more general topological quantum numbers results in a reduction of the entanglement entropy in  $(3 + 1)$ -dimensions. This analysis could be carried out for exactly solvable models [57, 68, 105, 106], or more generally using TQFT methods.

# Appendix A

## A.1 $\mathbb{Z}_2^{(1/2)}$ (Doubled Semion)

The  $\mathbb{Z}_2^{(1/2)}$  model[107] uses the  $\mathbb{Z}_2^{(1/2)}$  UFC:

- String types 0 and 1,
- Allowed branchings  $\{0, 0, 0\}$ ,  $\{0, 1, 1\}$ ,
- Quantum dimensions  $d_0 = 1$ ,  $d_1 = -1$ , and
- $F_{110}^{110} = -1$ . All other admissible  $F_{klm}^{ijm} = 1$ .

The Hamiltonian is

$$\mathbf{H}_{\mathbb{Z}_2^{(1/2)}}^{(0)} = - \sum_{\mathbf{v}} \mathbf{Q}_{\mathbf{v}} - \sum_{\mathbf{p}} \frac{1}{2} (\mathbf{B}_{\mathbf{p}}^0 - \mathbf{B}_{\mathbf{p}}^1). \quad (\text{A.1})$$

The ground state is given by:

$$|0\rangle = \sum_{|X\rangle \in \substack{\text{closed loop} \\ \text{string-nets}}} (-1)^{n_{\mathbb{C}}(|X\rangle)} |X\rangle, \quad (\text{A.2})$$

where  $n_{\mathbb{C}}(|X\rangle)$  is the number of closed loops in  $|X\rangle$ . Using Appendix A.5, the ground state degeneracy on a manifold with genus  $g$  is  $4^g$ .

If we represent the strings as spin- $\frac{1}{2}$  particles, where the 0 string is  $|+z\rangle$  and the 1 string is  $|-z\rangle$ , then  $\mathbf{Q}_v$  and  $\mathbf{B}_p^{(0)}$  can be written in terms of Pauli matrices:

$$\mathbf{Q}_v = \frac{1}{2} \left( 1 + \prod_{i \in v \text{ legs}} \sigma_i^z \right) \quad (\text{A.3})$$

$$\begin{aligned} \mathbf{B}_p^{(0)} &= \frac{1}{2} \left( 1 - \prod_{i \in p \text{ edges}} \sigma_i^x \cdot \prod_{j \in p \text{ legs}} i^{\frac{1-\sigma_j^z}{2}} \right) \\ &\times \prod_{v \in p \text{ vertices}} \mathbf{Q}_v \end{aligned} \quad (\text{A.4})$$

Omitting the  $\prod_v \mathbf{Q}_v$  term in  $\mathbf{B}_p^{(0)}$ , which acts trivially on the ground state, this Hamiltonian is equivalent to,

$$\mathbf{H} = - \sum_v \prod_{i \in v \text{ legs}} \sigma_i^z - \sum_p \prod_{i \in p \text{ edges}} \sigma_i^x \cdot \prod_{j \in p \text{ legs}} i^{\frac{1-\sigma_j^z}{2}}, \quad (\text{A.5})$$

up to a factor of 2 and an overall energy shift. (Actually, when written in terms of Pauli matrices,  $\mathbf{B}_p^{(0)}$  needs to be modified in order for  $\mathbf{H}_{\mathbb{Z}_2^{(1/2)}}^{(0)}$  to be exactly solvable. [108])

There are four string operators, which belong to the  $\mathbb{Z}_2^{(1/2)} \times \overline{\mathbb{Z}_2^{(1/2)}}$  MTC. When acting along a path P, they can be written in terms of Pauli matrices:

$$\mathbf{W}_I = I, \quad (\text{A.6})$$

$$\mathbf{W}_s = \prod_{i \in P \text{ edges}} \sigma_i^x \cdot \prod_{j \in P \text{ r-legs}} i^{\frac{1-\sigma_j^z}{2}} \cdot \prod_{k \in P \text{ l-legs}} (-1)^{\theta_k}, \quad (\text{A.7})$$

$$\mathbf{W}_{\bar{s}} = \prod_{i \in P \text{ edges}} \sigma_i^x \cdot \prod_{j \in P \text{ r-legs}} (-i)^{\frac{1-\sigma_j^z}{2}} \cdot \prod_{k \in P \text{ l-legs}} (-1)^{\theta_k}, \quad (\text{A.8})$$

$$\mathbf{W}_b = \prod_{i \in P \text{ r-legs}} \sigma_i^z. \quad (\text{A.9})$$

Here,  $\theta_k = \frac{1}{4}(1 - \sigma_i^z)(1 - \sigma_j^z)$ , where i and j are the links that come just before and just after the link k along the path, respectively. An open  $\mathbf{W}_s$  creates a  $\mathbf{Q}_v$  violating semion

$\mathbf{s}$  at each of its endpoints,  $\mathbf{W}_{\bar{\mathbf{s}}}$  creates a  $\mathbf{Q}_v$  violating semion  $\bar{\mathbf{s}}$ , and  $\mathbf{W}_{\mathbf{b}}$  creates a  $\mathbf{B}_p^{(0)}$  violating boson  $\mathbf{b}$ . (If we do not omit the  $\prod_v \mathbf{Q}_v$  term in the definition of  $\mathbf{B}_p^{(0)}$ , then  $\mathbf{W}_{\mathbf{s}}$  and  $\mathbf{W}_{\bar{\mathbf{s}}}$  also create three  $\mathbf{B}_p^{(0)}$  violations at their endpoints.)

The  $\mathcal{S}$  and  $\mathcal{T}$  matrices are:

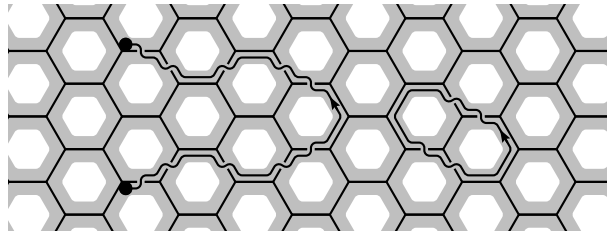
$$\mathcal{S}_{\mathbb{Z}_2^{(1/2)} \times \mathbb{Z}_2^{(1/2)}} = \frac{1}{2} \begin{bmatrix} 1 & 1 & 1 & 1 \\ 1 & -1 & 1 & -1 \\ 1 & 1 & -1 & -1 \\ 1 & -1 & -1 & 1 \end{bmatrix}, \quad (\text{A.10})$$

$$\mathcal{T}_{\mathbb{Z}_2^{(1/2)} \times \mathbb{Z}_2^{(1/2)}} = \text{diag}(1, i, -i, 1). \quad (\text{A.11})$$

The rows and columns of  $\mathcal{S}$  and  $\mathcal{T}$  correspond to  $\mathbf{I}$ ,  $\mathbf{s}$ ,  $\bar{\mathbf{s}}$ ,  $\mathbf{b}$ . The  $\mathbf{s}$  and  $\bar{\mathbf{s}}$  quasiparticles are anyons of opposite chiralities, while  $\mathbf{b}$  is a boson.

## A.2 String Operators

A string operators  $\mathbf{W}_a$  can be represented strings acting along an open or closed paths on the fattened honeycomb lattice.



The fattened honeycomb lattice is obtained by slightly thickening every link of a regular honeycomb lattice. The string operator on the fattened lattice can be reduced to lattice

states by using the following rules:

1.  =  $\sum_{jst} \Omega_{\mathbf{a},sti}^j$  .
2.  =  $\sum_{jst} \bar{\Omega}_{\mathbf{a},sti}^j$  .
3.  = .
4.  =  $d_i$  .
5.  =  $\delta_{ij}$  .
6.  =  $\sum_n F_{kln}^{ijm}$  .

Thus, the string operators are characterized by  $(\Omega_{\mathbf{a},sti}^j, \bar{\Omega}_{\mathbf{a},sti}^j)$ .

The  $\Omega$  symbols are constrained by the fact that string operators are isotopy invariant,

$$\img alt="Diagram 13: A box with input a and output i, and another box with input i* and output a." data-bbox="440 511 490 541"/> = , \tag{A.12}$$

and can be passed freely over the vertices of the lattice along their middle,

$$\img alt="Diagram 15: A vertex with inputs k, i and output j, and a string operator passing through it." data-bbox="450 618 500 652"/> = . \tag{A.13}$$

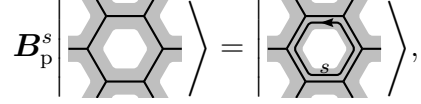
These two conditions are expressed, respectively, by the following equations:

$$\bar{\Omega}_{\mathbf{a},sti}^j = \sum_k \Omega_{\mathbf{a},sti^*}^k F_{i^*sj^*}^{it^*k}, \tag{A.14}$$

$$\sum_s \bar{\Omega}_{\mathbf{a},rsj}^m F_{kjm^*}^{sl^*i} \Omega_{\mathbf{a},sti}^l \frac{v_j v_s}{v_m} = \sum_n F_{t^*nl^*}^{ji^*k} \Omega_{\mathbf{a},rtk}^n F_{krm^*}^{jl^*n}. \tag{A.15}$$

For a given UFTC, there are only a finite number of irreducible solutions to these equations, due to Ocneanu rigidity.

The operator  $B_p^s$  is a string operator that creates a loop of string  $s$  in the plaquette  $p$ :

$$B_p^s \left| \begin{array}{c} \text{---} \\ \text{---} \\ \text{---} \\ \text{---} \\ \text{---} \\ \text{---} \end{array} \right\rangle = \left| \begin{array}{c} \text{---} \\ \text{---} \\ \text{---} \\ \text{---} \\ \text{---} \\ \text{---} \end{array} \right\rangle, \quad (\text{A.16})$$


which can be reduced to Eq. (2.8) using the above rules.

### A.3 Corrections to $\mathcal{S}$ and $\mathcal{T}$

The original  $\mathcal{S}$  and  $\mathcal{T}$  matrices were defined as:[24]

$$[\mathcal{S}]_{ab} = \frac{1}{\mathcal{D}_{D(c)}} \langle 0 | a \text{---} b | 0 \rangle, \quad (\text{A.17})$$

$$[\mathcal{T}]_{ab} = \frac{\langle 0 | \text{---} a | 0 \rangle}{\langle 0 | \text{---} a | 0 \rangle} \delta_{ab}. \quad (\text{A.18})$$

These are incorrect for models with underlying strings whose quantum dimension are negative.

For example, using the original definitions applied to the  $\mathbb{Z}_2^{(1/2)}$  model yields the incorrect results

$$\mathcal{S} = \mathcal{S}_{\mathbb{Z}_2^{(1/2)}} \otimes \mathcal{S}_{\mathbb{Z}_2^{(1/2)}}^* = \frac{1}{2} \begin{bmatrix} 1 & -1 & -1 & 1 \\ -1 & -1 & 1 & 1 \\ -1 & 1 & -1 & 1 \\ 1 & 1 & 1 & 1 \end{bmatrix}, \quad (\text{A.19})$$

$$\mathcal{T} = \mathcal{T}_{\mathbb{Z}_2^{(1/2)}} \otimes \mathcal{T}_{\mathbb{Z}_2^{(1/2)}}^* = \text{diag}(1, -i, i, 1), \quad (\text{A.20})$$

where  $\mathcal{S}_{\mathbb{Z}_2^{(1/2)}}$  and  $\mathcal{T}_{\mathbb{Z}_2^{(1/2)}}$  are from the  $\mathbb{Z}_2^{(1/2)}$  MTC:

$$\mathcal{S}_{\mathbb{Z}_2^{(1/2)}} = \frac{1}{\sqrt{2}} \begin{bmatrix} 1 & -1 \\ -1 & -1 \end{bmatrix}, \quad (\text{A.21})$$

$$\mathcal{T}_{\mathbb{Z}_2^{(1/2)}} = \text{diag}(1, i). \quad (\text{A.22})$$

(Compare Eq. (A.19) and (A.20) with Eq. (A.10) and (A.11).)

The origin of this correction lies in the distinction between diagrams in anyons models and diagrams in string-net models. In anyon models, diagrams represent states in the topological Hilbert space. For example, pair creating  $\mathbf{a}$  and  $\mathbf{a}^*$  from the vacuum results in the state:

$$|\mathbf{a}, \bar{\mathbf{a}}; \mathbf{0}\rangle = \begin{array}{c} \mathbf{a} \quad \mathbf{a}^* \\ \diagdown \quad / \\ \mathbf{0} \\ \vdots \end{array}, \quad (\text{A.23})$$

where we have omitted the usual isotopy normalization. Unitarity requires that all states in anyon models have non-negative norms. For example,

$$\langle \mathbf{a}, \bar{\mathbf{a}}; \mathbf{0} | \mathbf{a}, \bar{\mathbf{a}}; \mathbf{0} \rangle = \begin{array}{c} \mathbf{0} \\ \vdots \\ \mathbf{a} \quad \mathbf{a}^* \\ \diagdown \quad / \\ \mathbf{a} \quad \mathbf{a}^* \\ \diagup \quad \diagdown \\ \mathbf{0} \\ \vdots \end{array} = d_{\mathbf{a}} > 0. \quad (\text{A.24})$$

On the other hand, the above diagram in a string-net model represents a closed  $\mathbf{W}_{\mathbf{a}}$  string operator acting on the ground state,

$$\langle 0 | \mathbf{O}_{\mathbf{a}} | 0 \rangle, \quad (\text{A.25})$$

and could possibly be negative. The disagreement between these two results is captured by  $\varkappa_{\mathbf{a}}$ .

The  $\mathcal{S}$  matrix is technically defined by an inner product in the anyon model: create a pair of  $\mathbf{a}$  and  $\mathbf{a}^*$  and a pair of  $\mathbf{b}$  and  $\mathbf{b}^*$  from vacuum, braid  $\mathbf{a}^*$  around  $\mathbf{b}$ , and compute the inner product of the resulting state with the initial state before the braid.

$$[\mathcal{S}_{D(c)}]_{ab} = \frac{1}{\mathcal{D}_{D(c)}} \text{Diagram} \tag{A.26}$$

Thus, when expressing the  $\mathcal{S}$  matrix with a similar string-net diagram, we must be careful to include factors of  $\varkappa_a$  and  $\varkappa_b$ .

The same reasoning also applies to the  $\mathcal{T}$  matrix.

### A.4 Ising String Operators

The  $\Omega$  symbols that define the nine string operators of the Ising model are given in Table A.1.

We can view these string operators as a pair of Ising strings running above and below

| $\mathbf{a}$ | $(a_A, a_B)$       | $\theta_{\mathbf{a}}$ | $\Omega_{\mathbf{a},sti}^j$  | Visual Representation  |
|--------------|--------------------|-----------------------|--|--|
| <b>0</b>     | $(I, I)$           | 0                     | $\Omega_{\mathbf{0},III}^I = 1$<br>$\Omega_{\mathbf{0},II\sigma}^\sigma = 1$<br>$\Omega_{\mathbf{0},II\psi}^\psi = 1$  | $\diagup = \diagdown$<br>$\times = \times$<br>$\bowtie = \bowtie$  |
| <b>1</b>     | $(I, \sigma)$      | $-\frac{\pi}{8}$      | $\Omega_{\mathbf{1},\sigma\sigma I}^\sigma = 1$<br>$\Omega_{\mathbf{1},\sigma\sigma\sigma}^I = \frac{1}{\sqrt{2}}e^{-\frac{\pi i}{8}}, \Omega_{\mathbf{4},\sigma\sigma\sigma}^\psi = \frac{1}{\sqrt{2}}e^{\frac{3\pi i}{8}}$<br>$\Omega_{\mathbf{1},\sigma\sigma\psi}^\sigma = -i$           | $\diagup = \diagdown$<br>$\times = \frac{1}{\sqrt{2}}(e^{-\frac{\pi i}{8}} \times + e^{\frac{3\pi i}{8}} \times)$<br>$\bowtie = -i \bowtie$  |
| <b>2</b>     | $(I, \psi)$        | $\pi$                 | $\Omega_{\mathbf{2},\psi\psi I}^\psi = 1$<br>$\Omega_{\mathbf{2},\psi\psi\sigma}^\sigma = -i$<br>$\Omega_{\mathbf{2},\psi\psi\psi}^I = -1$   | $\diagup = \diagdown$<br>$\times = -i \times$<br>$\bowtie = -\bowtie$  |
| <b>3</b>     | $(\sigma, I)$      | $\frac{\pi}{8}$       | $\Omega_{\mathbf{3},\sigma\sigma I}^\sigma = 1$<br>$\Omega_{\mathbf{3},\sigma\sigma\sigma}^I = \frac{1}{\sqrt{2}}e^{\frac{\pi i}{8}}, \Omega_{\mathbf{3},\sigma\sigma\sigma}^\psi = \frac{1}{\sqrt{2}}e^{-\frac{3\pi i}{8}}$<br>$\Omega_{\mathbf{3},\sigma\sigma\psi}^\sigma = i$            | $\diagup = \diagdown$<br>$\times = \frac{1}{\sqrt{2}}(e^{\frac{\pi i}{8}} \times + e^{-\frac{3\pi i}{8}} \times)$<br>$\bowtie = i \bowtie$   |
| <b>4</b>     | $(\sigma, \sigma)$ | 0                     | $\Omega_{\mathbf{4},III}^I = 1, \Omega_{\mathbf{4},\psi\psi I}^\psi = 1$<br>$\Omega_{\mathbf{4},I\psi\sigma}^\sigma = e^{\frac{\pi i}{4}}, \Omega_{\mathbf{4},\psi I\sigma}^\sigma = e^{-\frac{\pi i}{4}}$<br>$\Omega_{\mathbf{4},II\psi}^\psi = -1, \Omega_{\mathbf{4},\psi\psi\psi}^I = 1$ | $\diagup = \diagdown + \bowtie$<br>$\times = e^{\frac{\pi i}{4}} \times + e^{-\frac{\pi i}{4}} \times$<br>$\bowtie = -\bowtie + \bowtie$     |
| <b>5</b>     | $(\sigma, \psi)$   | $-\frac{7\pi}{8}$     | $\Omega_{\mathbf{5},\sigma\sigma I}^\sigma = 1$<br>$\Omega_{\mathbf{5},\sigma\sigma\sigma}^I = \frac{1}{\sqrt{2}}e^{-\frac{7\pi i}{8}}, \Omega_{\mathbf{6},\sigma\sigma\sigma}^\psi = \frac{1}{\sqrt{2}}e^{\frac{5\pi i}{8}}$<br>$\Omega_{\mathbf{5},\sigma\sigma\psi}^\sigma = i$           | $\diagup = \diagdown$<br>$\times = -\frac{1}{\sqrt{2}}(e^{\frac{\pi i}{8}} \times + e^{-\frac{3\pi i}{8}} \times)$<br>$\bowtie = i \bowtie$  |
| <b>6</b>     | $(\sigma, I)$      | $\pi$                 | $\Omega_{\mathbf{6},\psi\psi I}^\psi = 1$<br>$\Omega_{\mathbf{6},\psi\psi\sigma}^\sigma = i$<br>$\Omega_{\mathbf{6},\psi\psi\psi}^I = -1$  | $\diagup = \diagdown$<br>$\times = i \times$<br>$\bowtie = -\bowtie$   |
| <b>7</b>     | $(\psi, I)$        | $\frac{7\pi}{8}$      | $\Omega_{\mathbf{7},\sigma\sigma I}^\sigma = 1$<br>$\Omega_{\mathbf{7},\sigma\sigma\sigma}^I = \frac{1}{\sqrt{2}}e^{\frac{7\pi i}{8}}, \Omega_{\mathbf{7},\sigma\sigma\sigma}^\psi = \frac{1}{\sqrt{2}}e^{-\frac{5\pi i}{8}}$<br>$\Omega_{\mathbf{7},\sigma\sigma\psi}^\sigma = -i$          | $\diagup = \diagdown$<br>$\times = -\frac{1}{\sqrt{2}}(e^{-\frac{\pi i}{8}} \times + e^{\frac{3\pi i}{8}} \times)$<br>$\bowtie = -i \bowtie$ |
| <b>8</b>     | $(\psi, \psi)$     | 0                     | $\Omega_{\mathbf{8},III}^I = 1$<br>$\Omega_{\mathbf{8},II\sigma}^\sigma = -1$<br>$\Omega_{\mathbf{8},II\psi}^\psi = 1$   | $\diagup = \diagdown$<br>$\times = -\times$<br>$\bowtie = \bowtie$   |

Table A.1: Ising model string operators.

the lattice, i.e.  $\mathbf{a} = (a_A, a_B)$ , where  $a_A, a_B \in \{I, \sigma, \psi\}$ . To show this, note that

$$\begin{aligned}
\frac{i}{\frac{a_A}{a_B}} \begin{array}{c} \text{---} \\ \text{---} \\ \text{---} \end{array} &= \sum_{stkl} \frac{v_s v_t}{d_{a_A} d_{a_B}} \frac{v_k v_l}{v_{a_A} v_{a_B} d_i} \\
&\quad \frac{i}{\frac{a_A}{a_B}} \begin{array}{c} \text{---} \\ \text{---} \\ \text{---} \end{array} \begin{array}{c} \text{---} \\ \text{---} \\ \text{---} \end{array} \\
&= \sum_{stkl} \frac{v_s v_t}{d_{a_A} d_{a_B}} \frac{v_k v_l}{v_{a_A} v_{a_B} d_i} (R_k^{a_A i})^{-1} R_l^{i a_B} \\
&\quad \frac{i}{\frac{a_A}{a_B}} \begin{array}{c} \text{---} \\ \text{---} \\ \text{---} \end{array} \begin{array}{c} \text{---} \\ \text{---} \\ \text{---} \end{array} \\
&= \sum_{stjkl} \frac{v_k v_l}{v_{a_A} v_{a_B} d_i} (R_k^{a_A i})^{-1} R_l^{i a_B} \\
&\quad F_{a_B l j}^{a_A k i} F_{i a_A s}^{a_B j k} F_{i a_B t}^{a_A j l} \frac{i}{\frac{a_A}{a_B}} \begin{array}{c} \text{---} \\ \text{---} \\ \text{---} \end{array} \begin{array}{c} \text{---} \\ \text{---} \\ \text{---} \end{array} \quad (A.27)
\end{aligned}$$

where we have used the  $R$  symbols of the Ising MTC. Since it can be explicitly checked that for all  $\mathbf{a}$ ,

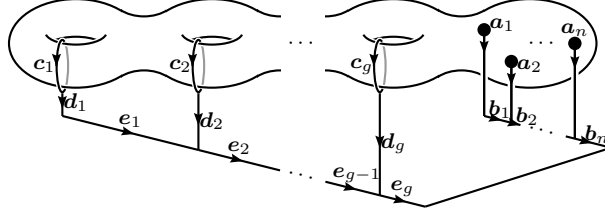
$$\Omega_{\mathbf{a}, sti}^j = \sum_{kl} \frac{v_k v_l}{v_s d_i} (R_k^{a_A i})^{-1} R_l^{i a_B} F_{a_B l j}^{a_A k i} F_{i a_A s}^{a_B j k} F_{i a_B t}^{a_A j l}, \quad (A.28)$$

and since the same argument holds for  $\bar{\Omega}_{\mathbf{a}, sti}^j$ , we can view the string operators as pairs of Ising strings.

## A.5 GSD from Verlinde Equation

Consider a system in an ideal topological phase with  $n$  quasiparticles on a manifold of genus  $g$ . The ground state degeneracy  $\mathcal{N}_{g, \{a_1, \dots, a_n\}}$  can be counted by threading an anyon through each of the handles, and then counting the degeneracy of the resulting

fusion tree.



This degeneracy is given by:

$$\begin{aligned}
& \sum_{c_1 \cdots c_g} \sum_{d_1 \cdots d_g} \sum_{e_1 \cdots e_g} \sum_{b_1 \cdots b_n} \delta_{d_1 e_1} \delta_{a_1 b_1} \delta_{e_g b_n^*} \\
& \quad \times [N_{c_1}]_{c_1^* d_1} \cdots [N_{c_g}]_{c_g^* d_g} \\
& \quad \times [N_{e_1}]_{d_2 e_2} \cdots [N_{e_{g-1}}]_{d_g e_g} \\
& \quad \times [N_{b_1}]_{a_2 b_2} \cdots [N_{b_{n-1}}]_{a_n b_n}. \tag{A.29}
\end{aligned}$$

Using the Verlinde formula, unitarity of  $\mathcal{S}$ , and  $[\mathcal{S}]_{ab} = [\mathcal{S}]_{ba} = [\mathcal{S}]_{a^*b}^*$  yields: [109]

$$\mathcal{N}_{g, \{a_1, \dots, a_n\}} = \sum_x [\mathcal{S}]_{0x}^{2-2g-n} [\mathcal{S}]_{a_1 x} \cdots [\mathcal{S}]_{a_n x}. \tag{A.30}$$

For doubled Chern-Simons theories, we can also calculate the ground state degeneracy using App. A.6.

## A.6 GSD for Doubled Chern-Simons Theories

For doubled Chern-Simons theories, a flux phase can be viewed as an underlying string passing through each plaquette. We can exploit this property to calculate the ground state degeneracy in a different way than App. A.5. We show this by considering the smooth phase and flux phases of the Ising model.

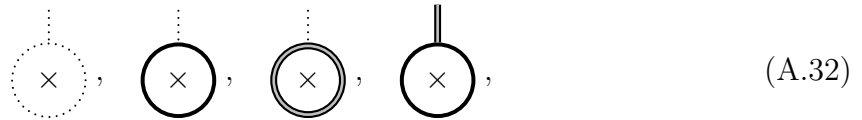
### A.6.1 Ising Smooth Phase

Consider the case when the lattice is supported by a manifold with genus  $g$ . Since there is  $I$  flux passing through every plaquette, every handle is free to have a  $I$ ,  $\sigma$ , or  $\psi$  string wrapping around it on the outside as long as we can form a fusion tree out of these strings that results in a net  $I$  string.

For example, on a torus there are three possibilities:



where  $i$  can be a  $I$ ,  $\sigma$ , or  $\psi$  string. In general, there are four ways of wrapping strings around a handle:



where  $\times$  represents a handle. Note that the fourth configuration must come in pairs, so that the resulting fusion is a  $I$  string. Counting the number of ways to assign pairs of the fourth configuration to some of the handles and the first three configurations to the rest yields:

$$\sum_{n=0}^{\lfloor g/2 \rfloor} \binom{g}{2n} 3^{g-2n} = 2^{g-1}(2^g + 1). \quad (\text{A.33})$$

Since the same argument can be applied independently inside the manifold, the ground state degeneracy is:

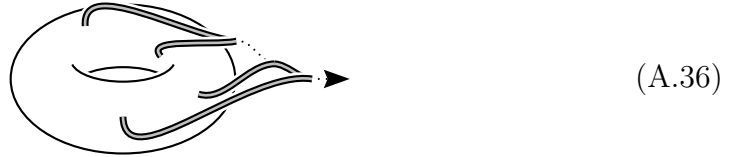
$$(2^{g-1}(2^g + 1))^2 = 4^{g-1}(2^g + 1)^2. \quad (\text{A.34})$$

This result agrees with App. A.5:

$$\mathcal{N}_g = 4^{g-1}(2^g + 1)^2. \quad (\text{A.35})$$

### A.6.2 Ising $\psi$ Flux Phase

Consider the case when a lattice with an even number of plaquettes is supported by a manifold with genus  $g$ . The  $\psi$  flux strings outside of the manifold can all be fused to a single string. Since there are an even number of plaquettes, the result of this fusion is a  $I$  string. For example, when a lattice with four plaquettes is supported by a torus, the fusion tree would look like:



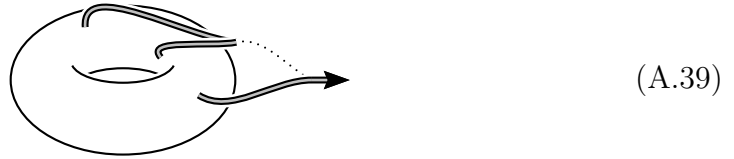
Therefore, every handle is free to have a  $I$ ,  $\sigma$ , or  $\psi$  string wrapping around it on the outside as long as we can form a fusion tree out of these strings that results in a net  $I$  string. For example, on the torus there are three possibilities:



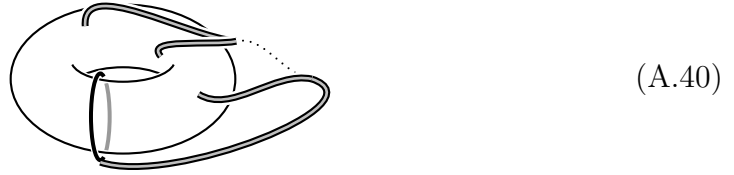
where the string  $i$  can be  $0$ ,  $\sigma$ , or  $\psi$ . This degeneracy was counted in Sec. A.6.1 to be  $2^{g-1}(2^g + 1)$ . Since the same argument can be applied independently inside the manifold, the ground state degeneracy is:

$$(2^{g-1}(2^g + 1))^2 = 4^{g-1}(2^g + 1)^2. \quad (\text{A.38})$$

Now consider the case when a lattice with an odd number of plaquettes is supported by a manifold with genus  $g$ . Again, the  $\psi$  flux strings outside of the manifold can all be fused to a single string. Since there are an odd number of plaquettes, the result of this fusion is a  $\psi$  string. For example, when the lattice with three plaquettes is supported by a torus, the fusion tree would look like:



Therefore, every handle is free to have a  $I$ ,  $\sigma$ , or  $\psi$  string wrapping around it on the outside as long as we can form a fusion tree out of these strings that results in a net  $\psi$  string. For example, on the torus there is only one possibility:



Counting the degeneracy of this, following an argument similar to that of Sec. A.6.1, yields:

$$\sum_{n=0}^{\lfloor g/2 \rfloor} \binom{g}{2n+1} 3^{g-(2n+1)} = 2^{g-1}(2^g - 1). \quad (\text{A.41})$$

Since the same argument can be applied independently inside the manifold, the ground state degeneracy is:

$$(2^{g-1}(2^g - 1))^2 = 4^{g-1}(2^g - 1)^2. \quad (\text{A.42})$$

These results agree with Appendix A.5:

$$\mathcal{N}_{g, \{(\psi, \psi), \dots, (\psi, \psi)\}} = 4^{g-1}(1 + (-1)^N 2^{g+1} + 4^g), \quad (\text{A.43})$$

where  $\{(\psi, \psi), \dots, (\psi, \psi)\}$  represents  $N$  number of  $(\psi, \psi)$ .

### A.6.3 Ising $\sigma$ Flux Phase

Consider the case when a lattice with an even number of plaquettes is supported by a manifold with genus  $g$ . Then, the  $\sigma$  fluxes outside of the manifold can all be fused to a single string. Since there are an even number of plaquettes, the result of this fusion is  $I$  or  $\psi$ , each with a degeneracy of  $2^{N/2-1}$ . Therefore, every handle is free to have a  $I$ ,  $\sigma$ , or  $\psi$  string wrapping around it on the outside as long as we can form a fusion tree out of these strings that results in a net  $I$  or  $\psi$  string. The degeneracy of this, following arguments similar to those of Sec. A.6.1, is  $4^g$ . Since the same argument can be applied independently inside the manifold, the ground state degeneracy is:

$$(2^{N/2-1}4^g)^2 = 2^{N-2}16^g. \quad (\text{A.44})$$

Now consider the case when a lattice with an odd number of plaquettes is supported by a manifold with genus  $g$ . The  $\sigma$  fluxes outside of the manifold can all be fused to a single string. However, since there are an odd number of plaquettes, the result of the fusion is now a  $\sigma$  string. Therefore, every handle is free to have a  $I$ ,  $\sigma$ , or  $\psi$  string wrapping around it on the outside as long as we can form a fusion tree out of these strings that results in a net  $\sigma$  string. However, this is impossible. So, we conclude that the ground state is frustrated and one of the  $N$  plaquettes must have a  $I$  or  $\psi$  flux, while the  $N - 1$  remaining plaquettes form a fusion tree with a degeneracy of  $2^{(N-1)-2}16^g$ . Thus, the ground state degeneracy is:

$$2N \times 2^{(N-1)-2}16^g = N2^{N-2}16^g. \quad (\text{A.45})$$

These results agree with Appendix A.5:

$$\mathcal{N}_{g,\{(\sigma,\sigma),\dots,(\sigma,\sigma)\}} = 2^{N-3}(1 + (-1)^N)16^g, \quad (\text{A.46})$$

where  $\{(\sigma, \sigma), \dots, (\sigma, \sigma)\}$  represents  $N$  number of  $(\sigma, \sigma)$ .

## A.7 $\mathbb{Z}_2^{(1/2)}$ Flux Phase

The Hamiltonian is:

$$\mathbf{H}_{\mathbb{Z}_2^{(1/2)}}^{(1)} = -\sum_{\mathbf{v}} \mathbf{Q}_{\mathbf{v}} - \sum_{\mathbf{p}} \frac{1}{2} (\mathbf{B}_{\mathbf{p}}^0 + \mathbf{B}_{\mathbf{p}}^1) \quad (\text{A.47})$$

$$\begin{aligned} &= -\sum_{\mathbf{v}} \frac{1}{2} \left( 1 + \prod_{i \in \mathbf{v} \text{ legs}} \sigma_i^z \right) \\ &\quad - \sum_{\mathbf{p}} \frac{1}{2} \left( 1 - \prod_{i \in \mathbf{p} \text{ edges}} \sigma_i^x \right), \end{aligned} \quad (\text{A.48})$$

where we have again omitted the  $\prod_{\mathbf{v}} \mathbf{Q}_{\mathbf{v}}$  in the definition of  $\mathbf{B}_{\mathbf{p}}^{(1)}$ .

Since the  $\mathbb{Z}_2^{(1/2)}$  UFTC can be made into a MTC, the ground state corresponds to having a 1 string passing through every plaquette. It is given by:

$$|0\rangle = \sum_{|X\rangle \in \substack{\text{closed loop} \\ \text{string-nets}}} (-1)^{n_{\mathbf{p}}(|X\rangle) + n_{\mathbf{c}}(|X\rangle)} |X\rangle, \quad (\text{A.49})$$

where  $n_{\mathbf{p}}(|X\rangle)$  is the number of plaquettes contained by closed loops in  $|X\rangle$  and  $n_{\mathbf{c}}(|X\rangle)$  is the number of closed loops. Using App. A.5, the ground state degeneracy for a lattice with an even number of plaquettes  $N$  on a manifold of genus  $g$  is  $\mathcal{N}_{g,\{(1,1),\dots,(1,1)\}} = 4^g$ , where  $\{(1,1), \dots, (1,1)\}$  represents  $N$  number of  $(1,1)$ . For a lattice with an odd number of plaquettes, the system is actually frustrated and the ground state degeneracy is  $4^g N$ .

The four string operators of the smooth phase can still be applied in the flux phase to create excitations, but  $\mathbf{W}_s$  and  $\mathbf{W}_{\bar{s}}$  now acquire a factor of  $-1$  every time they are passed over a plaquette.

### A.7.1 Even Plaquette Solution

For a lattice with an even number of plaquettes, we can use a change of basis to solve  $\mathbf{H}_{\mathbb{Z}_2}^{(1)}$ . We mark links on the lattice in such a way that each hexagon has exactly one marked link, as shown in Fig. 2.2, and apply the change of basis  $\mathbf{\Lambda}$ :

$$\mathbf{\Lambda} = \mathbf{\Lambda}^{-1} = \prod_{i \in \text{marked links}} \mathbf{\Lambda}_i \quad (\text{A.50})$$

where

$$\mathbf{\Lambda}_i = \boldsymbol{\sigma}_i^z = \begin{bmatrix} 1 & 0 \\ 0 & -1 \end{bmatrix} \quad (\text{A.51})$$

multiplies the amplitude of a lattice state by a factor of  $-1$  if its link  $i$  is occupied by a 1 string. Since every hexagon has exactly one marked link, and

$$\boldsymbol{\sigma}_i^z \boldsymbol{\sigma}_j^x \boldsymbol{\sigma}_i^z = \begin{cases} \boldsymbol{\sigma}_j^x, & i \neq j \\ -\boldsymbol{\sigma}_j^x, & i = j \end{cases}, \quad (\text{A.52})$$

the change of basis transforms the flux Hamiltonian into the smooth Hamiltonian:

$$\tilde{\mathbf{H}}_{\mathbb{Z}_2}^{(1)} = \mathbf{\Lambda}^{-1} \mathbf{H}_{\mathbb{Z}_2}^{(1)} \mathbf{\Lambda} = \mathbf{H}_{\mathbb{Z}_2}^{(0)}. \quad (\text{A.53})$$

Thus, we can understand the flux phase by applying the change of basis to the smooth phase results.

The ground state in the flux phase is

$$|0\rangle = \sum_{|X\rangle \in \substack{\text{closed loop} \\ \text{string-nets}}} (-1)^{n_M(|X\rangle) + n_C(|X\rangle)} |X\rangle, \quad (\text{A.54})$$

where  $n_M(|X\rangle) = n_P(|X\rangle)$  is the number of marked links occupied by 1 strings in the string-net  $|X\rangle$ . This agrees with Eq. (A.49).

The four modified string operators of the flux phase, which pass through plaquettes freely, are  $\mathbf{W}_I$ ,  $(-1)^{n_M(P)} \mathbf{W}_s$ ,  $(-1)^{n_M(P)} \mathbf{W}_{\bar{s}}$ ,  $\mathbf{W}_b$ , where  $n_M(P)$  is the number of marked links along the path P.

## A.8 $\mathbb{Z}_N$ Flux Phases

For every positive integer  $n$ , there is a  $\mathbb{Z}_n$  UFTC. When  $n$  is even, there is also a  $\mathbb{Z}_n^{(1/2)}$  UFTC, which differs from  $\mathbb{Z}_n$  in its quantum dimensions and  $F$  symbols.[26, 110]

The  $\mathbb{Z}_n$  model uses the  $\mathbb{Z}_n$  UFTC and realizes the  $D(\mathbb{Z}_n)$  phase. It is specified by:

- String types  $0, 1, \dots, n-1$ ,
- Allowed branchings  $\{i, j, [i+j]_n\}$ , where  $i, j \in \{0, 1, \dots, n-1\}$ ,
- Quantum dimensions  $d_i = 1$  for all  $i$ , and
- All admissible  $F_{klm}^{ijn} = 1$ .

The smooth phase Hamiltonian is

$$\mathbf{H}_{\mathbb{Z}_n}^{(0)} = - \sum_{\mathbf{v}} \mathbf{Q}_{\mathbf{v}} - \frac{1}{n} \sum_{\mathbf{p}} \mathbf{B}_{\mathbf{p}}^s. \quad (\text{A.55})$$

To define the flux Hamiltonian, we use the following unitary matrix, which simultaneously diagonalizes  $N_i$ :

$$[P]_{jk} = \frac{1}{\sqrt{n}} e^{\frac{2\pi i}{n} jk}. \quad (\text{A.56})$$

The  $j$  flux Hamiltonian is

$$\mathbf{H}_{\mathbb{Z}_n}^{(j)} = - \sum_{\mathbf{v}} \mathbf{Q}_{\mathbf{v}} - \frac{1}{n} \sum_{\mathbf{p}} \sum_{\mathbf{s}} e^{-\frac{2\pi i}{n} j\mathbf{s}} \mathbf{B}_{\mathbf{p}}^{\mathbf{s}}, \quad (\text{A.57})$$

where  $j \in \{1, \dots, n-1\}$ . We wish to find a map from the  $j$  flux phase Hamiltonian to the smooth phase Hamiltonian.

When the number of plaquettes in the lattice is a multiple of  $n$ , we can apply the following change of basis  $\mathbf{\Lambda}^{(j)}$ :

$$\mathbf{\Lambda}^{(j)} = \prod_{i \in \text{marked links}} \left( \mathbf{\Lambda}_i^{(j)} \right)^{m_i} \quad (\text{A.58})$$

where marked links and their associated  $m_i$  are shown in Fig. A.1, and  $\mathbf{\Lambda}_k^{(j)}$  acts on the link  $k$ , taken to be directed right for convention, as the diagonal matrix:

$$\mathbf{\Lambda}_k^{(j)} = \text{diag}(1, e^{\frac{2\pi i}{n} j}, e^{\frac{2\pi i}{n} 2j}, \dots, e^{\frac{2\pi i}{n} (n-1)j}). \quad (\text{A.59})$$

Under this change of basis, the branching matrices transform as:

$$\left( \mathbf{\Lambda}_k^{(j)} \right)^{-1} N_l \mathbf{\Lambda}_k^{(j)} = e^{\frac{2\pi i}{n} jl} N_l. \quad (\text{A.60})$$

Recall that the loop operator acts on a plaquette as:

$$\mathbf{B}_{\mathbf{p}}^{\mathbf{s}} \left| \begin{array}{c} \psi \\ \begin{array}{c} \text{g} \quad \text{h} \quad \text{g}' \\ \text{a} \quad \text{i} \quad \text{j} \quad \text{d} \\ \text{l} \quad \text{k} \quad \text{e} \end{array} \end{array} \right\rangle = \sum_{g'h'i'j'k'l'} B_{s,ghijkl}^{g'h'i'j'k'l'} \left| \begin{array}{c} \psi \\ \begin{array}{c} \text{h}' \quad \text{g}' \\ \text{a}' \quad \text{i}' \quad \text{j}' \quad \text{d}' \\ \text{l}' \quad \text{k}' \quad \text{e}' \end{array} \end{array} \right\rangle, \quad (\text{A.61})$$

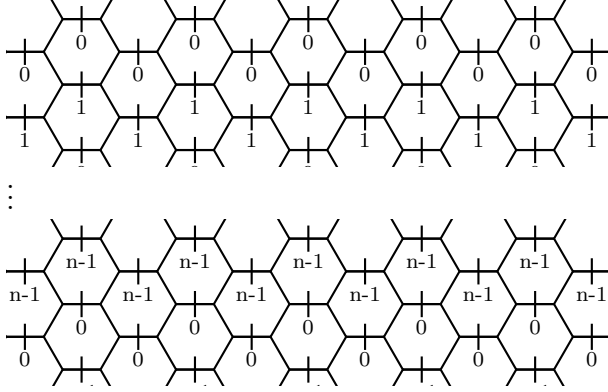


Figure A.1: Change of Basis

where

$$B_{s,ghijkl}^{g'h'i'j'k'l'} = F_{s^*g'l'^*}^{al^*g} \cdots F_{s^*l'k'^*}^{fk^*l} \quad (\text{A.62})$$

We can write this as

$$B_{s,ghijkl}^{g'h'i'j'k'l'} = B_{s,ghijkl}^{g'h'i'j'k'l'} [N_s]_{gg''} \cdots [N_s]_{ll''}, \quad (\text{A.63})$$

since

$$[N_s]_{gg''} \cdots [N_s]_{ll''} = \begin{cases} 1 & \text{if } B_{s,ghijkl}^{g'h'i'j'k'l'} \neq 0 \\ 0 & \text{if } B_{s,ghijkl}^{g'h'i'j'k'l'} = 0. \end{cases} \quad (\text{A.64})$$

Now, since  $\Lambda_k^{(j)}$  acts diagonally on the link  $k$ , Eq. (A.60) implies:

$$\sum_{k'k''} [\Lambda_k^{(j)}]_{k''k'''} B_{s,ghijkl}^{g'h'i'j'k''l'} [\Lambda_k^{(j)}]_{kk'} = e^{\frac{2\pi i}{n} js} B_{s,ghijkl}^{g'h'i'j'k''l'}. \quad (\text{A.65})$$

Every hexagon has two marked links, with the top link directed left and the bottom link directed right. Taking these directions into account, the above equation implies that

applying the change of basis to these two links results in:

$$(\mathbf{\Lambda}^{(j)})^{-1} \mathbf{B}_p^s \mathbf{\Lambda}^{(j)} = e^{\frac{2\pi i}{n} j s} \mathbf{B}_p^s. \quad (\text{A.66})$$

Thus,  $\mathbf{\Lambda}^{(j)}$  maps  $\mathbf{H}_{\mathbb{Z}_n}^{(j)}$  to  $\mathbf{H}_{\mathbb{Z}_n}^{(0)}$ , as desired.

The  $\mathbb{Z}_n^{(1/2)}$  model, for  $n$  even, uses the  $\mathbb{Z}_n^{(1/2)}$  UFTC and realizes the  $\mathbb{Z}_n^{(1/2)} \times \overline{\mathbb{Z}_n^{(1/2)}}$  phase. It is specified by:

- String types  $0, 1, \dots, n-1$ ,
- Allowed branchings  $\{i, j, [i+j]_n\}$ , where  $i, j \in \{0, 1, \dots, n-1\}$ ,
- Quantum dimensions  $d_i = (-1)^i$ , and
- All admissible  $F_{kln}^{ijm} = e^{\frac{\pi i}{n} i([j]_n + [k]_n - [j+k]_n)}$ .

The smooth phase Hamiltonian is

$$\mathbf{H}_{\mathbb{Z}_n^{(1/2)}}^{(0)} = - \sum_{\mathbf{v}} \mathbf{Q}_{\mathbf{v}} - \frac{1}{n} \sum_{\mathbf{p}} \mathbf{B}_{\mathbf{p}}^s. \quad (\text{A.67})$$

To define the flux Hamiltonian, we use the following unitary matrix, which simultaneously diagonalizes  $N_i$ :

$$[P]_{jk} = \frac{(-1)^{(j+k)}}{\sqrt{n}} e^{\frac{2\pi i}{n} jk}. \quad (\text{A.68})$$

The  $j$  flux phase Hamiltonian is

$$\mathbf{H}_{\mathbb{Z}_n^{(1/2)}}^{(j)} = - \sum_{\mathbf{v}} \mathbf{Q}_{\mathbf{v}} - \frac{1}{n} \sum_{\mathbf{p}} \sum_s e^{-\frac{2\pi i}{n} (j+n/2)s} \mathbf{B}_{\mathbf{p}}^s, \quad (\text{A.69})$$

where  $j \in \{1, \dots, n-1\}$ . We wish to find a map from the  $j$  flux phase Hamiltonian to the smooth phase Hamiltonian.

When the number of plaquettes in the lattice is a multiple of  $n$ , we can apply the change of basis  $\Lambda^{(j+n/2)}$ , defined above. Following the arguments above, this change of basis results in:

$$\left(\Lambda^{(j+n/2)}\right)^{-1} \mathbf{B}_p^s \Lambda^{(j+n/2)} = e^{\frac{2\pi i}{n}(j+n/2)s} \mathbf{B}_p^s. \quad (\text{A.70})$$

Thus,  $\Lambda^{(j+n/2)}$  maps  $\mathbf{H}_{\mathbb{Z}_n^{(1/2)}}^{(j)}$  to  $\mathbf{H}_{\mathbb{Z}_n^{(1/2)}}^{(0)}$ , as desired.

## A.9 Abelian vs. Non-Abelian Fluxes

A flux  $j$  is Abelian iff there exists some unique  $k$  (corresponding to  $j^*$ ) such that a plaquette with flux  $j$  and a plaquette with flux  $k$  will always have definite total flux 0:

$$\mathbf{B}_{p_1}^{(j)} \mathbf{B}_{p_2}^{(k)} = \mathbf{B}_{p_1}^{(j)} \mathbf{B}_{p_1 p_2}^{(0)}, \quad (\text{A.71})$$

where  $\mathbf{B}_{p_1 p_2}^{(0)}$  projects the total flux of plaquettes  $p_1$  and  $p_2$  onto trivial flux. Since

$$\begin{aligned} \mathbf{B}_{p_1}^{(j)} \mathbf{B}_{p_2}^{(k)} & \left| \begin{array}{c} \text{---} \\ \text{---} \\ \text{---} \\ \text{---} \\ \text{---} \\ \text{---} \end{array} \right. \left. \begin{array}{c} \text{---} \\ \text{---} \\ \text{---} \\ \text{---} \\ \text{---} \\ \text{---} \end{array} \right. \\ & = \sum_{st} a_s^{(j)} a_t^{(k)} \left| \begin{array}{c} \text{---} \\ \text{---} \\ \text{---} \\ \text{---} \\ \text{---} \\ \text{---} \end{array} \right. \left. \begin{array}{c} \text{---} \\ \text{---} \\ \text{---} \\ \text{---} \\ \text{---} \\ \text{---} \end{array} \right. \\ & = \sum_{stui} a_s^{(j)} a_t^{(k)} \frac{v_u}{v_s v_t} F_{uti}^{t^* u^* s^*} \left| \begin{array}{c} \text{---} \\ \text{---} \\ \text{---} \\ \text{---} \\ \text{---} \\ \text{---} \end{array} \right. \left. \begin{array}{c} \text{---} \\ \text{---} \\ \text{---} \\ \text{---} \\ \text{---} \\ \text{---} \end{array} \right. \end{aligned} \quad (\text{A.72})$$

and

$$\begin{aligned}
 & \mathbf{B}_{P_1}^{(j)} \mathbf{B}_{P_1 P_2}^{(0)} \left| \begin{array}{c} \text{---} \\ \text{---} \\ \text{---} \\ \text{---} \\ \text{---} \\ \text{---} \end{array} \right. \\
 & = \sum_{tu} a_u^{(j)} \frac{d_t}{\mathcal{D}_C^2} \left| \begin{array}{c} \text{---} \\ \text{---} \\ \text{---} \\ \text{---} \\ \text{---} \\ \text{---} \end{array} \right.
 \end{aligned} \tag{A.73}$$

we need

$$\sum_s a_s^{(j)} a_t^{(k)} \frac{v_u}{v_s v_t} F_{uti}^{t^* u^* s^*} = \begin{cases} a_u^{(j)} \frac{d_t}{\mathcal{D}_C^2} & \text{if } i = 0 \\ 0 & \text{if } i \neq 0. \end{cases} \tag{A.74}$$

After simplification, we find that flux  $j$  is Abelian iff there exists a unique  $k$  such that for all  $i \neq 0$ ,  $t$ , and  $u$ , we have

$$\frac{[P]_{tj}[P]_{tk}[P]_{0k}}{[P]_{0j}} = \frac{d_t^2}{\mathcal{D}_C^2}, \tag{A.75}$$

$$\sum_s v_s^{-1} [P]_{sj} F_{uti}^{t^* u^* s^*} = 0. \tag{A.76}$$

Otherwise, it is non-Abelian.

## A.10 Ising Change of Basis

The Hamiltonian for  $\psi$  flux phase of the Ising model is:

$$\mathbf{H}_{IS}^{(\psi)} = - \sum_v \mathbf{Q}_v - \sum_p \frac{1}{4} \left( \mathbf{B}_p^I - \sqrt{2} \mathbf{B}_p^\sigma + \mathbf{B}_p^\psi \right). \tag{A.77}$$

We wish to find a map from the flux Hamiltonian to the smooth Hamiltonian.

When number of plaquettes in the lattice is even, we can apply the change of basis

$\Lambda$ :

$$\Lambda = \Lambda^{-1} = \prod_{i \in \text{marked links}} \Lambda_i, \quad (\text{A.78})$$

where marked links are shown in Fig. 2.2 and

$$\Lambda_i = \text{diag}(1, -1, 1) \quad (\text{A.79})$$

multiplies the amplitude of a lattice state by a factor of  $-1$  if its link  $i$  is occupied by a  $\sigma$  string. Under this change of basis, the branching matrices transform as:

$$\Lambda_i^{-1} N_I \Lambda_i = N_I \quad (\text{A.80})$$

$$\Lambda_i^{-1} N_\sigma \Lambda_i = -N_\sigma \quad (\text{A.81})$$

$$\Lambda_i^{-1} N_\psi \Lambda_i = N_\psi. \quad (\text{A.82})$$

Therefore, by the arguments of Appendix A.8:

$$\Lambda^{-1} \mathbf{B}_p^I \Lambda = \mathbf{B}_p^I \quad (\text{A.83})$$

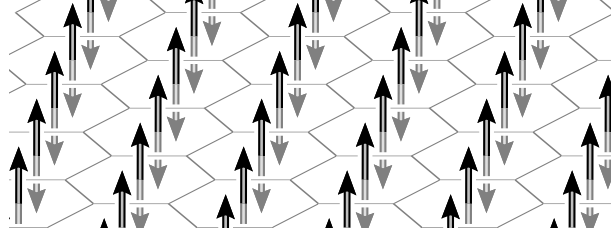
$$\Lambda^{-1} \mathbf{B}_p^\sigma \Lambda = -\mathbf{B}_p^\sigma \quad (\text{A.84})$$

$$\Lambda^{-1} \mathbf{B}_p^\psi \Lambda = \mathbf{B}_p^\psi. \quad (\text{A.85})$$

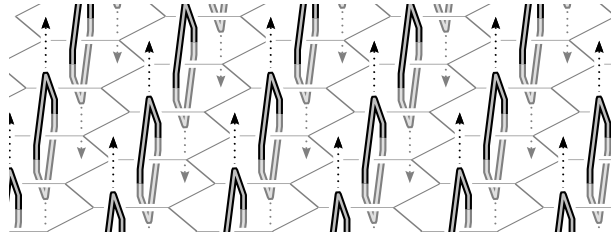
Thus,  $\Lambda$  maps  $\mathbf{H}_{IS}^{(\psi)}$  to  $\mathbf{H}_{IS}^{(I)}$ .

It is useful to visualize why this change of basis works. The ground state of the  $\psi$

flux phase has a  $\psi$  string passing through every plaquette.



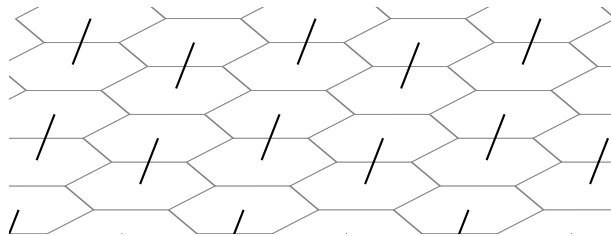
We can fuse the  $\psi$  flux strings of adjacent plaquettes above and below the lattice. Since two  $\psi$  strings must fuse into a  $I$  string, we are essentially left with loops of  $\psi$  strings enclosing certain links.



Using the facts:

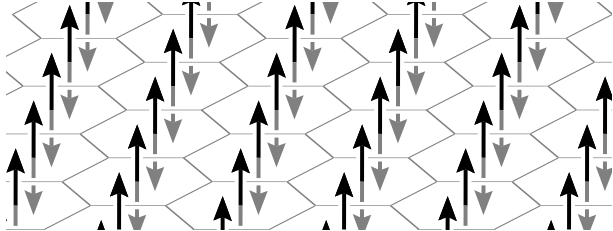
$$\begin{array}{c} \circlearrowleft \\ \vdots \end{array} = \vdots, \quad \begin{array}{c} \circlearrowright \\ \vdots \end{array} = -\vdots, \quad \begin{array}{c} \circlearrowleft \\ \vdots \\ \circlearrowright \end{array} = \parallel, \quad (\text{A.86})$$

we can replace every link enclosed by a  $\psi$  string loop with a marked link and apply the change of basis  $\Lambda$ .

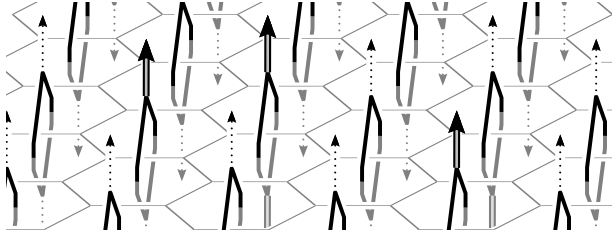


The result is a lattice with  $I$  flux through every plaquette.

This visualization also explains why changing basis does not work as simply for the  $\sigma$  flux phase. The ground state of the  $\sigma$  flux phase has a  $\sigma$  string passing through every plaquette.



Imagine fusing the  $\sigma$  flux strings of adjacent plaquettes above and below the lattice. For example:



Since we are not left with  $\sigma$  loops around links, we cannot reduce the  $\sigma$  flux phase to the smooth phase with a change of basis. Note that since two  $\sigma$  strings can fuse into a  $I$  or  $\psi$  string, there are  $2^{N-2}$  possible configurations of the fusion tree formed by flux lines above and below the lattice, which is precisely the degeneracy given by spectacle operators. In fact, the spectacle operator changes the the fusion channel between two 1 fluxes:

$$\begin{array}{c} | \\ \bigcirc \\ | \end{array} = \begin{array}{c} | \\ \text{---} \\ | \end{array} . \tag{A.87}$$

## A.11 Properties of Spectacle Operators

When applying the same minimal spectacle operator twice, we get  $\mathbf{S}_{p_1 p_2}^2 = \mathbf{B}_{p_1}^{(\sigma)} \mathbf{B}_{p_2}^{(\sigma)}$ :

$$\begin{aligned}
 \frac{1}{4} \left| \begin{array}{c} \text{Diagram 1} \\ \text{Diagram 2} \end{array} \right\rangle &= \frac{1}{4} \left| \begin{array}{c} \text{Diagram 3} \\ \text{Diagram 4} \end{array} \right\rangle, \\
 &= \frac{1}{4} \left| \begin{array}{c} \text{Diagram 5} \\ \text{Diagram 6} \end{array} \right\rangle,
 \end{aligned} \tag{A.88}$$

where

$$\begin{aligned}
 \frac{1}{2} \left| \begin{array}{c} \text{Diagram 7} \\ \text{Diagram 8} \end{array} \right\rangle &= \frac{1}{2} \left| \begin{array}{c} \text{Diagram 9} \\ \text{Diagram 10} \end{array} \right\rangle \\
 &\quad - \frac{1}{2} \left| \begin{array}{c} \text{Diagram 11} \\ \text{Diagram 12} \end{array} \right\rangle \\
 &= \mathbf{B}_p^{(\sigma)} \left| \begin{array}{c} \text{Diagram 13} \\ \text{Diagram 14} \end{array} \right\rangle.
 \end{aligned} \tag{A.89}$$

Therefore, when acting on the ground state of the  $\sigma$  flux Ising Hamiltonian,  $\mathbf{S}_{p_1 p_2}^2 = I$ .

Spectacle operators are also Hermitian. To show this we first note that:

$$\mathbf{S}_{p_1 p_2} = \sqrt{2} \mathbf{B}_{p_1 p_2}^\sigma - \mathbf{B}_{p_1}^\sigma \mathbf{B}_{p_2}^\sigma, \tag{A.90}$$

where  $\mathbf{B}_{p_1 p_2}^\sigma$  is a closed  $\mathbf{W}_{(\sigma, I)}$  enclosing the plaquettes  $p_1$  and  $p_2$ . Since  $\mathbf{B}_{p_1}^\sigma$  and  $\mathbf{B}_{p_2}^\sigma$  commute and are Hermitian, we only need to show  $\mathbf{B}_{p_1 p_2}^\sigma$  is Hermitian. In fact, we show

that any closed string operator enclosing two plaquettes is Hermitian.

$$\begin{aligned}
& \left( \text{Diagram of two adjacent plaquettes with vertices } a, b, c, d, e, f, g, h, i, j, k, l, m, n, o, p, q, r, s \text{ and a closed string operator path} \right) = \\
& = \sum_{\alpha, \beta, s''} v_\alpha v_\beta \Omega_{\beta\alpha s}^{s'} \bar{\Omega}_{\alpha\beta s}^{s''} \\
& \quad F_{\alpha s' k'}^{l k s} F_{\alpha k' j'}^{c j k} F_{\alpha j' i'}^{b i j} F_{\alpha i' r'}^{a r i} F_{\alpha r' q'}^{h q r} F_{\alpha q' s''}^{p s q} \\
& \quad F_{s \beta l'}^{l k' s'} F_{l' \beta m'}^{m d l} F_{m' \beta n'}^{n e m} F_{n' \beta o'}^{o f n} F_{o' \beta p'}^{p g o} F_{p' \beta s}^{s'' q' p} \\
& \quad \left( \text{Diagram of two adjacent plaquettes with vertices } a, b, c, d, e, f, g, h, i, j, k', l', m', n', o', p', q', r', s \text{ and a closed string operator path} \right)
\end{aligned} \tag{A.91}$$

So, we need to show:

$$\begin{aligned}
& \sum_{\alpha\beta s' s''} v_\alpha v_\beta \Omega_{\beta\alpha s}^{s'} \bar{\Omega}_{\alpha\beta s}^{s''} \\
& \quad F_{\alpha s' k'}^{l k s} F_{\alpha k' j'}^{c j k} F_{\alpha j' i'}^{b i j} F_{\alpha i' r'}^{a r i} F_{\alpha r' q'}^{h q r} F_{\alpha q' s''}^{p s q} \\
& \quad F_{s \beta l'}^{l k' s'} F_{l' \beta m'}^{m d l} F_{m' \beta n'}^{n e m} F_{n' \beta o'}^{o f n} F_{o' \beta p'}^{p g o} F_{p' \beta s}^{s'' q' p} \\
& = \sum_{\alpha\beta s' s''} v_\alpha v_\beta \bar{\Omega}_{\beta\alpha s}^{s'} \Omega_{\alpha\beta s}^{s''} \\
& \quad F_{\alpha s' k}^{l' k' s} F_{\alpha k j}^{c j' k'} F_{\alpha j i}^{b i' j'} F_{\alpha i r}^{a r' i'} F_{\alpha r q}^{h q' r'} F_{\alpha q s''}^{p' s q'} \\
& \quad F_{s \beta l}^{l' k s'} F_{l \beta m}^{m' d l'} F_{m \beta n}^{n' e m'} F_{n \beta o}^{o' f n'} F_{o \beta p}^{p' g o'} F_{p \beta s}^{s'' q p'}
\end{aligned} \tag{A.92}$$

Using  $F_{kln}^{ijm} = \frac{v_m v_n}{v_j v_l} F_{kmj}^{inl} = \frac{v_m v_n}{v_i v_k} F_{mli}^{njk}$  on the right-hand side yields:

$$\begin{aligned}
& \sum_{\alpha\beta s' s''} v_\alpha v_\beta \Omega_{\beta\alpha s'}^{s'} \bar{\Omega}_{\alpha\beta s}^{s''} \\
& \quad F_{\alpha s' k'}^{lks} F_{\alpha k' j'}^{cjk} F_{\alpha j' i'}^{bij} F_{\alpha i' r'}^{ari} F_{\alpha r' q'}^{hqr} F_{\alpha q' s''}^{psq} \\
& \quad F_{s\beta l'}^{lk's'} F_{l'\beta m'}^{mdl} F_{m'\beta n'}^{nem} F_{n'\beta o'}^{ofn} F_{o'\beta p'}^{pgo} F_{p'\beta s}^{s''q'p} \\
& = \sum_{\alpha\beta s' s''} v_\alpha v_\beta \bar{\Omega}_{\beta\alpha s'}^{s'} \Omega_{\beta\alpha s}^{s''} \\
& \quad F_{\alpha s k'}^{l'ks'} F_{\alpha k' j'}^{cjk} F_{\alpha j' i'}^{bij} F_{\alpha i' r'}^{ari} F_{\alpha r' q'}^{hqr} F_{\alpha q' s}^{p's''q} \\
& \quad F_{s'\beta l'}^{lks} F_{l'\beta m'}^{mdl} F_{m'\beta n'}^{nem} F_{n'\beta o'}^{ofn} F_{o'\beta p'}^{pgo} F_{p'\beta s''}^{sqp} \tag{A.93}
\end{aligned}$$

So we need to show:

$$\sum_{s'} \Omega_{\beta\alpha s'}^{s'} F_{\alpha s' k'}^{lks} F_{s\beta l'}^{lk's'} = \sum_{s'} \bar{\Omega}_{\beta\alpha s'}^{s'} F_{\alpha s k'}^{l'ks'} F_{s'\beta l'}^{lks}, \tag{A.94}$$

and:

$$\sum_{s''} \bar{\Omega}_{\alpha\beta s}^{s''} F_{\alpha q' s''}^{psq} F_{p'\beta s}^{s''q'p} = \sum_{s''} \Omega_{\beta\alpha s}^{s''} F_{\alpha q' s}^{p's''q} F_{p'\beta s''}^{sqp}. \tag{A.95}$$

To prove the first condition we use  $\bar{\Omega}_{sti}^j = \sum_k \Omega_{sti}^k F_{isj}^{itk}$ .

$$\sum_{s'} \Omega_{\beta\alpha s'}^{s'} F_{\alpha s' k'}^{lks} F_{s\beta l'}^{lk's'} = \sum_{s't} \Omega_{\beta\alpha s}^{s'} F_{s\beta t}^{s\alpha s'} F_{\alpha s k'}^{l'kt} F_{t\beta l'}^{lks} \tag{A.96}$$

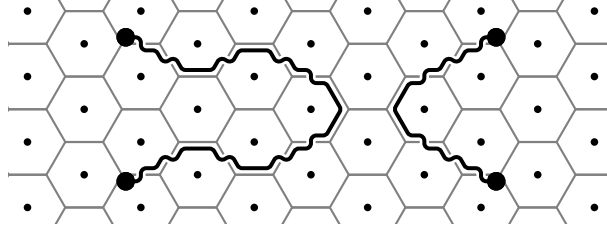
Finally, using  $F_{kln}^{ijm} = \frac{v_m v_n}{v_j v_l} F_{mkj}^{nil}$  and reordering yields:

$$F_{s\alpha k}^{k'ls'} F_{s'sk'}^{l'l\beta} = \sum_t F_{\alpha s k'}^{l'kt} F_{stk}^{l'l\beta} F_{s\beta t}^{s\alpha s'}, \tag{A.97}$$

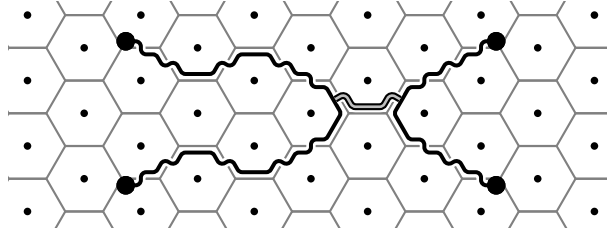
which is just the Pentagon equation. The proof for the second condition is similar. Thus, spectacle operators are Hermitian.



Let  $\mathcal{O}^{(I)}$  be composed of two non-intersecting open  $\mathbf{W}_{(\sigma,I)}$ , as shown below.

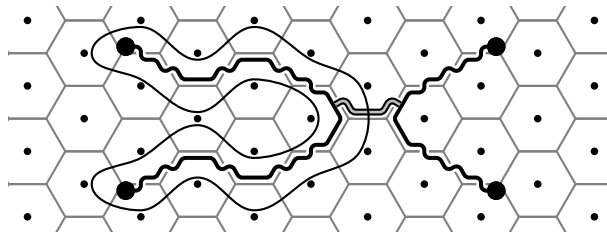


When acting on the ground state subspace this operator creates the subspace  $\mathcal{H}^{(I)}$  spanned by  $|\alpha^{(0)}\rangle = \mathcal{O}^{(I)}|\alpha\rangle$ . Let  $\mathcal{O}^{(\psi)}$  be  $\mathcal{O}^{(I)}$  with a  $\mathbf{W}_{(\psi,I)}$  string connecting the  $\mathbf{W}_{(\sigma,I)}$  strings, as shown below.



When acting on the ground state Hilbert space this operator creates the Hilbert space  $\mathcal{H}^{(\psi)}$ , spanned by  $|\alpha^{(\psi)}\rangle = \mathcal{O}^{(\psi)}|\alpha\rangle$ .

We show that  $\langle\alpha^{(I)}|\beta^{(\psi)}\rangle = 0$  for all  $\alpha$  and  $\beta$ . This is clear when  $\alpha \neq \beta$ , because  $|\alpha^{(0)}\rangle$  and  $|\beta^{(2)}\rangle$  will have mismatching  $\sigma$  strings. So, we need to show  $\langle\alpha^{(I)}|\alpha^{(\psi)}\rangle = 0$  for all  $\alpha$ . To show this, imagine drawing a Gaussian surface around one of the  $\mathbf{W}_{(\sigma,I)}$  strings.



In general, the links of  $|\alpha^{(I)}\rangle$  and  $|\alpha^{(\psi)}\rangle$  crossing this surface may have  $\sigma$  strings created by spectacle operators. However, we can remove these spectacle operators:

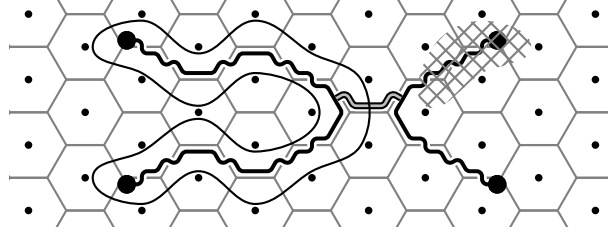
$$\begin{aligned}
\langle\alpha^{(I)}|\alpha^{(\psi)}\rangle &= \langle\alpha|(\mathbf{O}^{(I)})^\dagger\mathbf{O}^{(\psi)}|\alpha\rangle \\
&= \langle\tilde{\alpha}|(\prod\mathbf{s})^\dagger(\mathbf{O}^{(I)})^\dagger\mathbf{O}^{(\psi)}(\prod\mathbf{s})|\tilde{\alpha}\rangle \\
&= \langle\tilde{\alpha}|(\mathbf{O}^{(I)})^\dagger\mathbf{O}^{(\psi)}(\prod\mathbf{s})(\prod\mathbf{s})|\tilde{\alpha}\rangle \\
&= \langle\tilde{\alpha}|(\mathbf{O}^{(I)})^\dagger\mathbf{O}^{(\psi)}|\tilde{\alpha}\rangle \\
&= \langle\tilde{\alpha}^{(I)}|\tilde{\alpha}^{(\psi)}\rangle,
\end{aligned} \tag{A.100}$$

where in the second line  $|\tilde{\alpha}\rangle$  no longer has any 1 strings crossing the Gaussian surface, in the third line we have used the fact that spectacle operators commute with  $\mathbf{O}^{(I)}$  and  $\mathbf{O}^{(\psi)}$  and are Hermitian, and in the fourth line we used the fact that  $\mathbf{S}^2 = 1$  when acting on the ground state. But  $\langle\tilde{\alpha}^{(I)}|\tilde{\alpha}^{(\psi)}\rangle = 0$ , because  $|\tilde{\alpha}^{(I)}\rangle$  and  $|\tilde{\alpha}^{(\psi)}\rangle$  have different parity of 2 strings crossing the Gaussian surface. Thus,  $\langle\alpha^{(I)}|\beta^{(\psi)}\rangle = 0$  for all  $\alpha$  and  $\beta$ .

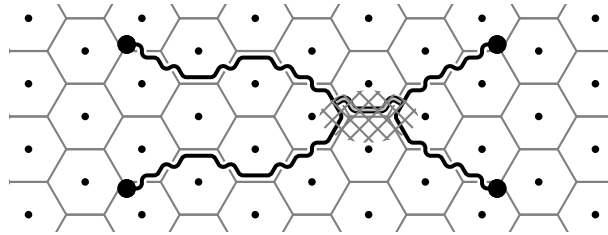
We may worry the above argument fails because spectacle operators acting on plaquettes containing the endpoints of the  $(1,0)$  strings may not commute with  $\mathbf{O}^{(0)}$  and  $\mathbf{O}^{(2)}$ , but we may circumvent this issue by simply enlarging the Gaussian surface at the endpoints so that it never passes through plaquettes which contain the endpoints.

Now we show that  $\langle\alpha^{(I)}|\mathbf{V}|\beta^{(\psi)}\rangle = 0$  for all  $\alpha$  and  $\beta$ , and any local operator  $\mathbf{V}$ , if the simply connected cover of the support of  $\mathbf{V}$  does not contain endpoints from both the  $\mathbf{W}_{(\sigma,I)}$  strings. Consider the case when we can draw a Gaussian surface around one of the  $\mathbf{W}_{(\sigma,I)}$  strings of  $\mathbf{O}^{(I)}$  and  $\mathbf{O}^{(\psi)}$  which is always at least a plaquette away from the

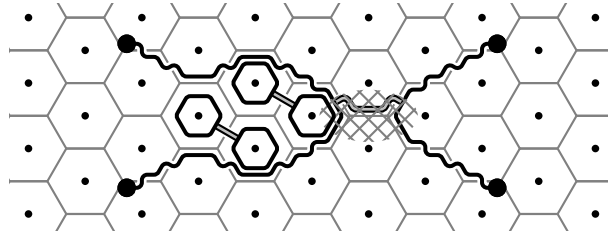
support of  $\mathbf{V}$ .



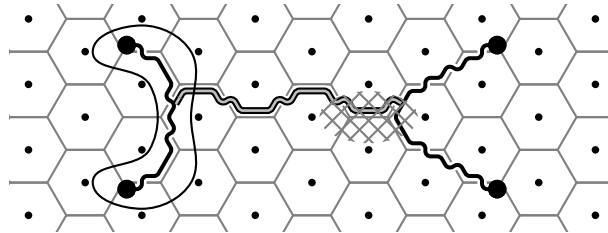
Then,  $\langle \alpha^{(I)} | \mathbf{V} | \beta^{(\psi)} \rangle = 0$  by the arguments of the previous paragraph. Now, consider the case when it is seemingly impossible to draw such a Gaussian surface.



Then, we can move one of the  $\mathbf{W}_{(\sigma, I)}$  strings using spectacle operators:



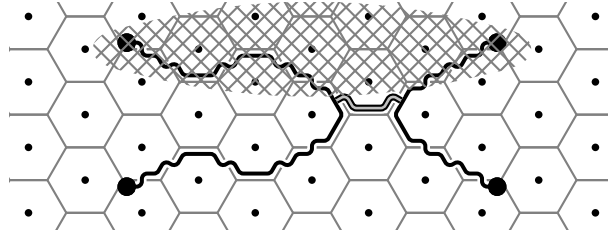
The new  $\mathcal{O}^{(\psi)}$  has a  $\mathbf{W}_{(\sigma, I)}$  string that can be surrounded by a Gaussian surface.



Mathematically,

$$\begin{aligned}
\langle \alpha^{(I)} | \mathbf{V} | \beta^{(\psi)} \rangle &= \langle \alpha | (\mathbf{O}^{(I)})^\dagger \mathbf{V} \mathbf{O}^{(\psi)} | \beta \rangle \\
&= \langle \tilde{\alpha} | \left( \prod S \right)^\dagger (\mathbf{O}^{(I)})^\dagger \mathbf{V} \mathbf{O}^{(\psi)} \left( \prod S \right) | \tilde{\beta} \rangle \\
&= \langle \tilde{\alpha} | \left( \tilde{\mathbf{O}}^{(0)} \right)^\dagger \mathbf{V} \tilde{\mathbf{O}}^{(\psi)} | \tilde{\beta} \rangle.
\end{aligned} \tag{A.101}$$

So, again  $\langle \alpha^{(I)} | \mathbf{V} | \beta^{(\psi)} \rangle = 0$  by the arguments of the previous paragraph. More generally, this is true as long as the simply-connected cover of the support of  $\mathbf{V}$  does not contain endpoints from both the  $\mathbf{W}_{(\sigma,I)}$  strings. For example, an operator whose action is nontrivial on the region shown below would not satisfy this condition.



In order to show that  $\mathcal{H}^{(I)}$  and  $\mathcal{H}^{(\psi)}$  are topologically protected, we also need to show that  $\langle \alpha^{(I)} | \mathbf{V} | \beta^{(I)} \rangle = \langle \alpha^{(\psi)} | \mathbf{V} | \beta^{(\psi)} \rangle$ . This is clear if the support of  $\mathbf{V}$  does not include the  $\mathbf{W}_{(\psi,I)}$  and  $\mathbf{W}_{(\sigma,I)}$  strings of  $\mathbf{O}^{(\psi)}$ . When the support of  $\mathbf{V}$  includes  $\mathbf{W}_{(\sigma,I)}$  string, we can move the  $\mathbf{W}_{(\sigma,I)}$  string away by passing it over an even number of plaquettes. When the support of  $\mathbf{V}$  also includes the  $\mathbf{W}_{(\sigma,I)}$  string, we can use spectacle operators to move the

$\mathbf{W}_{(\sigma,I)}$  string away:

$$\begin{aligned}
\langle \alpha^{(I)} | \mathbf{V} | \beta^{(I)} \rangle &= \langle \alpha | (\mathbf{O}^{(I)})^\dagger \mathbf{v} \mathbf{O}^{(I)} | \beta \rangle \\
&= \langle \alpha | (\tilde{\mathbf{O}}^{(I)})^\dagger (\prod \mathbf{s})^\dagger \mathbf{v} (\prod \mathbf{s}) \tilde{\mathbf{O}}^{(I)} | \beta \rangle \\
&= \langle \alpha | (\tilde{\mathbf{O}}^{(I)})^\dagger (\prod \mathbf{s})^\dagger (\prod \mathbf{s}) \mathbf{v} \tilde{\mathbf{O}}^{(I)} | \beta \rangle \\
&= \langle \alpha | (\tilde{\mathbf{O}}^{(I)})^\dagger \mathbf{v} \tilde{\mathbf{O}}^{(I)} | \beta \rangle
\end{aligned} \tag{A.102}$$

Here,  $\tilde{\mathbf{O}}^{(I)}$  no longer has its half spectacle in the support of  $\mathbf{V}$ , and is identical to  $\tilde{\mathbf{O}}^{(\psi)}$  in this region. Therefore,  $\langle \alpha^{(I)} | \mathbf{V} | \beta^{(I)} \rangle = \langle \alpha^{(\psi)} | \mathbf{V} | \beta^{(\psi)} \rangle$ . Note that we had to assume that the spectacle operators commute with  $\mathbf{V}$ .

# Appendix B

## B.1 Luttinger's Theorem for Kondo Model

Consider a 2D periodic lattice with  $\nu_c = \nu_{c\uparrow} + \nu_{c\downarrow}$  conduction electrons and  $\nu_s$  spin- $S$  localized spins per unit cell, governed by the translationally invariant Kondo model Hamiltonian

$$\mathbf{H} = -t \sum_{\langle jk \rangle, \alpha} (\mathbf{c}_{j\alpha}^\dagger \mathbf{c}_{k\alpha} + \text{h.c.}) + U \sum_j \mathbf{n}_{j\uparrow} \mathbf{n}_{j\downarrow} + K \sum_j \vec{s}_j \cdot \vec{\mathbf{S}}_j + J \sum_{\langle jk \rangle} \vec{\mathbf{S}}_j \cdot \vec{\mathbf{S}}_k \quad (\text{B.1})$$

$$\begin{aligned} &= -t \sum_{\langle jk \rangle, \alpha} (\mathbf{c}_{j\alpha}^\dagger \mathbf{c}_{k\alpha} + \text{h.c.}) + U \sum_j \mathbf{n}_{j\uparrow} \mathbf{n}_{j\downarrow} + \frac{1}{2} K \sum_j \left[ (\mathbf{n}_{j\uparrow} - \mathbf{n}_{j\downarrow}) \mathbf{S}_j^z + \mathbf{c}_{j\downarrow}^\dagger \mathbf{c}_{j\uparrow} \mathbf{S}_j^+ + \mathbf{c}_{j\uparrow}^\dagger \mathbf{c}_{j\downarrow} \mathbf{S}_j^- \right] \\ &\quad + J \sum_{\langle jk \rangle} \left[ \mathbf{S}_j^z \mathbf{S}_k^z + \frac{1}{2} (\mathbf{S}_j^+ \mathbf{S}_k^- + \text{h.c.}) \right], \end{aligned} \quad (\text{B.2})$$

where  $\vec{s}_j = \sum_{\alpha\beta} \mathbf{c}_{j\alpha}^\dagger \vec{\sigma}_{\alpha\beta} \mathbf{c}_{j\beta} / 2$ .

The above Hamiltonian has two global U(1) symmetries, corresponding to the conserved quantities  $\nu_{c\uparrow} + m_s \nu_s$  and  $\nu_{c\downarrow} - m_s \nu_s$ , where  $m_s$  is the magnetization per localized spin. The first of these, which we denote as U(1) $_{\uparrow}$ , is generated by the transformations:  $\mathbf{c}_{j\uparrow}^\dagger \rightarrow e^{i\theta} \mathbf{c}_{j\uparrow}^\dagger$ ,  $\mathbf{c}_{j\uparrow} \rightarrow e^{-i\theta} \mathbf{c}_{j\uparrow}$ , and  $\mathbf{S}_j^\pm \rightarrow e^{\pm i\theta} \mathbf{S}_j^\pm$ . This global symmetry can be promoted to a local symmetry by introducing a gauge field  $A_{jk}$  that couples to spin up electrons

and the localized spins, modifying the Hamiltonian to

$$\begin{aligned}
\mathbf{H}' = & -t \sum_{\langle jk \rangle} (e^{iA_{jk}} \mathbf{c}_{j\uparrow}^\dagger \mathbf{c}_{k\uparrow} + \mathbf{c}_{j\downarrow}^\dagger \mathbf{c}_{k\downarrow} + \text{h.c.}) + U \sum_j \mathbf{n}_{j\uparrow} \mathbf{n}_{j\downarrow} \\
& + \frac{1}{2} K \sum_j \left[ (\mathbf{n}_{j\uparrow} - \mathbf{n}_{j\downarrow}) \mathbf{S}_j^z + \mathbf{c}_{j\downarrow}^\dagger \mathbf{c}_{j\uparrow} \mathbf{S}_j^+ + \mathbf{c}_{j\uparrow}^\dagger \mathbf{c}_{j\downarrow} \mathbf{S}_j^- \right] \\
& + J \sum_{\langle jk \rangle} \left[ \mathbf{S}_j^z \mathbf{S}_k^z + \frac{1}{2} (e^{iA_{jk}} \mathbf{S}_j^+ \mathbf{S}_k^- + \text{h.c.}) \right], \tag{B.3}
\end{aligned}$$

which now has the local  $U(1)_\uparrow$  symmetry given by the transformations:  $\mathbf{c}_{j\uparrow} \rightarrow e^{i\theta_j} \mathbf{c}_{j\uparrow}$ ,  $\mathbf{c}_{j\uparrow}^\dagger \rightarrow e^{-i\theta_j} \mathbf{c}_{j\uparrow}^\dagger$ ,  $\mathbf{S}_j^\pm \rightarrow e^{\pm i\theta_j} \mathbf{S}_j^\pm$ , and  $A_{jk} \rightarrow A_{jk} + \theta_k - \theta_j$ .<sup>1</sup>

Consider starting in a ground state  $|\Psi(0)\rangle$  with  $\mathbf{R}_{T_x}$  eigenvalue  $e^{iP_x(0)}$  and threading a  $2\pi U(1)_\uparrow$  flux through the handle of the torus. This can be accomplished by tuning the vector potential from  $\vec{A}(0) = (0, 0)$  to  $\vec{A}(2\pi) = (2\pi/L_x, 0)$ , i.e.  $A_{jk} = \int_{\vec{r}_j}^{\vec{r}_k} d\vec{r} \cdot \vec{A} = \frac{[\vec{r}_j - \vec{r}_k]_x}{L_x}$  after the flux insertion. Although  $\mathbf{H}'(2\pi) \neq \mathbf{H}'(0)$ , the large gauge transformation

$$\mathcal{G}_\uparrow = e^{i2\pi \sum_j \frac{[\vec{r}_j]_x}{L_x} (\mathbf{n}_{j\uparrow} + \mathbf{S}_j^z)}, \tag{B.4}$$

removes the flux, i.e.  $\mathcal{G}_\uparrow \mathbf{H}'(2\pi) \mathcal{G}_\uparrow^{-1} = \mathbf{H}'(0)$ . Therefore, the state  $\mathcal{G}_\uparrow |\Psi(2\pi)\rangle$  must be an eigenstate of  $\mathbf{H}'(0)$ .

Since  $[\mathbf{R}_{T_x}, \mathbf{H}'(\Phi)] = 0$  throughout the flux threading process,  $|\Psi(2\pi)\rangle$  has momentum  $P_x(0)$ , and since

$$\mathcal{G}_\uparrow^{-1} \mathbf{R}_{T_x} \mathcal{G}_\uparrow = \mathbf{R}_{T_x} e^{i2\pi \left[ \frac{1}{L_x} \sum_j (\mathbf{n}_{j\uparrow} + \mathbf{S}_j^z) + \sum_{j|[\vec{r}_j]_x=1} \mathbf{S}_j^z \right]}, \tag{B.5}$$

<sup>1</sup>This  $U(1)$  symmetry may seem artificial. A more physical viewpoint is to let the conduction electrons have a  $U(1)_{S^z} \times U(1)_c$  spin and charge symmetry, and the localized spins have a  $U(1)_{S^z}$  spin symmetry. In this case, we carry out Oshikawa's argument by threading  $2\pi U(1)_{S^z}$  flux and  $\pi U(1)_c$  flux, so that the spin up electrons experience a  $2\pi(+\frac{1}{2}) + \pi = 2\pi$  flux, the spin down electrons experience a  $2\pi(-\frac{1}{2}) + \pi = 0$  flux, and the localized spins experience a  $2\pi S$  flux.

the state  $\mathcal{G}_\uparrow|\Psi(2\pi)\rangle$  has momentum  $P_x(0) + 2\pi[\nu_{c\uparrow} + (S + m_s)\nu_s]L_y \pmod{2\pi}$ .

This shift can be compared with the momentum shift of the emergent degrees of freedom. Assuming the system is a spinful Fermi liquid, threading the flux shifts the momentum of each of the  $N_{F\uparrow}$  spin up quasiparticles by  $2\pi/L_x$ .

Equating the two momentum shifts and repeating the argument in the other direction yields Luttinger's theorem for spin up quasiparticles:

$$\nu_{c\uparrow} + (S + m_s)\nu_s = \frac{V_{F\uparrow}}{(2\pi)^2} \pmod{1} \quad (\text{B.6})$$

where  $V_{F\uparrow} \equiv (2\pi)^2 N_{F\uparrow}/L_x L_y$  is the Fermi volume.

The  $U(1)_\downarrow$  symmetry is defined similarly for the spin down quasiparticles, and the same arguments give the corresponding Luttinger's theorem:

$$\nu_{c\downarrow} + (S - m_s)\nu_s = \frac{V_{F\downarrow}}{(2\pi)^2} \pmod{1}. \quad (\text{B.7})$$

Combining these results and using the fact that the number of filled bands for spin up electrons is equal to the number for spin down electrons gives the spin-summed Luttinger's theorem:

$$\nu_c + 2S\nu_s = \frac{V_F}{(2\pi)^2} \pmod{2}. \quad (\text{B.8})$$

## B.2 Gauge Equivalence Between Flux Threading and Creating Anyon Loop

In this appendix, we establish the equivalence between adiabatically threading a  $2\pi$   $U(1)$  through a handle of the torus and creating a vison  $v$  anyonic flux loop around the handle. Consider a system with on-site  $U(1)$  symmetry. Starting with the Hamiltonian

$\mathbf{H}(0)$  and state  $|\Psi(0)\rangle$ , threading a  $2\pi$  U(1) flux through the handle of the torus results in the Hamiltonian  $\mathbf{H}(2\pi)$  and state  $|\Psi(2\pi)\rangle$ , where  $\mathbf{H}(2\pi) = \mathcal{G}^{-1}\mathbf{H}(0)\mathcal{G}$  for some large gauge transformation

$$\mathcal{G} = e^{i2\pi \sum_j \frac{[\vec{r}_j]_x}{L_x} \mathbf{q}_j} = \prod_j \mathbf{R}_{2\pi[\vec{r}_j]_x/L_x}^{(j)}. \quad (\text{B.9})$$

Here,  $\mathbf{q}_j$  measures the U(1) charge of site  $j$ , while  $\mathbf{R}_\theta^{(j)} = e^{i\theta\mathbf{q}_j}$  rotates it by  $\theta$ . The state of the system after threading the flux and applying the gauge transformation is  $\mathcal{G}|\Psi(2\pi)\rangle$ .

For simplicity, let us assume that the Hamiltonian consists of on-site and nearest neighbor terms only, i.e.

$$\mathbf{H}(0) = \sum_j \mathbf{h}_j + \sum_{\langle jk \rangle} \mathbf{h}_{jk}, \quad (\text{B.10})$$

and investigate its transformation under  $\mathcal{G}^{-1}\mathbf{H}(0)\mathcal{G}$ . Since

$$\mathbf{R}_{-\theta}^{(j)} \mathbf{h}_j \mathbf{R}_\theta^{(j)} = \mathbf{R}_{-\theta} \mathbf{h}_j \mathbf{R}_\theta = \mathbf{h}_j, \quad (\text{B.11})$$

the on-site terms in the Hamiltonian are unaffected by  $\mathcal{G}$ :

$$\mathcal{G}^{-1} \mathbf{h}_j \mathcal{G} = \mathbf{h}_j. \quad (\text{B.12})$$

Similarly, since

$$\mathbf{R}_{-\theta}^{(j)} \mathbf{R}_{-\theta}^{(k)} \mathbf{h}_{jk} \mathbf{R}_\theta^{(j)} \mathbf{R}_\theta^{(k)} = \mathbf{h}_{jk}, \quad (\text{B.13})$$

the  $y$ -direction nearest neighbor terms in the Hamiltonian are unaffected. Only the  $x$ -direction nearest neighbor terms are transformed nontrivially by  $\mathcal{G}$ . Specifically, we have

$$\mathcal{G}^{-1} \mathbf{h}_{jk} \mathcal{G} = \begin{cases} \mathbf{R}_{2\pi/L_x}^{(k)} \mathbf{h}_{jk} \mathbf{R}_{-2\pi/L_x}^{(k)} & \text{if } \vec{r}_j - \vec{r}_k = (1, 0), \\ \mathbf{R}_{2\pi/L_x}^{(j)} \mathbf{h}_{jk} \mathbf{R}_{-2\pi/L_x}^{(j)} & \text{if } \vec{r}_j - \vec{r}_k = (-1, 0), \\ \mathbf{h}_{jk} & \text{otherwise.} \end{cases} \quad (\text{B.14})$$

This modification is identical to that created by defect loops winding around the  $y$ -direction, as we now explain.

Following the construction of on-site symmetry defects specified in Ref. [30], consider an  $I_\theta$  defect loop that winds in the negative  $y$ -direction along the line  $x = r_x^* - \frac{1}{2}$ , where  $r_x^* \in \{1, 2, \dots, L_x\}$ . Let  $C_L = \{j : [\vec{r}_j]_x = r_x^*\}$  be all the sites to the immediate left of  $I_\theta$  and  $C_R = \{j : [\vec{r}_j]_x = r_x^* - 1\}$  be all the sites to the immediate right. For the nearest neighbor Hamiltonian with on-site U(1) symmetry assumed in this section,  $I_\theta$  can be created by the modification:

$$\mathbf{h}_j \rightarrow \mathbf{h}_j \tag{B.15}$$

$$\mathbf{h}_{jk} \rightarrow \begin{cases} \mathbf{R}_\theta^{(k)} \mathbf{h}_{jk} \mathbf{R}_{-\theta}^{(k)} & \text{if } [\vec{r}_j]_x = r_x^*, [\vec{r}_k]_x = r_x^* - 1, \\ \mathbf{R}_\theta^{(j)} \mathbf{h}_{jk} \mathbf{R}_{-\theta}^{(j)} & \text{if } [\vec{r}_j]_x = r_x^* - 1, [\vec{r}_k]_x = r_x^*, \\ \mathbf{h}_{jk} & \text{otherwise.} \end{cases} \tag{B.16}$$

By comparing this modification with Eq. (B.12) and Eq. (B.14), we see that  $\mathbf{H}(2\pi)$  is essentially  $\mathbf{H}(0)$  with  $I_{2\pi/L_x}$  defect loops wrapping the torus in the negative  $y$ -direction along the lines  $x = \frac{1}{2}, x = \frac{3}{2}, \dots, x = L_x - \frac{1}{2}$ . Since  $|\Psi(2\pi)\rangle$  is a ground state of  $\mathbf{H}(2\pi)$ , it is essentially  $|\Psi(0)\rangle$  with these defect loops.

Finally, we turn to  $\mathcal{G}|\Psi(2\pi)\rangle$ . Rewriting the large gauge transformation as

$$\mathcal{G} = \prod_{j: [\vec{r}_j]_x=1} \mathbf{R}_{2\pi/L_x}^{(j)} \prod_{j: [\vec{r}_j]_x=2} \mathbf{R}_{4\pi/L_x}^{(j)} \cdots \prod_{j: [\vec{r}_j]_x=L_x-1} \mathbf{R}_{2\pi-2\pi/L_x}^{(j)}, \tag{B.17}$$

and recalling that defects lines obey the fusion rules

$$I_{\theta_1} \times I_{\theta_2} = \mathbf{w}(\theta_1, \theta_2) I_{[\theta_1+\theta_2]_{2\pi}}, \tag{B.18}$$

where  $\mathbf{w}(\theta_1, \theta_2)$  describes the U(1) fractionalization, we can study the action of  $\mathcal{G}$  on  $|\Psi(2\pi)\rangle$  *range* step by step.

**Step 1** Applying  $\prod_{j: [\vec{r}_j]_x=1} \mathbf{R}_{2\pi/L_x}^{(j)}$  moves  $I_{2\pi/L_x}$  at  $x = \frac{1}{2}$  to  $x = \frac{3}{2}$ , where it can be fused with  $I_{2\pi/L_x}$  already there to form  $I_{4\pi/L_x}$ .

**Step 2** Applying  $\prod_{j: [\vec{r}_j]_x=2} \mathbf{R}_{4\pi/L_x}^{(j)}$  moves  $I_{4\pi/L_x}$  at  $x = \frac{3}{2}$  to  $x = \frac{5}{2}$ , where it can be fused with  $I_{2\pi/L_x}$  already there to form  $I_{6\pi/L_x}$ .

⋮

**Step  $L_x - 1$**  Applying  $\prod_{j: [\vec{r}_j]_x=L_x-1} \mathbf{R}_{2\pi-2\pi/L_x}^{(j)}$  moves  $I_{2\pi-2\pi/L_x}$  at  $x = L_x - \frac{3}{2}$  to  $x = L_x - \frac{1}{2}$ , where it can be fused with  $I_{2\pi/L_x}$  already there to form a  $v$  anyon loop along the negative  $y$  direction, where  $v = \mathbf{w}(\theta, 2\pi - \theta)$ .

Since  $|\Psi(2\pi)\rangle$  is  $|\Psi(0)\rangle$  with defect loops wrapping around the torus in the  $y$ -direction, and  $\mathcal{G}|\Psi(2\pi)\rangle$  is  $|\Psi(2\pi)\rangle$  with all these defects loops fused to form a single  $v$  anyon loop around the  $y$ -direction of the torus, we conclude that  $\mathcal{G}|\Psi(2\pi)\rangle = \mathbf{W}_v|\Psi(0)\rangle$ .

# Appendix C

## C.1 Anyon Models on a Sphere

In this appendix, we review the description of anyon models on a sphere [82, 83]. Since punctures may be represented by anyons existing on their boundaries, this section also applies to spheres with punctures, e.g., a disk.

### C.1.1 Fusion Algebra

Anyon models, or modular tensor categories (MTCs), consist of a finite set of objects, or *anyons*, which obey a commutative, associative fusion algebra:

$$a \times b = \sum_c N_{ab}^c c, \tag{C.1}$$

where  $N_{ab}^c$  is a non-negative integer that specifies the number of different ways anyons  $a$  and  $b$  can fuse to  $c$ . An anyon  $a$  is *non-Abelian* if  $\sum_c N_{ab}^c > 1$  for some  $b$ , and *Abelian* otherwise.

The fusion algebra must obey certain conditions. There must exist a unique *vacuum* anyon  $0$  such that  $N_{a0}^c = \delta_{ac}$ , and each anyon  $a$  must have a *dual* anyon  $\bar{a}$  such that

$N_{ab}^0 = \delta_{b\bar{a}}$ . We also have the important relation

$$d_a d_b = \sum_c N_{ab}^c d_c, \quad (\text{C.2})$$

where  $d_a$ , the *quantum dimension* of  $a$ , is the largest eigenvalue of the fusion matrix  $N_a$ , (whose elements are  $[N_a]_{bc} = N_{ab}^c$ .) For non-Abelian anyons,  $d_a > 1$ , while for Abelian anyons,  $d_a = 1$ .

The total quantum dimension of an anyon model  $\mathcal{C}$  is

$$\mathcal{D} = \sqrt{\sum_{a \in \mathcal{C}} d_a^2}. \quad (\text{C.3})$$

### C.1.2 Anyonic Hilbert Space

The *anyonic Hilbert space* of topological system consists of all of its possible topologically distinct states. It can be constructed and expressed diagrammatically as follows.

#### Basis

The building blocks of the anyonic Hilbert space for the sphere is the space  $V_c^{ab}$  of two anyons  $a$  and  $b$  with definite total charge  $c$ , which is spanned by the vectors

$$|a, b; c, \mu\rangle = \left( \frac{d_c}{d_a d_b} \right)^{1/4} \begin{array}{c} \nearrow a \quad \nwarrow b \\ \searrow \mu \\ \swarrow c \end{array}, \quad (\text{C.4})$$

where  $\mu = 1, \dots, N_{ab}^c$ . The dual space  $V_{ab}^c$  is spanned by the covectors

$$\langle a, b; c, \mu| = \left( \frac{d_c}{d_a d_b} \right)^{1/4} \begin{array}{c} \uparrow c \\ \swarrow a \quad \searrow b \\ \nearrow \mu \end{array}. \quad (\text{C.5})$$

Larger spaces are constructed by taking tensor products. For example, the space  $V_d^{abc}$

of three anyons  $a$ ,  $b$ , and  $c$  with definite total charge  $d$  can be constructed as

$$V_d^{abc} \cong \bigoplus_e V_e^{ab} \otimes V_d^{ec}, \quad (\text{C.6})$$

which is spanned by

$$|a, b; e, \mu\rangle |e, c; d, \nu\rangle = \left( \frac{d_d}{d_a d_b d_c} \right)^{1/4} \begin{array}{c} \begin{array}{ccc} a & & b \\ \swarrow & & \searrow \\ \mu & & e \\ \swarrow & & \searrow \\ e & & c \\ \swarrow & & \searrow \\ \nu & & d \\ \swarrow & & \searrow \\ & & d \end{array} \end{array}, \quad (\text{C.7})$$

where  $\mu = 1, \dots, N_{ab}^e$ ,  $\nu = 1, \dots, N_{ec}^d$ , and  $e$  is any anyon such that  $N_{ab}^e \geq 1$  and  $N_{ec}^d \geq 1$ .

The space  $V_d^{abc}$  can also be constructed as

$$V_d^{abc} \cong \bigoplus_e V_e^{bc} \otimes V_d^{ae}, \quad (\text{C.8})$$

which is spanned by

$$|b, c; e, \mu\rangle |a, e; d, \nu\rangle = \left( \frac{d_d}{d_a d_b d_c} \right)^{1/4} \begin{array}{c} \begin{array}{ccc} & & b \\ & & \swarrow \\ & & \mu \\ & & e \\ & & \swarrow \\ & & c \\ & & \swarrow \\ & & \nu \\ & & \swarrow \\ & & d \\ & & \swarrow \\ & & a \end{array} \end{array}. \quad (\text{C.9})$$

where  $\mu = 1, \dots, N_{bc}^e$ ,  $\nu = 1, \dots, N_{ae}^d$ , and  $e$  is any anyon such that  $N_{bc}^e \geq 1$  and  $N_{ae}^d \geq 1$ .

These constructions are isomorphic, and their basis vectors are related by an  $F$ -move:

$$\begin{array}{c} \begin{array}{ccc} a & & b \\ \swarrow & & \searrow \\ \mu & & e \\ \swarrow & & \searrow \\ e & & c \\ \swarrow & & \searrow \\ \nu & & d \\ \swarrow & & \searrow \\ & & d \end{array} = \sum_f [F_d^{abc}]_{(e,\mu,\nu)(f,\alpha,\beta)} \begin{array}{c} \begin{array}{ccc} & & b \\ & & \swarrow \\ & & \alpha \\ & & f \\ & & \swarrow \\ & & c \\ & & \swarrow \\ & & \beta \\ & & \swarrow \\ & & d \\ & & \swarrow \\ & & a \end{array} \end{array}, \quad (\text{C.10})$$

where the  $F$ -symbols  $F_d^{abc}$  are unitary matrices that must satisfy the Pentagon consistency equations.

In general, the space  $V_c^{a_1 \dots a_n}$  of anyons  $a_1, \dots, a_n$  with definite combined charge  $c$

can be constructed as

$$V_c^{a_1 \dots a_n} \cong \bigoplus_{\vec{b}} V_{b_2}^{a_1 a_2} \otimes V_{b_3}^{b_2 a_3} \otimes \dots \otimes V_c^{b_{n-1} a_n}, \quad (\text{C.11})$$

which is spanned by

$$\begin{aligned} |\vec{a}, \vec{b}, \vec{\alpha}; c\rangle &= |a_1, a_2; b_2, \alpha_2\rangle \dots |b_{n-1}, a_n; c, \alpha_n\rangle \\ &= \left( \frac{d_c}{d_{a_1} \dots d_{a_n}} \right)^{1/4} \begin{array}{c} \begin{array}{c} a_1 \quad a_2 \quad \dots \\ \swarrow \quad \searrow \quad \nearrow \\ \alpha_2 \quad \alpha_3 \quad \dots \\ \swarrow \quad \searrow \quad \nearrow \\ b_{n-1} \quad c \end{array} \end{array}. \end{aligned} \quad (\text{C.12})$$

where  $\vec{b}$  and  $\vec{\alpha}$  take values that are allowed by fusion.

We can also write the  $F$ -move with two lower and two upper legs. This basis change is given by

$$\begin{array}{c} a \quad b \\ \uparrow \quad \uparrow \\ \diagdown \quad \diagup \\ e \\ \uparrow \\ c \quad d \end{array} = \sum_{f, \mu, \nu} [F_{cd}^{ab}]_{(e, \alpha, \beta)(f, \mu, \nu)} \begin{array}{c} a \quad b \\ \swarrow \quad \searrow \\ f \\ \swarrow \quad \searrow \\ c \quad d \end{array}, \quad (\text{C.13})$$

where the  $F$ -symbol in the above equation is related to the regular  $F$ -symbol by

$$[F_{cd}^{ab}]_{(e, \alpha, \beta)(f, \mu, \nu)} = \sqrt{\frac{d_e d_f}{d_a d_d}} [F_f^{ceb}]_{(a, \alpha, \mu)(d, \beta, \nu)}^* \quad (\text{C.14})$$

and is also a unitary transformation.

### Dimension

The dimension of  $V_c^{a_1 \dots a_n}$  is given by

$$\dim(V_c^{a_1 \dots a_n}) = \sum_{\vec{b}} N_{a_1 a_2}^{b_2} N_{b_2 a_3}^{b_3} \dots N_{b_{n-1} a_n}^c \equiv N_{a_1 \dots a_n}^c. \quad (\text{C.15})$$

The total dimension of the space of anyons  $a_1, \dots, a_n$  is

$$\sum_c \dim(V_c^{a_1 \dots a_n}) = \sum_c N_{a_1 \dots a_n}^c \equiv N_{a_1 \dots a_n}, \quad (\text{C.16})$$

In particular, if  $a_1 = \dots = a_n = a$ , then the dimension grows as  $N_{a \dots a} \sim d_a^n$  for large  $n$ . Note that a collection of Abelian anyons can only produce 1-dimensional spaces, but non-Abelian anyons can give rise to higher dimensional spaces. When considered by itself, a single anyon does not possess a multi-dimensional Hilbert space, so, from the perspective of individual anyons, the meaning of the quantum dimension is not so clear. We also define

$$d_{\vec{a}} \equiv d_{a_1} \cdots d_{a_n} = \sum_c N_{a_1 \dots a_n}^c d_c. \quad (\text{C.17})$$

Note that  $N_{a_1 \dots a_n} = \text{Tr}(I_{a_1 \dots a_n})$  and  $d_{\vec{a}} = \widetilde{\text{Tr}}(I_{a_1 \dots a_n})$ , where  $\text{Tr}$  and  $\widetilde{\text{Tr}}$  are defined below, and that they both grow with the same scaling as  $n \rightarrow \infty$ .

## Inner Product

Inner products can be evaluated by stacking diagrams, e.g. the fact that

$$\langle a', b'; c', \mu' | a, b; c, \mu \rangle = \delta_{a,a'} \delta_{b,b'} \delta_{c,c'} \delta_{\mu,\mu'} I_c \quad (\text{C.18})$$

can be expressed as

$$\left( \frac{d_c^2}{d_a d_b d_{a'} d_{b'}} \right)^{1/4} \begin{array}{c} \begin{array}{c} \downarrow c' \\ \swarrow a' \quad \searrow b' \\ \mu' \\ \downarrow \mu \\ \swarrow a \quad \searrow b \\ \downarrow c \end{array} \end{array} = \delta_{a,a'} \delta_{b,b'} \delta_{c,c'} \delta_{\mu,\mu'} \left| \begin{array}{c} \\ \\ \\ \\ \\ \end{array} \right|^c. \quad (\text{C.19})$$

Note that in the diagrammatic notation,  $\delta_{a,a'}$  and  $\delta_{b,b'}$  ensure that the branches of the splitting vertex can be joined with those of the fusion vertex, while  $\delta_{c,c'}$  enforces the

conservation of anyonic charge. More complicated diagrams can be similarly evaluated.

### Operators

The space  $V_{a_1 \dots a_n}^{a'_1 \dots a'_n}$  of operators acting on anyons  $a_1, \dots, a_n$  can be constructed as

$$V_{a_1 \dots a_n}^{a'_1 \dots a'_n} = \bigoplus_c V_{a_1 \dots a_n}^c \otimes V_c^{a'_1 \dots a'_n}, \quad (\text{C.20})$$

which is spanned by

$$|\vec{a}', \vec{b}', \vec{\alpha}'; c\rangle \langle \vec{a}, \vec{b}, \vec{\alpha}; c| = \left( \frac{d_c^2}{d_{\vec{a}} d_{\vec{a}'}} \right)^{1/4} \begin{array}{c} \begin{array}{c} a'_1 \quad a'_2 \quad \dots \\ \alpha_2 \quad \alpha_n \\ \swarrow \quad \downarrow \quad \searrow \\ b'_{n-1} \quad c \\ \swarrow \quad \downarrow \quad \searrow \\ b_{n-1} \quad c \\ \swarrow \quad \downarrow \quad \searrow \\ \alpha_2 \quad \alpha_n \\ a_1 \quad a_2 \quad \dots \end{array} \end{array}, \quad (\text{C.21})$$

where  $\vec{b}$ ,  $\vec{\alpha}$ ,  $\vec{b}'$ , and  $\vec{\alpha}'$  take values that are allowed by fusion.

For example, the identity operator for a pair of anyons  $a$  and  $b$  is

$$I_{ab} = \sum_{c, \mu} |a, b; c, \mu\rangle \langle a, b; c, \mu|, \quad (\text{C.22})$$

or, diagrammatically,

$$\begin{array}{c} | \\ a \end{array} \begin{array}{c} | \\ b \end{array} = \sum_{c, \mu} [F_{ab}^{ac}]_{0, (c, \mu, \nu)} \begin{array}{c} a \quad b \\ \mu \\ \swarrow \quad \searrow \\ c \\ \swarrow \quad \searrow \\ a \quad b \\ \nu \end{array} = \sum_{c, \mu} \sqrt{\frac{d_c}{d_a d_b}} \begin{array}{c} a \quad b \\ \mu \\ \swarrow \quad \searrow \\ c \\ \swarrow \quad \searrow \\ a \quad b \\ \mu \end{array}, \quad (\text{C.23})$$

and the braiding operator for the pair is

$$R^{ab} = \sum_{c, \mu} [R_c^{ab}]_{\mu\nu} |a, b; c, \mu\rangle \langle b, a; c, \nu|, \quad (\text{C.24})$$

or, diagrammatically,

$$\begin{array}{c} \diagup \\ \diagdown \\ \diagdown \\ \diagup \end{array} = \sum_{c,\mu,\nu} \sqrt{\frac{d_c}{d_a d_b}} [R_c^{ab}]_{\mu\nu} \begin{array}{c} \diagup \\ \diagdown \\ \diagup \\ \diagdown \end{array}, \quad (\text{C.25})$$

where the  $R$  symbols  $R_c^{ab}$  are unitary matrices that must satisfy the Hexagon consistency equations.

### $\mathcal{S}$ -matrix

The topological  $S$ -matrix is defined by

$$S_{ab} = \frac{1}{\mathcal{D}} \widetilde{\text{Tr}} (R^{b\bar{a}} R^{\bar{a}b}). \quad (\text{C.26})$$

The quantum dimension is related to the  $S$ -matrix by

$$d_a = \frac{S_{0a}}{S_{00}}. \quad (\text{C.27})$$

For a modular tensor category (MTC), the  $S$ -matrix is unitary and provides a unitary projective representation of the modular  $\mathcal{S}$ -transformations. In this case, the fusion coefficients can be expressed in terms of the  $\mathcal{S}$ -matrix by the Verlinde formula

$$N_{ab}^c = \sum_x \frac{\mathcal{S}_{ax} \mathcal{S}_{bx} \mathcal{S}_{cx}^*}{\mathcal{S}_{0x}}. \quad (\text{C.28})$$

It follows that the dimension of  $V_c^{a_1 \dots a_n}$ , given in Eq. (C.15), can also be expressed in terms of the  $\mathcal{S}$ -matrix as

$$N_{a_1 \dots a_n}^c = \sum_x \mathcal{S}_{0x}^{1-n} \mathcal{S}_{a_1 x} \cdots \mathcal{S}_{a_n x} \mathcal{S}_{cx}^*. \quad (\text{C.29})$$

**$\omega_a$ -loops**

The  $\omega_a$ -loop is defined by

$$\omega_a \circlearrowleft = \sum_x \mathcal{S}_{0a} \mathcal{S}_{ax}^* \circlearrowleft_x, \quad (\text{C.30})$$

and acts a projector on all charges threading the loop,

$$\omega_a \circlearrowleft \uparrow b = \delta_{ab} \uparrow b. \quad (\text{C.31})$$

**Trace**

The *trace* of an operator is defined, as usual, to be the sum of its diagonal elements, e.g.

$$\text{Tr}(|a', b'; c, \mu'\rangle \langle a, b; c, \mu|) = \delta_{a,a'} \delta_{b,b'} \delta_{\mu,\mu'} \quad (\text{C.32})$$

Its diagrammatic equivalent is the *quantum trace*  $\widetilde{\text{Tr}}$ , (also called the *anyonic trace*,) which is obtained by joining the outgoing anyon lines of the operator's diagram back onto the corresponding incoming lines, e.g.

$$\begin{aligned} \widetilde{\text{Tr}} \left( \left( \frac{d_c^2}{d_a d_b d_{a'} d_{b'}} \right)^{1/4} \begin{array}{c} a' \nearrow \\ \mu' \nearrow \\ c \uparrow \\ \mu \downarrow \\ a \swarrow \\ b \searrow \end{array} \right) &= \left( \frac{d_c^2}{d_a d_b d_{a'} d_{b'}} \right)^{1/4} \begin{array}{c} a' \nearrow \\ \mu' \nearrow \\ c \uparrow \\ \mu \downarrow \\ a \swarrow \\ b \searrow \end{array} \\ &= d_c \delta_{a,a'} \delta_{b,b'} \delta_{\mu,\mu'}, \end{aligned} \quad (\text{C.33})$$

which agrees with Eq. (C.32) except for the factor of  $d_c$ . In general, the anyonic trace of an operator  $X \in V_{a'_1 \dots a'_n}^{a_1 \dots a_n}$  is related to its ordinary trace by

$$\widetilde{\text{Tr}}(X) = \sum_c d_c \text{Tr}([X]_c), \quad (\text{C.34})$$

$$\text{Tr}(X) = \sum_c \frac{1}{d_c} \widetilde{\text{Tr}}([X]_c) \quad (\text{C.35})$$

where  $[X]_c = \Pi_c X \Pi_c \in V_c^{a_1 \dots a_n} \otimes V_{a'_1 \dots a'_n}^c$  is the projection of  $X$  onto definite total charge  $c$ , with  $X = \sum_c [X]_c$ .

The *partial anyonic trace* is obtained by joining only the outgoing and incoming lines of the anyons being traced over, e.g.

$$\begin{aligned} \widetilde{\text{Tr}}_b \left( \left( \frac{d_c^2}{d_a d_b d_{a'} d_{b'}} \right)^{1/4} \begin{array}{c} \text{---} a' \text{---} \\ \diagup \quad \diagdown \\ \mu' \quad \mu \\ \diagdown \quad \diagup \\ \text{---} a \text{---} \\ \text{---} b \text{---} \end{array} \right) &= \left( \frac{d_c^2}{d_a d_b d_{a'} d_{b'}} \right)^{1/4} \begin{array}{c} \text{---} a' \text{---} \\ \diagup \quad \diagdown \\ \mu' \quad \mu \\ \diagdown \quad \diagup \\ \text{---} a \text{---} \\ \text{---} b \text{---} \end{array} \\ &= \frac{d_c}{d_a} \delta_{a,a'} \delta_{b,b'} \delta_{\mu,\mu'} \begin{array}{c} \text{---} a \text{---} \\ | \\ \text{---} a \text{---} \end{array}. \end{aligned} \quad (\text{C.36})$$

Before computing the partial trace, all the anyons being traced over must be moved to the edge of the diagram by braiding them past the other anyons, a process which is not necessarily unique. In general, the partial anyonic trace of  $X \in V_{a'_1 \dots a'_n b'_1 \dots b'_m}^{a_1 \dots a_n b_1 \dots b_m}$  over the anyons  $b_1, \dots, b_m$  is related to its ordinary partial trace by

$$\widetilde{\text{Tr}}_{b_1 \dots b_m}(X) = \sum_{c,a} \frac{d_c}{d_a} [\text{Tr}_{b_1 \dots b_m}([X]_c)]_a, \quad (\text{C.37})$$

$$\text{Tr}_{b_1 \dots b_m}(X) = \sum_{c,a} \frac{d_a}{d_c} [\widetilde{\text{Tr}}_{b_1 \dots b_m}([X]_c)]_a. \quad (\text{C.38})$$

### C.1.3 Anyonic Density Matrix

An *anyonic density matrix*  $\tilde{\rho}$  is an anyonic operator normalized by the quantum trace  $\widetilde{\text{Tr}}\tilde{\rho} = 1$ , that describes the topological state of the system. The anyonic density matrix  $\tilde{\rho}$  determines the expectation value of anyonic operators acting on the system,  $\langle X \rangle = \widetilde{\text{Tr}}(\tilde{\rho}X)$ . For example, the density matrix describing a pair of anyons  $a$  and  $b$  with definite total charge  $c$  is

$$\tilde{\rho}_{ab} = \frac{1}{d_c} |a, b; c, \mu\rangle \langle a, b; c, \mu| = \frac{1}{\sqrt{d_a d_b d_c}} \begin{array}{c} a \quad b \\ \diagdown \quad \diagup \\ \mu \\ \diagup \quad \diagdown \\ a \quad b \\ c \end{array}, \quad (\text{C.39})$$

which is normalized such that  $\widetilde{\text{Tr}}(\tilde{\rho}^{ab}) = 1$ , while the most general state for the pair is given by

$$\begin{aligned} \tilde{\rho}_{ab} &= \sum_{\substack{a, b, \mu \\ a', b', \mu'}} \frac{\rho_{(a, b; c, \mu)(a', b'; c, \mu')}}{d_c} |a, b; c, \mu\rangle \langle a', b'; c, \mu'| \\ &= \sum_{\substack{a, b, \mu \\ a', b', \mu'}} \frac{\rho_{(a, b; c, \mu)(a', b'; c, \mu')}}{(d_a d_b d_{a'} d_{b'} d_c^2)^{1/4}} \begin{array}{c} a' \quad b' \\ \diagdown \quad \diagup \\ \mu' \\ \diagup \quad \diagdown \\ a \quad b \\ c \end{array}, \end{aligned} \quad (\text{C.40})$$

where the coefficients are normalized such that  $\sum_{a, b, \mu, c} \rho_{(a, b; c, \mu)(a, b; c, \mu)} = 1$ .

For a collection of anyons  $a_1, \dots, a_n, b_1, \dots, b_n$ , the reduced anyonic density matrix

$$\tilde{\rho}_{a_1 \dots a_n} = \widetilde{\text{Tr}}_{b_1 \dots b_n}(\tilde{\rho}_{a_1 \dots a_n b_1 \dots b_n}) \quad (\text{C.41})$$

describes the topological state of the anyons  $a_1, \dots, a_n$ , i.e. for any operator  $X \in V_{a'_1 \dots a'_n}^{a_1 \dots a_n}$ ,

$$\langle X \rangle = \widetilde{\text{Tr}}(\tilde{\rho}_{a_1 \dots a_n b_1 \dots b_n} X) = \widetilde{\text{Tr}}(\tilde{\rho}_{a_1 \dots a_n} X). \quad (\text{C.42})$$

## C.2 Examples of Braided Tensor Categories

In this Appendix, we provide additional details of the braided tensor categories (BTCs) mentioned in this paper. In particular, we list the fusion rules (which are commutative), quantum dimensions, and topological twist factors. (The  $F$ -symbols and  $R$ -symbols for these theories are uniquely determined, up to gauge freedom, by this data, and can be found in the literature, such as Ref. [82].)

### C.2.1 $\mathbb{Z}_N^{(p)}$

The  $\mathbb{Z}_N^{(p)}$  BTC for  $N$  a positive integer can have  $p \in \mathbb{Z}$  for all  $N$  and  $p \in \mathbb{Z} + \frac{1}{2}$  for  $N$  even. The total quantum dimension is  $\mathcal{D}^2 = N$ . This BTC has  $N$  topological charges labeled by  $\{0, 1, \dots, N - 1\}$ , for which the fusion rules, quantum dimensions, and twist factors are

$$a \times b = [a + b]_N, \quad (\text{C.43})$$

$$d_a = 1, \quad (\text{C.44})$$

$$\theta_a = e^{i\frac{2\pi p}{N}a^2}, \quad (\text{C.45})$$

where  $[a]_N = a \pmod{N}$ .

For odd  $N$ ,  $\mathbb{Z}_N^{(p)}$  is modular when  $[p]_N \neq 0$  and  $\gcd(N, [p]_N) = 1$ . For even  $N$ ,  $\mathbb{Z}_N^{(p)}$  is modular when  $p \in \mathbb{Z} + \frac{1}{2}$  and  $\gcd(N, 2[p]_N) = 1$ . Notice that  $p$  is periodic in  $N$ , so we can restrict our attention to  $0 \leq p < N$ . In some cases, there is a redundancy where distinct values of  $p$  describe the same BTC when the topological charge values are relabeled (i.e.  $a \mapsto a' = [na]_N$  for some integer  $n$ ). For example, in the case of  $\mathbb{Z}_5^{(p)}$ ,  $p = 1$  and  $4$  are the same BTC, and  $p = 2$  and  $3$  are the same BTC; in the case of  $\mathbb{Z}_7^{(p)}$ ,  $p = 1, 2$ , and  $4$  are the same BTC, and  $p = 3, 5$ , and  $6$  are the same BTC.

The trivial fermion SMTTC is described by  $\mathbb{Z}_2^{(1)}$ .

### C.2.2 $\text{Fib}^{\pm 1}$

The Fibonacci ( $\text{Fib}^{\pm 1}$ ) MTCs has two topological charges  $\{0, 1\}$ , for which the fusion rules are given by

$$0 \times a = a, \quad 1 \times 1 = 0 + 1. \quad (\text{C.46})$$

The quantum dimensions are given by

$$d_0 = 1, \quad d_1 = \phi, \quad (\text{C.47})$$

where  $\phi = \frac{1+\sqrt{5}}{2}$  is the Golden ratio, so  $\mathcal{D}^2 = \phi + 2$ . The twist factors are

$$\theta_0 = 1, \quad \theta_1 = e^{\pm i \frac{4\pi}{5}}. \quad (\text{C.48})$$

### C.2.3 $\mathcal{K}_\nu$

We use the notation  $\mathcal{K}_\nu$  with  $\nu = 0, 1, \dots, 15$  to denote Kitaev's 16-fold way of MTCs [81], which have chiral central charge  $c_-(\text{mod})8 = \nu$  and total quantum dimension  $\mathcal{D}^2 = 4$ .

For  $\nu$  odd, there are three topological charge values, which we denote  $\{I, \sigma, \psi\}$ , where the vacuum charge here is denoted  $I$ . The fusion rules are given by

$$I \times a = a, \quad \psi \times \psi = I, \quad \psi \times \sigma = \sigma, \quad \sigma \times \sigma = I + \psi. \quad (\text{C.49})$$

The quantum dimensions and twist factors are given by

$$\begin{aligned} d_I &= 1, & d_\sigma &= \sqrt{2}, & d_\psi &= 1, \\ \theta_I &= 1, & \theta_\sigma &= e^{i\frac{\pi}{8}\nu}, & \theta_\psi &= -1. \end{aligned} \tag{C.50}$$

$\nu = 1$  corresponds to the Ising TQFT,  $\nu = 3$  corresponds to  $SU(2)_2$ , and  $\nu \geq 5$  can be realized by  $SO(\nu)_1$  Chern-Simons field theory.

For  $\nu$  even, there are four topological charge values, all of which have quantum dimension  $d_a = 1$ . It is useful to further split them into two categories, as follows.

For  $\nu = 0, 4, 8$ , and  $12$ , the fusion rules are  $\mathbb{Z}_2 \times \mathbb{Z}_2$ . The twist factors are

$$\theta_{(0,0)} = 1, \quad \theta_{(0,1)} = \theta_{(1,0)} = e^{i\frac{\pi}{8}\nu}, \quad \theta_{(1,1)} = -1. \tag{C.51}$$

$\nu = 0$  corresponds to the toric code  $D(\mathbb{Z}_2)$ ,  $\nu = 8$  corresponds to the three fermion theory  $SO(8)_1$ , and  $\nu = 4$  and  $12$  correspond to  $\mathbb{Z}_2^{(\pm 1/2)} \times \mathbb{Z}_2^{(\pm 1/2)}$ , respectively.

For  $\nu = 2, 6, 10$ , and  $14$ , the fusion rules are  $\mathbb{Z}_4$ . The twist values are

$$\theta_0 = 1, \quad \theta_1 = \theta_3 = e^{i\frac{\pi}{8}\nu}, \quad \theta_2 = -1. \tag{C.52}$$

Thus, these correspond to the  $\mathbb{Z}_4^{(\nu/4)}$  MTCs.

### C.2.4 $SO(3)_6$

The  $SO(3)_6$  SMTC can be obtained as the restriction of the  $SU(2)_6$  MTC to its integer spin topological charge values. It has four topological charge values  $\{0, 1, 2, 3\}$ , which have the fusion rules

$$0 \times a = a, \quad 3 \times a = 3 - a, \quad 1 \times 2 = 1 + 2 + 3, \quad 1 \times 1 = 2 \times 2 = 0 + 1 + 2. \tag{C.53}$$

The quantum dimensions and twist factors are given by

$$\begin{aligned} d_0 = 1, \quad d_1 = 1 + \sqrt{2}, \quad d_2 = 1 + \sqrt{2}, \quad d_3 = 1, \\ \theta_0 = 1, \quad \theta_1 = i, \quad \theta_2 = -i, \quad \theta_3 = -1. \end{aligned} \tag{C.54}$$

### C.3 Proofs

We now prove various properties of anyonic entropy  $\tilde{S}$ , following Ref. [84] and adapting the proofs appropriately. We make use of the following definitions: the anyonic relative entropy is

$$\tilde{S}(\tilde{\rho}||\tilde{\sigma}) \equiv \widetilde{\text{Tr}}(\tilde{\rho} \log \tilde{\rho} - \tilde{\rho} \log \tilde{\sigma}). \tag{C.55}$$

and the anyonic mutual information between the two subsystems is

$$\tilde{I}(A : B) \equiv \tilde{S}(\tilde{\rho}_A) + \tilde{S}(\tilde{\rho}^B) - \tilde{S}(\tilde{\rho}^{AB}). \tag{C.56}$$

#### Anyonic Entropy is non-negative

**Statement:**  $\tilde{S}(\tilde{\rho}) \geq 0$  with equality iff  $\tilde{\rho}$  is pure.

**Proof:** Positivity follows from the definition. To see this, it may be helpful to write the anyonic density matrices in diagonalized form

$$\tilde{\rho} = \sum_{c, \alpha_c} \frac{p_{\alpha_c}}{d_c} |\alpha_c\rangle \langle \alpha_c| \tag{C.57}$$

where  $|\alpha_c\rangle$  are orthonormal states with total charge  $c$ . This gives

$$\tilde{S}(\tilde{\rho}) = - \sum_{c, \alpha_c} p_{\alpha_c} \log \left( \frac{p_{\alpha_c}}{d_c} \right) \tag{C.58}$$

$$= H(\{p_{\alpha_c}\}) + \sum_{c, \alpha_c} p_{\alpha_c} \log d_c, \tag{C.59}$$

which is positive, since  $d_c \geq 1$  (and  $d_c = 1$  iff  $c$  is Abelian).

### Relative Anyonic Entropy is non-negative

**Statement:**  $\tilde{S}(\tilde{\rho}||\tilde{\sigma}) \geq 0$  with equality iff  $\tilde{\rho} = \tilde{\sigma}$ .

**Proof:** Start by diagonalizing the anyonic density matrices

$$\tilde{\rho} = \sum_{c, \alpha_c} \frac{p_{\alpha_c}}{d_c} |\alpha_c\rangle \langle \alpha_c|, \quad (\text{C.60})$$

$$\tilde{\sigma} = \sum_{c, \beta_c} \frac{q_{\beta_c}}{d_c} |\beta_c\rangle \langle \beta_c|, \quad (\text{C.61})$$

where  $|\alpha_c\rangle$  and  $|\beta_c\rangle$  are possibly different orthonormal bases for the space of states with total charge  $c$ . Now we can write

$$\begin{aligned} \tilde{S}(\tilde{\rho}||\tilde{\sigma}) &= \sum_{c, \alpha_c} \left[ p_{\alpha_c} \log \left( \frac{p_{\alpha_c}}{d_c} \right) - d_c \langle \alpha_c | \tilde{\rho} \log \tilde{\sigma} | \alpha_c \rangle \right] \\ &= \sum_{c, \alpha_c} p_{\alpha_c} \left[ \log \left( \frac{p_{\alpha_c}}{d_c} \right) - \sum_{\beta_c} P_{\alpha_c, \beta_c} \log \left( \frac{q_{\beta_c}}{d_c} \right) \right] \\ &= \sum_{c, \alpha_c} p_{\alpha_c} \left[ \log p_{\alpha_c} - \sum_{\beta_c} P_{\alpha_c, \beta_c} \log q_{\beta_c} \right], \end{aligned} \quad (\text{C.62})$$

where we used

$$P_{\alpha_c, \beta_c} \equiv \langle \alpha_c | \beta_c \rangle \langle \beta_c | \alpha_c \rangle \geq 0, \quad (\text{C.63})$$

and the fact that it satisfies

$$\sum_{\alpha_c} P_{\alpha_c, \beta_c} = \sum_{\beta_c} P_{\alpha_c, \beta_c} = 1 \quad (\text{C.64})$$

because the basis states are orthonormal. Now the rest of the proof from Ref. [84] applies.

### Maximum of Anyonic Entropy

**Statement:** The entropy for a state  $\tilde{\rho}$  of anyons with topological charges  $a_1, \dots, a_n$  satisfies the bound

$$\tilde{S}(\tilde{\rho}) \leq \log \left( \prod_{i=1}^n d_{a_i} \right) = \sum_j \log d_{a_j}, \quad (\text{C.65})$$

with equality obtained iff

$$\tilde{\rho} = \frac{I_{a_1 \dots a_n}}{\prod_{i=1}^n d_{a_i}} = \tilde{\rho}_{a_1} \otimes \tilde{\rho}_{a_2} \otimes \dots \otimes \tilde{\rho}_{a_n}. \quad (\text{C.66})$$

**Proof:** Using the relative entropy with  $\tilde{\sigma} = \frac{I_{a_1 \dots a_n}}{\prod_{i=1}^n d_{a_i}}$ , we see

$$0 \leq \tilde{S}(\tilde{\rho} \parallel \tilde{\sigma}) = -\tilde{S}(\tilde{\rho}) + \log \left( \prod_{i=1}^n d_{a_i} \right) \quad (\text{C.67})$$

### Anyonic Entanglement Entropy of Pure States

**Statement:** The entanglement entropy of a composite system in a pure state  $\tilde{\rho}_{AB} = |\psi_c\rangle \langle \psi_c|$  has  $\tilde{S}(\tilde{\rho}_A) = \tilde{S}(\tilde{\rho}_B)$ .

*Corollary:* For a pure state  $\tilde{\rho}_{AB}$ ,  $I(A : B) = 2\tilde{S}(\tilde{\rho}_A)$ .

**Proof:** Begin by Schmidt decomposing the state

$$|\psi_c\rangle = \sum_{a, \alpha_a} \sqrt{p_{\alpha_a}} |\alpha_a\rangle_A |\alpha_b\rangle_B, \quad (\text{C.68})$$

where  $b = \bar{a} \times c$  is uniquely determined by  $a$  and has  $d_b = d_a$ , since  $c$  is Abelian. Now

we have

$$\tilde{\rho}_A = \sum_{a, \alpha_a} \frac{p_{\alpha_a}}{d_a} |\alpha_a\rangle \langle \alpha_a| \quad (\text{C.69})$$

$$\tilde{\rho}_B = \sum_{a, \alpha_a} \frac{p_{\alpha_a}}{d_a} |\alpha_{\bar{a} \times c}\rangle \langle \alpha_{\bar{a} \times c}| \quad (\text{C.70})$$

which clearly gives

$$\tilde{S}(\tilde{\rho}_A) = \tilde{S}(\tilde{\rho}_B) = - \sum_{a, \alpha_a} p_{\alpha_a} \log \left( \frac{p_{\alpha_a}}{d_a} \right). \quad (\text{C.71})$$

### Entropy of Tensor Product of States

**Statement:** The entropy of the tensor product  $\tilde{\rho}_{AB} = \tilde{\rho}_A \otimes \tilde{\rho}_B$  of two states is  $\tilde{S}(\tilde{\rho}_{AB}) = \tilde{S}(\tilde{\rho}_A) + \tilde{S}(\tilde{\rho}_B)$ .

*Corollary:* If  $\tilde{\rho}_{AB} = \tilde{\rho}_A \otimes \tilde{\rho}_B$ , then  $\tilde{I}(A : B) = 0$

**Proof:** Same as proof in Ref. [84].

### Entropy of Distribution of Orthogonal States

**Statement:** For a probability distribution  $p_i$  of states  $\tilde{\rho}_i$  with orthogonal support ( $\tilde{\rho}_i \tilde{\rho}_j = 0$  for  $i \neq j$ ), the entropy is

$$\tilde{S} \left( \sum_i p_i \tilde{\rho}_i \right) = H(\{p_i\}) + \sum_i p_i \tilde{S}(\tilde{\rho}_i). \quad (\text{C.72})$$

**Proof:** Begin by decomposing the density matrix  $\tilde{\rho}_i$  as

$$\tilde{\rho}_i = \sum_{c, \alpha_c^{(i)}} \frac{q_{\alpha_c^{(i)}}}{d_c} |\alpha_c^{(i)}\rangle \langle \alpha_c^{(i)}|. \quad (\text{C.73})$$

It follows that

$$\begin{aligned}
\tilde{S} \left( \sum_i p_i \tilde{\rho}_i \right) &= - \sum_{i,c,\alpha_c^{(i)}} p_i q_{\alpha_c^{(i)}} \log \left( \frac{p_i q_{\alpha_c^{(i)}}}{d_c} \right) \\
&= - \sum_i p_i \log p_i - \sum_i p_i \left( \sum_{c,\alpha_c^{(i)}} q_{\alpha_c^{(i)}} \log \left( \frac{q_{\alpha_c^{(i)}}}{d_c} \right) \right) \\
&= H(\{p_i\}) + \sum_i p_i \tilde{S}(\tilde{\rho}_i).
\end{aligned} \tag{C.74}$$

### Joint Entropy

**Statement:** For a set of states  $\tilde{\rho}_i$  and an orthogonal set of pure states  $|i\rangle \langle i|$ , then

$$\tilde{S} \left( \sum_i p_i |i\rangle \langle i| \otimes \tilde{\rho}_i \right) = H(\{p_i\}) + \sum_i p_i \tilde{S}(\tilde{\rho}_i). \tag{C.75}$$

**Proof:** This follows from the previous result. If necessary, we could introduce a set of unpure orthogonal states  $|i\rangle \langle i|$  with non-Abelian collective charge, which will require modification of this equation.

### Decoherence Due to Projective Measurement Increases Anyonic Entropy

**Statement:** Consider a projective measurement given by the complete, orthogonal set of projectors  $\Pi_i$ . The decoherence of a state  $\tilde{\rho}$  due to this measurement is given by the transformation  $\tilde{\rho}' = \sum_i \Pi_i \tilde{\rho} \Pi_i$ . Then  $\tilde{S}(\tilde{\rho}') \geq \tilde{S}(\tilde{\rho})$ , with equality iff  $\tilde{\rho} = \tilde{\rho}'$ .

**Proof:** We use the fact that

$$\begin{aligned}
\widetilde{\text{Tr}}[\tilde{\rho} \log \tilde{\rho}'] &= \widetilde{\text{Tr}} \left[ \tilde{\rho} \log \left( \sum_i \Pi_i \tilde{\rho} \Pi_i \right) \right] \\
&= \widetilde{\text{Tr}} \left[ \sum_j \Pi_j \tilde{\rho} \log \left( \sum_i \Pi_i \tilde{\rho} \Pi_i \right) \Pi_j \right] \\
&= \widetilde{\text{Tr}} \left[ \sum_j \Pi_j \tilde{\rho} \Pi_j \log \left( \sum_i \Pi_i \tilde{\rho} \Pi_i \right) \right] \\
&= \widetilde{\text{Tr}}[\tilde{\rho}' \log \tilde{\rho}']
\end{aligned} \tag{C.76}$$

and the previous results to get

$$\begin{aligned}
0 \leq \tilde{S}(\tilde{\rho} \|\tilde{\rho}') &= -\tilde{S}(\tilde{\rho}) - \widetilde{\text{Tr}}[\tilde{\rho} \log \tilde{\rho}'] \\
&= -\tilde{S}(\tilde{\rho}) + \tilde{S}(\tilde{\rho}').
\end{aligned} \tag{C.77}$$

### Subadditivity

**Statement:** For a composite state  $\tilde{\rho}_{AB}$ , we have

$$\tilde{S}(\tilde{\rho}_{AB}) \leq \tilde{S}(\tilde{\rho}_A) + \tilde{S}(\tilde{\rho}_B), \tag{C.78}$$

with equality iff  $\tilde{\rho}_{AB} = \tilde{\rho}_A \otimes \tilde{\rho}_B$ .

**Proof:** Let  $\tilde{\rho} = \tilde{\rho}_{AB}$  and  $\tilde{\sigma} = \tilde{\rho}_A \otimes \tilde{\rho}_B$ . Then we have

$$\begin{aligned}
0 \leq \tilde{S}(\tilde{\rho} \|\tilde{\sigma}) &= -\tilde{S}(\tilde{\rho}) - \widetilde{\text{Tr}}[\tilde{\rho}_{AB} \log \tilde{\sigma}] \\
&= -\tilde{S}(\tilde{\rho}_{AB}) + \tilde{S}(\tilde{\rho}_A) + \tilde{S}(\tilde{\rho}_B).
\end{aligned} \tag{C.79}$$

### Triangle Inequality

**Statement:** For a composite state  $\tilde{\rho}_{AB}$ , we have  $\tilde{S}(\tilde{\rho}_{AB}) \geq \left| \tilde{S}(\tilde{\rho}_A) - \tilde{S}(\tilde{\rho}_B) \right|$ , with equality iff  $\tilde{\rho}_A$  is already maximally entangled with the environment by its existing correlations with  $\tilde{\rho}_B$ .

**Proof:** Let  $R$  be a system which purifies systems  $A$  and  $B$ . Then  $\tilde{S}(\tilde{\rho}_{AR}) = \tilde{S}(\tilde{\rho}_B)$  and  $\tilde{S}(\tilde{\rho}_R) = \tilde{S}(\tilde{\rho}_{AB})$  because  $\tilde{\rho}_{ABR}$  is a pure state. If we consider the composite state of  $\tilde{\rho}_{AR}$ , then from subadditivity we have

$$\begin{aligned} \tilde{S}(\tilde{\rho}_{AR}) &\leq \tilde{S}(\tilde{\rho}_A) + \tilde{S}(\tilde{\rho}_R) \\ \tilde{S}(\tilde{\rho}_B) &\leq \tilde{S}(\tilde{\rho}_A) + \tilde{S}(\tilde{\rho}_{AB}) \\ \tilde{S}(\tilde{\rho}_{AB}) &\geq \tilde{S}(\tilde{\rho}_B) - \tilde{S}(\tilde{\rho}_A). \end{aligned} \tag{C.80}$$

Similarly,

$$\begin{aligned} \tilde{S}(\tilde{\rho}_{BR}) &\leq \tilde{S}(\tilde{\rho}_B) + \tilde{S}(\tilde{\rho}_R) \\ \tilde{S}(\tilde{\rho}_A) &\leq \tilde{S}(\tilde{\rho}_B) + \tilde{S}(\tilde{\rho}_{AB}) \\ \tilde{S}(\tilde{\rho}_{AB}) &\geq \tilde{S}(\tilde{\rho}_A) - \tilde{S}(\tilde{\rho}_B). \end{aligned} \tag{C.81}$$

Taken together, the above equations imply

$$\tilde{S}(\tilde{\rho}_{AB}) \geq \left| \tilde{S}(\tilde{\rho}_A) - \tilde{S}(\tilde{\rho}_B) \right|. \tag{C.82}$$

From subadditivity we know that  $\tilde{S}(\tilde{\rho}_{AR}) = \tilde{S}(\tilde{\rho}_A) + \tilde{S}(\tilde{\rho}_R)$  iff  $\tilde{\rho}_{AR} = \tilde{\rho}_A \otimes \tilde{\rho}_R$ .

### Concavity

**Statement:**  $\tilde{S}\left(\sum_j p_j \tilde{\rho}_j\right) \geq \sum_j p_j \tilde{S}(\tilde{\rho}_j)$ , with equality iff all the  $\tilde{\rho}_j$  are the same.

**Proof:** Let the sum on  $j$  run from 1 to  $n$ . We introduce an auxillary system  $B$  whose

state space has an orthonormal basis  $\{|\psi_k\rangle\}$ , such that at least  $n$  basis states have Abelian total charge. We enlarge the set  $\{p_j\}$  by setting  $p_j = 0$  for  $j > n$ . One choice of auxiliary system is for a particular basis state  $|\psi_k\rangle$  to correspond to  $k$  copies of  $\bar{c}$  and  $c$  fusing to vacuum for some nontrivial charge  $c$  in the anyon model describing the system. The proof from here follows that in Ref. [84].

# Bibliography

- [1] L. D. Landau, *Collected papers*, .
- [2] V. L. Berezinskii, *Destruction of long-range order in one-dimensional and two-dimensional systems having a continuous symmetry group ii. quantum systems*, *Sov. Phys. JETP* **34** (1972), no. 3 610–616.
- [3] J. M. Kosterlitz and D. J. Thouless, *Ordering, metastability and phase transitions in two-dimensional systems*, *Journal of Physics C: Solid State Physics* **6** (1973), no. 7 1181.
- [4] K. v. Klitzing, G. Dorda, and M. Pepper, *New method for high-accuracy determination of the fine-structure constant based on quantized hall resistance*, *Phys. Rev. Lett.* **45** (Aug, 1980) 494–497.
- [5] R. B. Laughlin, *Quantized hall conductivity in two dimensions*, *Phys. Rev. B* **23** (May, 1981) 5632–5633.
- [6] D. C. Tsui, H. L. Stormer, and A. C. Gossard, *Two-dimensional magnetotransport in the extreme quantum limit*, *Phys. Rev. Lett.* **48** (May, 1982) 1559–1562.
- [7] A. Kitaev and J. Preskill, *Topological entanglement entropy*, *Phys. Rev. Lett.* **96** (2006) 110404, [hep-th/0510092].
- [8] M. Levin and X.-G. Wen, *Detecting topological order in a ground state wave function*, *Phys. Rev. Lett.* **96** (2006) 110405, [cond-mat/0510613].
- [9] J. M. Leinaas and J. Myrheim, *On the theory of identical particles*, *Nuovo Cimento B* **37B** (1977) 1.
- [10] F. Wilczek, *Quantum mechanics of fractional-spin particles*, *Phys. Rev. Lett.* **49** (1982) 957–959.
- [11] G. A. Goldin, R. Menikoff, and D. H. Sharp, *Comments on “General Theory for Quantum Statistics in Two Dimensions”*, *Phys. Rev. Lett.* **54** (1985) 603.

- [12] K. Fredenhagen, K. H. Rehren, and B. Schroer, *Superselection sectors with braid group statistics and exchange algebras*, *Commun. Math. Phys.* **125** (1989) 201–226.
- [13] J. Fröhlich and F. Gabbiani, *Braid statistics in local quantum theory*, *Rev. Math. Phys.* **2** (1990) 251–353.
- [14] X.-G. Wen, *Topological orders in rigid states*, *Int. J. Mod. Phys. B* **04** (1990), no. 02 239–271.
- [15] A. Kitaev, *Fault-tolerant quantum computation by anyons*, *Annals of Physics* **303** (2003), no. 1 2 – 30.
- [16] C. Nayak, S. H. Simon, A. Stern, M. Freedman, and S. Das Sarma, *Non-abelian anyons and topological quantum computation*, *Rev. Mod. Phys.* **80** (Sep, 2008) 1083–1159.
- [17] S. Eilenberg and S. MacLane, *General theory of natural equivalences*, *Transactions of the American Mathematical Society* **58** (1945), no. 2 231–294.
- [18]
- [19]
- [20] R. B. Laughlin, *Anomalous quantum hall effect: An incompressible quantum fluid with fractionally charged excitations*, *Phys. Rev. Lett.* **50** (May, 1983) 1395–1398.
- [21] X.-G. Wen, *Vacuum degeneracy of chiral spin states in compactified space*, *Phys. Rev. B* **40** (Oct, 1989) 7387–7390.
- [22] L. Balents, *Spin liquids in frustrated magnets*, *Nature* **464** (03, 2010) 199–208.
- [23] T.-H. Han, J. S. Helton, S. Chu, D. G. Nocera, J. A. Rodriguez-Rivera, C. Broholm, and Y. S. Lee, *Fractionalized excitations in the spin-liquid state of a kagome-lattice antiferromagnet*, *Nature* **492** (12, 2012) 406–410.
- [24] M. A. Levin and X.-G. Wen, *String-net condensation: A physical mechanism for topological phases*, *Phys. Rev. B* **71** (Jan, 2005) 045110.
- [25] V. G. Turaev and O. Y. Viro, *State sum invariants of 3-manifolds and quantum 6j-symbols*, *Topology* **31** (1992) 865–902.
- [26] P. Bonderson, *Non-Abelian Anyons and Interferometry*. PhD thesis, Caltech, 2007.
- [27] A. Kitaev, *Anyons in an exactly solved model and beyond*, *Annals of Physics* **321** (2006), no. 1 2–111.

- [28] M. de Wild Propitius, *Topological interactions in broken gauge theories*, hep-th/9511195.
- [29] A. M. Essin and M. Hermele, *Classifying fractionalization: Symmetry classification of gapped  $F_2$  spin liquids in two dimensions*, *Phys. Rev. B* **87** (Mar, 2013) 104406.
- [30] M. Barkeshli, P. Bonderson, M. Cheng, and Z. Wang, *Symmetry, defects, and gauging of topological phases*, arXiv:1410.4540.
- [31] M. Cheng, M. Zaletel, M. Barkeshli, A. Vishwanath, and P. Bonderson, *Translational Symmetry and Microscopic Constraints on Symmetry-Enriched Topological Phases: A View from the Surface*, *Phys. Rev. X* **6** (Oct., 2016) 041068, [1511.0226].
- [32] P. Bonderson and C. Nayak, *Quasi-topological phases of matter and topological protection*, *Phys. Rev. B* **87** (May, 2013) 195451.
- [33] F. J. Burnell, S. H. Simon, and J. K. Slingerland, *Condensation of achiral simple currents in topological lattice models: Hamiltonian study of topological symmetry breaking*, *Phys. Rev. B* **84** (Sep, 2011) 125434.
- [34] J. M. Luttinger, *Fermi surface and some simple equilibrium properties of a system of interacting fermions*, *Phys. Rev.* **119** (Aug, 1960) 1153–1163.
- [35] M. Oshikawa, *Topological approach to luttinger’s theorem and the fermi surface of a kondo lattice*, *Phys. Rev. Lett.* **84** (Apr, 2000) 3370–3373, [cond-mat/0002392].
- [36] R. Tao and Y.-S. Wu, *Gauge invariance and fractional quantum hall effect*, *Phys. Rev. B* **30** (Jul, 1984) 1097–1098.
- [37] R. Tao and F. D. M. Haldane, *Impurity effect, degeneracy, and topological invariant in the quantum hall effect*, *Phys. Rev. B* **33** (Mar, 1986) 3844–3850.
- [38] E. Lieb, T. Schultz, and D. Mattis, *Two soluble models of an antiferromagnetic chain*, *Annals of Physics* **16** (1961), no. 3 407 – 466.
- [39] T. Senthil, S. Sachdev, and M. Vojta, *Fractionalized fermi liquids*, *Phys. Rev. Lett.* **90** (May, 2003) 216403, [cond-mat/0209144].
- [40] T. Senthil, M. Vojta, and S. Sachdev, *Weak magnetism and non-fermi liquids near heavy-fermion critical points*, *Phys. Rev. B* **69** (Jan, 2004) 035111, [cond-mat/0305193].
- [41] A. Paramekanti and A. Vishwanath, *Extending luttinger’s theorem to  $Z_2$  fractionalized phases of matter*, *Phys. Rev. B* **70** (Dec, 2004) 245118, [cond-mat/0406619].

- [42] M. Oshikawa, *Commensurability, excitation gap, and topology in quantum many-particle systems on a periodic lattice*, *Phys. Rev. Lett.* **84** (Feb, 2000) 1535–1538, [cond-mat/9911137].
- [43] M. B. Hastings and X.-G. Wen, *Quasiadiabatic continuation of quantum states: The stability of topological ground-state degeneracy and emergent gauge invariance*, *Phys. Rev. B* **72** (Jul, 2005) 045141, [cond-mat/0503554].
- [44] M. B. Hastings, *Lieb-schultz-mattis in higher dimensions*, *Phys. Rev. B* **69** (Mar, 2004) 104431, [cond-mat/0305505].
- [45] M. P. Zaletel and A. Vishwanath, *Constraints on topological order in mott insulators*, *Phys. Rev. Lett.* **114** (Feb, 2015) 077201, [arXiv:1410.2894].
- [46] D. Chowdhury and S. Sachdev, *Density-wave instabilities of fractionalized fermi liquids*, *Phys. Rev. B* **90** (Dec, 2014) 245136, [arXiv:1409.5430].
- [47] A. Thomson and S. Sachdev, *Fractionalized Fermi liquid on the surface of a topological Kondo insulator*, arXiv:1509.0331.
- [48] A. Hamma, R. Ionicioiu, and P. Zanardi, *Ground state entanglement and geometric entropy in the Kitaev model [rapid communication]*, *Physics Letters A* **337** (Mar., 2005) 22–28, [quant-ph/0406202].
- [49] C. W. von Keyserlingk, F. J. Burnell, and S. H. Simon, *Three-dimensional topological lattice models with surface anyons*, *Phys. Rev. B* **87** (Jan, 2013) 045107, [arXiv:1208.5128].
- [50] M. Cheng, *Symmetry Fractionalization in Three-Dimensional  $\mathbb{Z}_2$  Topological Order and Fermionic Symmetry-Protected Phases*, arXiv:1511.0256.
- [51] E. Schrödinger, *Discussion of probability relations between separated systems*, *Proceedings of the Cambridge Philosophical Society* **31** (1935) 555.
- [52] P. Calabrese and J. Cardy, *Entanglement entropy and quantum field theory*, *Journal of Statistical Mechanics: Theory and Experiment* **6** (June, 2004) 06002, [hep-th/0405152].
- [53] P. Calabrese and J. Cardy, *Entanglement entropy and conformal field theory*, *Journal of Physics A Mathematical General* **42** (Dec., 2009) 504005, [0905.4013].
- [54] L. Savary and L. Balents, *Quantum spin liquids: a review*, *Reports on Progress in Physics* **80** (Jan., 2017) 016502, [1601.0374].
- [55] M. H. Freedman, *P/NP, and the quantum field computer*, *Proc. Natl. Acad. Sci. USA* **95** (1998) 98–101.

- [56] S. Dong, E. Fradkin, R. G. Leigh, and S. Nowling, *Topological entanglement entropy in chern-simons theories and quantum hall fluids*, *JHEP* **05** (2008) 016, [0802.3231].
- [57] C. Castelnovo and C. Chamon, *Topological order in a three-dimensional toric code at finite temperature*, *Phys. Rev. B* **78** (Oct., 2008) 155120, [0804.3591].
- [58] I. D. Rodríguez and G. Sierra, *Entanglement entropy of integer quantum Hall states*, *Phys. Rev. B* **80** (Oct., 2009) 153303, [0811.2188].
- [59] T. Grover, A. M. Turner, and A. Vishwanath, *Entanglement entropy of gapped phases and topological order in three dimensions*, *Phys. Rev. B* **84** (Nov., 2011) 195120, [1108.4038].
- [60] B. J. Brown, S. D. Bartlett, A. C. Doherty, and S. D. Barrett, *Topological entanglement entropy with a twist*, *Phys. Rev. Lett.* **111** (Nov, 2013) 220402, [1303.4455].
- [61] I. H. Kim, *Long-range entanglement is necessary for a topological storage of quantum information*, *Phys. Rev. Lett.* **111** (Aug, 2013) 080503, [1304.3925].
- [62] I. H. Kim and B. J. Brown, *Ground-state entanglement constrains low-energy excitations*, *Phys. Rev. B* **92** (Sep, 2015) 115139, [1410.7411].
- [63] X. Wen, S. Matsuura, and S. Ryu, *Edge theory approach to topological entanglement entropy, mutual information, and entanglement negativity in Chern-Simons theories*, *Phys. Rev. B* **93** (June, 2016) 245140, [1603.0853].
- [64] A. Bullivant and J. K. Pachos, *Entropic manifestations of topological order in three dimensions*, *Phys. Rev. B* **93** (Mar., 2016) 125111, [1504.0286].
- [65] S. Furukawa and G. Misguich, *Topological entanglement entropy in the quantum dimer model on the triangular lattice*, *Phys. Rev. B* **75** (Jun, 2007) 214407, [cond-mat/0612227].
- [66] M. Haque, O. Zozulya, and K. Schoutens, *Entanglement entropy in fermionic Laughlin states*, *Phys. Rev. Lett.* **98** (2007) 060401, [cond-mat/0609263].
- [67] O. S. Zozulya, M. Haque, K. Schoutens, and E. H. Rezayi, *Bipartite entanglement entropy in fractional quantum Hall states*, *Phys. Rev. B* **76** (2007) 125310, [0705.4176].
- [68] O. S. Zozulya, M. Haque, and N. Regnault, *Entanglement signatures of quantum Hall phase transitions*, *Phys. Rev. B* **79** (Jan., 2009) 045409, [0809.1589].
- [69] H. Yao and X.-L. Qi, *Entanglement entropy and entanglement spectrum of the kitaev model*, *Phys. Rev. Lett.* **105** (Aug, 2010) 080501, [1001.1165].

- [70] S. V. Isakov, M. B. Hastings, and R. G. Melko, *Topological entanglement entropy of a Bose-Hubbard spin liquid*, *Nature Physics* **7** (Oct., 2011) 772–775, [1102.1721].
- [71] A. Sterdyniak, A. Chandran, N. Regnault, B. A. Bernevig, and P. Bonderson, *Real-space entanglement spectrum of quantum Hall states*, *Phys. Rev. B* **85** (Mar., 2012) 125308, [1111.2810].
- [72] Y. Zhang, T. Grover, A. Turner, M. Oshikawa, and A. Vishwanath, *Quasiparticle statistics and braiding from ground-state entanglement*, *Phys. Rev. B* **85** (Jun, 2012) 235151, [1111.2342].
- [73] H.-C. Jiang, Z. Wang, and L. Balents, *Identifying topological order by entanglement entropy*, *Nature Physics* **8** (Dec., 2012) 902–905, [1205.4289].
- [74] M. P. Zaletel and R. S. K. Mong, *Exact matrix product states for quantum hall wave functions*, *Phys. Rev. B* **86** (Dec, 2012) 245305, [1208.4862].
- [75] M. P. Zaletel, R. S. K. Mong, and F. Pollmann, *Topological characterization of fractional quantum hall ground states from microscopic hamiltonians*, *Phys. Rev. Lett.* **110** (Jun, 2013) 236801, [1211.3733].
- [76] L. Cincio and G. Vidal, *Characterizing topological order by studying the ground states on an infinite cylinder*, *Phys. Rev. Lett.* **110** (Feb, 2013) 067208, [1208.2623].
- [77] B. Estienne, N. Regnault, and B. Bernevig, *Correlation lengths and topological entanglement entropies of unitary and nonunitary fractional quantum hall wave functions*, *Phys. Rev. Lett.* **114** (2015), no. 18 186801, [1406.6262].
- [78] A. G. Grushin, J. Motruk, M. P. Zaletel, and F. Pollmann, *Characterization and stability of a fermionic  $\nu = 1/3$  fractional chern insulator*, *Phys. Rev. B* **91** (Jan, 2015) 035136, [1407.6985].
- [79] G. Moore and N. Seiberg, *Classical and quantum conformal field theory*, *Commun. Math. Phys.* **123** (1989) 177–254.
- [80] J. Preskill, “lecture notes.”  
<http://www.theory.caltech.edu/~preskill/ph219/topological.pdf>.
- [81] A. Kitaev, *Anyons in an exactly solved model and beyond*, *Annals Phys.* **321** (2006) 2–111, [cond-mat/0506438].
- [82] P. H. Bonderson, *Non-Abelian anyons and interferometry*. PhD thesis, California Institute of Technology, 2007.
- [83] P. Bonderson, K. Shtengel, and J. K. Slingerland, *Interferometry of non-abelian anyons*, *Annals of Physics* **323** (2008) 2709, [0707.4206].

- [84] M. A. Nielsen and I. L. Chuang, *Quantum Computation and Quantum Information: 10th Anniversary Edition*. Cambridge University Press, New York, NY, USA, 10th ed., 2011.
- [85] M. A. Levin and X.-G. Wen, *String-net condensation: A physical mechanism for topological phases*, *Phys. Rev. B* **71** (2005) 045110, [cond-mat/0404617].
- [86] H. Li and F. D. M. Haldane, *Entanglement spectrum as a generalization of entanglement entropy: Identification of topological order in non-abelian fractional quantum hall effect states*, *Phys. Rev. Lett.* **101** (Jul, 2008) 010504, [0805.0332].
- [87] P. Bruillard, S.-H. Ng, E. C. Rowell, and Z. Wang, *Rank-finiteness for modular categories*, *J. Amer. Math. Soc.* **29** (2016) [1310.7050].
- [88] E. Rowell, R. Stong, and Z. Wang, *On classification of modular tensor categories*, *Comm. Math. Phys.* **292** (2009) 343, [0712.1377].
- [89] P. Bonderson and J. K. Slingerland in preparation.
- [90] P. Bonderson, M. Freedman, and C. Nayak, *Measurement-only topological quantum computation via anyonic interferometry*, *Annals of Physics* **324** (Apr., 2009) 787–826, [0808.1933].
- [91] P. Bonderson, M. Freedman, and C. Nayak, *Measurement-Only Topological Quantum Computation via Anyonic Interferometry*, *Annals Phys.* **324** (2009) 787, [0808.1933].
- [92] P. Bonderson, M. Freedman, and C. Nayak, *Measurement-only topological quantum computation*, *Phys. Rev. Lett.* **101** (2008) 010501, [0802.0279].
- [93] K. Hikami, *Skein theory and topological quantum registers: Braiding matrices and topological entanglement entropy of non-Abelian quantum Hall states*, *Annals of Physics* **323** (July, 2008) 1729–1769, [0709.2409].
- [94] K. Kato, F. Furrer, and M. Murao, *Information-theoretical formulation of anyonic entanglement*, *Phys. Rev. A* **90** (Dec., 2014) 062325, [1310.4140].
- [95] R. N. C. Pfeifer, *Measures of entanglement in non-Abelian anyonic systems*, *Phys. Rev. B* **89** (Jan., 2014) 035105, [1310.0373].
- [96] J. Cardy, *Boundary Conformal Field Theory*, *Encyclopedia of Mathematical Physics* (2006) [hep-th/0411189].
- [97] R. N. C. Pfeifer, O. Buerschaper, S. Trebst, A. W. W. Ludwig, M. Troyer, and G. Vidal, *Translation invariance, topology, and protection of criticality in chains of interacting anyons*, *Phys. Rev. B* **86** (Oct., 2012) 155111, [1005.5486].

- [98] E. Witten, *Quantum field theory and the Jones polynomial*, *Comm. Math. Phys.* **121** (1989) 351–399.
- [99] T. Stevens, *Speech Opposing Network Neutrality*. United States Senate, Washington DC, USA, 2006.
- [100] S. T. Flammia, A. Hamma, T. L. Hughes, and X.-G. Wen, *Topological Entanglement Rényi Entropy and Reduced Density Matrix Structure*, *Phys. Rev. Lett.* **103** (Dec., 2009) 261601, [0909.3305].
- [101] R. Dijkgraaf and E. Witten, *Topological gauge theories and group cohomology*, *Commun. Math. Phys.* **129** (1990), no. 2 393–429.
- [102] P. Bonderson, M. Cheng, R. Mong, and A. Tran in preparation.
- [103] T. Lan, L. Kong, and X.-G. Wen, *Theory of (2+1)-dimensional fermionic topological orders and fermionic/bosonic topological orders with symmetries*, *Phys. Rev. B* **94** (Oct., 2016) 155113, [1507.0467].
- [104] M. Barkeshli, P. Bonderson, C.-M. Jian, M. Cheng, and K. Walker, *Reflection and time reversal symmetry enriched topological phases of matter: path integrals, non-orientable manifolds, and anomalies*, 1612.0779.
- [105] C. W. von Keyserlingk, F. J. Burnell, and S. H. Simon, *Three-dimensional topological lattice models with surface anyons*, *Phys. Rev. B* **87** (Jan., 2013) 045107, [1208.5128].
- [106] K. Walker and Z. Wang, *(3+1)-TQFTs and topological insulators*, *Frontiers of Physics* **7** (Apr., 2012) 150–159, [1104.2632].
- [107] M. Freedman, C. Nayak, K. Shtengel, K. Walker, and Z. Wang, *A class of  $p, t$ -invariant topological phases of interacting electrons*, *Annals of Physics* **310** (4, 2004) 428–492.
- [108] C. W. von Keyserlingk, F. J. Burnell, and S. H. Simon, *Three-dimensional topological lattice models with surface anyons*, *Phys. Rev. B* **87** (Jan, 2013) 045107.
- [109] G. Moore and N. Seiberg, *Lectures on rcft*, in *Physics, Geometry and Topology* (H. Lee, ed.), vol. 238 of *NATO ASI Series*, pp. 263–361. Springer US, 1990.
- [110] L.-Y. Hung and Y. Wan, *String-net models with  $Z_N$  fusion algebra*, *Phys. Rev. B* **86** (Dec, 2012) 235132.